Secondary Control of Multi-chamber Cylinders for Low-speed, High-force, Offshore Applications

Donkov, Viktor Hristov

Publication date:
2020

Document Version
Publisher's PDF, also known as Version of record

SECONDARY CONTROL OF MULTI-CHAMBER CYLINDERS FOR LOW-SPEED, HIGH-FORCE OFFSHORE APPLICATIONS

BY
VIKTOR HRISTOV DONKOV

DISSERTATION SUBMITTED 2020

AALBORG UNIVERSITY
DENMARK

Secondary Control of Multi-chamber Cylinders for Low-speed, High-force Offshore Applications

Ph.D. Dissertation
Viktor Hristov Donkov

Dissertation submitted month 09, 2020

Dissertation submitted:	September 2020
PhD supervisor:	Prof. Torben Ole Andersen Aalborg University, Denmark
Assistant PhD supervisor:	Prof. Morten Kjeld Ebbesen University of Agder, Norway
PhD committee:	Associate Professor Mads Pagh Nielsen (chairman) Aalborg University
	Professor Leonid Freidovich Umeå University
	Professor Kalevi Huhtala Tampere University
PhD Series:	Faculty of Engineering and Science, Aalborg University
Department:	Department of Energy Technology

ISSN (online): 2446-1636
ISBN (online): 978-87-7210-810-0

Published by:
Aalborg University Press
Kroghstræde 3
DK – 9220 Aalborg Ø
Phone: +45 99407140
aauf@forlag.aau.dk
forlag.aau.dk

Printed in Denmark by Rosendahls, 2020

Abstract

The ongoing global warming crisis and the increasing cost of energy demand improvements in many industries. Technologies and methods, which were once sufficient, must again and again be examined and improved. One of these technologies is hydraulic actuation. Hydraulic systems may have efficiencies as low as 30 %. Due to their many benefits such inefficiencies have been disregarded to some extent. In recent years both academia and industry have put a higher focus on efficiency, and different paradigm shifts are being investigated. Digital hydraulics is one such paradigm, which relies on the notion that a component, which is switched off, does not incur losses, while one that is used to its maximum potential can be designed to be efficient for that operation condition.

Multi-chamber cylinders are a part of the digital hydraulics field. They are hydraulic cylinders, which have more than two chambers. Each chamber has a different cross-sectional area. Different forces can be generated by connecting the chambers to different predefined pressures. This concept removes the need for proportional control valves and throttling. Removing throttling removes a major part of the losses in hydraulic systems. When a system is controlled in such a way as to only extract the necessary energy from a source, without changing the sources output, it is called secondary control.

One of the challenges in implementing secondary controlled multi-chamber cylinders is that the hydraulic cylinder in such a solution is more complex than a standard hydraulic cylinder. Very limited research has been conducted, documenting the performance of digitally controlled cylinders on low-speed, high-force applications. Concerns about the smoothness of motion, the possibility of pressure spikes, and the computational complexity of the control structure have been raised. This thesis addresses these difficulties. First it investigates the performance of a multi-chamber cylinder in a low-speed, high-force application such as a knuckle boom crane. It is shown that while simpler control structures can get the job done, a more

complicated structure such as Model Predictive Control (MPC) can give better performance. The optimization problem inherent in MPC, the controllers sensitivity, and the controllers robustness are also studied. In trying to study the smoothness of motion of a cylinder, the project faced a lack of tools with which to measure it and the use of total harmonic distortion, a concept from electrical engineering is proposed.

The project concludes that multi-chamber cylinders can have smooth, energy efficient motion if MPC with integral action is used and certain conditions are met - mostly known or selected system parameters. When changes are introduced the energy efficiency suffers first followed by smoothness of motion. The project also concludes that when MPC is used for position control, a short time horizon can be sufficient. In this case a much simpler optimization method can still give good results. In this case MPC works more like model based control. Overall, multi-chamber cylinders are an intriguing solution, but more research into making their performance more robust is needed before they can find wider popularity.

Resumé

Den igangværende klimakrise og de stigende energiomkostninger kræver reduktion af energibehov i mange brancher. Teknologier og metoder, der engang var tilstrækkelige, skal igen undersøges og forbedres. En af disse teknologier er hydraulisk aktuering. Historisk set har hydrauliske systemer haft effektivitet helt ned til 30 %. På grund af hydrauliske systemers vigtighed er denne ineffektivitet i nogen grad blevet ignoreret. I de senere år har både akademia og industri sat et højere fokus på energieffektivitet, og forskellige paradigmeskift undersøges. Digital hydraulik er et sådant paradigmeskifte, der bygger på faktummet om, at en komponent, der er slukket, er tabsfri, mens en, der benyttes ved sit maksimale effektniveau, kan blive designet til at være effektiv i denne driftsbetingelse.

Multikammercylindre er en del af det digitalt hydrauliske felt. Det er hydrauliske cylindre med mere end to kamre. Alle kamre har forskellige tværsnitsarealer. Forskellige kræfter kan genereres ved at forbinde kamrene til forskellige foruddefinerede tryk. Dette koncept fjerner behovet for proportionalventiler og drøvling. Ved at fjerne drøvling fjernes en væsentlig kilde til tab i hydrauliske systemer. Når et system styres på en sådan måde, at det kun benytter den nødvendige energi fra en kilde, uden at ændre kildens output, benænes det sekundær kontrol.

En af udfordringerne ved implementering af sekundært kontrollerede multikammercylindre er, at den hydrauliske cylinder i en sådan løsning er mere kompleks end en standard hydraulisk cylinder. Der er lavet begrænset forskning, der dokumenterer ydeevnen for digitalt kontrollerede cylindre på lav-hastighed, høj-kraft applikationer. Bevægelsens glathed, muligheden for trykspidser og beregningskompleksiteten i kontrolstrukturen er. Denne afhandling vedrører disse vanskeligheder. Først undersøges ydeevnen af en multikammercylinder i en lav-hastighed, høj-kraft applikation, som f.eks. en knuckle boom kran. Det vises, at selvom enkle kontrolstrukturer er brugbare, kan en mere kompliceret struktur såsom Model Predictive Control (MPC) forbedre ydeevnen. Optimeringsproblemet, der er forbundet med MPC, reg-

ulatorens følsomhed og robusthed undersøges også. Hertil foreslås at evaluere den såkaldte total harmonisk forvrængning, der er et velkendt koncept fra effektelektronikken.

Projektet konkluderer, at multikammercylindre kan have en jævn, energieffektiv bevægelse, hvis MPC bruges, og visse betingelser er opfyldt - heriblandt kendte eller valgte systemparametre. Når ændringer indføres, forringes energieffektiviteten først efterfulgt af glathed i bevægelsen. Når MPC bruges til positionskontrol, kan en kort tidshorisont være tilstrækkelig, i hvilket tilfælde en meget enklere optimeringsmetode stadig kan give gode resultater. I dette tilfælde fungerer MPC som modelbaseret kontrol. Generelt er multikammercylindre en interessant teknologi, men der kræves mere forskning i at gøre deres ydeevne mere robust, før de kan vinde indpas i industrielle sammenhænge.

Reading Guidelines

This thesis is a paper-based thesis. It consists of a summarizing text and a number of individual papers published independently of each other. The papers all relate to the same subject and as such constitute a scientific whole corresponding to the contents of a monographic thesis. This thesis is divided into four parts. Part I, Part II and Part III summarize the papers contained in Part IV.

Part I contains background information, which explains multi-chamber cylinders, their advantages and disadvantages, and the state of the art in this technology. The state of the art chapter is based on paper A. The research questions, which this thesis attempts to answer are defined in this part of the thesis.

Part II contains the models and control structures used in the published papers. Chapter 3 details the model of a seesaw test bench defined in paper D, the model of a knuckle boom crane defined in paper C, and goes into greater detail into the model of a multi-chamber cylinder. Chapter 4 describes the two control structures in the thesis - direct force control and model predictive control. First direct force control is explained which is used in papers B and C. Model predictive control is then defined. This control structure is used in papers C, D, and E.

Part III contains the results of papers B, C, D, and E. Laboratory results are only available for the seesaw test bench and come from paper D. The rest of the results are obtained through simulations. Part III also contains Chapter 6, where the conclusions of the thesis can be found.

Part IV contains the papers on which the thesis is based on.

Each chapter has its own reference section. Reference numbers only refer to the chapter in which they are used.

List of publications

A Digital Hydraulic Technology for linear Actuation: A state of the art review, Viktor Donkov, Torben Ole Andersen, Matti Linjama, Morten Kjeld Ebbesen, under review at *International Journal of Fluid Power, 2020*

B Applying Digital Hydraulic Technology on a Knuckle Boom Crane, Viktor Donkov, Torben Ole Andersen, Morten Kjeld Ebbesen, Henrik Clemmensen Pedersen, in *The Ninth Workshop on Digital Fluid Power, September 7-8, 2017, Aalborg, Denmark*

C Application of Model Predictive Control in Discrete Displacement Cylinders to Drive a Knuckle Boom Crane, Viktor Donkov, Torben Ole Andersen, Morten Kjeld Ebbesen, Henrik Clemmensen Pedersen, in *The Global Fluid Power Society PhD Symposium, July 18-20, 2018, Samara, Russia*

D Investigation of the Fault Tolerance of Digital Hydraulic Cylinders, Viktor Donkov, Torben Ole Andersen, Morten Kjeld Ebbesen, Matti Linjama, Miika Paloniity, in *The Sixteenth Scandinavian Conference on Fluid Power, May 22-24, 2019, Tampere, Finland*

E An analysis of Model Predictive Control with Integral Action Applied to Digital Displacement Cylinders, Viktor Donkov, Torben Ole Andersen, Morten Kjeld Ebbesen, under review at *Modeling, Identification and Control, 2020*

Contents

Abstract iii

Resumé v

Reading Guidelines vii

Preface xi

I Introduction 1

1 Introduction 3
References 8

2 State of the art 9
2.1 Multi-chamber cylinders 9
2.2 Multi-pressure cylinder 11
2.3 Conclusion 12
References 14

II Modelling and Control 17

3 System and model 19
3.1 Seesaw model 19
3.2 Crane model 24
3.3 Multi-chamber cylinder 29
3.3.1 Force level number and density 30
References 36

4 Control 37
4.1 Direct Force control 37
4.2 Model Predictive Control 41

4.2.1 Prediction Model 43
4.2.2 Model with integral action 45
4.2.3 The optimization problem 47
4.2.4 Using neural networks to approximate an MPC 60
4.2.5 Fault tolerant control 63
References 67

III Results and Conclusions 69

5 Results 71
5.1 Crane results 71
5.1.1 Results with a constant pressure rail compared with DFC 71
5.1.2 Results with a load sensing system compared with MPC and DFC 74
5.2 Seesaw results 77
5.2.1 Trajectories 78
5.2.2 Total harmonic distortion analysis 78
5.2.3 Algorithm results 81
5.2.4 Neural network approximation 85
5.2.5 Laboratory results 86
5.2.6 Sensitivity analysis 88

6 Conclusion 95
6.1 Answering the research questions 95
6.2 Future Work 97

IV Papers 99

A Digital Hydraulic Technology for Linear Actuation: A state of the art review 101

B Applying Digital Hydraulic Technology on a Knuckle Boom Crane 135

C Application of Model Predictive Control in Discrete Displacement Cylinders to Drive a Knuckle Boom Crane 153

D Investigation of the Fault Tolerance of Digital Hydraulic Cylinders 163

E An analysis of Model Predictive Control with Integral Action Applied to Digital Displacement Cylinders 177

Preface

This thesis was written at the Department of Energy Technology at Aalborg University during the period 2017-2020. The work received funding from The Research Council of Norway, SFI Offshore mechatronics, project number 237896/O30.

I am thankful to my supervisors Prof. Torben Ole Andersen and Prof. Morten Kjeld Ebbesen for their continued support and guidance.

I would also like to thank my colleagues at Aalborg university and my hosts at Tampere University of Technology for their advice and help.

Finally, I would like to thank my friends and family for their support.

Viktor Hristov Donkov
Aalborg University, September 18, 2020

Part I

Introduction

Chapter 1

Introduction

Fluid power is used in many industries. One of its benefits is a high force-to-weight ratio. One alternative is the use of electric motors which require a gearbox with large gear ratios, especially for linear actuation. The inclusion of the gearbox reduces the force-to-weight ratio of the system. Cranes and mobile work platforms (such as excavators or forestry machines) mostly use hydraulic cylinders to do their job. Large scale machines, see for example Fig. 1.1 and Fig. 1.2, can be quite powerful. Unfortunately, the overall efficiency of their hydraulic transmission can be very low. In some cases, it can be as low as 30 %. Research has shown that this is partly due to the hydraulic components, which have changing efficiency - high in certain operating conditions and low otherwise.

Figure 1.1: A 25 ton knuckle-boom crane. ©NOV, Geir-Arne Moslått 2018.

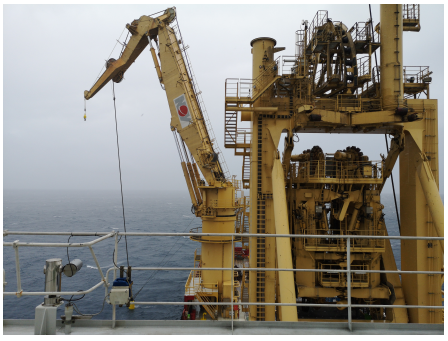

Figure 1.2: A 250 ton knuckle-boom crane. ©NOV, Geir-Arne Moslått 2019.

Specifically, the proportional valve, which is used to control almost all linear hydraulic actuators, can account for a large portion of the losses in a

system. This occurs, because the valve throttles the flow of hydraulic fluid passing through it in order to control it. This throttling process can be seen in Fig. 1.3. In the figure the pressure in the chamber is lower than the supply pressure, because of the orifice of the proportional valve. This pressure difference represents energy losses, because the energy was converted to unwanted heat as the fluid is accelerated. The process allows for very convenient velocity control of a cylinder, but with the rise in the cost of energy, it becomes less and less desirable. A common solution of the problem has been to manipulate the output of the pump, so the desired flow is delivered without the need of throttling. However in most machines multiple actuators are supplied by the same pump. From all the actuators supplied by the pump, the one with the largest pressure requirement dictates the supply. In many cases this leads to the necessity of throttling. A crane systems of the type seen in Fig. 1.1, for instance, would have a pressure compensated mobile hydraulic valve. An operator gives velocity references for the cylinders with a pair of joysticks. The cylinder of the main boom carries more weight, because it carries the weight of the main boom, the knuckle boom, the load and the second cylinder. The cylinder of the main boom will determine the supply pressure in this case. The proportional valve will then throttle this pressure down as dictates by the requirement of the second cylinder. Some research attempts to solve this problem through the decentralisation of the supply i.e. having a separate pump and electric motor for each actuator [2]. Other research focuses on the use of electro-mechanical cylinders which altogether avoid hydraulics [1]. Digital hydraulics is a third alternative, which draws inspiration from the area of electronics.

Digital hydraulics is a new paradigm in fluid power technology, which is founded on the notion that a component, which is switched off, does not incur losses, while a component that is used to its maximum potential is efficient. This research field in the hydraulic community has been gaining some attention with multiple papers and conference keynote speeches argueing for its benefits e.g. [3] and [4].

Multi-chamber cylinders are a specific subset of digital hydraulics. They enables a new development in the field of linear actuation - secondary control of hydraulic cylinders. The idea behind secondary control is to change the output of the actuator by changing its displacement instead of throttling the flow. In the field of rotary hydraulics this can already be achieved by the use of, for example, swash-plate motors. This approach has shown itself to be useful and efficient. It is not possible to apply the same approach to a standard cylinder as the parameter that needs to change is the cross-sectional area of the cylinder's chambers. So far no way has been found to allow for the change of the area in a continuous fashion. Digital hydraulics proposes

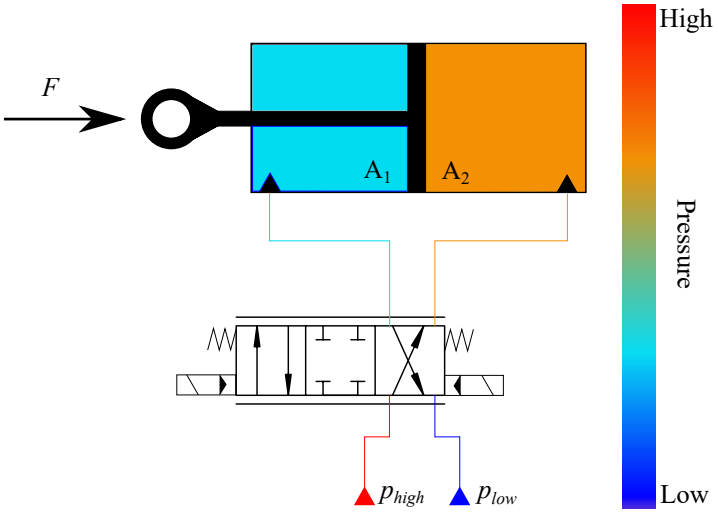

Figure 1.3: Simplified classic cylinder with throttling valve for control

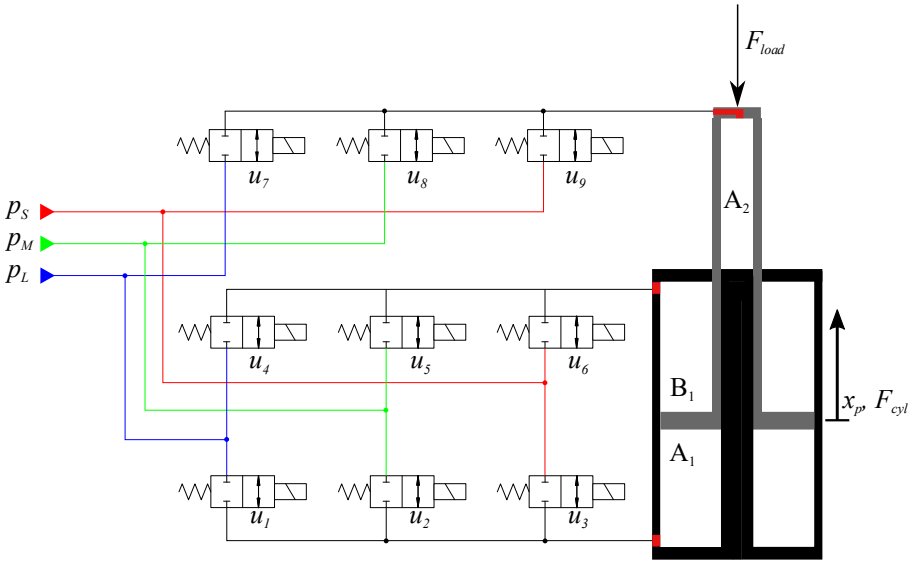

Figure 1.4: Example of a three-chamber multi-chamber cylinder.

the use of multi-chamber cylinders in order to do this in a discrete manner.

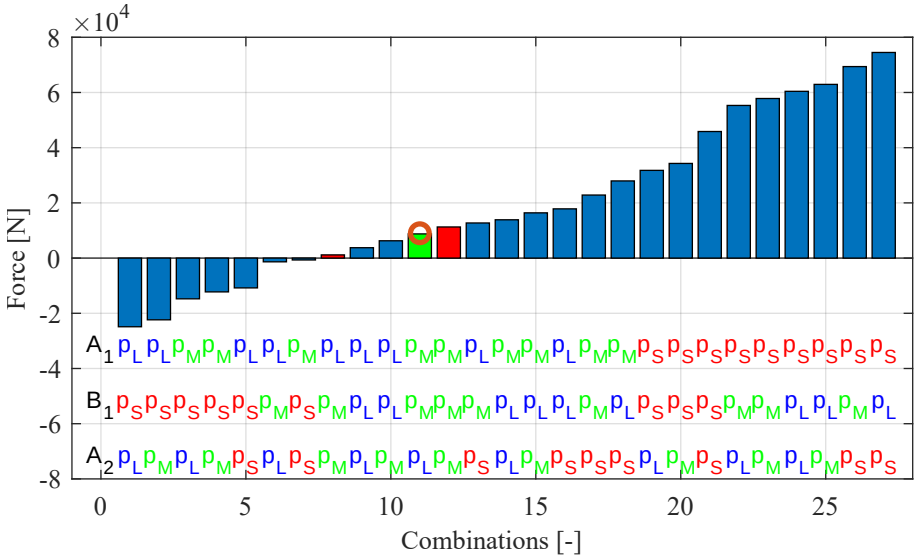

Figure 1.5: Example of a force resolution.

Multi-chamber cylinders are hydraulic cylinders, which have more than two chambers. Each chamber has a different area. The same flow supplied to different chambers results in different output velocities. In this way the cylinders velocity can be changed, without changing the output of the pump or throttling the flow. A further refinement on the concept leads to the idea of using constant pressure rail similar to the concept of an electric grid. By connecting different chambers to pressure rails with different values, the force output of the cylinder is changed. An example of a multi-chamber cylinder with three chambers and three pressure rails can be seen in Fig. 1.4. In the figure p_S is a high-pressure line with a pressure value of 122 bar, p_L is a low pressure line with a value of 10 bar, and p_M is a pressure line with a pressure value between the high and low pressures 30 bar. The areas of the chambers A_1, B_1, and A_2 are $5059 \cdot 10^{-6}$, $2557 \cdot 10^{-6}$ and $1257 \cdot 10^{-6}$ m^2 respectively. The forces this cylinder can generate are shown in Fig. 1.5. In the figure each bar represents one force level. The pressures in the three chambers can be seen below each force level. For example force level 11 is achieved by using pressure p_M in chambers A1 and B1, and using pressure p_L in chamber A2. A red circle above this force level represents a load force applied to the cylinder. If a higher force level e.g. force level 12 is selected, then cylinder will start accelerating in the positive direction. If force level eight is selected then the cylinder will start accelerating in the negative direction. Using this

method the cylinder can be used to follow a force reference. Since the valve connecting a chamber to a pressure supply is fully open, it does not throttle the flow. The valve itself still has some losses, but these are much smaller than the ones incurred when throttling.

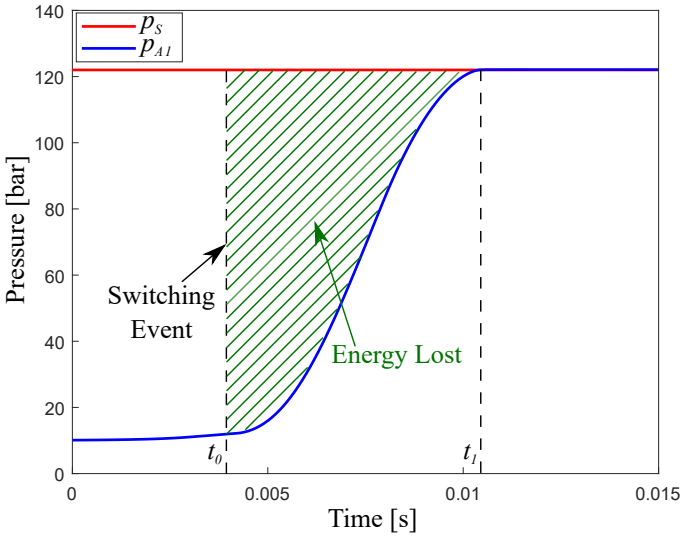

Figure 1.6: Energy lost during pressure shift

Using a multi-chamber cylinder removes the problem of throttling but introduces other issues. The hydraulic fluid in the system is compressible, which means that energy is lost when switching between pressure lines. This is illustrated in Fig. 1.6, where a chamber previously connected to the low-pressure rail is now connected to the high-pressure rail. The pressure in the chamber raises as flow enters the chamber. The same amount of fluid exits the pressure rail. Energy is defined as the integration of the product of flow and pressure. So the energy extracted from the pressure rail is:

$$E_{supply} = \int_{t_0}^{t_1} p_s(t)Q(t)dt \tag{1.1}$$

where p_s is the pressure of the high pressure rail and $Q(t)$ is the flow of fluid exciting the pressure rail. It can be seen that the pressure in the chamber gradually reaches the pressure of the pressure line. During this time the pressure in the pressure line stays constant. The difference in pressure results in lost energy, because the energy of the chamber is defined as:

$$E_{A1} = \int_{t_0}^{t_1} p_{A1}(t)Q(t)dt \tag{1.2}$$

where p_{A1} is the pressure in chamber A1 and $Q(t)$ is the same flow, t_0 is the time at which the switch happens and t_1 is the time at which the pressure of the chamber reaches the pressure of the pressure line. A smaller number is being integrated, because the chamber pressure p_{A1} is smaller than the pressure rail pressure p_s. The energy losses occur only when a switch in pressure is commanded, so they are called switching losses. Since it is highly unlikely that the desired cylinder force will exactly match one of the available forces, this switching will occur often. The losses can be reduced though, through various means discussed in this thesis: choosing appropriate pressure levels, using model predictive control, and improving the optimization procedure inside the controller.

This project builds upon the current state of the art, which will be discussed in the next section, in order to improve the technology.

References

[1] D. Hagen, W. Pawlus, M. K. Ebbesen, and T. O. Andersen, "Feasibility study of electromechanical cylinder drivetrain for offshore mechatronic systems," *Modeling, Identification and Control*, vol. 38, no. 2, 2017.

[2] S. Ketelsen, D. Padovani, T. O. Andersen, M. K. Ebbesen, and L. Schmidt, "Classification and review of pump-controlled differential cylinder drives," *Energies*, vol. 12, no. 7, p. 1293, 2019.

[3] M. S. A. Laamanen and M. Vilenius, "Is it time for digital hydraulics?" in *The Eighth Scandinavian International Conference on Fluid Power*, 2003.

[4] R. Scheidl, M. Linjama, and S. Schmidt, "Is the future of fluid power digital?" *Proceedings of the Institution of Mechanical Engineers, Part I: Journal of Systems and Control Engineering*, vol. 226, no. 6, pp. 721–723, 2012.

Chapter 2

State of the art

This chapter summarizes the state of the art concerning multi-chamber cylinders. Since multi-pressure cylinders have some similar properties a small section is also devoted to them. An in-depth analysis of the existing literature can be found in Appendix paper A.

2.1 Multi-chamber cylinders

Multi-chamber cylinders have been examined by multiple researchers over the years. Multi-chamber cylinders can be considered as a move from a resistive technology to a switching technology. In terms of electrical systems, this would be equivalent to exchanging a resistor for a number of transistors. In the field of electricity this greatly improved energy efficiency. Using multi-chamber cylinders can completely remove throttling, in which case the main losses are due to switching between pressure levels. The shift can improve overall energy efficiency. In [25] input energy was reduced by 62 % compared with a classical hydraulic system, e.g. a load sensing pump and throttling valve. This efficiency has been the driving force behind multi-chamber cylinder research over the years.

While the concept of multi-chamber cylinders was first considered in the 80s, the first resurgence in recent years can be linked to a paper by Matti Linjama in 2009 [25]. This paper examines a four-chamber cylinder which is connected to two pressure lines - a low-pressure line and a high-pressure line. To control the cylinder, a PID controller generates a force reference. A digital controller follows the reference by choosing one of the available force levels. A cost is included in this digital controller in order to reduce switching activity, since switching is the main source of losses. The system is found to be very efficient with the previously stated 62 % reduction in input energy. The paper identifies pressure spikes and oscillatory movement as problems

of the system.

Due to their efficiency multi-chamber cylinders have then been considered for use in wave-energy converters [14], [10], [11], [15], [12], [13], [9], [8], [3], [5], [7], [4], and [6]. In this case, the cylinder does not need to follow a position trajectory. Instead it is used to extract energy from sea waves.

This research project [14] introduced an extra pressure line. Initially the idea behind the extra pressure line is to use the fact that chamber pressure can overshoot. Since switching losses depend on the pressure difference between the initial and the new pressure, the extra line is supposed to be used every time a switching event occurs. The event follows these steps. First, the chamber is connected to the intermediate rail. The pressure in the chamber starts rising, reaches the level of the pressure rail, and due to momentum of the fluid overshoots. At the peak of the overshoot the controller switches to the high pressure line [11]. In order for this concept to work, it requires long hoses. Long hoses increase the volume in which a switch takes place. For this reason long hoses increase switching losses [25]. This is the reason why the concept from [11] has not been investigated in any other papers. Instead the intermediate pressure line is used to increase the number of available forces. At first, a digital controller similar to [25] is used. The controller is then improved by calculating the specific losses for each switch. Since the losses are based on pressure and chamber cross-sectional area, switching between some forces is more expensive.

The technology has also started to get attention from other researchers who want to use it in mobile hydraulic machines such as excavators [1], [16], [26], and [17]. Most of the literature still uses the same controller involving a force reference and a separate switching algorithm. Heybroek et al. [16] proposed a Model Predictive Controller (MPC) in which the transition between two force levels is smoothed out. In order to do this, throttling is introduced. More specifically the pressures in the chambers are being controlled by controlling the spool position of the on/off valves involved in the switching. Hansen et al. [8] and [3] proposed an alternative approach - the valve opening trajectory is selected off-line. In this way it does not add any computational complexity to the controller. This off-line generated trajectory will not fit all operating conditions, so it will be less effective than the MPC solution of Heybroek et al.

Model predictive control also gets introduced for sea energy extraction in [5]. The paper showed that the model predictive controller has some benefits over the previously used force selection algorithms. Two more articles have been published [7] and [6], which further investigate the benefits of MPC in energy extraction. The focus in these papers is on following a force reference. The paper [5] was the only paper focusing on MPC to follow a position reference. In [5] the system is a linear spring damper load.

A downside to the MPC method is that a much more complicated opti-

mization problem needs to be solved compared with the force selection algorithm of [25]. The results of the optimization problem determine not only the quality of the optimum, but also the frequency at which the controller can run. The issue lies in the fact that using switched technology implies the use of integer values in the optimization problem. Since the rest of the hydraulic system has continuous outputs i.e. cylinder position, the optimization problem becomes a mixed-integer optimization problem. Far fewer methods can solve integer problems compared with linear or even convex problems. Many researchers in the digital hydraulic field have avoided researching better optimization algorithms e.g. [17] and [5]. Some researchers use model based controllers which iteratively check large numbers of combinations e.g. 421 [22] or 784 [24]. Some researchers [19], [23], [2], and [21] concentrate on reducing the computation complexity of such model based controllers.

Another gap in the literature can be defined as the lack of structured knowledge on the subject. It is claimed that a smaller mass leads to uneven movement of the cylinder. This is similar to the current ripple in a direct torque controlled electric motor. But it is not clear how big the mass should be in order to avoid this. Furthermore it is not clear how to compare a slow ripple with a large amplitude and a fast ripple with small amplitude, as most research papers only contain a sum of position error.

It is also not clear how many chambers and pressure lines a cylinder should have. Some researchers use a four chamber cylinder with two pressure lines [25] and [16]; others use three-chamber cylinders with three pressure lines [20] and [8]. In the case where three pressure lines are used the middle-pressure line has been chosen to be in the exact middle between the high and the low pressure lines [8], [7], and [6].

2.2 Multi-pressure cylinder

Multi-pressure actuators function on a similar principle as multi-chamber cylinders, because they achieve motion by switching between multiple force levels. In the case of multi-pressure cylinders, a differential cylinder is connected to the different pressures. In order to achieve good controllability, seven or more pressure levels might be needed. The benefit of using multiple pressure lines is that switching losses are greatly reduced. A Further benefit is that the differential cylinder is a widely available component. In order to create these many pressure lines a pressure transformer was proposed by [18]. One high pressure rail is connected to the rod side chamber of a row of small cylinders as can be seen in Fig. 2.1. The ratio between piston and rod side produces different pressures in the piston side chamber. These chambers are used as the constant pressure rails. Because of the small volume in each chamber care has to be taken not to empty one of them.

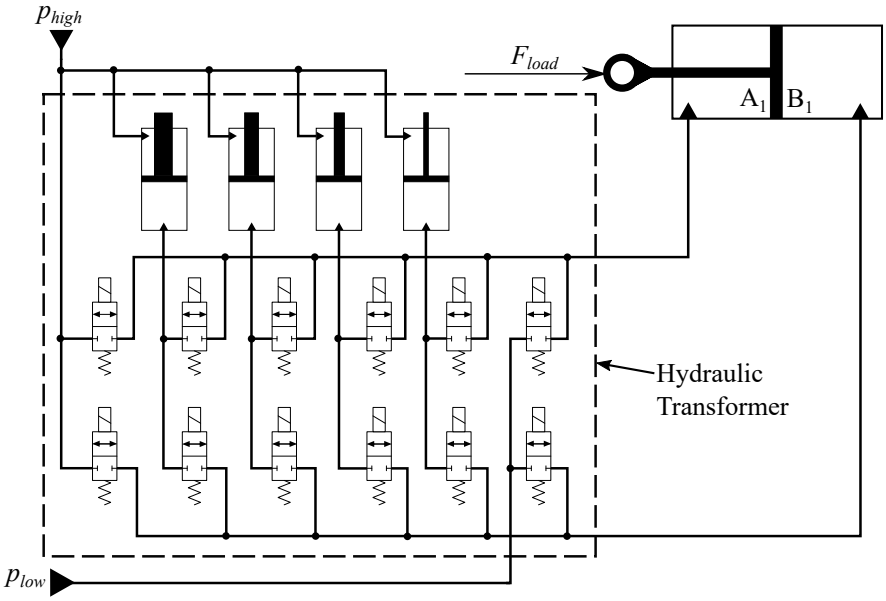

Figure 2.1: Concept for a multi-pressure cylinder with 6 pressures.

Energy efficiency is the main advantage of the multi-pressure concept. Multi-pressure cylinders can be more efficient than multi-chamber cylinders. This is because switching losses scale with the difference between pressure levels. The key drawback is the high number of components needed to make the concept work. A multi-pressure cylinder with six pressure lines like the one in Fig. 2.1 requires 12 on/off valves and four cylinders. If this concept is used on a crane which requires two actuators, then a transformer will be needed for each actuator. In contrast each multi-chamber cylinder requires nine valves, but multiple multi-chamber cylinders can be connected to the same pressure lines.

2.3 Conclusion

Based on this analysis of the existing literature, it was decided that this research project should focus on the following questions

- What performance may be expected if multi-chamber cylinders are used for the control of systems with large inertias like cranes?
- How robust are multi-chamber cylinder drives with respect to valve faults?

- Which system parameters (inertia, noise, etc.) are important to multi-chamber cylinder performance?
- How do different optimization algorithms affect the performance of model predictive control applied to multi-chamber cylinders?

Papers B and C address the first question. Paper D addresses the second question. Paper E addresses the third and fourth questions.

References

[1] A. Dell'Amico, M. Carlsson, E. Norlin, and M. Sethson, "Investigation of a digital hydraulic actuation system on an excavator arm," in *The* 13^{th} *Scandinavian International Conference on Fluid Power; June 3-5; 2013; Linköping; Sweden*, no. 092. Linköping University Electronic Press, 2013, pp. 505–511.

[2] J. Ersfolk, P. Bostrlöm, V. Timonen, J. Westerholm, J. Wiik, O. Karhu, M. Linjama, and M. Waldèn, "Optimal digial valve control using embedded gpu," in *The Eighth Workshop on Digital Fluid Power, Tampere, Finland, May*, 2016, pp. 239–250.

[3] A. Hansen and H. Pedersen, "Reducing fatigue loading due to pressure shift in discrete fluid power force systems," in 9^{th} *FPNI Ph. D. Symposium on Fluid Power*. American Society of Mechanical Engineers, 2016, pp. V001T01A002–V001T01A002.

[4] A. H. Hansen, M. F. Asmussen, and T. O. Andersen, "Valve shifting time in a digital fluid power system-energy efficiency versus fatigue loading," in *Proceedings of the* 6^{th} *International Conference on Control, Mechatronics and Automation*. ACM, 2018, pp. 128–132.

[5] A. H. Hansen, M. F. Asmussen, and M. M. Bech, "Energy optimal tracking control with discrete fluid power systems using model predictive control," in *Proceedings of the Ninth Workshop on Digital Fluid Power, Aalborg, Denmark*, 2017, pp. 7–8.

[6] ——, "Hardware-in-the-loop validation of model predictive control of a discrete fluid power power take-off system for wave energy converters," *Energies*, vol. 12, no. 19, p. 3668, 2019.

[7] ——, "Model predictive control of a wave energy converter with discrete fluid power power take-off system," *Energies*, vol. 11, no. 3, p. 635, 2018.

[8] A. H. Hansen and H. C. Pedersen, "Energy cost of avoiding pressure oscillations in a discrete fluid power force system," in *ASME/BATH 2015 Symposium on Fluid Power and Motion Control*. American Society of Mechanical Engineers, 2015, pp. V001T01A044–V001T01A044.

[9] R. H. Hansen, T. O. Andersen, H. C. Pedersen, and A. H. Hansen, "Control of a 420 kn discrete displacement cylinder drive for the wavestar wave energy converter," in *ASME/BATH 2014 Symposium on Fluid Power and Motion Control*. American Society of Mechanical Engineers, 2014, pp. V001T01A021–V001T01A021.

[10] R. H. Hansen, T. O. Andersen, and H. C. Perdersen, "Analysis of discrete pressure level systems for wave energy converters," in *Fluid Power and Mechatronics (FPM), 2011 International Conference on*. IEEE, 2011, pp. 552–558.

[11] R. H. Hansen, A. Hansen, and T. O. Andersen, "Influence and utilisation of pressure propagation in pipelines for secondary controlled discrete displacement cylinders," in *Applied Mechanics and Materials*, vol. 233. Trans Tech Publ, 2012, pp. 72–75.

[12] ——, "Simulation of utilisation of pressure propagation for increased efficiency of secondary controlled discrete displacement cylinders," in *Applied Mechanics and Materials*, vol. 233. Trans Tech Publ, 2012, pp. 3–6.

[13] R. H. Hansen, M. M. Kramer, and E. Vidal, "Discrete displacement hydraulic power take-off system for the wavestar wave energy converter," *Energies*, vol. 6, no. 8, pp. 4001–4044, 2013.

[14] R. H. Hansen, "Design and control of the powertake-off system for a wave energy converter with multiple absorbers," *Videnbasen for Aalborg UniversitetVBN, Aalborg UniversitetAalborg University, Det Teknisk-Naturvidenskabelige Fakultet, The Faculty of Engineering and Science*, 2013.

[15] R. H. Hansen, T. O. Andersen, and H. C. Pedersen, "Determining required valve performance for discrete control of pto cylinders for wave energy," 2012.

[16] K. Heybroek, E. Norlin, and A. Sipola, "Hydraulic multi-chamber cylinders in construction machinery," in *Hydraulikdagarna, March 16-17, 2015*, 2015.

[17] K. Heybroek and J. Sjöberg, "Model predictive control of a hydraulic multi-chamber actuator: A feasibility study," *IEEE/ASME Transactions on Mechatronics*, vol. 23, no. 3, pp. 1393–1403, 2018.

[18] M. Huova, A. Aalto, M. Linjama, K. Huhtala, T. Lantela, and M. Pietola, "Digital hydraulic multi-pressure actuator–the concept, simulation study and first experimental results," *International Journal of Fluid Power*, pp. 1–12, 2017.

[19] M. Huova, M. Ahopelto, V. Ahola, M. Linjama, and K. Huhtala, "Characteristics of digital hydraulics with commercial controllers," in *The Seventh Workshop on Digital Fluid Power, Linz, Austria, February*, 2015, pp. 114–128.

[20] M. Huova, A. Laamanen, and M. Linjama, "Energy efficiency of three-chamber cylinder with digital valve system," *International Journal of Fluid Power*, vol. 11, no. 3, pp. 15–22, 2010.

[21] M. Linjama, "On the numerical solution of steady-state equations of digital hydraulic valve-actuator system," in *The Eighth Workshop on Digital Fluid Power, Tampere, Finland, May*, 2016, pp. 144–155.

[22] ——, "Model-based control of a digital hydraulic transformer-based hybrid actuator," in *BATH/ASME 2018 Symposium on Fluid Power and Motion Control*. American Society of Mechanical Engineers Digital Collection, 2018.

[23] M. Linjama and M. Huova, "Numerically efficient flow model for on/off valves," in *The Seventh Workshop on Digital Fluid Power, Linz, Austria, February*, 2015, pp. 164–172.

[24] ——, "Model-based force and position tracking control of a multi-pressure hydraulic cylinder," *Proceedings of the Institution of Mechanical Engineers, Part I: Journal of Systems and Control Engineering*, vol. 232, no. 3, pp. 324–335, 2018.

[25] M. Linjama, H. Vihtanen, A. Sipola, and M. Vilenius, "Secondary controlled multi-chamber hydraulic cylinder," in *The* 11^{th} *Scandinavian International Conference on Fluid Power, SICFP*, vol. 9, 2009, pp. 2–4.

[26] K. Pettersson, K. Heybroek, P. Mattsson, and P. Krus, "A novel hydromechanical hybrid motion system for construction machines," *International Journal of Fluid Power*, vol. 18, no. 1, pp. 17–28, 2017.

Part II

Modelling and Control

Chapter 3

System and model

This chapter presents the two systems on which a multi-chamber cylinder was used in this Ph.D. project. The two systems chosen were a seesaw setup and a crane. The seesaw was chosen because it has been used to test several digital hydraulic solutions, and therefore there is plenty of information on this test bench. This will make it easier to compare results. The seesaw test bench was used in papers D and E. The crane was chosen because it represents a high-force, low-speed system of particular interest to the SFI offshore project which funded this research. Multi-chamber cylinders have not been tested on this type of system, and therefore this area holds potential for innovation. Certain types of off-shore cranes are connected to a constant high-pressure rail. In these cases, pressure is constantly being throttled. A crane of this type is used in paper B. Other cranes have their own hydraulic power unit. This type of crane typically has a load sensing system. A crane of this type is used in paper C.

3.1 Seesaw model

The seesaw test bench consists of two bodies connected with a pin joint. Weights can be distributed over four locations. Changing the arrangement of the weights changes the load and the inertia experienced by the cylinder. The system can be seen in Fig. 3.1.

The kinematics are described in paper D. The kinematic description of the system is based on two reference frames - a stationary reference frame and a rotating reference frame. The stationary reference frame is denoted with x_0 and y_0. The origin of this reference frame is attached to point A. The rotating reference frame is denoted with x_1, y_1 and is also attached at point A. The frame is oriented so the y axis points towards the center of mass of Body 2. The vector r_{cm1} defined in this reference frame always has an x value of 0.

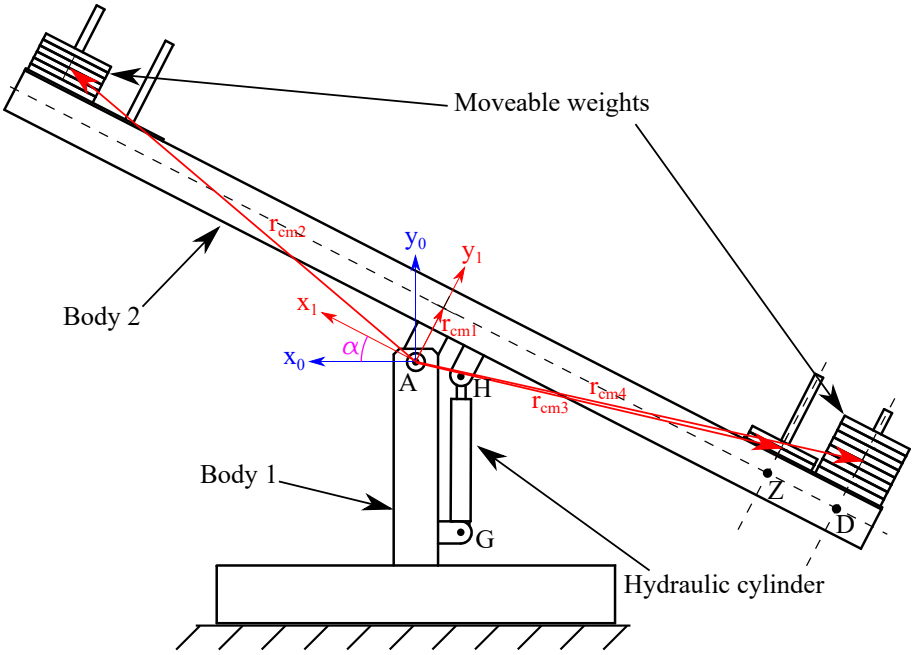

Figure 3.1: Kinematics of the seesaw test bench

Three more vectors are defined pointing to the centres of mass of the stacks of weights. In this case the stacks of weights are treated as point masses at the geometric centres of the stacks. In order to calculate the equivalent inertia and the load seen by the cylinder the kinematics presented in the figure, the dimensions of the components, and the parallel axis theorem were used. The cylinder was modelled with one degree of freedom. The equivalent mass can be seen in Fig. 3.2 and the equivalent load in Fig. 3.3. These values agree with the results obtained from other researchers using this test bench.

The cylinder model is:

$$\ddot{x}_p = \frac{\sum F}{m_{eq}(x_p)} \tag{3.1}$$

$$\sum F = F_{cyl} - F_{fric} - F_{eq}(x_p) \tag{3.2}$$

where $\ddot{x}_p$ is the acceleration of the cylinder, m_{eq} is the position dependent mass seen in Fig. 3.2, F_{cyl} is the force produced by the pressures in the cylinder's chambers, F_{eq} is the position dependent load due to gravity, F_{fric} is the friction of the cylinder.

For the friction in the cylinder the LuGre friction model was used. The LuGre model approximates friction between two surfaces as a phenomenon

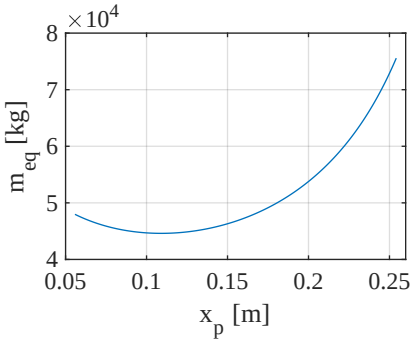

Figure 3.2: Equivalent mass as a function of cylinder stroke.

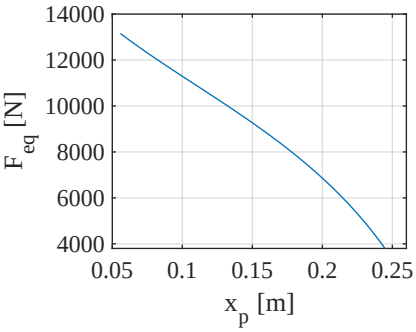

Figure 3.3: Equivalent load as function of cylinder stroke.

caused by bristles in contact. The friction model is defined as:

$$F_{fric} = \sigma_0 z + \sigma_1 \dot{z} + \sigma_2 \dot{x}_p \tag{3.3}$$

$$\dot{z} = \dot{x}_p - \frac{|\dot{x}_p|}{g(\dot{x}_p)} z \tag{3.4}$$

$$g(\dot{x}_p) = \frac{1}{\sigma_0}\left[F_c + (F_s - F_c)e^{-(\dot{x}_p/v_{str})}\right] \tag{3.5}$$

where z is the average deflection of the bristles, σ_0, σ_1, and σ_2 are friction parameters, $g(\dot{x}_p)$ is a non-linear function describing the effects of the different friction forces, where F_c is the Coulomb friction, F_s is the static friction, and v_{str} is the Stribeck velocity. The parameters for this friction model have been obtained experimentaly for this specific cylinder by Ho et al. in [7]. All parameters are shown in Tab. 3.1.

Table 3.1: Friction parameters

F_s	$1214/-1646$ N
F_c	$500/-600$ N
v_{str}	$0.026/-0.035$ m/s
σ_0	$8 \cdot 10^6/-6 \cdot 10^6$ N/m
σ_1	$700/-700$ N/ms^{-1}
σ_2	$10 \cdot 10^3/-9 \cdot 10^3$ N/ms^{-1}

The hydraulic circuit for the system can be seen in Fig. 3.4. The system consists of a constant speed, fixed displacement pump, four manifolds of 16 on/off valves each, three accumulators and a four-chamber cylinder. Each pressure line is fitted with one accumulator. The pump is activated when the pressure of the high-pressure line falls below a certain value. Two suboptimal design decisions had to be made when assembling the test bench. Firstly,

on/off valves are used to charge the middle-pressure line from the high-pressure line instead of directly from the pump. Secondly, only three of the cylinder's four chambers were used. Both of these decisions were made, because of the limitations of the manifolds. Specifically each manifold has been designed with a check valve between two of the ports. Due to this one of the two inputs has to be the low-pressure line. In the figure it can be seen that all the right input ports are connected to low pressure. Due to these limitations a lot of the valves in each manifold were not used. A legend is added in the figure showing which valves were used for controlling the cylinder, which were used for charging and discharging the pressure lines, and which were not used at all.

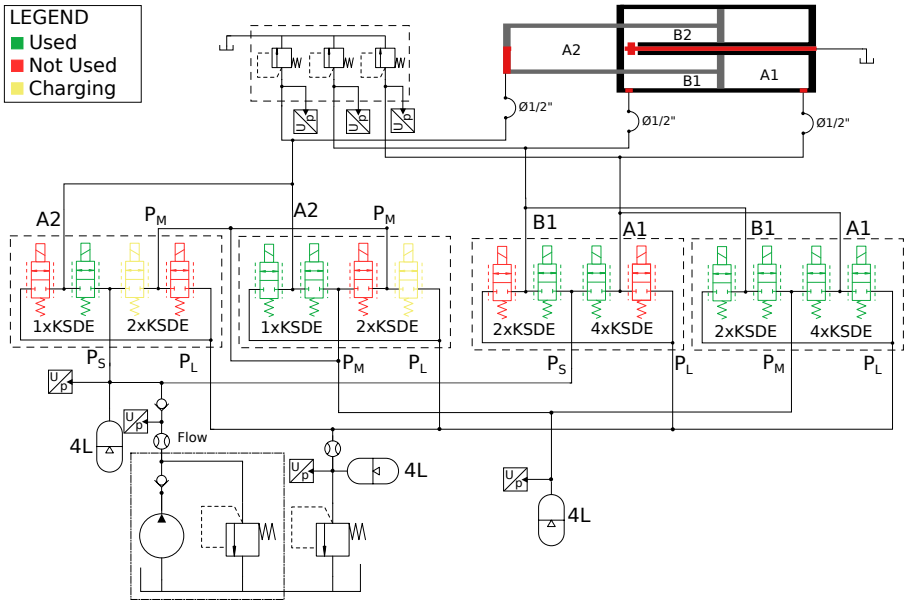

Figure 3.4: Hydraulic circuit for the seesaw model

The accumulators are modelled according to the method used in [4]. The model is based on the temperature and volume of the gas as

$$\dot{T} = \frac{T_{wall} - T}{\tau} - \frac{RT\dot{V}_g}{c_v V_g} \tag{3.6}$$

$$\dot{V}_g = \dot{p}_{acc}\frac{V_{oil}}{\beta_v} - Q_{in} \tag{3.7}$$

where T_{wall} is the temperature of the accumulator wall, τ is the heat exchange time constant, R is the thermal resistance of the accumulator, c_v is the heat

capacitance, $\dot{p}_{acc}$ is the gradient of the pressure in the accumulator, V_{oil} is the volume of the oil, β_v is the bulk modulus of the oil, and Q_{in} is the flow of oil into the accumulator. The volume of the oil is found from the current volume of the gas and the size of the accumulator

$$V_{oil} = V_{acc} + V_0 - V_g \tag{3.8}$$

From these equations the change in pressure of the hydraulic fluid can be described by

$$\dot{p}_{acc} = \frac{Q_{in} + \frac{1}{1+\frac{R}{c_v}} \frac{V_g}{T} \frac{1}{\tau} \left(T_{wall} - T\right)}{\frac{V_{oil}}{\beta_v} + \frac{1}{1+\frac{R}{c_v}} \frac{V_g}{p_{acc}}} \tag{3.9}$$

From Eq. 3.6, Eq. 3.7 and Eq. 3.9 the dynamics of an accumulator can be described. The bladders were pre-charged to a value of 22.5 bar and 105 bar for the mid- and high-pressure rails respectively. As the trajectory is followed losses are inevitable, which means that the accumulators pressures will drop. A simple combinatorial logic-based controller is used to charge the mid- and high-pressure accumulators. The rules for charging the high pressure rail are:

- If $p_S < 115$ bar, then turn pump on
- If $p_S > 125$ bar, then turn pump off

In a similar manner if p_M reaches 25 bar it is supposed to be charged. But as previously stated the fluid for charging the mid-pressure rail comes from the high pressure rail. In order to avoid draining the high-pressure rail completely, charging does not start unless the high pressure line is above the desired value. The rules for charging the high pressure rail are:

- If $p_M < 25$ bar and $p_S > 115$ bar, then open charging valves
- If $p_M > 35$ bar, then close charging valves

If the charging condition is fulfilled, two on/off valves are opened between the high- and middle-pressure lines. The charging occurs with a large pressure drop across the charging valves and it is very inefficient. In most cases charging the mid-pressure rail, dropped the pressure in the high-pressure rail and triggered the charging condition for that rail. The two valves between middle- and low-pressure lines can be used to drain all the accumulators, so the system can be de-pressurised. This is done by opening all of the charging valves which connects p_S to p_M to p_L.

It is known that long hoses introduce pressure spikes in the system. In order for the model to reflect the pressure spikes, the hoses have to be modeled as well. The hoses in the system are modelled according to the method used in [4]. Each hose is divided into segments as seen in Fig. 3.5.

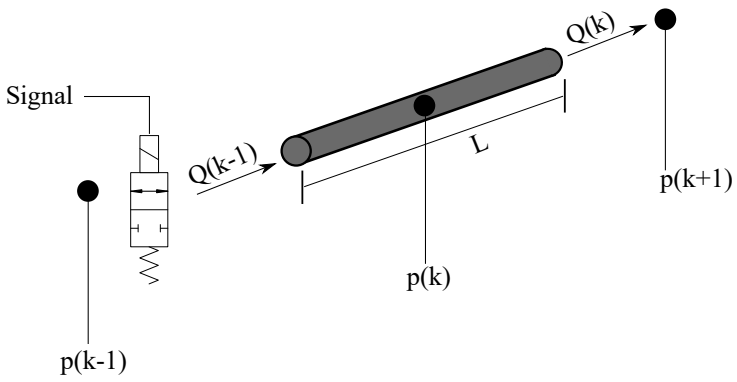

Figure 3.5: Illustration of a hose segment.

The time derivatives of the flow and the pressure for each hose segment are modelled as

$$\dot{Q}(k) = \frac{A\left(p(k) - p(k+1)\right)}{L\rho} \tag{3.10}$$

$$\dot{p}(k) = \frac{\beta(p(k))}{AL}\left(Q(k-1) - Q(k)\right) \tag{3.11}$$

where A and L are the cross-sectional area and length of the hose segment, ρ is the density of oil, and k denotes segment number, $\beta(p(k))$ is the bulk modulus of the oil as a function of the pressure in that segment. Losses in the hoses and fittings are ignored in the model. Hoses length was minimised as much as possible, so as to minimize not only these losses, but also the pressure spikes associated with longer hoses.

3.2 Crane model

The crane type and scale was suggested from the SFI Offshore Mechatronics organization, which is funding this project. Cranes of this type are known as knuckle boom cranes. By offshore standards, the crane used in this project is not large. While it is not a copy of a real crane, the sizing and hydraulic circuit is to scale for a crane in the 20-25 ton lifting range. The crane model was used in papers B and C, as well as [9].

The crane structure has been modeled as a number of bodies according to the method presented by Nikravesh in [11]. The method allows for kinematic chains with constraints to be modelled in a straightforward way. The equations are nearly identical for each body and they can be collected in a matrix form. The dynamic modelling of this crane is not the main topic of this paper,

so the model has been presented in a compact form. The equations of motion for the crane can be seen in Eq. 3.12.

$$\begin{bmatrix} \mathbf{M} & \mathbf{D}^T \\ \mathbf{D} & \mathbf{0} \end{bmatrix} \begin{bmatrix} \dot{\mathbf{v}} \\ \lambda \end{bmatrix} = \begin{bmatrix} \mathbf{g}_{ext} - \mathbf{b} \\ \gamma \end{bmatrix} \tag{3.12}$$

where $\mathbf{M}$ is matrix of masses and inertias for each body, $\mathbf{D}$ is the constraint Jacobian, λ is the vector of Lagrange multipliers, $\dot{\mathbf{v}}$ is a vector of the linear and rotational accelerations of the bodies, $\mathbf{g}_{ext}$ is the vector of external forces including gravity and cylinder forces, $\mathbf{b}$ is the gyroscopic term, and γ is calculated from the derivation of the kinematic constraints of the system.

The inputs to the mechanical model are the cylinder forces obtained from the hydraulic model, which is presented later in the chapter. The forces are inserted into the vector $\mathbf{g}_{ext}$. The outputs of the model are the accelerations of the bodies contained in vector $\dot{\mathbf{v}}$, which are integrated over time using the Runge-Kutta 4-step method. The velocity and position of the cylinder bodies are in turn inputs to the hydraulic model. In this way the two models are coupled.

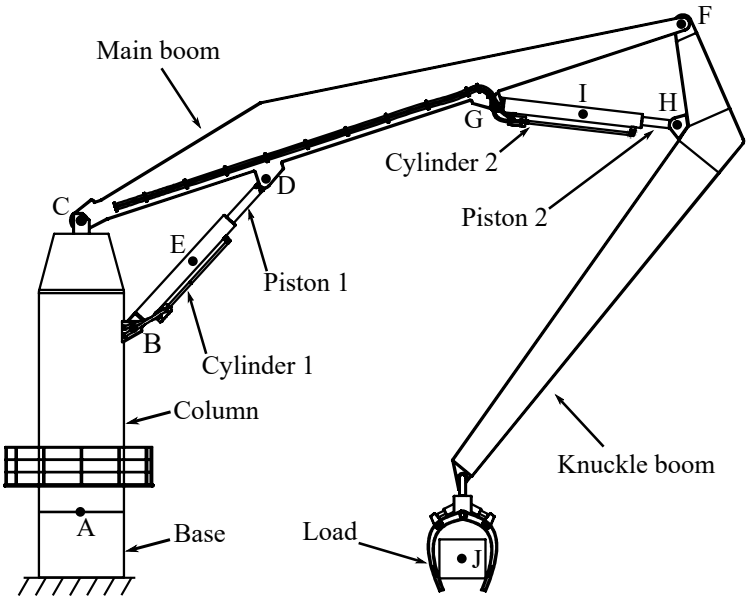

Figure 3.6: Simplified representation of a knuckle boom crane

The crane has eight bodies when each cylinder is divided into two bodies. The bodies are Column, Main boom, Cylinder 1, Piston 1, Knuckle boom, Cylinder 2, Piston 2, and Load. They can be seen in Fig. 3.6. There are 3 linear and 3 rotational coordinates used to describe the location of each body

creating a generalised coordinate vector $\mathbf{q} \in \mathbb{R}^{48\times 1}$. The accelerations of the system are collected in $\dot{\mathbf{v}}$ as seen in Eq. (3.13).

$$\dot{\mathbf{v}} = \begin{bmatrix} \ddot{\mathbf{r}}_1 \\ \dot{\boldsymbol{\omega}}'_1 \\ \vdots \\ \ddot{\mathbf{r}}_8 \\ \dot{\boldsymbol{\omega}}'_8 \end{bmatrix} \quad \mathbf{q} = \begin{bmatrix} \mathbf{r}_1 \\ \boldsymbol{\Theta}_1 \\ \vdots \\ \mathbf{r}_8 \\ \boldsymbol{\Theta}_8 \end{bmatrix} \tag{3.13}$$

The mechanical system is modelled as 7 revolute joints (A, B, C, D, F, G, and H in Fig. 3.6) and two translational joints (E, I in Fig. 3.6) similar to how a knuckle boom crane was modeled in [1]. Pin joint A allows the entire crane to rotate around its base. The load is a body with center of mass at J, constrained with a distance constraint (between point J and the tip of the jib in Fig. 3.6). This allows the load to swing from side to side as if connected by a rope. Finally $\mathbf{b}$ is the gyroscopic term seen in Eq. (3.14), where $\mathbf{J}_i$ is the matrix of mass moment of inertia of body i.

$$\mathbf{b} = \begin{bmatrix} \mathbf{0}^{3\times 1} \\ \tilde{\boldsymbol{\omega}}'_1 \mathbf{J}_1 \boldsymbol{\omega}'_1 \\ \vdots \\ \mathbf{0}^{3\times 1} \\ \tilde{\boldsymbol{\omega}}'_8 \mathbf{J}_8 \boldsymbol{\omega}'_8 \end{bmatrix} \tag{3.14}$$

In the equation $\tilde{\boldsymbol{\omega}}'_1$ is the skew symmetric matrix constructed from the elements of $\boldsymbol{\omega}'_1$ in order to represent cross product.

As previously mentioned, the cylinder forces are included in $\mathbf{g}_{ext}$. The magnitude of the cylinder forces are calculated from the pressure and the cross-sectional area of each cylinder chamber. The one-dimensional force calculated in this way is converted into a three-dimensional force vector by using the unit vector of the cylinder orientation.

The crane's dimensions are collected in Tab. 3.2. As previously mentioned, these dimensions do not describe a real crane, but rather are a good example of what is possible.

Table 3.2: Crane dimensions

Body	Length [m]	Mass [kg]
Inner Jib	13.75	6000
Outer Jib	9.24	3300
Cylinder 1	2.33	1500
Cylinder 2	2.84	750

The purpose of the crane model is to implement multi-chamber cylinders and investigate their performance. It was decided that having a baseline performance for this crane would make evaluating the multi-chamber cylinders'

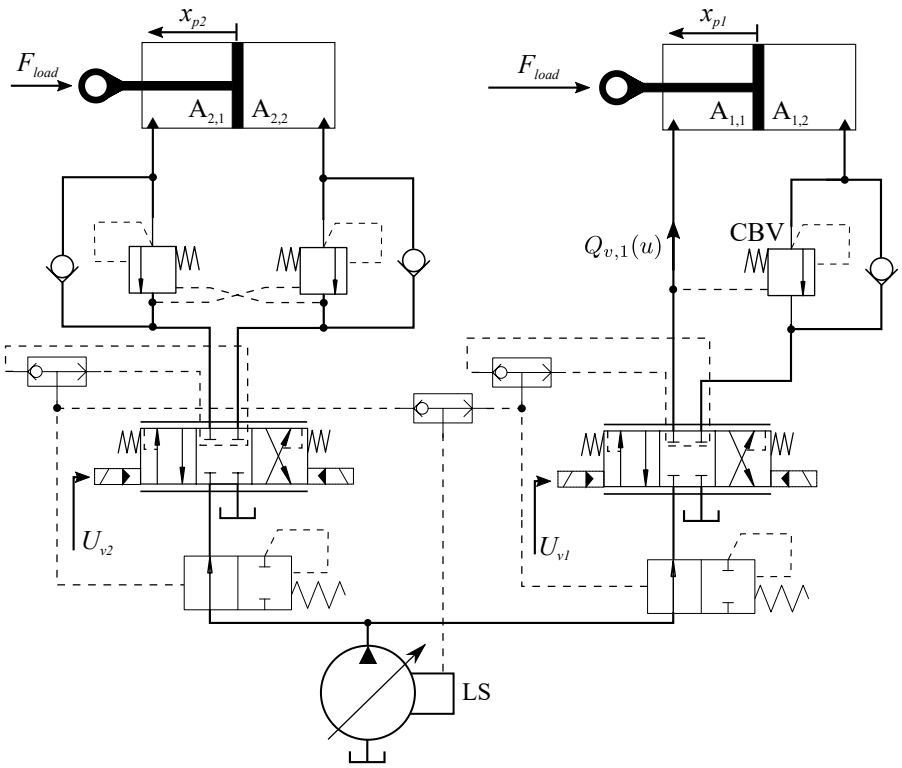

Figure 3.7: Knuckle Boom Crane hydraulic circuit

performance easier. For this reason a hydraulic system typical for this kind of crane was also modelled. The hydraulic schematic for the knuckle boom crane can be seen in Fig. 3.7. The system consists of two cylinders, controlled through pressure compensated, directional proportional valves. The system is supplied by a variable displacement pump with load sensing (LS) capabilities. The pressure compensated valves normally receive control inputs U_{v1} and U_{v2} from a set point generator. The set point generator generates these values based on user selected inputs. In the case where open loop operation is selected U_{v1} and U_{v2} are directly proportional to the inputs of the user. Typically this is done with two joysticks. In the case where closed loop mode is selected, the joystick signal are transformed into position and velocity references. The position reference is followed with a feedback controller, while the velocity reference is given as a feedforward signal [2]. In paper B, instead of a load sensing system, the crane is supplied by a constant pressure rail. This sort of centralized pressure supply is also in use on some offshore platforms. The change in pressure in the chambers has been modelled as in Eq.

3.15.

$$\dot{p}_p = \frac{\beta_1}{V_{1,1}} \left(-A_{1,1}\dot{x}_p + Q_{v,1}(u) \right) \tag{3.15}$$

where β_1 is the bulk modulus of the fluid, $V_{1,1}$ is the volume of chamber $A_{1,1}$, $A_{1,1}$ is the area of chamber $A_{1,1}$, $\dot{x}_{p1}$ is the velocity of the piston, and $Q_{v,1}$ is the flow through the valve. Mobile hydraulic valves are often pressure compensated, which makes it easier to model them. Certainly, for the example crane discussed in paper C, industry partners suggested that this would be the case. The flow through the valve to the chamber is simplified to a linear equation directly proportional to the control signal. The return flow follows the standard orifice equation as seen in Eq. 3.16.

$$Q_{v,1}(u) = \begin{cases} Q_{max}u & u \geq 0 \\ k_q u \text{sign}(p_p - p_t)\sqrt{|p_p - p_t|} & u < 0 \end{cases} \tag{3.16}$$

where k_q is the discharge coefficient, p_p is chamber pressure, and u is the spool position.

Most cranes are required by law to be equipped with safety equipment for load holding. This functionality is provided by a valve which is commonly known as a Counter-Balance Valve (CBV). Its opening is controlled by the ratio between the pressure in the load holding chamber $A_{1,2}$ and the forward chamber of the cylinder $A_{1,1}$. If the pressure in chamber $A_{1,1}$ drops because the load is overrunning the flow capacity of the pump or because the crane has lost power the CBV closes. The cylinder in the main boom sees loading conditions in only one direction due to the geometry of the crane, so it has only one CBV. The cylinder actuating the knuckle boom can experience loads in both directions, so it has CBVs on both chambers. The opening of a CBV is calculated as in Eq. 3.17.

$$x_{CBV1,1} = \begin{cases} \frac{p_p R + p_r - p_{CP}}{K_s} & p_p R + p_r > p_{CP} \\ 0 & p_p R + p_r < p_{CP} \\ 1 & p_p R + p_r - p_{CP} > K_s \end{cases} \tag{3.17}$$

where $x_{CBV1,1}$ is the normalised CBV opening, R is the ratio of the areas of the pressures acting on the spool of the CBV, p_{CP} is the crack pressure, and K_s is the spring stiffness. The ratio R of the valve dictates how easy it is to open the valve. High ratios of R are more energy efficient, because the pressure in the forward chamber can be lower. At the same time this makes the valve more sensitive to pressure fluctuations. It is a well known fact that high ratios of R can introduce instabilities in the system. In this case a ratio of 5:1 was used.

The flow from the piston side chamber to tank, which passes through the counterbalance valve is calculated by the orifice equation. In order to

simplify the model, the fluid volume between the CBV and the directional valve has been ignored. Instead the two orifices (CBV and direction valve) are considered as a single equivalent orifice as in Eq. 3.18.

$$A_{eq} = \begin{cases} \sqrt{\frac{1}{\frac{1}{(|u|A_{dv})^2} + \frac{1}{(x_{CBV1,1}A_{check})^2}}} & |u|, x_{CBV1,1} > 0 \\ 0 & |u|, x_{CBV1,1} = 0 \end{cases} \tag{3.18}$$

3.3 Multi-chamber cylinder

The same multi-chamber cylinder type has been used in all the papers comprising this project. A simplified schematic can be seen in Fig. 3.8. The cylinder has two chambers A_1 and A_2, which can provide a positive force. Positive in this sense, as indicated on the figure, is a force acting in the positive direction of piston position x_p. The third chamber B_1 produces a negative force e.g. a force that retracts the cylinder. Three constant pressure rails are available. The bank of nine valves is used to connect the pressure lines to the chambers.

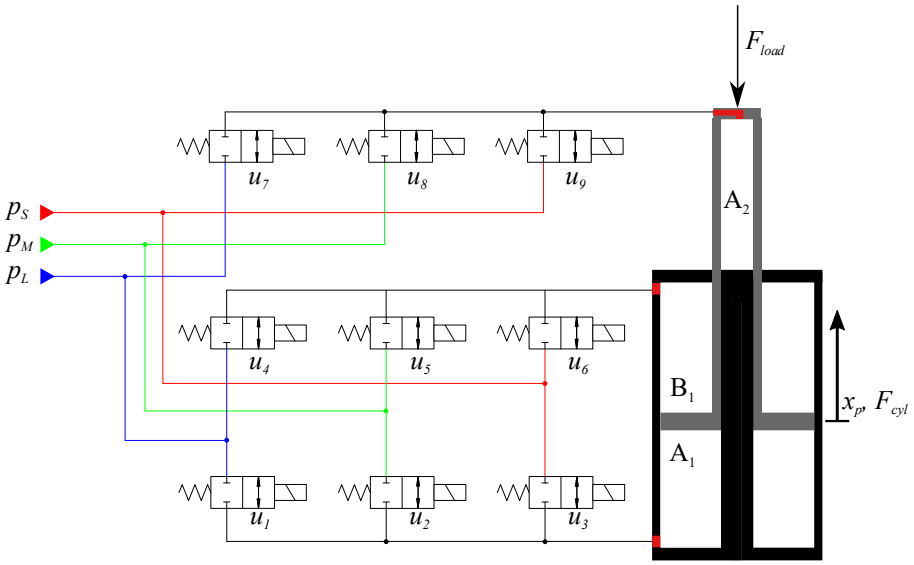

Figure 3.8: Representation of the multi-chamber cylinder used in the project

The pressure dynamics of the cylinder is:

$$\dot{p}_i = \frac{\beta_i}{V_i}\left(A_i \dot{x}_p + Q_{v,i,n}(u)\right) \tag{3.19}$$

$$Q_{v,i,n}(u) = k_q u \text{sign}(p_i - p_n)\sqrt{|p_i - p_n|} \tag{3.20}$$

$$\ddot{x}_p = \frac{1}{m_{eq}}\left(F_{cyl} - F_{load} - F_{fric}\right) \tag{3.21}$$

where $\dot{p}_i$, β_i, V_i, and A_i are the pressure gradient, bulk modulus, volume, and cross-sectional area of chamber i. x_p, $\dot{x}_p$, and $\ddot{x}_p$ are the position, velocity and the acceleration of the piston. x_p varies from $-L_S/2$ to $L_S/2$, where L_S is the maximum stroke of the cylinder. $Q_{v,i,n}(u)$ is the flow to chamber i, through valve n. The flow is defined by the orifice equation with k_q being the valve specific coefficient, p_n being the n^{th} pressure line and u being the normalized valve opening. m is the mass of the system, F_{cyl} is the force provided by the cylinder, F_{load} is the equivalent load on the cylinder, and F_{fric} is the frictional force.

3.3.1 Force level number and density

The operation of the controller is heavily influenced by the number of possible force levels of the cylinder. This is known as the force resolution of the cylinder. The force resolution determines how accurately a force trajectory can be followed. The equation for the number of available force levels is:

$$F_{num} = {n_c}^{n_p} \tag{3.22}$$

where F_{num} is the number of force levels that are available, n_c is the number of chambers and n_p is the number of pressure lines. As previously mentioned some researchers have chosen to use a four-chamber cylinder with two pressure lines - this gives 16 force levels [10] and [6]. Others have chosen to use a three-chamber cylinder with three pressure lines - this gives 27 force levels [8] and [3]. In general adding more pressure lines increases the possible force levels more than increasing the number of chambers e.g. going from three chamber and three pressure lines to three chambers and four pressure lines results in 81 force levels (an increase of 54), while going to four chambers and three pressure lines results in 64 force levels (an increase of only 37). In this thesis a three-chamber three-pressure cylinder was used in all papers.

An important concept for multi-chamber cylinders is the cost of switching. Hansen et al. defined this cost in [5] as:

$$E = \frac{1}{2}\frac{V}{\beta}\left(p_1 - p_0\right)^2 \tag{3.23}$$

This cost scales with the difference between the initial and final pressure value, and the volume of the chamber. The bulk modulus of the oil is also of importance, but this cannot be controlled by the force selection algorithm.

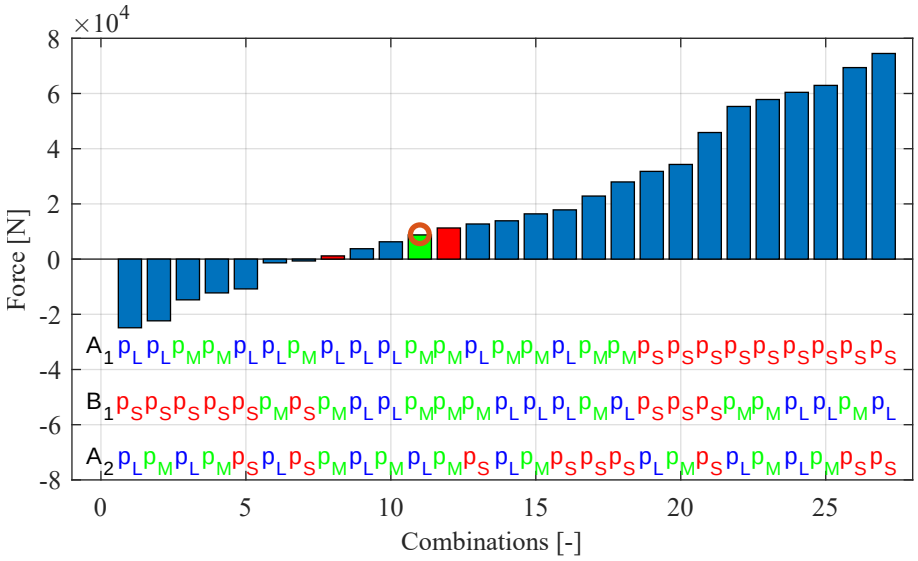

Figure 3.9: Force resolution of a three chamber, three pressure cylinder.

Choosing middle pressure line through extensive search

It can be concluded from Eq. 3.23 that having smaller differences between pressure levels improves efficiency. One way to achieve this is by introducing more pressure lines. This can be costly due to the number of components required. Another way to reduce the difference between pressure levels is to change the values of the available pressure levels. In papers B and C the maximum and minimum force levels had to match the maximum and minimum of a predetermined standard cylinder. The low-pressure rail and the high-pressure rail could not be changed due to this. The middle-pressure rail had no limitations, so that is the parameter which was varied.

In paper B an extensive search was conducted with 16 pressures between 50 bar and 200 bar. The search also included variation of a control parameter, which has to be set after the pressures are known. This control parameter W was varied in 20 steps. The entire search space was then the product of the two which is 320 possibilities. A full 40 second simulation was conducted for each possibility. In the end the search showed that the middle pressure should not be placed as the average of the high- and low-pressure values, but 60 bar below that value. The changes in energy consumption are shown

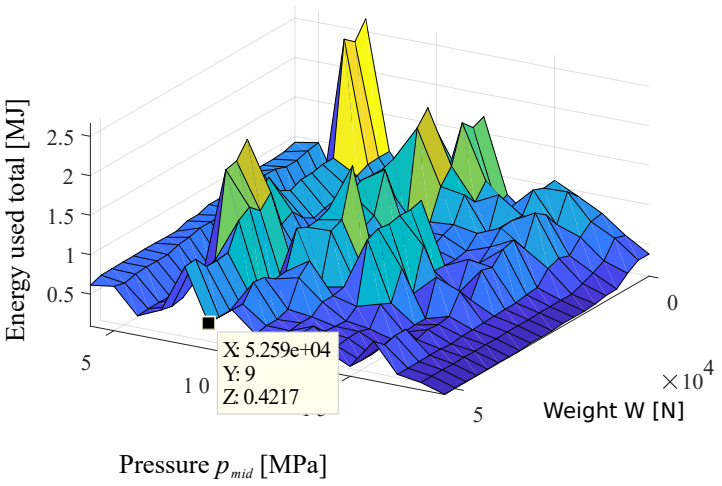

Figure 3.10: Changes to energy consumption as a function of middle pressure value and control parameter W.

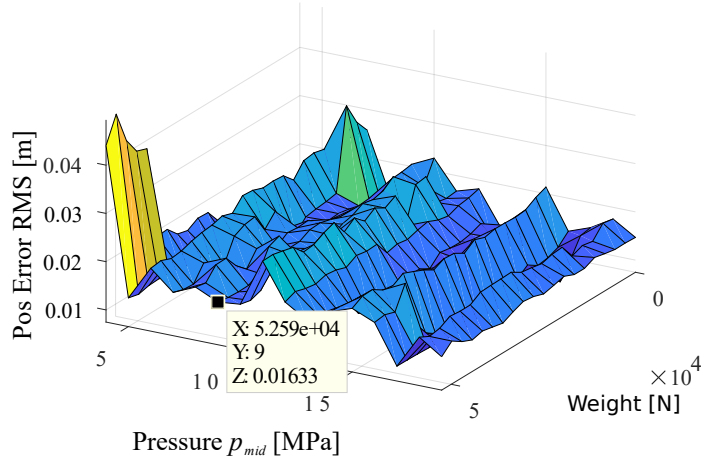

Figure 3.11: Changes to position error RMS as a function of middle pressure value and control parameter W.

in Fig. 3.10 and changes to positional accuracy are shown in Fig. 3.11. From Fig. 3.11 it can be seen that the middle pressure line had a bigger effect on the tracking performance of the cylinder than the control parameter.

In paper D another extensive search was conducted with values between 20 and 100 bar. These extensive searches based on full simulations required several hours in both cases. In both papers it was found that choosing the middle pressure line based on the load improves both energy efficiency and tracking performance as numbers indicate in Fig. Fig. 3.11 and Fig. Fig. 3.10. In paper D it was known that the systems inertia produces a nearly constant load force of 9000 N inside the defined position trajectory. In Fig. 3.9 this constant force is shown as a red circle. The force levels are obtained with the parameters seen in Tab. 3.3. With the chosen middle pressure it can be seen that force 11, indicated in green, is very close to the load. Furthermore the force levels close to this working point have small differences. The force resolution of the cylinder has not improved, but by manipulating the middle pressure line, the force resolution has improved in a specific area which is of interest.

Table 3.3: Multi-chamber cylinder parameters

A_{A_1}	$5059 \cdot 10^{-6}$ m^2	p_L	10 bar
A_{B_1}	$2557 \cdot 10^{-6}$ m^2	p_M	30 bar
A_{A_2}	$1257 \cdot 10^{-6}$ m^2	p_S	122 bar

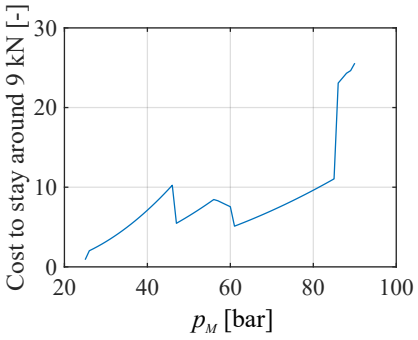

Figure 3.12: Cost to stay in one place with a load of 9 kN with different mid pressure levels

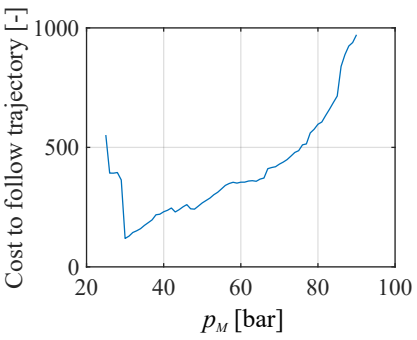

Figure 3.13: Cost to follow trajectory with different mid pressure levels

Choosing middle pressure line analytically

Choosing the middle pressure line as a function of load showed to have advantages, but the extensive search process is slow. For this reason an analytical method was devised to perform the same search.

Since it is unlikely to have a force which exactly matches the load the controller will have to optimally switch between two forces - one above and one below the load. In Fig. 3.9, the two forces with the smallest cost between them have been coloured in red. A less time consuming method than the extensive search is presented in Fig. 3.14. This method is based on finding these two forces.

for $i = 1 : p_{res}$ **do**
  $\mathbf{F}_{res}$ = ForceLevels($\mathbf{p}_{mid}(i)$) ;
  F_{close} = min($\mathbf{F}_{res}$, F_{target}) ;
  [F_+, F_-] = Cheapest($\mathbf{F}_{res}$, $F_{closest}$) ;
  $\mathbf{y}(i)$ = Cost(F_+, F_-) ;
end

Figure 3.14: Choosing Middle-pressure level with known constant force

In the algorithm p_{res} stands for size of vector $\mathbf{p}_{mid}(i)$. This vector contains the possible choices for middle-pressure line magnitude. The function ForceLevels() calculates the force resolution seen in Fig. 3.9. $F_{closest}$ is the force closest to the target force F_{target}. The function Cheapest finds one force above the target and one below the target. These are F_+ and F_- respectively. This is done through using Eq. 3.23 to calculate the cost between all possible force combinations. Finally the cost to switch between forces F_+ and F_- is recorded as $\mathbf{y}(i)$. The 9000 N constant force was chosen as F_{target} and the cost $\mathbf{y}$ was calculated for p_{mid} values between 25 bar and 90 bar. The result is shown in Fig. 3.12. According to this analysis choosing the mid-pressure as low as possible will give the best energy efficiency. The extensive search showed that this is not the case.

for $i = 1 : p_{res}$ **do**
  for $ii = 1 : T$ **do**
    $\mathbf{F}_{res}$ = ForceLevels($\mathbf{p}_{mid}(i)$) ;
    F_{close} = min($\mathbf{F}_{res}$, $\mathbf{F}_{target}(ii)$) ;
    [F_+, F_-] = Cheapest($\mathbf{F}_{res}$, F_{close}) ;
    $\mathbf{y}(ii)$ = Cost(F_+, F_-) ;
  end
  c(i) = sum($\mathbf{y}$) ;
end

Figure 3.15: Choosing Middle-pressure level with known trajectory

The algorithm was augmented to take into account that the full force trajectory is known as seen in Fig. 3.15. Here $\mathbf{F}_{target}$ is a vector of target

forces with length T. The vector of costs $\mathbf{y}$ is summed so the actual cost for pressure i is $\mathbf{c}(i)$. The results of using the algorithm in Fig. 3.15 are shown in Fig. 3.13. In the figure it can be seen that switching costs increase when p_{mid} is reduced below 30 bar. This result agrees with the results of the extensive search. The benefit of using this analytical method is that the analysis can be conducted in a matter of seconds. The parameter sweeps each took several hours. The improved costs and force density around the load comes at a price of course - there is only one force level between 34000 N and 55000 N, these are combinations 20 and 22 in Fig. 3.13.

References

[1] M. K. Bak and M. R. Hansen, "Analysis of offshore knuckle boom crane-part one: modeling and parameter identification," *Modeling, Identification and Control*, vol. 34, no. 4, p. 157, 2013.

[2] D. Hagen, W. Pawlus, M. K. Ebbesen, and T. O. Andersen, "Feasibility study of electromechanical cylinder drivetrain for offshore mechatronic systems," *Modeling, Identification and Control*, vol. 38, no. 2, 2017.

[3] A. H. Hansen and H. C. Pedersen, "Energy cost of avoiding pressure oscillations in a discrete fluid power force system," in *ASME/BATH 2015 Symposium on Fluid Power and Motion Control*. American Society of Mechanical Engineers, 2015, pp. V001T01A044–V001T01A044.

[4] A. H. Hansen, H. C. Pedersen, and R. H. Hansen, "Validation of simulation model for full scale wave simulator and discrete fuild power pto system," in 9^{th} *JFPS International Symposium on Fluid Power*. Japan Fluid Power System Society, 2014.

[5] R. H. Hansen, T. O. Andersen, and H. C. Perdersen, "Analysis of discrete pressure level systems for wave energy converters," in *Fluid Power and Mechatronics (FPM), 2011 International Conference on*. IEEE, 2011, pp. 552–558.

[6] K. Heybroek, E. Norlin, and A. Sipola, "Hydraulic multi-chamber cylinders in construction machinery," in *Hydraulikdagarna, March 16-17, 2015*, 2015.

[7] S. Ho Cho, O. Niemi-Pynttäri, and M. Linjama, "Friction characteristics of a multi-chamber cylinder for digital hydraulics," *Proceedings of the Institution of Mechanical Engineers, Part C: Journal of Mechanical Engineering Science*, vol. 230, no. 5, pp. 685–698, 2016.

[8] M. Huova, A. Laamanen, and M. Linjama, "Energy efficiency of three-chamber cylinder with digital valve system," *International Journal of Fluid Power*, vol. 11, no. 3, pp. 15–22, 2010.

[9] S. Ketelsen, L. Schmidt, V. H. Donkov, and T. O. Andersen, "Energy saving potential in knuckle boom cranes using a novel pump controlled cylinder drive," *Modeling, Identification and Control*, 2018.

[10] M. Linjama, H. Vihtanen, A. Sipola, and M. Vilenius, "Secondary controlled multi-chamber hydraulic cylinder," in *The* 11^{th} *Scandinavian International Conference on Fluid Power, SICFP*, vol. 9, 2009, pp. 2–4.

[11] P. E. Nikravesh, *Computer-aided analysis of mechanical systems*. Prentice-Hall, Inc., 1988.

Chapter 4

Control

It was established in chapter 2, that multi-chamber cylinders are a part of the digital hydraulics field. In order to avoid throttling the multi-chamber cylinder is controlled by choosing which chambers are connected to which pressure lines. In this thesis this has been done in two ways - a Force Selection Algorithm (FSA) and Model Predictive Control (MPC).

The FSA method requires a controller design with nested loops. The algorithm is very simple and computationally simple. The method was implemented in papers B and C.

The MPC method does not require nested loops. The method is based on a model of the system and an optimization algorithm. MPC has started gaining attention within multi-chamber cylinder control as well as electric motor control. This method was used in papers C, D, and E.

4.1 Direct Force control

The most widely referenced paper on the control of multi-chamber cylinders is [12]. The method in [12] uses a force control scheme which can be seen in Fig. 4.1. An outer loop with a proportional-integral controller generates a reference for the inner loop. In this case the outer loop controls position. Then the proportional-integral controller generates a force reference. On a machine with a operator, the input to the outer loop can be the velocity signal given by the operator as for example the implementation in [9].

In the inner loop the Force Selection Algorithm (FSA) determines the force level. The force is switched when the force error becomes sufficiently large. In paper B and paper C a three-chamber cylinder with three pressure lines was used such as the one seen in Fig. 3.8. This gives a force resolution of 27 forces as discussed in section 3.3.1. The control algorithm can be expressed as choosing a control combination $\mathbf{u}_i$ where i is one of the 27 possible combi-

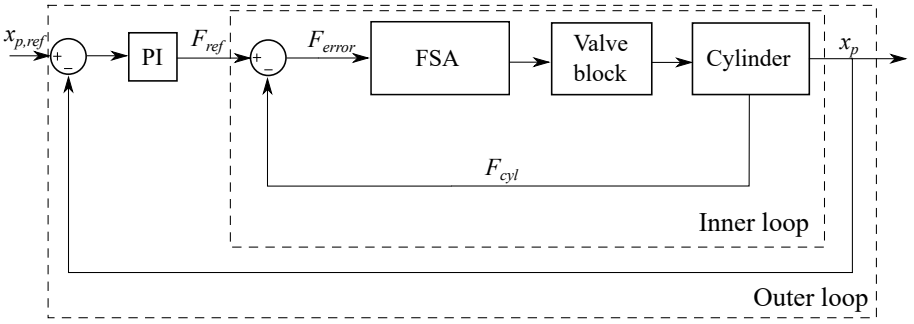

Figure 4.1: Multi-chamber cylinder with simple direct force control cascade.

nations, which minimises a cost function as seen in Eq. 4.1.

$$\mathbf{u}_i(k) = \underset{\mathbf{u}_i(k)}{\operatorname{argmin}} \{|F_{ref} - F_i(\mathbf{u}_i(k))| + W u_{change}(\mathbf{u}_i(k), \mathbf{u}_i(k-1))\} \quad i = 1, \cdots, 27 \tag{4.1}$$

where F_{ref} is a force reference, $F_i(\mathbf{u}_i(k))$ is the force produced by valve combination i, W is a weight to be chosen, $u_{change}(\mathbf{u}_i(k), \mathbf{u}_i(k-1))$ is a binary value, which is equal to 1 if combination i is different from the previous valve combination i.e if the control combination $\mathbf{u}_i$ at time $k-1$ is the same as the one at time k then $u_{change} = 1$. $W u_{change}(\mathbf{u}_i(k), \mathbf{u}_i(k-1))$ penalizes switching between force levels. The cost function contains two parts - force error and a penalty on switching force levels. The two parts work in opposite directions. The reason for defining the control in this way is to produce accurate position tracking by closely following the force trajectory, but to also reduce the energy consumption which comes from compressibility losses at every force switch [12].

The output of the controller is $\mathbf{u}_i$ which is the input to the bank of valves seen in Fig. 3.8. Each combination i is associated with a force output. For instance $i = 27$ can be seen in Eq. 4.3, where valves three, four and nine are opened. This means that high pressure is connected to chamber A_1 and A_2, and low pressure is connected to chamber B_1. The combination produces the largest force output as seen in Fig. 3.9.

$$\mathbf{u}_i = \begin{bmatrix} u_{i,1} & u_{i,2} & u_{i,3} & u_{i,4} & u_{i,5} & u_{i,6} & u_{i,7} & u_{i,8} & u_{i,9} \end{bmatrix}^T \tag{4.2}$$

$$\mathbf{u}_{27} = \begin{bmatrix} 0 & 0 & 1 & 1 & 0 & 0 & 0 & 0 & 1 \end{bmatrix}^T \tag{4.3}$$

The weight W and the change indicator u_{change} are scalar values. They treat all force switches equally. In section 3.3.1, it was shown that some force switches are more costly. The algorithm does not take this into account. In its current definition is treats frequent switching as something to be avoided.

In order to explore if this is the case an augmented controller was proposed in paper B.

The augmentation was in the form of two additional weights. One term $W_{large}u_{i,3}$ penalizes combinations which involve opening the valve between the high-pressure rail and chamber A_1. The second term $W_{large}u_{i,6}$ penalizes combinations in which the valve between the high-pressure rail and chamber B_1 is opened. The augmented algorithm is:

$$\mathbf{u} = \underset{\mathbf{u}}{\operatorname{argmin}} \{|F_{ref} - F_i| + Wu_{change} + W_{large}u_{i,3} + W_{large}u_{i,6}\} \tag{4.4}$$

The weight W for both controllers was found through an extensive search with a simulation at each point. The results of the search can be seen in paper B or in section 3.3.1. The weight W_{large} was simply chosen as a number significantly larger than the maximum possible force error. The experiment revealed two possible switching patterns for the multi-chamber cylinder seen in Fig. 4.2 and Fig. 4.3. The cylinder used is the same as in Fig. 3.8.

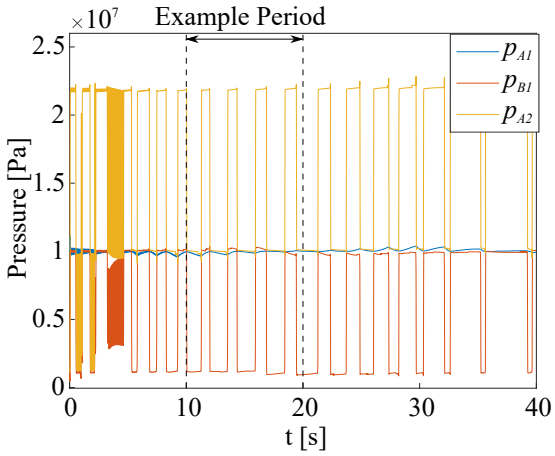

Figure 4.2: Pressures in the cylinder chambers using the augmented DFC.

Every force change is a switching event. Based on the two figures the original controller produces fewer switching events over the entire trajectory. This is the case because in the time period between 10 and 20 s in Fig. 4.2 the force changes 9 times. In the same time period the force changes 5 times in Fig. 4.3. In this period the augmented controller modulates the force output in order to produce an average force. This can be seen better in Fig. 4.4, where the force chosen by the augmented controller alternates between being above and below the reference. At approximately 3 seconds the augmented controller begins to chatter between two for levels, which results in a large number of switching events. This increases the overall number of switching

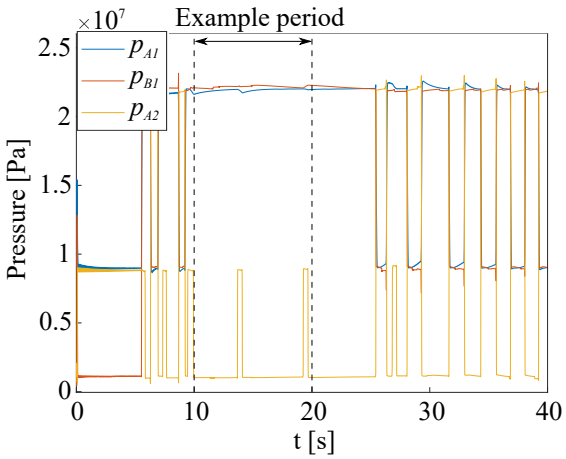

Figure 4.3: Pressures in the cylinder chambers using the original DFC.

events produced by the augmented controller. The forces produced by the two controllers can be seen in Fig. 4.4.

According to [12] reducing the number of switching events should reduce energy use and force spikes, but it should also increase position error. In Fig. 4.4 it can be seen that the original controller does produce fewer force spikes, but the spikes are larger. The largest force spike is at 25 s. These large spikes are produced when the chamber A_1 switches between high pressure and mid pressure. In Fig. 4.4 the augmented controller modulates the force output in order to produce an average force output.

The force produced by the original controller follows the force trajectory closely, which according to [12] should produce better position tracking with less vibrations. This showed itself not to be the case. Both controllers had nearly identical position tracking and energy efficiency. The original controller had a Root-Mean-Square(RMS) position error of 0.0097 m, while the augmented controller had a RMS position error of 0.0074 m. The energy consumed by the system with the original controller over the trajectory was 0.27357 MJ, while the same system with the augmented controller consumed 0.21672 MJ. This results shows that simply having fewer force switches does not necessarily produce better results. For a different trajectory the augmented controller still consumed less energy, but it could not follow the position trajectory accurately. From the full set of results, which can be found in paper B or in Chapter 5 it can be concluded that it is not possible to draw a direct correlation between the frequency of switching and the performance of the system.

These two switching patterns can also be observed in [7], where an investigation is conducted into the difference between using a FSA and using

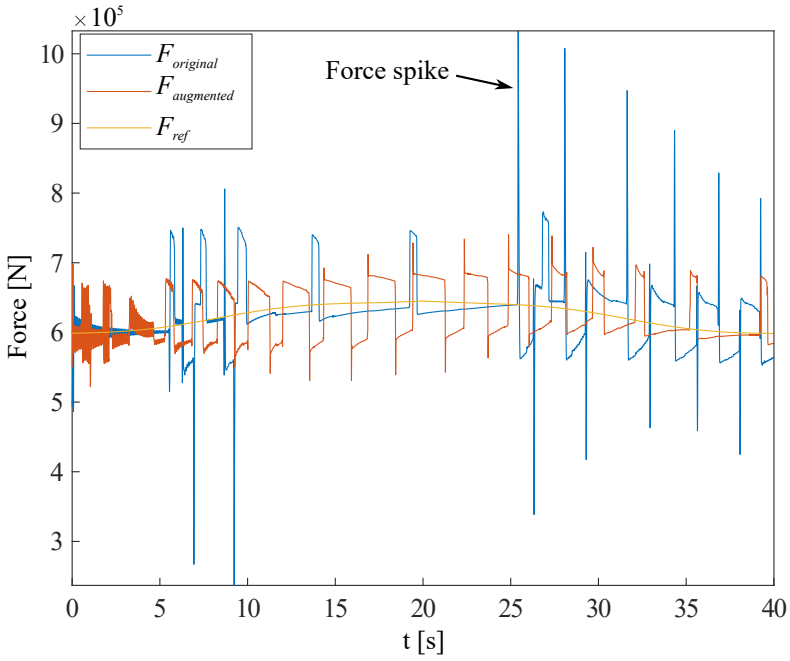

Figure 4.4: Force produced by the two controllers compared with the force reference.

an MPC to control a multi-chamber cylinder. The FSA produced a switching pattern similar to the controller presented in Eq. 4.1 i.e. fewer changes in force output, but when they happen they involve changing the pressures in all chambers. The MPC produced a switching pattern closer to the augmented controller presented here - more frequent changes in force output, but the change happens only in the smallest chamber. The MPC in [7] also produced better results overall.

From the results of paper B and paper [7] it can be concluded that the FSA does not take the complexity of the system into account. Specifically, it does not take into account that creating a larger force error at the current time step can be necessary in order to allow for a better control step in the future. For this reason MPC is investigated in this project.

4.2 Model Predictive Control

The second method to control a multi-chamber cylinder used in this thesis is model predictive control. The method allows for multiple conflicting objectives to be collected in the same cost function. In this case the conflicting objectives are accuracy and energy use. One of the disadvantages of the al-

gorithm is that it requires a known trajectory. Possible ways of obtaining a position reference is to integratate the velocity signal given by the operator [1] or to use a path generator algorithms where the operator selects a beginning and end point and the algorithm generates the neccesary position reference. Some more advanced implementations can be to prediction a possible trajectory through Bayesian inference for data based short term trajectory prediction together with correlation analysis in order to detect recurrent cycles [17]. Neural network are being used for trajectory prediction of vehicles [11]. Finally the SFI offshores mechatronics project has nine researchers working on autonomous systems. The mining industry for instance has begun to automate many of its machines such as excavators and trucks [14]. The possible implementation of MPC on a crane has not been tested in this thesis. As mentioned in chapter 3.2 where the control of a knuckle boom crane was discussed, according to [6] not all cranes are operated in open loop. Some cranes have position reference generators. For this project it was assumed that a position reference is available. The controller is constructed from an optimization procedure and a model of the system as can be seen in the block diagram in Fig. 4.5. The model is used to predict how the system will react to future inputs up to a certain point in time. An example is shown in Fig. 4.6. A prediction horizon is a term which describes how far in the future is the prediction conducted. In the example this is denoted with M. The optimization algorithm finds the best possible control inputs depending on criteria chosen by the user. Only the first of these optimal values is implemented and the optimization is repeated the next time the controller is executed. This is done because the model used to predict the future becomes inaccurate over larger horizons. By repeating the optimization the controller predicts a feedforward signal, but corrects it with feedback from the signal.

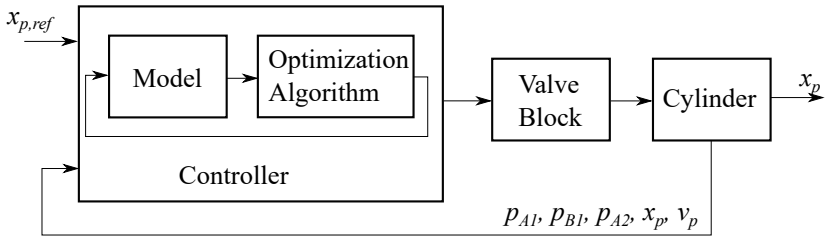

Figure 4.5: A block diagram of a multi-chamber cylinder with Model Predictive Control.

The method from its conception was most popular in chemical process control. This can mainly be attributed to its computational complexity. The controller has to run at a frequency higher than the natural frequency of the plant. Chemical processes can have large time constants, which reduces the hardware requirements to implement a MPC in real-time. Computation

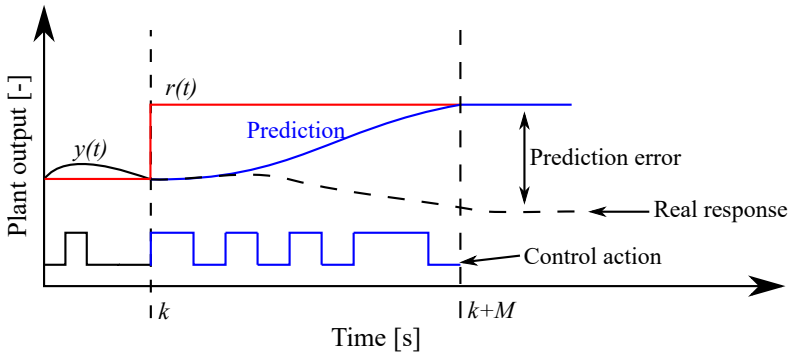

Figure 4.6: Model predictive control example.

hardware has been steadily improving in its performance and has steadily been decreasing in price. These improvements have enabled MPC to be considered for controlling electric motors and wave-energy converters. It was shown in [7] that MPC can improve the performance of multi-chamber cylinders, but the computational complexity prevented a real-time implementation. The complexity comes from having to solve an optimization problem each time the controller is executed. Larger problems generally take more time to solve, so the size of the optimization problem depends on the prediction horizon.

This section will be divided into the prediction model, the optimization problem, a subsection on neural network implementation, and fault tolerant control.

4.2.1 Prediction Model

Model prediction control uses a model to predict the future outputs of a plant based on possible controller inputs. It then uses an optimization algorithm in order to find the optimal input, which will produce the optimal output. Two prediction models have been used in this thesis.

In paper C the following model was presented:

$$\mathbf{x}(k+1) = \mathbf{A}\mathbf{x}(k) + \mathbf{B}\mathbf{u}(k) \tag{4.5}$$

$$y(k+1) = \mathbf{C}\mathbf{x}(k+1) \tag{4.6}$$

where $\mathbf{x}(k)$ is a vector of the five internal states of the system at time step k. The states are p_{A_1} - pressure in chamber A_1, p_{B_1} - pressure in chamber B_1, p_{A_2} - pressure in chamber A_2, x_p - position of piston, and v_p is the velocity of piston. $\mathbf{u}(k)$ is the vector of valve openings at time step k. It includes opening values for the nine valves as in Eq. 4.2.

The matrices **A** and **B** are defined as:

$$\mathbf{A} = \begin{bmatrix} 0 & 0 & 0 & 0 & 0 \\ 0 & 0 & 0 & 0 & 0 \\ 0 & 0 & 0 & 0 & 0 \\ 0 & 0 & 0 & 1 & T_s \\ \frac{A_{A_1} T_s}{M_{eq}} & -\frac{A_{B_1} T_s}{M_{eq}} & \frac{A_{A_2} T_s}{M_{eq}} & 0 & 1 \end{bmatrix} \tag{4.7}$$

$$\mathbf{B} = \begin{bmatrix} p_t & p_{mid} & p_{high} & 0 & 0 & 0 & 0 & 0 & 0 \\ 0 & 0 & 0 & p_t & p_{mid} & p_{high} & 0 & 0 & 0 \\ 0 & 0 & 0 & 0 & 0 & 0 & p_t & p_{mid} & p_{high} \\ 0 & 0 & 0 & 0 & 0 & 0 & 0 & 0 & 0 \\ 0 & 0 & 0 & 0 & 0 & 0 & 0 & 0 & 0 \end{bmatrix} \tag{4.8}$$

No pressure dynamics is present in the model as the first three rows of the **A** matrix are zeros. The pressures in the system are directly defined by the valve vector $\mathbf{u}(k)$ and the matrix **B**. For example if u_3 is equal to one at time step k, then p_{A_1} is predicted to be equal to p_{high} at time step $k+1$. An equivalent mass M_{eq}, areas A_{A_1}, A_{B_1}, and A_{A_2}, and the sampling time T_s define the dynamics of the model. In reality the equivalent mass depends on the position of the cylinder. In paper C this was chosen as a constant value. In paper D the mass was recalculated and the prediction matrices were updated each time the controller was called. In paper E the influence of changing mass on controller performance was investigated. The specific values for these parameters are different for the different systems.

Matrix **C** has been defined as Eq. 4.9. This makes $y(k+1)$ a scalar.

$$\mathbf{C} = \begin{bmatrix} 0 & 0 & 0 & 1 & 0 \end{bmatrix} \tag{4.9}$$

The model Eq. 4.5 can be used to predict future plant outputs. The predictions for time steps $k = \{1, 2, 3\}$ can be seen below:

$$\mathbf{x}(1) = \mathbf{A}\mathbf{x}(0) + \mathbf{B}\mathbf{u}(0) \tag{4.10}$$

$$\mathbf{x}(2) = \mathbf{A}\mathbf{x}(1) + \mathbf{B}\mathbf{u}(1) \tag{4.11}$$

$$\mathbf{x}(3) = \mathbf{A}\mathbf{x}(2) + \mathbf{B}\mathbf{u}(2) \tag{4.12}$$

These predictions cannot be used in an optimization algorithm directly, since for instance the states at time step two depend on controller input $\mathbf{u}(1)$ and states $\mathbf{x}(1)$. $\mathbf{u}(1)$ is to be chosen by an algorithm, but $\mathbf{x}(1)$ is a future value. A number of mathematical manipulations need to be done as in [7], before the model can be used in an optimization algorithm. Inserting the value for $\mathbf{x}(1)$ into $\mathbf{x}(2)$ gives:

$$\mathbf{x}(2) = \mathbf{A}(\mathbf{A}\mathbf{x}(0) + \mathbf{B}\mathbf{u}(0)) + \mathbf{B}\mathbf{u}(1) \tag{4.13}$$

$$= \mathbf{A}^2\mathbf{x}(0) + \mathbf{A}\mathbf{B}\mathbf{u}(0) + \mathbf{B}\mathbf{u}(1) \tag{4.14}$$

In this way $\mathbf{x}(2)$, depends on $\mathbf{x}(0)$, $\mathbf{u}(0)$, and $\mathbf{u}(1)$. The equation for $\mathbf{x}(2)$ in turn can be inserted into $\mathbf{x}(3)$:

$$\mathbf{x}(3) = \mathbf{A}(\mathbf{A}^2\mathbf{x}(0) + \mathbf{AB}\mathbf{u}(0) + \mathbf{B}\mathbf{u}(1)) + \mathbf{B}\mathbf{u}(2) \tag{4.15}$$

$$= \mathbf{A}^3\mathbf{x}(0) + \mathbf{A}^2\mathbf{B}\mathbf{u}(0) + \mathbf{AB}\mathbf{u}(1) + \mathbf{B}\mathbf{u}(2) \tag{4.16}$$

Observing the pattern in Eq. 4.16 it is possible to give an equation in general form, that can be used to predict the system's states for time step M:

$$\mathbf{x}(M) = \mathbf{A}^M\mathbf{x}(0) + \sum_{n=1}^{M} \mathbf{A}^{M-n}\mathbf{B}\mathbf{u}(n-1) \tag{4.17}$$

This gives an equation for predicting future outputs of the plant based on the current state $\mathbf{x}(0)$ which is known from available measurements and the controller inputs $\mathbf{u}(n-1)$, where n varies from zero to $M-1$. Since the position of the cylinder is of interest, the definition $y(k+1) = \mathbf{C}\mathbf{x}(k+1)$ is used to produce:

$$y(M) = \mathbf{C}\mathbf{A}^M\mathbf{x}(0) + \sum_{n=1}^{M} \mathbf{C}\mathbf{A}^{M-n}\mathbf{B}\mathbf{u}(n-1) \tag{4.18}$$

In matrix form this is written as:

$$\mathbf{G} = \begin{bmatrix} \mathbf{CB} & \mathbf{0} & \cdots & \mathbf{0} \\ \mathbf{CAB} & \mathbf{CB} & \cdots & \mathbf{0} \\ \vdots & \vdots & \ddots & \vdots \\ \mathbf{CA}^{M-1}\mathbf{B} & \mathbf{CA}^{M-2}\mathbf{B} & \cdots & \mathbf{CB} \end{bmatrix} \tag{4.19}$$

$$\hat{\mathbf{x}}_o = \begin{bmatrix} \mathbf{CA} \\ \vdots \\ \mathbf{CA}^M \end{bmatrix} \mathbf{x}(0) \tag{4.20}$$

where $\mathbf{G}$ is a gain matrix and $\hat{\mathbf{x}}_o$ is a vector containing the influence of the initial condition $\mathbf{x}(0)$. Using this matrix equation, a vector of system outputs $\hat{\mathbf{y}}$ can be predicted from a vector of inputs $\hat{\mathbf{u}}$:

$$\hat{\mathbf{y}} = \mathbf{G}\hat{\mathbf{u}} + \hat{\mathbf{x}}_o \tag{4.21}$$

where $\hat{\mathbf{y}} = [y(1),\ y(2),\ \cdots,\ y(M)]^T$ and $\hat{\mathbf{u}} = [\mathbf{u}(0),\ \mathbf{u}(1), \cdots, \mathbf{u}(M-1)]^T$. Eq. 4.21 is used in the cost function of an optimization algorithm in order to find the optimal control inputs.

4.2.2 Model with integral action

It was found in paper C that the prediction model Eq. 4.21 is not suitable for use in situations with large disturbances. According to [15] integral action

MPC can deal with this problem and so it was introduced in paper D. In order to introduce integral action to the control structure the following variables need to be defined:

$$\Delta \mathbf{u}(k) = \mathbf{u}(k) - \mathbf{u}(k-1) \tag{4.22}$$

$$\Delta \mathbf{x}(k) = \mathbf{x}(k) - \mathbf{x}(k-1) \tag{4.23}$$

$\Delta \mathbf{u}(k)$ is the change in input and $\Delta \mathbf{x}(k)$ is the change in internal state. With these definitions Eq. 4.5 is rewritten as:

$$\Delta \mathbf{x}(k+1) = \mathbf{A}\Delta \mathbf{x}(k) + \mathbf{B}\Delta \mathbf{u}(k) \tag{4.24}$$

$$y(k+1) - y(k) = \mathbf{CA}\Delta \mathbf{x}(k) + \mathbf{CB}\Delta \mathbf{u}(k) \tag{4.25}$$

The integral action can be seen because the equation for $y(k+1)$ can be viewed as:

$$y(k+1) = y(k) + \mathbf{C}\Delta \mathbf{x}(k+1) \tag{4.26}$$

In this equation the new output $y(k+1)$ is equal to the old output $y(k)$ plus the change in internal states. This can be considered a form of simple integration. Following the procedure from [15] a new state vector is introduced:

$$\overline{\mathbf{x}}(k) = \begin{bmatrix} \Delta \mathbf{x}(k) \\ y(k) \end{bmatrix} \tag{4.27}$$

The system equations become:

$$\overline{\mathbf{x}}(k+1) = \overline{\mathbf{A}}\overline{\mathbf{x}}(k) + \overline{\mathbf{B}}\Delta \mathbf{u}(k) \tag{4.28}$$

$$y(k) = \overline{\mathbf{C}}\overline{\mathbf{x}}(k) \tag{4.29}$$

where

$$\overline{\mathbf{A}} = \begin{bmatrix} \mathbf{A} & \mathbf{0} \\ \mathbf{CA} & \mathbf{I} \end{bmatrix} \tag{4.30}$$

$$\overline{\mathbf{B}} = \begin{bmatrix} \mathbf{B} \\ \mathbf{CB} \end{bmatrix} \tag{4.31}$$

$$\overline{\mathbf{C}} = \begin{bmatrix} 0 & 0 & 0 & 0 & 0 & 1 \end{bmatrix} \tag{4.32}$$

The new model can be written as a matrix equation using the same procedure:

$$\overline{\mathbf{y}} = \overline{\mathbf{G}}\Delta \hat{\mathbf{u}} + \overline{\mathbf{x}}_o \tag{4.33}$$

The matrices are constructed the same way, but inside instead of matrices $\mathbf{A}$, $\mathbf{B}$, $\mathbf{C}$, the new matrices $\overline{\mathbf{A}}$, $\overline{\mathbf{B}}$, $\overline{\mathbf{C}}$ are used. This is denoted by the bar on $\overline{\mathbf{G}}$ and $\overline{\mathbf{x}}_o$.

The two prediction models are described by the two matrix equations Eq. 4.21 and Eq. 4.33. These models are to be used in the optimization algorithms described in the next section.

4.2.3 The optimization problem

MPC is based on an optimization approach, where the effectiveness of this depends on the convergence rate and the formulation of the optimization problem. The problem can be divided into three parts - the cost function, the constraints, and the optimization algorithm. The shape of the cost function and the constraints will influence which optimization algorithms can solve this problem and to some extent how fast. First the cost function will be described followed by the number of algorithms, which have been developed and tested.

Cost Function Definition

To use the simple model for prediction and optimization a Lasso cost function was chosen in paper C:

$$J = ||\hat{\mathbf{r}} - (\mathbf{G}\hat{\mathbf{u}} + \hat{\mathbf{x}}_o)||_2^2 + |\mathbf{F}\hat{\mathbf{u}}|_1 \tag{4.34}$$

where $\hat{\mathbf{r}}$ is the reference vector. The symbol $\hat{\mathbf{u}}$ denotes the vector of valves, which starts with the current valve combination followed by the vector to be found by optimization:

$$\hat{\mathbf{u}} = \begin{bmatrix} \mathbf{u}(0) \\ \mathbf{u}(1) \\ \vdots \\ \mathbf{u}(M-1) \end{bmatrix} \tag{4.35}$$

These variables can only take on values of 0 or 1. This denotes the valve being closed or opened respectively. $\mathbf{F}$ is a difference matrix which calculates the cost of switching from one pressure to another.

$$F(i,j) = \begin{cases} -V_{chamb_n} p_z, & \text{if} \quad i = j \\ V_{chamb_n} p_z, & \text{elseif} \quad j = i + 9 \\ 0, & \text{otherwise} \end{cases} \tag{4.36}$$

where V_{chamb_n} is the volume of chamber n where n changes at each increment of i and j:

$$V_{chamb_n} = \begin{cases} V_{A_1} & \text{if} \quad \text{floor}((n-1)/3) = 0 \\ V_{B_1} & \text{if} \quad \text{floor}((n-1)/3) = 1 \\ V_{A_2} & \text{if} \quad \text{floor}((n-1)/3) = 2 \end{cases} \tag{4.37}$$

$$n = \begin{cases} 1 & \text{if} \quad n = 9 \\ n+1 & \text{otherwise} \end{cases} \tag{4.38}$$

where floor is a function which truncates a real number to an integer. For $i = 1$, $j = 1$ then $n = 1$ and $\text{floor}((n-1)/3) = 0$. When j is incremented then

$n = 2$, but floor$((n-1)/3)$ is still equal to zero. When j reaches nine, the counter n is reset. According to this definition, changes in valves u_1, u_2 and u_3 will be multiplied with V_{A_1}. This is the volume of chamber A_1 and these three valves are connected to this chamber. Furthermore p_z is defined by:

$$p_z = \begin{cases} \frac{p_L}{p_S} \cdot 10^5 & \text{if} \quad \text{Mod}(n,3) = 1 \\ \frac{p_M}{p_S} \cdot 10^5 & \text{if} \quad \text{Mod}(n,3) = 2 \\ \frac{p_S}{p_S} \cdot 10^5 & \text{if} \quad \text{Mod}(n,3) = 0 \end{cases} \tag{4.39}$$

where Mod$(n,3)$ is the modulo operator, which returns the remainder of a division of two integers. For the example above changes in valve opening u_1, u_2 and u_3 will be multiplied with $\frac{p_L}{p_S}$, $\frac{p_M}{p_S}$, and $\frac{p_S}{p_S}$ respectively. In this way $|\mathbf{F}\hat{\mathbf{u}}|_1$ grows with larger changes in pressure and larger chamber volumes. The term penalizes energy use.

When using the integral action model the cost function can be written as:

$$J_{int} = \left|\left| \hat{\mathbf{r}} - \underbrace{\left(\overline{\mathbf{G}}\mathbf{Q}\hat{\mathbf{u}} + \overline{\mathbf{x}}_o\right)}_{\Psi} \right|\right|_2^2 + |\mathbf{F}\hat{\mathbf{u}}|_1 \tag{4.40}$$

The cost function Eq. 4.40 was used in papers D and E.

The matrix $\mathbf{Q}$ is used to connect the vector $\hat{\mathbf{u}} \in \{0,1\}$ with the difference vector $\Delta\hat{\mathbf{u}} \in \{-1,0,1\}$. The first one shows the actual valve openings, while the second one shows the change in control action. The matrix $\mathbf{Q}$ is defined as:

$$\mathbf{Q}(i,j) = \begin{cases} -1, & \text{if} \quad i = j \\ 1, & \text{elseif} \quad j = i + 9 \\ 0, & \text{otherwise} \end{cases} \tag{4.41}$$

By this definition of $\mathbf{Q}$ the term Ψ in Eq. 4.40 becomes:

$$\Psi = \left(\overline{\mathbf{G}}\mathbf{Q}\hat{\mathbf{u}} + \overline{\mathbf{x}}_o\right) = \overline{\mathbf{G}}\Delta\hat{\mathbf{u}} + \overline{\mathbf{x}}_o \tag{4.42}$$

From Eq. 4.33 and Eq. 4.42:

$$\Psi = \overline{\mathbf{y}} \tag{4.43}$$

The cost function then becomes

$$J_{int} = \underbrace{||\hat{\mathbf{r}} - \overline{\mathbf{y}}||_2^2}_{\text{Accuracy term}} + \underbrace{w\,|\mathbf{F}\hat{\mathbf{u}}|_1}_{\text{Energy term}} \tag{4.44}$$

In Eq. 4.44 the constant w is added, in order to scale the energy term. This produces a relative weighing between the two terms. The constant can be used to tune the controller. The cost function can also be rewritten as:

$$J_{int} = \left|\left| - \overline{\mathbf{G}}\mathbf{Q}\hat{\mathbf{u}} + (\hat{\mathbf{r}} - \hat{\mathbf{x}}_o)\right|\right|_2^2 + w\,|\mathbf{F}\hat{\mathbf{u}}|_1 \tag{4.45}$$

Then a matrix $\mathbf{T}$ and a vector $\hat{\mathbf{j}}$ can be defined as:

$$\mathbf{T} = -\overline{\mathbf{G}}\mathbf{Q} \tag{4.46}$$

$$\hat{\mathbf{j}} = \hat{\mathbf{r}} - \hat{\mathbf{x}}_o \tag{4.47}$$

which results in the cost function being written on the form:

$$J_{int} = ||\mathbf{T}\hat{\mathbf{u}} + \hat{\mathbf{j}}||_2^2 + w\,|\mathbf{F}\hat{\mathbf{u}}|_1 \tag{4.48}$$

Putting the cost function on the form in Eq. 4.48 makes it a well known optimization problem called Classic Lasso. Since the problem is known the performance of different algorithm with respect to solving the problem can be found in the literature. Cost functions Eq. 4.34 and Eq. 4.48 are used in the algorithms presented in section 4.2.3.

Cost Function Analysis

The cost function is made of two parts. One part is the cost of not following the reference denoted as accuracy term in Eq. 4.44 and can be seen in Fig. 4.7. The second part is the cost incurred due to switching between pressure lines denoted with Energy term in Eq. 4.44 and can be seen in Fig. 4.8.

The two costs for a prediction horizon of 4 steps are presented in the figures. The x-axis shows the cost calculated by Eq. 4.44. All the possible force combinations are arranged on the y-axes. With 4 prediction steps and 27 possible control inputs per step, the total number of possible combinations is 531441. On the very left $\hat{\mathbf{u}} = [\mathbf{u}_9,\ \mathbf{u}_1,\ \mathbf{u}_1,\ \mathbf{u}_1,\ \mathbf{u}_1]^T$. On the far right, combination 531441 corresponds to $\hat{\mathbf{u}} = [\mathbf{u}_9,\ \mathbf{u}_{27},\ \mathbf{u}_{27},\ \mathbf{u}_{27},\ \mathbf{u}_{27}]^T$. The initial conditions for the calculations are an initial force output corresponding to combination nine, and a cylinder position equal to the reference at time step zero. The reference is increased by 0.5 mm at the last time step. This corresponds to a small error of $\hat{\mathbf{r}} - \overline{\mathbf{y}} = [0,\ 0,\ 0,\ 0.5 \cdot 10^{-3}]^T$. In paper D a maximum error of 0.5 mm was desired, due to previous results with the same test stand. The tuning parameter w was selected as $1.2 \cdot 10^{-7}$ in paper E. It can be seen that with this parameter the two costs have similar magnitude as indicated by the scale on the y-axis.

In Fig. 4.9 the two parts of the cost function have been plotted against each-other with blue points being specific combinations of valve openings. A Pareto optimal front can be identified by the points which are not dominated by any other points in at least one dimension. In this case the front has been denoted with red points. Changing the value of w will change which of these points will be found.

The two cost functions are added together and the optimum can be seen as a red star in Fig. 4.10. This corresponds to a situation with zero switching

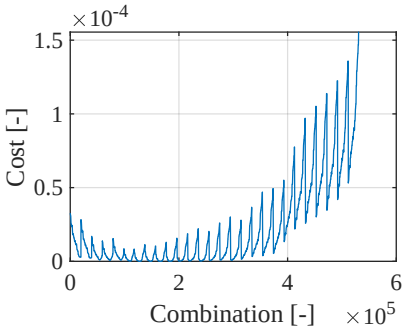

Figure 4.7: Cost of position accuracy.

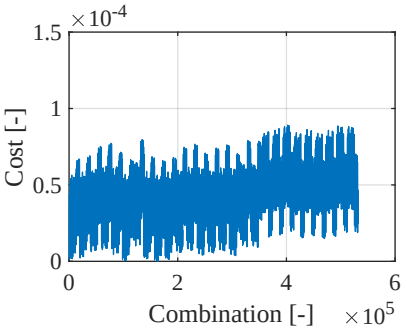

Figure 4.8: Cost of switching scaled with w.

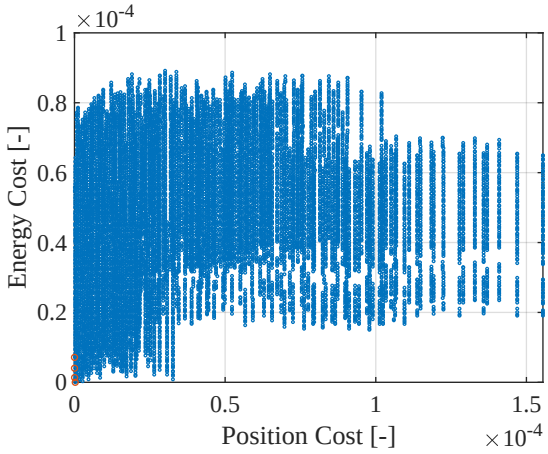

Figure 4.9: Scatter plot of valve combinations according to position and energy cost.

costs. This happens only if no change in force is required over the prediction horizon. Considering the small position error it is not unexpected that the optimal control input is to not change force level. A maximum error of 0.5 mm was desired in paper D, so it was expected that the algorithm would produce this result many times. Considering this, all algorithms were started at this point in order to accelerate convergence.

With the shape and properties of the cost function identified, it should be considered if modification can be introduced to help the convergence rate of the optimization algorithms. Modifications were made to the cost function in paper D. The cost function was implemented as:

$$J_{int} = \left|\mathbf{T}\hat{\mathbf{u}} + \hat{\mathbf{j}}\right|_1 + \left|\mathbf{F}\hat{\mathbf{u}}\right|_1 \tag{4.49}$$

Instead of a second norm squared, a first norm was implemented. This was done in order to reduce the number of computations, since squaring matri-

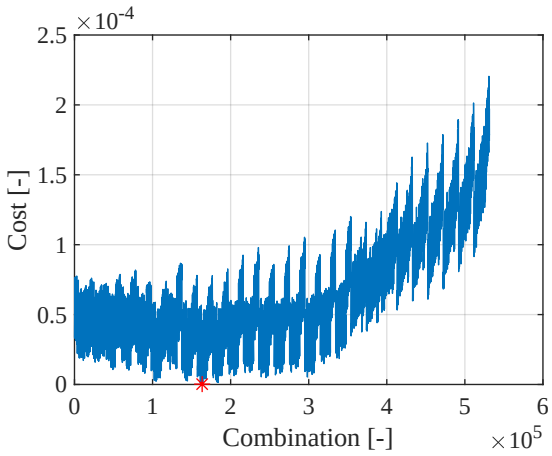

Figure 4.10: Combined cost for energy and position.

ces can be computationally costly. The method proved to speed up the algorithm's convergence on the test stand, but later tests in paper E showed no improvement. It can be concluded that hardware and compilation method, play a large role in the performance of the algorithms as discussed in paper E. The following function was also introduced in paper E:

$$J_{int} = \left|\left|\mathbf{T}\hat{\mathbf{u}} + \hat{\mathbf{j}}\right|\right|_2^2 + ||\mathbf{F}\hat{\mathbf{u}}||_2^2 \tag{4.50}$$

Here both components are a second norm squared. This reduces the complexity when gradient descent methods are used, because the second norm squared has a defined gradient. The first norm does not have a defined gradient at zero so the sub-gradient has to be used. This complicates the derivation of the gradient descent method. It was found that neither modification produces smaller costs or faster computation times. The shape of the cost function prevents the use of linear programming algorithms, because it is not linear. Either quadratic programming methods or non-linear programming methods have to be used.

Constraints

The second part of the optimization problem is the constraints. Several constraints are necessary for this project. These further limit the possible number of algorithms which can be used to solve the optimization problem. The vector $\hat{\mathbf{u}}$ describes opened and closed valves and so has to be constrained to:

$$\hat{\mathbf{0}} \leq \hat{\mathbf{u}} \leq \hat{\mathbf{1}} \tag{4.51}$$

were $\hat{0}$ and $\hat{1}$ denote vectors of zeros and ones respectively with size determined by $\hat{\mathbf{u}}$. This constraint is necessary because a valve opening larger than

one would introduce pressures larger than the pressure rail capability to the cylinders chambers. Furthermore, since only one pressure line should be connected to a chamber at a time, an additional constraint is added:

$$\mathbf{L\hat{u}} = \begin{bmatrix} u_1(k) + u_2(k) + u_3(k) \\ \vdots \\ u_7(M) + u_8(M) + u_9(M) \end{bmatrix} \quad \mathbf{L\hat{u}} = \hat{\mathbf{1}} \tag{4.52}$$

Considering that $u_1(k)$, $u_2(k)$, and $u_3(k)$ are already constrained to be between zero and one, if their sum is equal to one, it means that more than one valve cannot be opened at the same time. Unfortunately this constraint does not prevent a situation in which all three valves are opened to a value of 0.333. Under that situation the model of the system does not agree with the reality of a test bench. A final constraint is required to secure that only one valve per chamber is opened at a time. This constraint is that the input vector is constrained to only having integer values. The integrality constraint, breaks the convexity of the cost function. This limits the possible optimization algorithms to integer programming and non-linear/stochastic programming algorithms.

Algorithms

Three optimization algorithms were applied to the problem: a differential evolution algorithm, a branch and bound algorithm, and a path-finding algorithm. The first algorithm is stochastic based. The second is an integer programming algorithm. The third is a path-finding algorithm. The algorithms are presented in the following subsections.

Evolution based algorithm The differential evolution algorithm is a stochastic algorithm inspired by natural processes [16]. It can solve a large variety of problems including the mixed-integer non-linear problems. The algorithm was chosen because it has been proven to work for this specific problem in [7]. The algorithm was used in papers D and E. The algorithm in its current implementation can be seen in Fig. 4.11. In Fig. 4.11 $\mathbf{x}$ stands for the current population, **ind** is a matrix of TRUE/FALSE values, **rand** is a random number generator outputting values between 0 and 1, and CR is a number describing the crossover ratio. $\mathrm{mod}(*,*)$ is the modulus function returning the remainder of the division of two numbers. Notation $\mathbf{x}(\min(\mathbf{f}) == \mathbf{f})$ is taken from Matlab and stands for those members of $\mathbf{x}$ which produce the minimum value of $\mathbf{f}$. In the algorithm a population of size $[NP, D]$ is initiated, where NP is the size of the population and D is the control horizon for the MPC. For each NP, a D-number of forces are selected based on a randomization of a initial seed. The seed can be a previous optimum or something else. In

```
x = Initiate(seed) ;
stop = 0 ;
f = J(x) ;
while stop ==0 do
    x_new = Mutate(x, min(f));
    ind = rand > CR ;
    x_new(ind) = x(ind) ;
    f = J(x_new) ;
    h_indx = mod(G,Tf)+1 ;
    h(h_indx) = sum(f) ;
    G = G + 1 ;
    best = x(min(f) == f);
    x = x_new ;
    if std(h) > Tol OR G ≥ G_max then
        stop = 1 ;
    end
end
```

Figure 4.11: Differential Evolution algorithm

papers D and E the initial seed was a vector filled with the force number 12. This was found to be a good solution through trial and error. The number is chosen because the force level is close to the center of the search space, but it is also close to the constant load applied to the cylinder. For problems where the load changes significantly a different way of choosing the initial seed will be required.

The randomization ensured that the initial population had forces between force levels 8 and 16. The algorithm then uses the cost function J to find the fitness of each member. Each new generation is created based on the best members from the previous generations and a random mutation. The crossover ratio CR determines how many members can be kept from the previous generation. Mutation was implemented as:

$$\mathbf{x}_{new} = \mathbf{x}_{r_1} + F(\mathbf{x}(\min(\mathbf{f}) == \mathbf{f}) - \mathbf{x}_{r_1}) + F(\mathbf{x}_{r_2} - \mathbf{x}_{r_3}) \tag{4.53}$$

where r_1, r_2, and r_3 are randomly chosen vectors from the previous population. The first part $\mathbf{x}_{r_1} + F(\mathbf{x}(\min(\mathbf{f}) == \mathbf{f}) - \mathbf{x}_{r_1})$, moves the new population towards the best solution from the previous iteration, since if $F = 1$, the equation simplifies to $\mathbf{x}(\min(\mathbf{f}) == \mathbf{f})$. In the algorithm a F value of 0.7 was used as in [8]. The second part - $F(\mathbf{x}_{r_2} - \mathbf{x}_{r_3})$, prevents the algorithm from converging prematurely as it moves the answer in a random direction. As the algorithm converges, the population become more and more homogeneous and so the effect of the second part is reduced.

Branch and Bound based algorithm Another way of solving mixed integer problems is to use branch and bound algorithms. The algorithm separates the problem into two parts. One part is the original convex problem, but without the integrality constraint. The second part is the branching on a chose variable. Dropping the integrality constraint simplifies the problem and a quadratic programming algorithm can be used. The quadratic programming algorithm produces real numbers. Once the result is obtained, a variable is selected to be branched on. The specific variable is chosen according to a branching rule. The action is called branching, because it creates two new cases. In one case the variable is constrained to be an integer below the current value, in the other case - an integer above the current value. These two problems are solved and the one, which produces a better solution, is chosen. The algorithm was used in paper E. The reasoning behind choosing this algorithm comes from it being one of few possible for solving integer programming problems. Furthermore multiple variables can be constrained to integers at the same time. This can happen, because if one valve is open, the other two valves connected to the same chamber have to be closed. There is a large cost associated with switching between force levels, so constraining the first nine values of the optimization variable can force the rest of the variable to be the same. This was seen in the cost function analysis in section 4.2.3. The algorithm as implemented consists of several steps as can be seen in Fig. 4.12. The variable being selected for branching $\mathbf{x}_b$ is chosen chamber by

```
while stop == 0 do
    x_opt, f_opt = ADMM(J, A) ;
    if Binary(x_opt) OR I > I_max then
        stop = 1 ;
    end
    x_b = BranchVar(x_opt) ;
    A_1 = AddConstaintOne(x_b) ;
    x_1, f_1 = ADMM(J,A_1) ;
    A_0 = AddConstaintZero(x_b) ;
    x_0, f_0 = ADMM(J,A_0) ;
    if f_0 > f_1 then
        A = A_1 ;
    else
        A = A_0
    end
    I = I + 1 ;
end
```

Figure 4.12: Branch and bound algorithm based on ADMM

chamber. That is to say that values earlier in the time horizon are chosen first. From the three valves connected to the same chamber the one with the largest value is chosen for branching. This is done because if a value is constrained to a value of one the valve is open and the other two valves connected to that chamber have to be closed. In this way two branching operations are avoided. The branching operation produces two constraint matrices $\mathbf{A}_1$ and $\mathbf{A}_0$. A convex solver solves finds the optimum for both branches $\mathbf{x}_1$ and $\mathbf{x}_0$, and the one which produces a smaller optimal value f_1 or f_0 is kept for the next iterations of the algorithm. In this thesis an Alternating Directions Method of Multipliers (ADMM) algorithm was selected for a convex solver. This algorithm was chosen because it shows good properties for solving the Classic Lasso problem [5]. In order to use this method the cost function is separated into two functions as seen in [4]. In this thesis the two functions are:

$$f(\mathbf{x}) = 0.5 \left|\left|\mathbf{T}\mathbf{x} + \hat{\mathbf{j}}\right|\right|_2^2 + w \left|\mathbf{F}\mathbf{x}\right|_2^2 \tag{4.54}$$

$$g(\mathbf{z}) = I(\mathbf{z}) \tag{4.55}$$

where $f(\mathbf{x})$ is the original cost function and $g(\mathbf{z})$ is an indication function connected with the constraints as:

$$I(\mathbf{z}) = \begin{cases} 0 & \mathbf{x} \in \mathbf{C} \\ \infty & \text{otherwise} \end{cases} \tag{4.56}$$

In this case $\mathbf{C}$ is the set $\mathbf{A}\mathbf{x} = \mathbf{b}$ satisfying the constraints Eq. 4.52 and $\mathbf{x} \geq 0$. Then the problem can be described as:

$$\min\{f(\mathbf{x}) + g(\mathbf{z})\} \tag{4.57}$$

$$\text{subject to } \mathbf{x} - \mathbf{z} = 0 \tag{4.58}$$

The ADMM iterations to solve this problem are:

$$\mathbf{x}^{k+1} = \min(f(\mathbf{x}) + 0.5\rho \left|\left|\mathbf{x}^{k+1} - \mathbf{z}^k + \mathbf{u}^k\right|\right|_2^2) \tag{4.59}$$

$$\mathbf{z}^{k+1} = \min(g(\mathbf{z}) + 0.5\rho \left|\left|\mathbf{x}^{k+1} - \mathbf{z}^{k+1} + \mathbf{u}^k\right|\right|_2^2) \tag{4.60}$$

$$\mathbf{u}^{k+1} = \mathbf{u}^k + \mathbf{x}^{k+1} - \mathbf{z}^{k+1} \tag{4.61}$$

For this type of problem the proximity function of the $\mathbf{x}^{k+1}$ and $\mathbf{z}^{k+1}$ iteration are known [5]. At first the Lasso cost function Eq. 4.48 was used in paper C. Using a first norm in the cost function of an optimization problem can under certain circumstances promote sparsity. A vector can be considered sparse when the majority of its entries are equal to zero. Considering the constraints placed on the input vector $\mathbf{x}$, a sparse solution would be one where only one valve per chamber is open. During the project it was found

that due to the relative weight on the two parts of the cost function, the optimal solutions are never sparse. Sparse results can be obtained if the the weight w is reduced. This allows the algorithm to converge faster, but this also increases the position error. The ADMM iterations for the Lasso cost function Eq. 4.48 are more complicated than the ones for Eq. 4.50 and the only reason for using Eq. 4.48 is because it promotes sparse results. Since it was found that sparse results cannot be obtained with the tuning parameter chosen, the cost function Eq. 4.50 was used in the thesis.

Path-finding algorithm Different stochastic algorithms were considered before the differential evolution algorithm was selected. Some of the other algorithms were the ant colony and swarm algorithms. The algorithms were not suited to the task, but the ant algorithm in particular inspired the implementation of a path-finding algorithm. The ant algorithm is described to work as a colony of ants trying to find the best path to a food source. Ants who take the shortest path return quicker and make more trips. In the metaphor the ants are random guesses on the solution of the problem and the length of the path is the size of the minimum. In the $A^\star$ path-finding algorithm a single worker traverses a tree of choices, but the cost of travelling each path is calculated and the worker only takes the fastest route. Once a minimum is found the algorithm is stopped if the other paths are already longer. The A* algorithm is a well known algorithm which can be used to explore a tree or grid. It combines the best parts of the depth-first and width-first search algorithms. In order to apply it to this problem the optimization has to be considered as a tree of branching choices. Time steps are considered as nodes. From each node 27 possibilities branch out. A naming convention was chosen, to not only distinguish between different nodes but also to implicitly encode which force level does the node represent and which time step does the node belong to. The first node is named node 1. From it branch nodes 2 through 28. From node 2 branch nodes 29 through 55. The equation for naming new nodes is:

$$\mathbf{n}_{new} = (n_{current} - 1)27 + [2, 3, \cdots, 28]^T \tag{4.62}$$

With this equation it can be found that nodes between 29 and 757 represent the second time step as can be seen in Fig. 4.13. The ending condition or the goal for the path-finding algorithm is to find any nodes which belong to a user chosen time step. As an example a 4 step horizon was chosen in paper E. Using the equation shows that the algorithm is searching for a node with a number above 20440. The algorithm has been described in Fig. 4.14. In the algorithm N is the list of unexplored nodes. It starts with only one node in it. Each node is a row in the array - the first number is the node name, the second is the cost associated with this node, and the third number is the node from which the branch came. At each step of the algorithm the branch

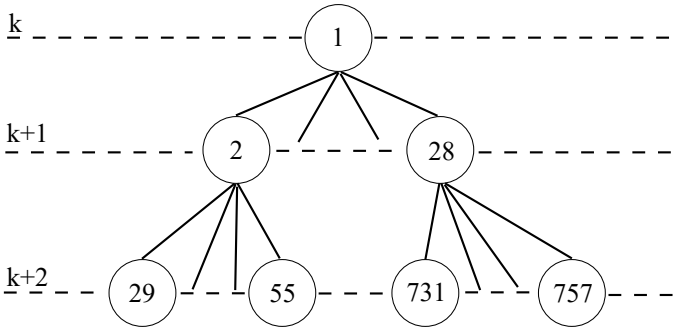

Figure 4.13: Tree branching for the first two time steps

with the smallest cost gets selected. The 27 branches that stem from it get created by the function Branch. The new branches are evaluated according to the cost function J. The function AddNodes adds these new branches to the array of nodes N. Then the function RemoveNode removes the already explored node, so it does not get selected for branching again. Finally a check is performed to see if any of the new nodes have values large enough to indicate the Goal has been found. If the goal has been found, then the cost to reach this goal is compared with the costs of all the unexplored nodes. If all other nodes have larger costs then the algorithm can stop.

```
N = [1, 0, 0] ;
stop = 0 ;
while stop ==0 do
    n_branch, n_cost = min(N(:,2));
    n_new = Branch(n_branch) ;
    n_new,costs = J(n_new) ;
    N = AddNodes([ n_new, n_new,costs, n_branch]) ;
    N = RemoveNode(n_branch) ;
    if Any(n_new > Goal) AND n_new,costs < N(:,2) then
        stop = 1 ;
    end
end
```

Figure 4.14: A* search algorithm

Without any heuristic the algorithm tends to search through the tree width first. This happens because each new time step makes the prediction vector $\hat{\mathbf{y}}$ longer. Since position error and cost of switching rarely disappear completely, the cost naturally grows with each time step. This can result in a large number of explored branches. An example of an explored tree with

no heuristic can be seen in Fig. 4.15. The red dot in middle is first node in the three and corresponds to the current force level. From it a number of blue lines branch out leading to a blue dot. Each blue dot is a node i.e. a possible force to be chosen at the first time step. From these nodes more blue lines branch out. The red dot in the lower left corner is the found optimum. Exploring more nodes, results in a longer convergence time.

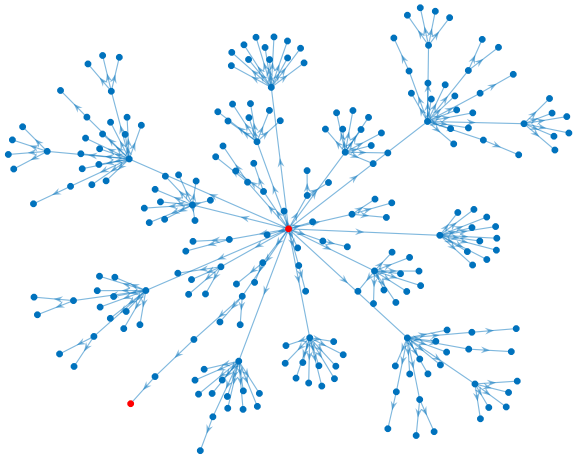

Figure 4.15: Tree exploration without heuristic. Explored nodes 229.

To help the algorithm converge an oracle is added. An oracle is an initial guess on the correct answer, which can be used to explore promising paths first. The ADMM algorithm was used to produce a vector of optimal valve openings. An Euclidean distance was used between the optimal values produced by the ADMM and the branches of the tree. This distance was added as an additional cost to the cost function J. In this case branches closer to the optimum would produce a smaller cost and so should be explored first. The proposed heuristic was implemented and tested, but instead of reducing the number of explored branches it increased it. The real number values of the ADMM result did not guide the algorithm in any specific direction and the added cost forced the algorithm to explore more nodes. This can be seen in Fig. 4.16. The number of explored nodes has increased from 229 to 3423. This in turn increases convergence time. In order to improve the oracle, the results of the ADMM algorithm were rounded, so inconclusive results i.e. those below 0.5 are removed. This reduced the number of explored branches as can be seen in Fig. 4.17 where only 84 nodes were explored.

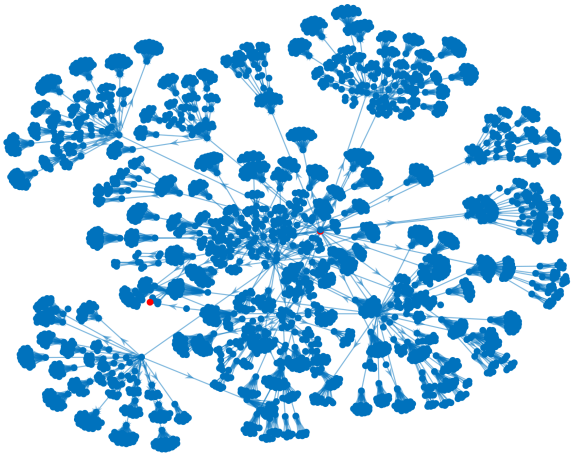

Figure 4.16: Tree exploration with heuristic but no rounding. Explored nodes 3423.

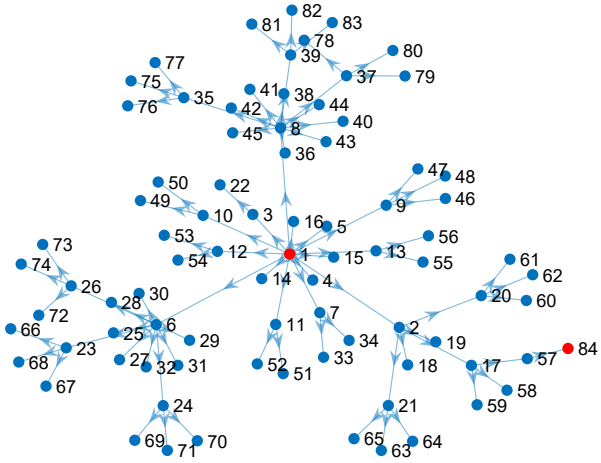

Figure 4.17: Tree exploration with heuristic with rounding. Explored nodes 84.

The algorithm still had a convergence time of over 6 seconds. A considerable amount of time was dedicated to profiling and optimizing the algorithms implementation e.g. vectorizing calculations, avoiding repeated calculations, changing the structure in which the nodes are stored. These modifications did not bring the algorithm convergence time below the target of 60 ms, so further a modification was introduced. Up to this point each new time step increased the number of variables. The new algorithm predicts for the entire time horizon with the assumption that the selected force level will not be changed. For example when calculating the cost of node 10 (which corresponds to the choice of force 9 at the first time step) the prediction is for the full 5 time steps with force 9 being kept constant. The first branch stemming from this choice is node 272. To calculate the cost of this node the valve vector is constructed with force level 9 (previous node) first and then the rest of the vector being filled with force level 1 (current node). This prevents the optimization algorithm from finding combinations in which a more costly step is taken first in order to use a much cheaper step later in the prediction horizon. On the other hand it greatly increased the convergence rate to below 60 ms.

4.2.4 Using neural networks to approximate an MPC

Neural networks are receving more attention from the research comunity. A neural network can be trained to approximate an arbitrary function [10]. The MPC used in this project is a complicated function, but MPC of similar complexity has succesfully been aproximated by a neural network in order to control an electric converter in [13]. In that paper a one layer neural network with 15 neurons has been trained on 200 000 data instances, until it reaches an accuracy of 69 %. This means that the output of the neural network and the output of the MPC were the same in 69 % of the cases. The neural network achieved better results than the MPC which it was meant to approximate with a lower THD, a fast and safe transient response, and excellent steady and dynamic performance [13]. Something similar has been done in this thesis. The training data was obtained by using the A* algorithm. The possible inputs to the algorithm were varied and the chosen force level was saved. In this case the outputs were converted from binary vectors specifying valve openings into the 28 possible force levels including the zero vector. In order to learn the integral action of the MPC the previous position, velocity, and force levels are used as well. A sine wave trajectory was used as a basis for possible position and velocity references. In this way 1.6 million data points were generated. Another 200 000 points were generated from full simulink simulations of the seesaw system. A histogram showing how many of each force number were produced can be seen in Fig. 4.18. The training data was saved in a comma separated values (CSV) file using Matlab's writematrix() built-in function. The values were then loaded in a data frame using Python's

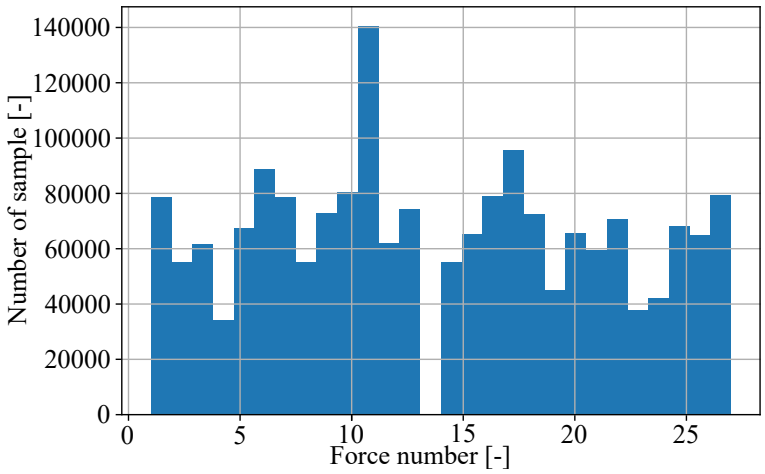

Figure 4.18: Histogram of training data target distribution

pandas library. The data was organized as seen in Tab. 4.1, where the each column corresponded to a different input, except the last column which was the output. In order to train the neural network, the current and previous position, the current and previous velocity, the current and previous force, and the trajectory vector were used as inputs. For each combination of inputs the A* algorithm produced an output which is the force level selected by the algorithm in this situation.

Table 4.1: Data structure

Data samples	Pos	Pos Prev	Vel	Vel Prev	Force	Force Prev	Traj	Output
Sample 1								
Sample 2								
⋮								
Sample $1.8 \cdot 10^6$								

The data were split into a 80 % - 20 % training-testing split. Training and neural network architecture were done using the Tensorflow and Keras libraries in Python. Bigger problems require more complex neural networks, so networks of increasing size were tested. The prediction accuracy according to neural network size can be seen in Tab. 4.2. The rows represent the size of the first layer and the columns the size of the second layer. Prediction accuracy in this sense reflects how often does the network's prediction agree with the real value obtained from the optimization algorithm. An accuracy value of 100 % would indicate that for the test data provided, the neural

network guessed the correct answer for every sample.

Table 4.2: Accuracy results with neural networks with different numbers of nodes in the first and second layer

Node number	128	256	512	1024
128	58.53 %	60.71 %	56.50 %	63.96 %
256	58.21 %	63.00 %	59.06 %	60.33 %
512	58.93 %	63.43 %	59.00 %	66.13 %
1024	61.38 %	57.84 %	48.05 %	52.92 %

The table shows that the largest network with 1024 nodes in both layers does not have the best accuracy. As a fair trade-off a structure with 128 neurons in the first layer and 1024 neurons in the second layer were chosen. The accuracy of the selected network is 63.96 %. The neural network was trained using the Keras library in python. The Adamax training algorithm was chosen after it was found to give better results than the Adam algorithm. A dropout layer with a 50 % dropout was inserted after the second layer. This means that during any training run, half of the neurons are not trained. This prevents the neural network from overfitting on the data. Overfitting occurs when a function is too closely fit to a limited number of data points and no longer describes the actual function which produced the data points. The 63.96 % accuracy is obtained with this dropout layer implemented during training.

It is a good idea to visualize the inaccuracy of the neural network. This can be done in a confusion matrix plot. The confusion matrix collects all guesses by the network and compares them to the correct answer. The confusion matrix can be seen in Fig. 4.19. Deeper colour indicates that the network guessed this number correctly more often. For example when the MPC would have selected output 10, the neural network would almost predict correctly. When the MPC would have selected out 22 or 23, the neural network is almost always wrong as indicated by the lack of a blue square for these two outputs. In an ideal situation where the network is 100 % accurate, the confusion matrix would have deep blue squares across its entire diagonal. In this case the matrix has an accuracy of 63.96 % so it predicts incorrectly nearly half the time. There are no coloured squares very far from the diagonal, which shows that the confusion is between close forces e.g. force number 5 might be selected instead of force number 7. From a position accuracy perspective choosing adjacent forces might not be problematic, but from a energy cost perspective it can pose a much bigger problem. This is because as discussed previously in the thesis, adjacent force levels can have very similar force values, but they might require that all chamber pressures have to be switched.

The neural network was implemented as matrix vector multiplication and

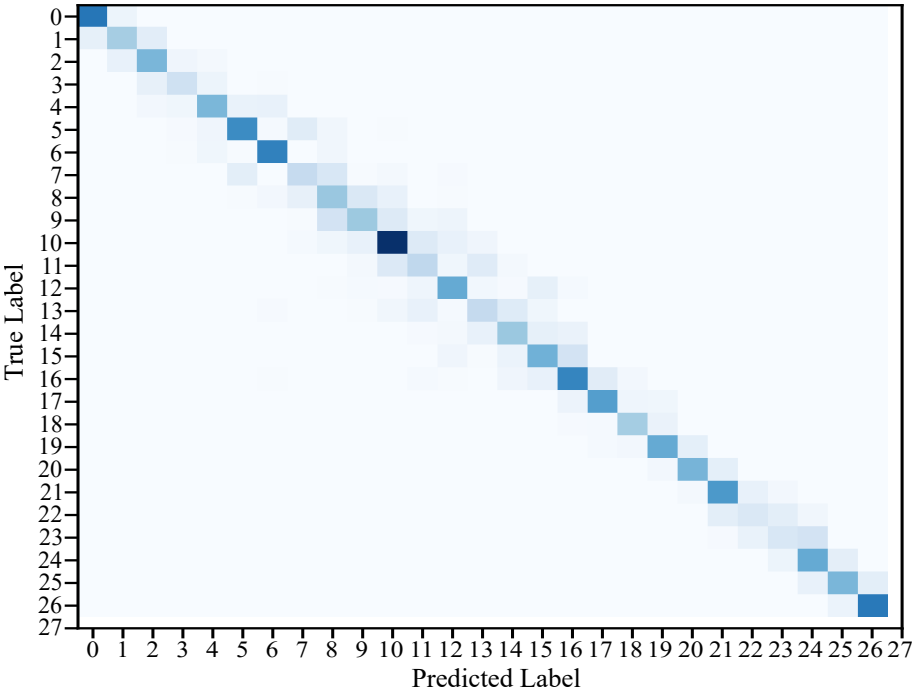

Figure 4.19: Confusion matrix of the trained neural network

tested in the full non-linear model. It was found that the system is unable to follow the reference trajectory with the neural network trained on the 1.8 million data points. A second training procedure was conducted but this time only the 200 000 simulation data points were used. The training resulted in the same accuracy level of 63 %, but when the network was implemented in the non-linear simulation it produced results comparable with the MPC controller. The comparison can be seen in the results chapter 5.2.4.

4.2.5 Fault tolerant control

To control a multi-chamber cylinder multiple valves are opened and closed repeatedly with a high frequency. The reliability of digital valves, which are often of the seat type variety, has been a major topic in their research. These valve are designed to open and close as fast as possible and this results in repeated impacts of the seat and the poppet of the valve [3]. This results in valve failures [2]. A full reliability study of a multi-chamber cylinder is out of the scope of this thesis. Nevertheless reliability in the sense of extended operational time for a multi-chamber cylinder has been addressed in paper D.

In the mentioned paper a fault tolerance study was conducted. The focus was on valve failures. Furthermore a way to recover from some of these faults was proposed. The seesaw test-bench was used as a basis for the study. The multi-chamber cylinder in the test-bench used nine valves to connect chambers to pressure lines. For each valve two faults were considered - one where the valve fails in closed position, and one where the valve fails in an open position. For the study it is considered that the fault is already detected and identified.

For each case a trajectory run was simulated where the fault was introduced from time zero. To show the inherent fault tolerance of multi-chamber cylinders no changes were made to the controller and the results are collected in Tab. 4.3. These tests consider a valve being stuck. In the table faults are denoted as "$*$ to $\bullet$", which should be understood as a fault in the valve connecting pressure line $*$ to chamber $\bullet$. The absolute position error during the simulation is summed and the energy used is collected and divided by the length of the trajectory in mm. Some simulations merely result in poor performance, other result in the cylinder moving to one end-stop and staying there for the entire simulation time. Any simulations with a absolute position error sum of over 900 m (450 m being a normal run) have been labelled as critical and have a red coloured cell. The column Energy refers to the energy used per millimetre of movement measured in J/mm. Smaller values are preferred. More information is available in the paper D itself or in the results chapter. In this section the number themselves are less important than the colours.

Some faults do not result in failure or even considerable worsening of results. As discussed in paper D the basis for this fault tolerance is that some of these valves are not used for this trajectory. It can be seen in Tab. 4.3, that the three last results are critical failures. All three results are for faults in the low-pressure line. The position error sum is also much larger in these cases. From this it can be concluded that faults in the low-pressure line are more dangerous, because the low-pressure line sees a lot more use for this trajectory.

Table 4.3: Results with valve stuck closed without detection. Red indicates critical fail.

Fault	Pos Error [m]	Energy [J/mm]
p_s to A_1	615.57	20.32
p_s to B_1	1417.39	18.52
p_s to A_2	810.23	20.16
p_m to A_1	1694.33	33.62
p_m to B_1	659.43	26.85
p_m to A_2	735.09	25.70
p_l to A_1	12220.05	18.03
p_l to B_1	9062.45	14.41
p_l to A_2	9231.42	19.53

A fault tolerant controller is proposed in paper D by the addition of an extra matrix in the cost function:

$$J_{int} = \left|\left|\mathbf{T}\hat{\mathbf{u}} + \hat{\mathbf{j}}\right|\right|_2^2 + \omega_2 \left| \mathbf{W}_f \mathbf{F}\hat{\mathbf{u}} \right|_1 \tag{4.63}$$

where $\mathbf{W}_f$ is a diagonal matrix with a large weight at the position of the faulty valve and ones at all other positions of the diagonal. This makes combinations involving the faulty valve more costly.

The results for the same tests as in Tab. 4.3 with the fault tolerance controller are collected in Tab. 4.4. It can be seen that some faults which were critical are now not. The weight on energy cost ω_2 had to be reduced. This is necessary, because the controller now needs to pick less energy efficient combinations. It can be seen that in the first fault "p_s to A_2" position error has been reduced, but energy consumption has gone up from 20 to 29 J/mm. The result for fault "p_l to B_1" has the largest increase in energy use. Fault "p_l to A_1" is indicated as critical, but simply decreasing the weight on switching can improve accuracy.

Table 4.4: Results with valve stuck closed with detection.

Fault	Pos Error [m]	Energy [J/mm]
p_s to A_1	490.19	36.45
p_s to B_1	509.69	18.22
p_s to A_2	422.55	29.98
p_m to A_1	486.97	20.67
p_m to B_1	414.85	21.49
p_m to A_2	487.97	24.86
p_l to A_1	1034.89	22.83
p_l to B_1	590.81	46.28
p_l to A_2	376.04	30.12

Tests where the valve is stuck open instead are collected in Tab. 4.5. In the table, nearly all results are critical as indicated by the red colour of the cells. Comparing the five critical results in Tab. 4.3 with the eight critical results in Tab. 4.5 shows that valves failing open results in more critical failures. This is because if a valve is stuck open it leads the controller opening a chamber to two pressure rails at the same time. This produces a pressure level between the two pressure rails in the chamber, which does not agree with the model used in the controller. It also drains the pressure lines.

The fault tolerant controller is applied to these cases as well. Now the task rather than to avoid a certain valve is to make sure that the valve is always used. This prevents the controller from opening two valves to the same chamber. The weights are put on the two healthy valves connected to the same chamber. The results can be seen in Tab. 4.6. Again, some faults which were critical without the fault tolerant controller are not critical now. Faults "p_s to A_1" and "p_s to B_1" are still critical. In these cases the fault tolerant

Table 4.5: Results with valve stuck open without detection

Fault	Pos Error [m]	Energy [J/mm]
p_s to A_1	38422.09	13.38
p_s to B_1	31687.24	15.63
p_s to A_2	31879.61	9.23
p_m to A_1	4208.14	29.85
p_m to B_1	596.53	21.75
p_m to A_2	16711.33	49.24
p_l to A_1	15956.17	1.43
p_l to B_1	2735.25	46.93
p_l to A_2	13078.48	21.69

controller cannot help. The faults reduce the number of available forces. In these two cases none of the remaining available forces are sufficient to follow the trajectory.

Table 4.6: Results with valve stuck open with detection

Fault	Pos Error [m]	Energy [J/mm]
p_s to A_1	23455.80	13.65
p_s to B_1	17781.12	20.80
p_s to A_2	778.69	38.51
p_m to A_1	473.98	25.87
p_m to B_1	522.98	20.05
p_m to A_2	618.81	22.57
p_l to A_1	853.26	17.15
p_l to B_1	876.16	12.58
p_l to A_2	721.17	32.92

Overall it can be concluded that when a valve fails to a closed state it removes nine forces from the force resolutions of the cylinder. When a valve fails to an open state it limits the resolution to those same nine forces which were removed in the first case. This is a much more dangerous situation, because it is much more difficult to follow a trajectory with the smaller force resolution.

References

[1] J. Backas and R. Ghabcheloo, "Nonlinear model predictive energy management of hydrostatic drive transmissions," *Proceedings of the Institution of Mechanical Engineers, Part I: Journal of Systems and Control Engineering*, vol. 233, no. 3, pp. 335–347, 2019.

[2] N. C. Bender, H. C. Pedersen, A. Plöckinger, and B. Winkler, "Reliability analysis of a hydraulic on/off fast switching valve," in *Proc. of The Ninth Workshop on Digital Fluid Power, Aalborg, Denmark*, 2017.

[3] N. C. Bender, H. C. Pedersen, B. Winkler, and A. Plöckinger, "Numerical investigation of switching features of a hydraulic seat valve with annular flow geometry," *International Journal of Fluid Power*, vol. 19, no. 3, pp. 152–164, 2018.

[4] S. Boyd, N. Parikh, E. Chu, B. Peleato, J. Eckstein *et al.*, "Distributed optimization and statistical learning via the alternating direction method of multipliers," *Foundations and Trends® in Machine learning*, vol. 3, no. 1, pp. 1–122, 2011.

[5] B. R. Gaines, J. Kim, and H. Zhou, "Algorithms for fitting the constrained lasso," *Journal of Computational and Graphical Statistics*, vol. 27, no. 4, pp. 861–871, 2018.

[6] D. Hagen, W. Pawlus, M. K. Ebbesen, and T. O. Andersen, "Feasibility study of electromechanical cylinder drivetrain for offshore mechatronic systems," *Modeling, Identification and Control*, vol. 38, no. 2, 2017.

[7] A. H. Hansen, M. F. Asmussen, and M. M. Bech, "Energy optimal tracking control with discrete fluid power systems using model predictive control," in *Proceedings of the Ninth Workshop on Digital Fluid Power, Aalborg, Denmark*, 2017, pp. 7–8.

[8] ——, "Hardware-in-the-loop validation of model predictive control of a discrete fluid power power take-off system for wave energy converters," *Energies*, vol. 12, no. 19, p. 3668, 2019.

[9] K. Heybroek and M. Sahlman, "A hydraulic hybrid excavator based on multi-chamber cylinders and secondary control–design and experimental validation," *International Journal of Fluid Power*, vol. 19, no. 2, pp. 91–105, 2018.

[10] K. Hornik, M. Stinchcombe, H. White *et al.*, "Multilayer feedforward networks are universal approximators." *Neural networks*, vol. 2, no. 5, pp. 359–366, 1989.

[11] B. Kim, C. M. Kang, J. Kim, S. H. Lee, C. C. Chung, and J. W. Choi, "Probabilistic vehicle trajectory prediction over occupancy grid map via recurrent neural network," in *2017 IEEE 20th International Conference on Intelligent Transportation Systems (ITSC)*, 2017, pp. 399–404.

[12] M. Linjama, H. Vihtanen, A. Sipola, and M. Vilenius, "Secondary controlled multi-chamber hydraulic cylinder," in *The* 11^{th} *Scandinavian International Conference on Fluid Power, SICFP*, vol. 9, 2009, pp. 2–4.

[13] I. S. Mohamed, S. Rovetta, T. D. Do, T. Dragicević, and A. A. Z. Diab, "A neural-network-based model predictive control of three-phase inverter with an output *lc* filter," *IEEE Access*, vol. 7, pp. 124 737–124 749, 2019.

[14] T. Peinsitt, H. Haubmann, H. Kargl, and C. Kary, "Recent developments towards autonomous tunneling and mining machinery," *Tunnels and Underground Cities: Engineering and Innovation Meet Archaeology, Architecture and Art: Volume 6: Innovation in Underground Engineering, Materials and Equipment-Part 2*, p. 2849, 2020.

[15] M. A. Stephens, C. Manzie, and M. C. Good, "Model predictive control for reference tracking on an industrial machine tool servo drive," *IEEE Transactions on Industrial Informatics*, vol. 9, no. 2, pp. 808–816, 2013.

[16] R. Storn, "Differrential evolution-a simple and efficient adaptive scheme for global optimization over continuous spaces," *Technical report, International Computer Science Institute*, vol. 11, 1995.

[17] J. Unger, M. Kozek, and S. Jakubek, "Nonlinear model predictive energy management controller with load and cycle prediction for non-road hev," *Control Engineering Practice*, vol. 36, pp. 120–132, 2015.

Part III

Results and Conclusions

Chapter 5

Results

In this chapter the results from all the articles are collected. The results are divided into results for the crane system and results for the seesaw system. Results for the crane system come from papers B and C. Results for the seesaw system come from papers D and E. Laboratory results are available only for the seesaw system.

5.1 Crane results

The result showing the performance of multi-chamber cylinders applied on an example knuckle-boom crane are shown in this section. The section is divided into two subsections. Each subsection shows results from one paper. In one paper the crane is supplied from a constant pressure rail, in the other paper the crane is supplied by a load sensing pump. Both types of cranes are available on offshore platforms.

5.1.1 Results with a constant pressure rail compared with DFC

In paper B the boom of the knuckle-boom crane described in chapter 3 was actuated with the DFC algorithm. In chapter 4 it was explained that the controller was augmented to avoid certain force levels in order to enforce different switching patterns. The results for the trajectory tracking of the cylinder can be seen in Fig. 5.1 and the energy consumed to follow the trajectory can be seen in Fig. 5.2. It can be seen that the multi-chamber cylinders use nearly half as much energy as the normal cylinder. Furthermore both multi-chamber cylinder controllers use almost the same amount of energy even though they use different switching patterns as discussed in chapter 4. In this point of the project switching patterns are of greater interest than

accurate position tracking. Better position tracking results can be seen later on for instance in 5.5. The results denoted as normal cylinder are obtained from a standard differential cylinder controlled by a servo valve and supplied from a constant pressure rail. This kind of rail is commonly available on oil platforms where the example crane would normally be placed. The normal cylinder using throttling control provides the best tracking performance.

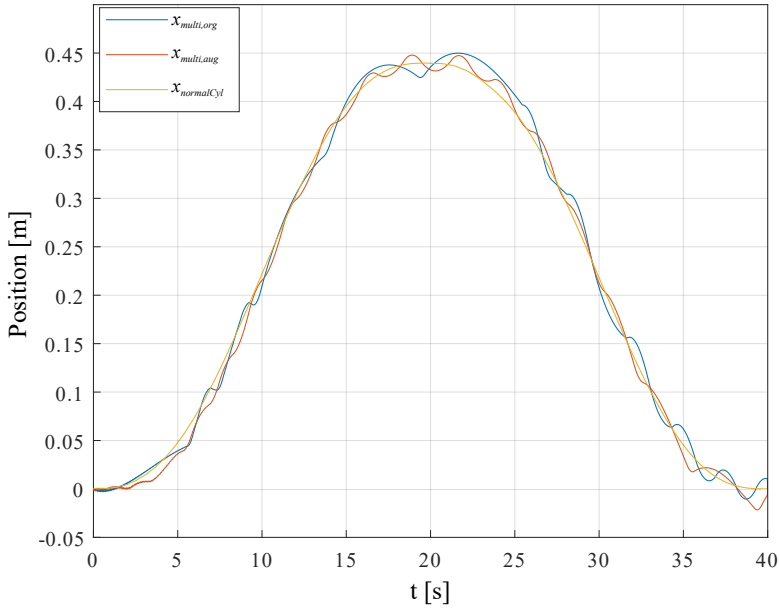

Figure 5.1: Trajectory tracking with the different controllers

Two more tests were conducted in this paper. The same shape of position trajectory was used again, but the required velocity was increased in the first test and decreased in the second. The point of the tests was to investigate the robustness of the control structure. The results are shown it Tab. 5.1. The results for the most part are not surprising. The normal cylinder's constant throttling wastes a lot of energy, but it provides the best position accuracy. The multi-chamber cylinder has worse position accuracy due to the oscillation around the actual trajectory, but spends a lot less energy. It is surprising that, when the velocity of the trajectory is decreased, the non-augmented controller wastes a significant amount of energy 0.72 MJ, which is nearly the same energy use as the normal cylinder. The two DFC controllers otherwise have nearly identical position tracking performance with the augmented controller actually delivering consistently better position accuracy and lower energy use as seen in Tab. 5.1. As discussed in chapter 4, this is significant,

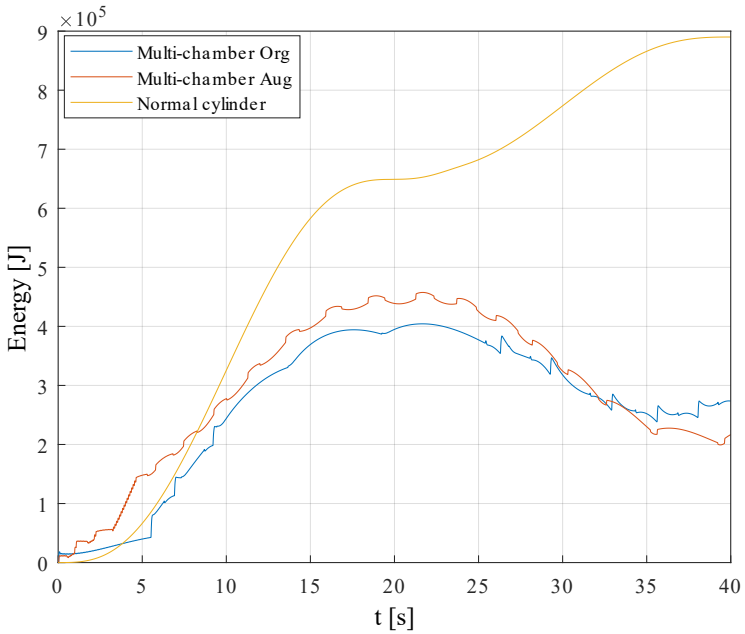

Figure 5.2: Energy used to follow the trajectory

because it is expected that a switching controller that switches more often will produce better position tracking but will waste significant amounts of energy.

Table 5.1: Result of simulations with trajectories with three different velocities

	Energy used [MJ]			Error RMS [m]		
Velocity	Normal	Fast	Slow	Normal	Fast	Slow
Normal Cylinder	0.89007	0.89308	0.88867	0.002	0.0026	0.0013
Controller Original	0.27357	0.28364	0.71907	0.0097	0.0113	0.0098
Controller Augmented	0.21672	0.14764	0.22810	0.0074	0.0124	0.0074

The same tests were repeated again but with an increased load on the crane. The results follow a similar pattern, but this time the augmented controller, also delivered poor energy performance with the slow trajectory.

This first paper in the thesis showed several things. It is possible to save a large amount of energy if the standard cylinders on a knuckle-boom crane are swapped for multi-chamber cylinders. The tests also showed that different switching patterns can result in largely similar performance. A higher average switching ratio can indicate better position performance, but it does not necessarily lead to high energy use. It showed that it is better to consider the switching costs between each force level, rather than simply punish

Table 5.2: Result of simulations with trajectories with three different velocities and increased load

	Energy used [MJ]			Error RMS [m]		
Velocity	Normal	Fast	Slow	Normal	Fast	Slow
Normal Cylinder	0.89455	0.91036	0.89207	0.0054	0.0087	0.0028
Controller Original	0.47680	0.39424	0.79168	0.0078	0.0090	0.0088
Controller Augmented	0.37959	0.28645	0.65295	0.0118	0.0180	0.0133

switching events. The paper also showed that tailoring the middle-pressure line's pressure value can give much better results instead of just choosing to have it in the mathematical middle between the low- and high-pressure lines.

5.1.2 Results with a load sensing system compared with MPC and DFC

The purpose of paper C was to investigate several things. The first was the difference in performance in multi-chamber cylinder with MPC compared with the DFC algorithm used in B. The second, was to investigate the energy efficiency of the multi-chamber cylinders when the crane is using a load sensing system. Both of the crane's cylinders were actuated at the same time. The trajectory mimics a realistic work cycle - the crane begins in one position moves to a second position, picks up a large mass and moves it to the first location. This can be a loading or unloading cycle. The position tracking performance of the multi-chamber cylinder of the boom, as well as the standard hydraulic cylinder, can be seen in Fig. 5.3. The same results but for the second cylinder can be seen in Fig. 5.4. The results clearly show that when the large mass of 20 ton is picked up at 50 seconds, the standard cylinder keeps its performance, but the multi-chamber cylinder does not as indicated by the large deviation in position. An error of 0.2 m in cylinder position is not acceptable. It was found that with a much harder tuned DFC algorithm, the tracking performance can be recovered, but the energy consumption increases. This agrees with the results of paper B that changing the trajectory can result in large energy use. Since the main use of a crane is to lift and lower large load, this is a big problem for multi-chamber cylinders.

In order to test that the performance decrease is due to mass change another test was conducted, but with a constant load of 200 kg. The results can be seen in Fig. 5.5 and Fig. 5.6. The tracking error is reduced but the problem is not completely removed, since there is still an increased error from time 40 s to 70 s. It is assumed that the reason for the error is that the equivalent mass seen by the cylinder has changed significantly at this point of greatest extension of the crane.

The energy used by Cylinder 1 and Cylinder 2 to follow the trajectory have been summed for the two multi-chamber cylinder controllers and for

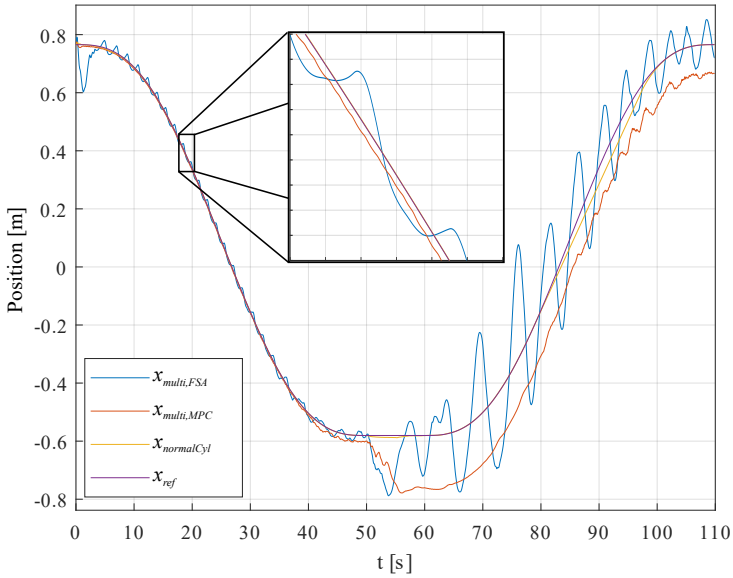

Figure 5.3: Tracking results of Cylinder 1 with a changing load.

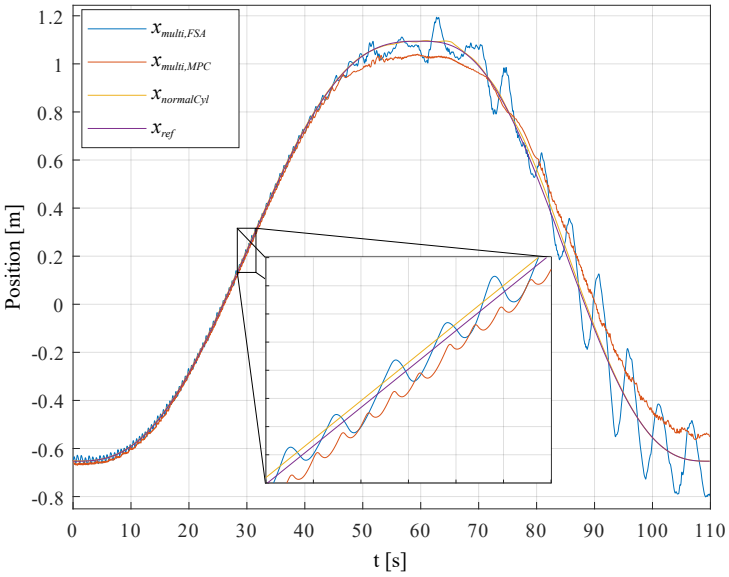

Figure 5.4: Tracking results of Cylinder 2 with a changing load.

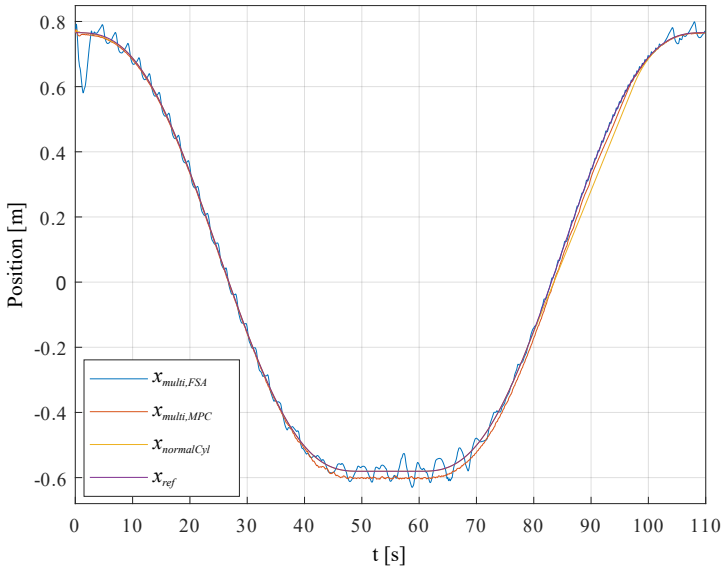

Figure 5.5: Tracking results of Cylinder 1 with a constant load.

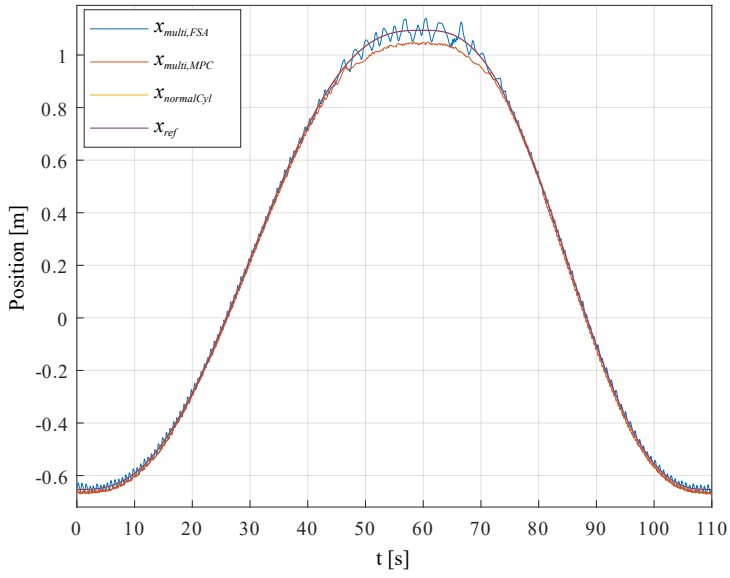

Figure 5.6: Tracking results of Cylinder 2 with a constant load.

the load sensing system. The results for the changing load can be seen in Fig. 5.7 and the results with the constant load can be seen in Fig. 5.8. When the load is constant both the FSA and the MPC consume less energy than the LS system, though for the FSA the difference is not large. Tuning the force controller in the FSA harder produced better tracking results, but increased energy use above the LS system even in the constant load case. Since multi-chamber cylinders are primarily considered due to their energy efficiency this tuning was discarded.

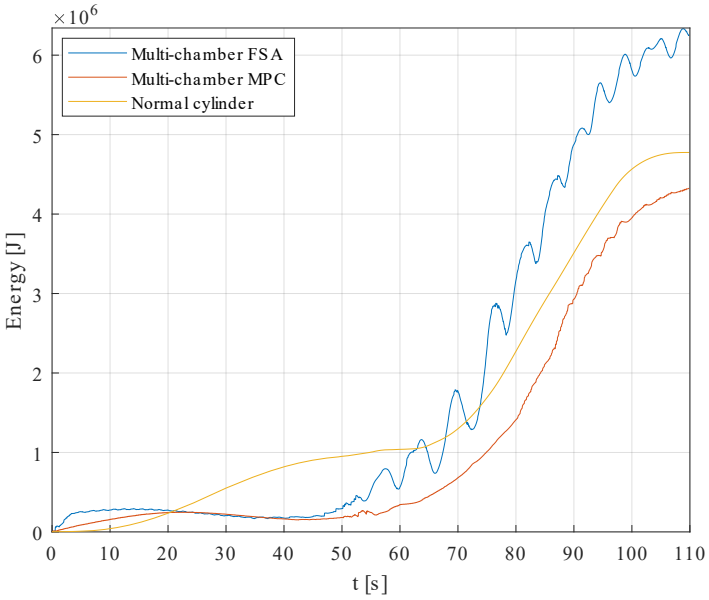

Figure 5.7: Energy used by the system if changing load.

The results from this paper confirmed that MPC control can give better performance than DFC. The results also showed that multi-chamber cylinder are not robust to system parameter changes. The large steady state error for the MPC case lead to research into MPC with integral action in paper D and a sensitivity study in paper E.

5.2 Seesaw results

This section presents the results obtained with the seesaw test-bench described in chapter 3. The results shown concern fault tolerance and model verification obtained in paper D. Results for integral action MPC, algorithm performance and MPC sensitivity to parameter changes are obtained in paper E.

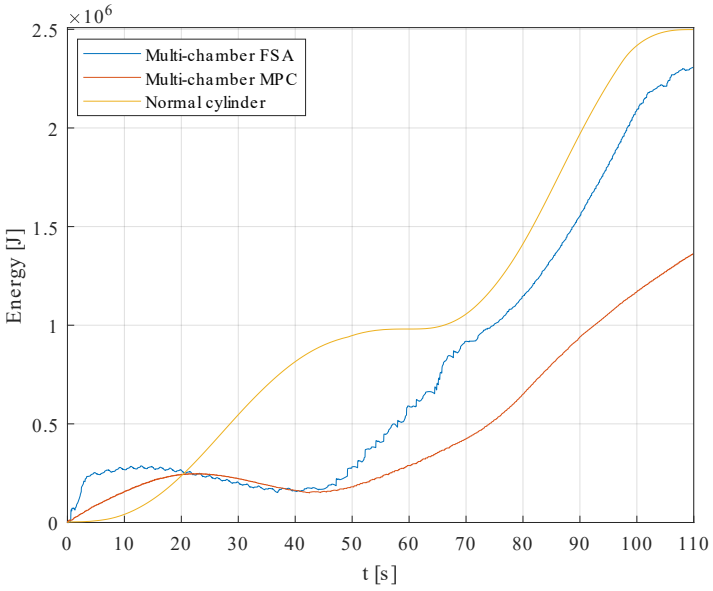

Figure 5.8: Energy used by the system if constant load.

5.2.1 Trajectories

Two trajectories have been used in the various tests in papers D and E. The trapezoid trajectory seen in Fig. 5.9 has been used in many papers. This allows for easy comparison of energy consumption results. The other trajectory used specifically in the sensitivity analysis in paper E is a sine trajectory seen in Fig. 5.10. The sinewave trajectory is necessary, because when a Fast Fourier Transform is applied to it, it will appear in the results as a single easily identifiable spike.

5.2.2 Total harmonic distortion analysis

The smoothness of motion of digital hydraulic linear actuation has been of great importance since the very beginning of the field of study. The switching events associated with the control of multi-chamber cylinders result in vibrations. Common conjectures are that increased mass and better control can result in smoother motion. This is difficult to determine, because no attempts have been made to quantify what smooth motion means. The standard is to take the root mean square of the position error signal. This is not necessarily always the truth as was shown in paper B. Different switching patterns can result in very similar numbers. Furthermore, a larger number can also indicate the the position is lagging behind the reference. Compar-

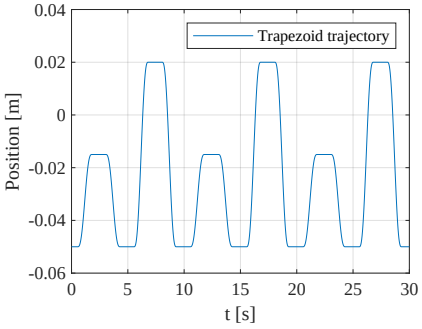

Figure 5.9: Trapezoid trajectory repeated three times

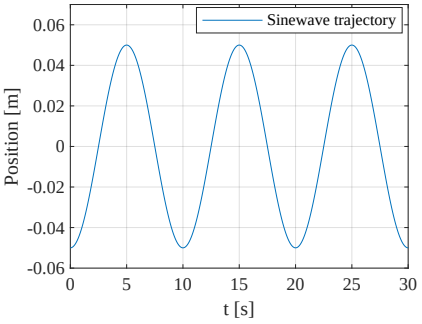

Figure 5.10: Sine-wave trajectory repeated three times

ing results from different papers is also difficult, because longer trajectories will naturally result in a larger accumulation of numbers. In paper E it was proposed to use the Total Harmonic Distortion (THD) measure. In electrical theory the measure reflects the ratio between the sum of powers of the harmonic components and the power of the fundamental frequency. In the paper E it was more specifically proposed that the THD+N or total harmonic distortion plus noise can be applied to the position signal in order to establish a qualitative measure of the distortions due to switching. The procedure used to calculate this THD was to take a Fast Fourier transform of the position, velocity, and force output signals of the cylinder. The single-sided amplitude spectrum of the position signal of a normal simulation run can be seen in Fig. 5.11. The sine wave reference appears as spike at 0.1 Hz. The distortion due to switching is too small to see in this plot. Looking at the FFT of the velocity signal in Fig. 5.12 it can be seen that the reference appears as a spike at 0.1 Hz, but now noise can be seen between 0.1 and 10 Hz. This is the distortion due to switching. Finally the analysis has been done on the force output of the cylinder and the result can be seen in Fig. 5.13. In the figure the constant load of 9000 N can be seen as a spike is at 0 Hz. Furthermore two harmonics appear around 8 Hz which is half the frequency of the controller. These harmonics then periodically repeat. In order to calculate the THD measure the following formula is used

$$THD = \frac{\sqrt{(\sum_{f=1}^{L} P_{pos}(f)^2) - \max(P_{pos}(f))^2}}{A_{ref,rms}} \tag{5.1}$$

where L is the length of the amplitude spectrum signal, $P_{pos}(f)$ is the value of the signal at frequency f, $\max(P_{pos}(f))$ is the maximum value of the signal which corresponds to the amplitude of the reference signal, and $A_{ref,rms}$ is the RMS value of the reference signal. The length of the signal is determined

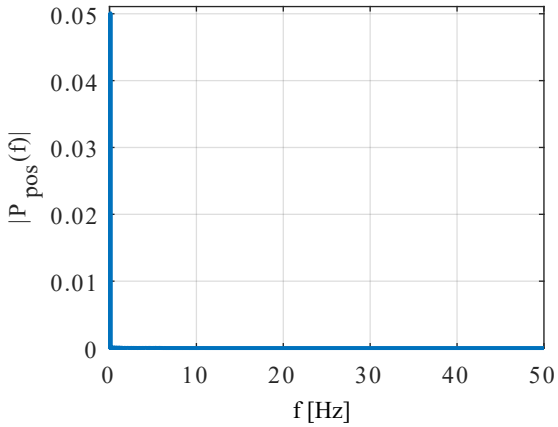

Figure 5.11: The single-sided amplitude spectrum of the position signal of a multi-chamber cylinder in the seesaw system.

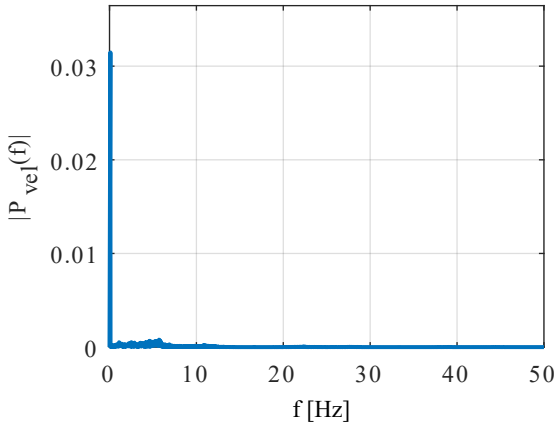

Figure 5.12: The single-sided amplitude spectrum of the velocity signal of a multi-chamber cylinder in the seesaw system..

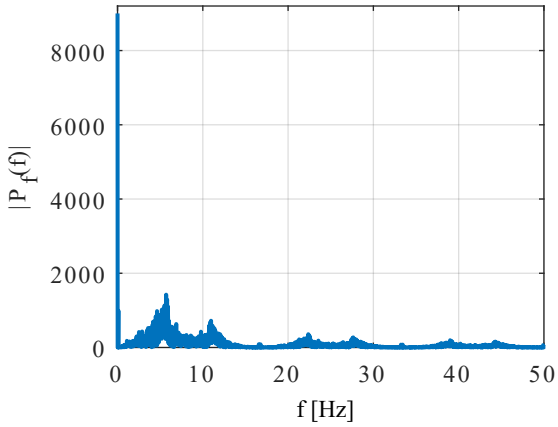

Figure 5.13: The single-sided amplitude spectrum of the force signal of a multi-chamber cylinder in the seesaw system..

by the sampling frequency and in this case all tests have been done with a sampling frequency of 10000 Hz. In table 5.3 the results of five tests are shown. The frequency of the reference signal is increased in each subsequent test, until the frequency is too high for the cylinder to follow. In the last case the THD becomes 48 %, because the cylinder cannot produce a force large enough to follow the reference. The length of the trajectory is always the same. It is determined as 3 periods of the sine wave. Slower frequencies result in longer simulations, which is why the RMS of position error is used. It can be seen that for faster trajectories the error increases, but the THD does not. Furthermore the energy use for the second test is much lower than for the first, but the total harmonic distortion has increased. From these tests it can be concluded that the THD is a better measure of the distortion in position tracking due to the constant switching of the controller. The normally used RMS of position error includes phase lag, so larger number do not necessarily mean more oscillatory behaviour of the cylinder. Energy measure alone is also not a good indicator, because different switching patterns can produce the same energy use as was shown in paper B. For this reason RMS of position error and THD are both used in the paper E.

5.2.3 Algorithm results

The algorithms presented in the previous chapter have been tested and the results are shown here. It is not clear what effect a small difference in the optimum will have when the optimization algorithm is used in the MPC controller. To investigate this full simulations were done with MPC based on

Table 5.3: Sine wave tracking of a multi-chamber cylinder in the seesaw system.

Sine freq [Hz]	Error sum [m]	Energy measure [J/mm]	THD [%]
0.1	0.0024	6.36	1.25
0.2	0.0047	2.66	1.79
0.4	0.0102	4.40	1.43
0.6	0.0171	8.02	4.99
0.8	0.0356	8.36	48.04

each optimization algorithm. The seesaw system was used for these simulations. The performance of the various algorithms has been tested in paper E. The cost of the minimum can be found in Fig. 5.14. The time it takes for these algorithms to find the minimum can be seen in Fig. 5.15. The x-axis in these figure represents different starting conditions for the algorithms. The tests are repeated five times and the results in the figures are the average.

From Fig. 5.15 it can be determined that the Mosek industrial solver and

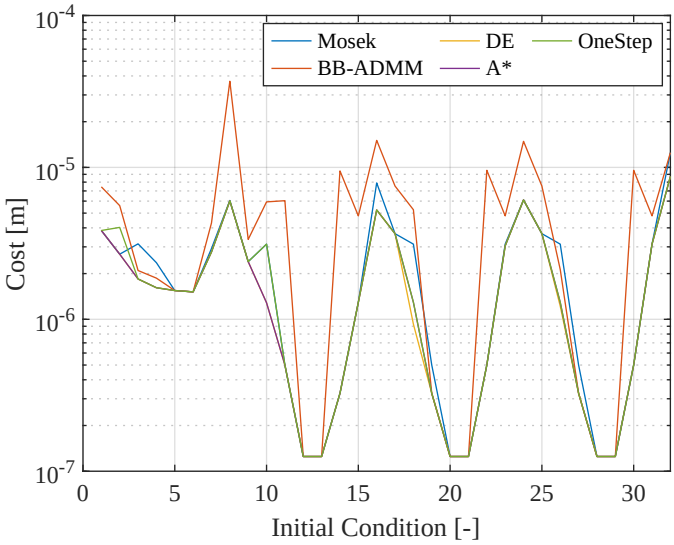

Figure 5.14: The value of the minimums found by the different algorithms

the BB-ADMM algorithms are the slowest to find an optimum. In the case of BB-ADMM the found optimum is very often not the global optimum, which is why the red line is above the others in Fig. 5.14. It was found that the ADMM part of the algorithm finds the same optimum as the Mosek solver if the integrality constraint is dropped. It can be concluded then that the poor performance is due to the branching rules. In this implementation the algorithm could not branch more than nine times. The initial choice of Lasso

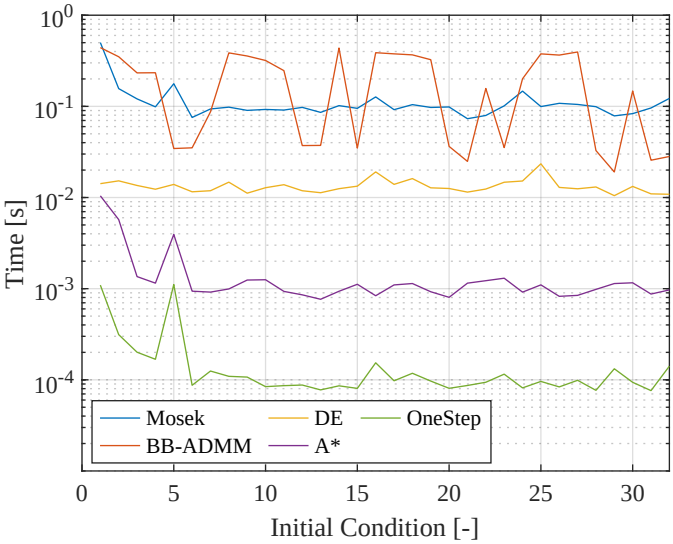

Figure 5.15: Time needed to find the minimum with different algorithms

cost function was made due to the sparsity which a 1-norm can introduce. Unfortunately it was found that when the MPC is tuned to follow a position trajectory with this accuracy the results of the ADMM are never sparse, so it is not possible to find an optimum with just two or three branches. This is due to the tuning parameter in the cost function reducing size of the 1-norm. All other algorithms produced similar optimums. As was previously stated, it is difficult to determine how the quality of the optimum affects the overall performance of the controller. After all the MPC calls the optimization algorithm once every 60 ms. Over a 30 s simulation small differences can add up. To see this effect the optimization algorithms have been tested on the non-linear model of the seesaw test bench with the trapezoid trajectory. The results can be seen in Tab. 5.4.

Table 5.4: Result for full simulation of the seesaw test bench with different optimization algorithms in the MPC.

	Accuracy [m]	Energy measure [J/mm]	Sim Time
BB-ADMM	0.00433±0	12.77±0	187.61±4.17
DE	0.00284±0.00003	5.35±0.29	56.61±2.44
A*	0.00283±0	5.55±0	42.82±0.68
OneStep	0.00283±0	5.55±0	37.56±0.20

The DE algorithm produces fast result and the best optimum. It also is the only algorithm which is stochastic in nature, so there is a variance to

its results. This can be seen in Tab. 5.4 by the fact that it is the only algorithm which has variations in its accuracy and energy measure results. The A* search algorithm produces good results and is the second fastest. Unfortunately it can be seen that in its current implementation it operates as the OneStep algorithm. This is to say that at each time step it chooses the same force level as it chose at the first time step. The A* in its original implementation where the cost vector grows at each time step, could find better minimum, but it was also significantly slower. Due to the similar optimums found in Tab. 5.4 it can be concluded that the OneStep algorithm, which can be considered almost a Model Based control, can be considered sufficient to use for these short time horizons.

A figure of the position, velocity, pressures and force obtained from a simulation with the MPC controller and the DE algorithm can be seen in Fig. 5.16.

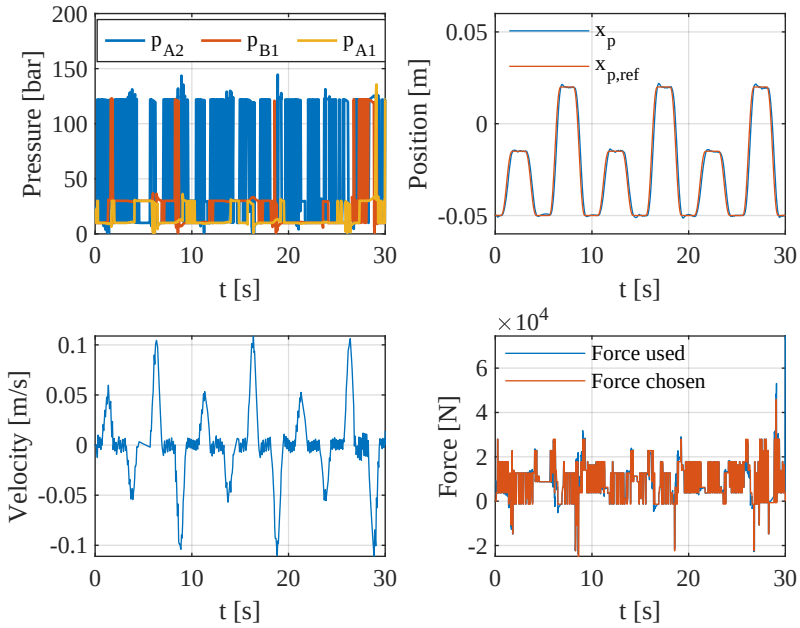

Figure 5.16: Simulation of the seesaw system with the DE algorithm.

The top left sub-plot in Fig. 5.16 illustrates that the pressure in chamber A_2 is changed most often as indicated by the blue line. This is the case because the mid-pressure line and the tuning of the controller were selected in way that allows the pressure in the other two chamber to be nearly constant, while the smallest chamber is being modulated to provide tracking. The

bottom right sub-plot shows how the actual force follows the theoretically chosen force. It can be seen that in certain cases the real force (blue color) jumps above the red force. This coincides with the change in pressure of the larger chambers in a similar fashion as in Fig. 4.4. It can be concluded that MPC together with a well chosen mid-pressure line reduces these kinds of pressure spikes compared with DFC, but sometimes the use of these dangerous switching combinations is unavoidable.

5.2.4 Neural network approximation

The results for using a neural network to approximate a MPC can be seen in this subsection. The trajectory used to gather data point for training was the trapezoid trajectory seen in Fig. 5.9. The results for position, velocity, chamber pressures and force can be seen in Fig. 5.17 The figure shows that the

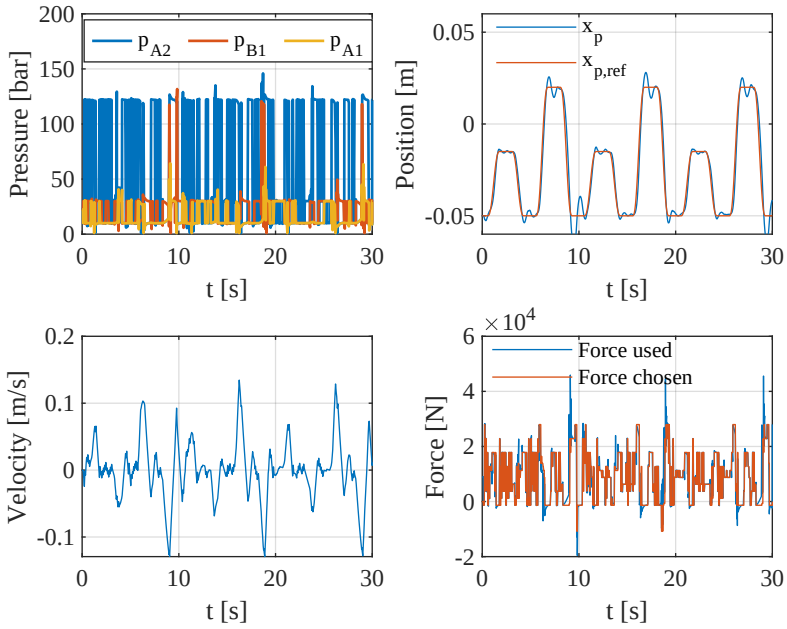

Figure 5.17: Simulation of the seesaw system with the neural network approximating the A* controller.

controller has suffered on position accuracy. Overshoot has appeared, where it is not evident when the training controller is used. It can be seen in Fig. 5.17 that the neural network uses high pressure in chamber B_1 at time 9.8 seconds. This is due to the problem discussed in chapter 4 - the neural network confuses forces which are close to each other. The force values can be close,

but the cost of switching can be very different. In this case the negative force chosen is costly, so the position error has to become large before a switch is possible. The error sum is 1016.24 m, which is an increase over the error sum of 839.46 m in Fig. 5.16. The energy measure for this simulation is 5.83 J/mm. This is an improvement on the 7.44 J/mm of the training controller. Finally the simulation time is 156.37 seconds. This is not a reduction over the training controller, a possible reason for this is the Matlab implementation of neuron activation function, which was not profiled and optimized for fast execution. Overall it can be concluded that the neural network has not approximated the training controller in a satisfactory manner due to the large position error.

5.2.5 Laboratory results

A simulation of the seesaw test bench was created in paper D as was mentioned in the systems section. The simulation was verified with the real test bench. The results are presented here.

Comparison

It was very difficult to verify that the simulation data agrees to a high degree with the measured data. In order to determine how well the simulation reflects reality two tests were conducted. In the first test the multi-chamber cylinder is considered fault free. In the second it is considered that a fault between the high-pressure line and chamber A2 is introduced, which corresponds to fault p_s to A_2 in section 4.2.5. The comparison between simulation and experiment can be see in Fig. 5.18. The results for the second case can be seen in Fig. 5.19.

The results do not agree very well especially in energy use. It was found that the pressure line in the laboratory drain much faster than in the simulation. Trying to fit the models by varying the opening time and delay of the valves, and the time constant of the accumulators produced some improvement in result, but no perfect agreement was found. The controller follows the trajectory better when a fault is introduced, because the large overshoot at the top of the trapezoid trajectory is reduced and the delay before the downward motion is also removed. This implied that an actual fault is present in the valves and using different force levels avoids those broken valves. The valves were tested individually when the test bench was being prepared and no faults were present. After the test were conducted and the paper was published, the valves were tested again and it was found that a fault was present in the valve connected to chamber B_1. This is the reason why the cylinder overshoots at the top of the trapezoid trajectory. The motion of the cylinder needs to be stopped, so the controller applies a negative force. This

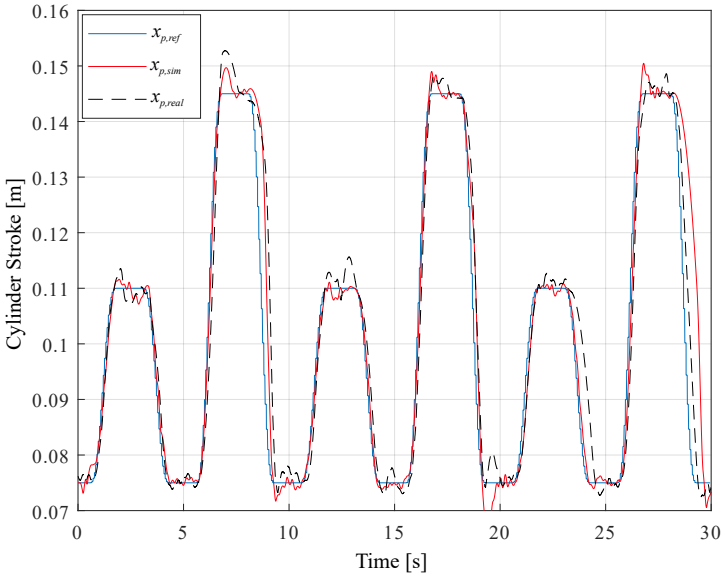

Figure 5.18: Comparison of laboratory and simulated results without fault

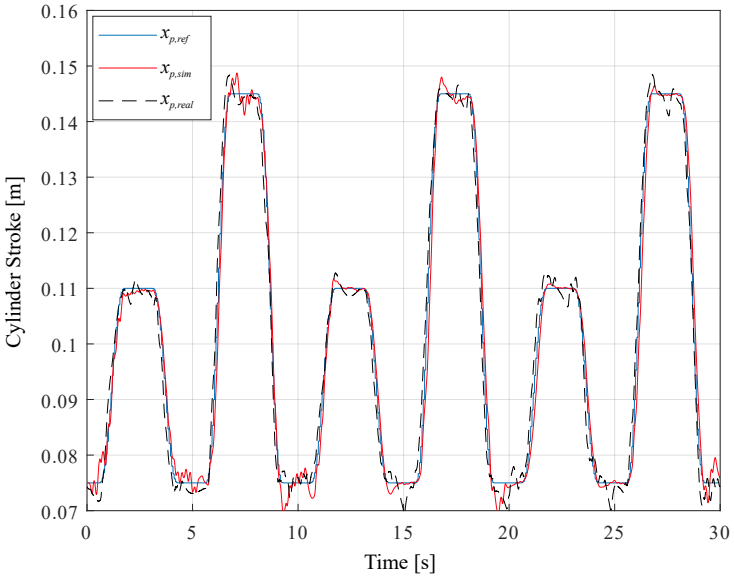

Figure 5.19: Comparison of laboratory and simulated results with fault p_s to A_2

requires that pressure be changed in chamber B_1. The force shift is not delivered on time and the cylinder overshoots the trajectory. A similar thing happens when the downward motion starts - the controller gives a negative force command, but this is not deliver on time. At the time of publishing of paper D this was not known and so it was attempted to make the simulation agree with reality by changing simulation parameters. Increasing the valve opening delay by 5 ms and increasing the closing time by 2 ms on the valves brought the simulation closest to the real results. Specifically it produced the overshoot seen on the upward slope of the 0.07 m trapezoid shapes and the downward slope of the same shape as seen in Fig. 5.18.

Having valves which close slower means that at some point multiple valves are open to the same chamber which wastes energy. This short circuiting of pressure lines can explain some of the poor energy consumption results, but it cannot be concluded that this is the sole reason. In order to investigate which other factors can cause multi-chamber cylinders to produce poor results a sensitivity analysis was conducted in paper E. Considering the results of the sensitivity analysis it can be concluded that the software delay and the low noise estimation frequency also contributed to the poor laboratory results.

5.2.6 Sensitivity analysis

This sensitivity analysis was inspired by the poor laboratory results obtained in paper E. The parameters which were investigated are equivalent mass, software delays, noise and velocity estimation, and supply pressure. Each parameter was varied in both directions until a poor results was obtained or the variation becomes so big that it becomes absurd. A vector of 50 values is then generated between these outer points. For each of these values a simulation is conducted with the MPC controller and the A* algorithm. All results were normalized with the results from a standard run. Only one parameter was varied at a time. The results for the change in position accuracy can be seen in Fig. 5.20. The results for the change in THD can be seen in Fig. 5.21. These are box plots. A box is shown for each experiment. The red line inside the box shows the median for the 50 results. The blue box shows between which values does 50 % of the data falls. The vertical lines above and below the box show the minimum and maximum results. The red dots represent outliers in the data. Due to limited space some of the names for the tests are abbreviated. The column "m known" refers to tests where the mass of the system is varied and the real value is given to the controller. When this is the case the model in the MPC matches the system. The column "m unknown" refers to a test where the mass of the system is varied, but the correct value is not given to the controller. Instead the model in the MPC has a constant mass of 50 ton. "Est freq" is a test where a velocity measurement is not available so

the cylinders velocity is estimated as in paper D. "Pos noise" and "vel noise" refer to test where position noise and velocity noise respectively are added to the measurements signals. The results in these plots are normalized, so values closer to 1 indicate that the system is not sensitive to changes in this parameter.

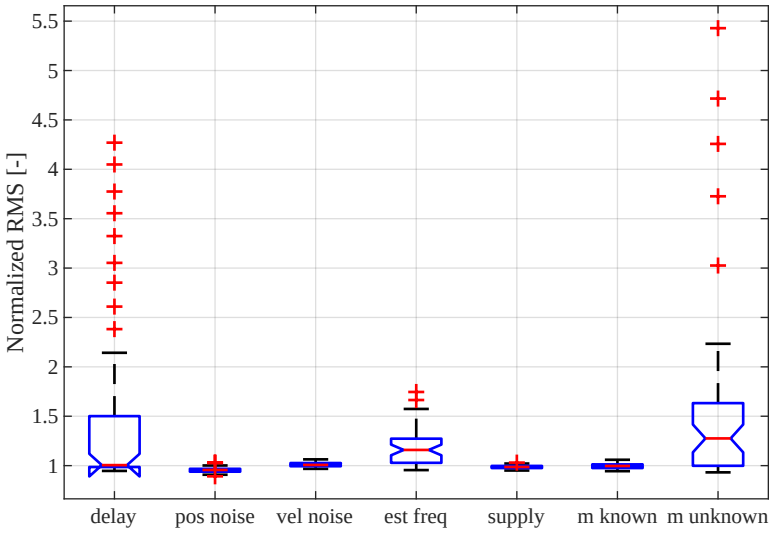

Figure 5.20: Collected result for accuracy.

It can be seen that some parameters produce larger variations. The results for changing mass, system delays and noise estimation frequency produces the largest variation in result. It can be concluded that the system is sensitive to these parameters. These results will be presented here as they are more important. The rest of the results can be seen in paper E. From the difference is scale in Fig. 5.20 and Fig. 5.20 it can be concluded that RMS sum of position error changes significantly less than THD. This means that the integral action of the MPC works and position accuracy is maintained at the cost of control effort. Larger control effort can be linked to larger energy consumption, but it is not guaranteed as seen in Tab. 5.3, where changes in energy use were present without increases in control effort.

Changing mass

In order to test how the controller reacts to a change in load mass, this parameter has been varied from 25 ton to 100 ton. In Fig. 5.22 the mass is varied, but the controller uses only 50 ton. In Fig. 5.23. It can be seen that

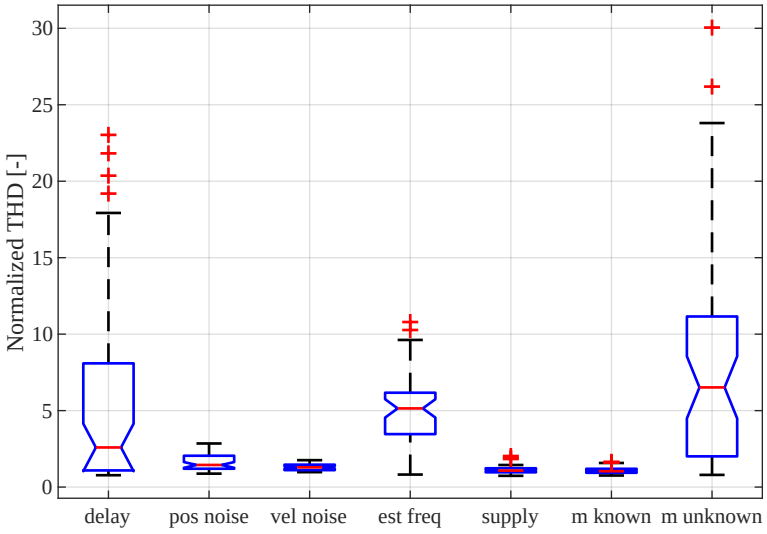

Figure 5.21: Collected result for THD.

reducing mass below 40 ton increases error significantly. On the other hand the position error and THD of the system does not change significantly when the controller is provided with the correct value.

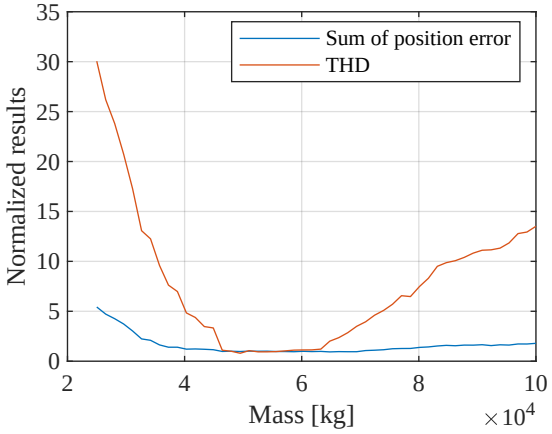

Figure 5.22: Result from varying mass without providing the controller the correct value.

Multi-chamber cylinders have been known to work poorly with low system inertia. It can be seen in Fig. 5.23 that performance remains consistent if

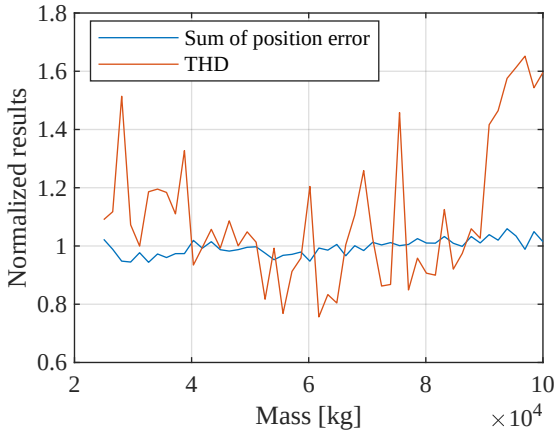

Figure 5.23: Result from varying mass and providing the controller the correct value.

the model parameters are known. It is true that at masses below 15 ton, the system stops being stable. This can be attributed to the fact that as system inertia decreases, natural frequency increases. The controller should also work at a higher frequency in order to keep the system stable. It is not possible to increase the frequency of the controller in this case, because the time necessary to switch force level, should be smaller than the controller sampling time. In this case the on/off valves requires 15 ms to close or open. One valve needs to be fully closed before a second can be opened. It was assumed that spool travel time is only 5 of the 15 ms and the other 10 ms are current build up and delay. It would then be possible to give a close signal to one valve and 5 ms later an open signal to another valve. Both valves would switch state in 20 ms and they are not connected to the same chamber at the same time. After the valves have switched state, the pressure dynamics require another 15-20 ms for the pressure in the chamber to reach its new desired value. These limitation require that the controller sampling time is not smaller than 40 ms. These factors prevent the system from working with less than 15 ton. Faster valves, smaller chambers and appropriately tuned force levels can enable multi-chamber cylinders to work with smaller system inertias. Referring back to the problem laid out in section 5.1.2, when a crane equipped with multi-chamber cylinder controlled by integral action MPC picks up a large unknown mass, the integral action MPC will compensate for the position error, but the control effort will increase. This can concluded from Fig. 5.22, where increasing the test mass increases THD, while position error remains relatively unchanged.

Software delays

The system delays have a large effect on the performance of the controller. In this case delays are all the delays between the controller starting a computation and the pressure in the cylinders chambers changing. This includes computation delays, software delays, and valve delays. These delays are of a significant size compared with the sampling time of the model. In order to deal with them the output of the controller is further delayed. If the added delay together with the system delays perfectly match one sample of the controller, then these can be incorporated into the MPC. In this way the calculated force level changes in the real system and in the model at the same time. The delay compensation implemented in paper E and paper D is static and user chosen. The real delays are variable and unknown. In this study the representation of the software delay is varied, while the user chosen delay is kept constant at 30 ms. The results in Fig. 5.24 illustrate how the performance of the controller degrades when the real delays and the estimation of their size do not match. Delays between 25 ms and 35 ms do not result in increased error or increased control effort. This is because the delay compensation is set to 30 ms and the actual delays are another 30 ms which matches the controller sampling time of 60 ± 5 ms. Outside this area THD suffers first followed by position error. It can also be seen that assuming that the delays are smaller than they are in reality results in poorer performance compared with assuming that they are larger.

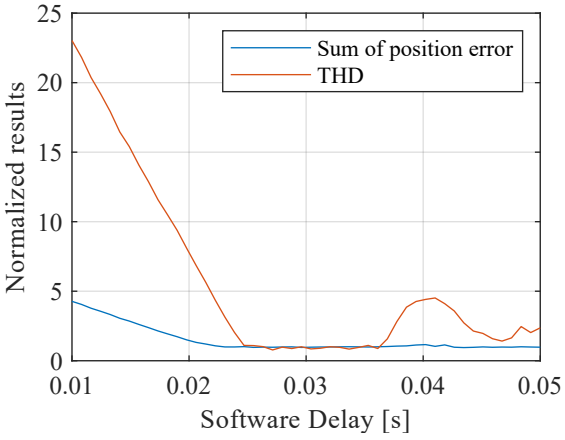

Figure 5.24: Result from varying software delays.

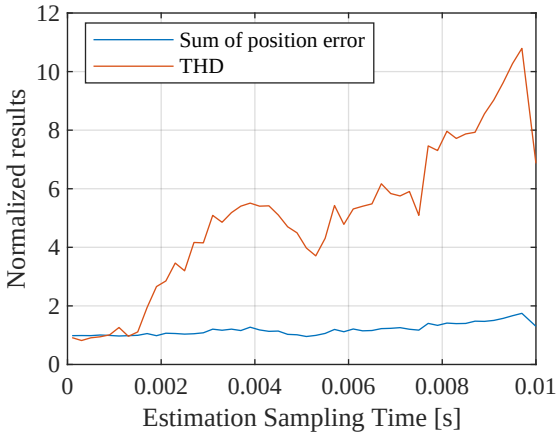

Figure 5.25: Result from varying the frequency of velocity estimation.

Velocity estimation frequency

In some cases a velocity measurement will not be available. This was the case in paper D. The velocity signal is necessary for the controller to work correctly, so a velocity was estimated from the available position measurement. For this test, the sampling time of the estimation process was varied from 0.1 ms to 10 ms and the results can be seen in Fig. 5.25. The results show that having a slow estimator results in large control effort as indicated by the increase in THD. The sampling time for the estimation in paper D was selected as 5 ms. According to this test the choice resulted in increased control effort.

Chapter 6

Conclusion

This thesis has focused on secondary control of multi-chamber cylinders. Three controller structures have been studied - Direct Force Control, Model Predictive Control and Model Predictive Control with integral action. Three different algorithms were implemented for solving the optimization problem of the Model Predictive Controllers - Differential Evolution, Branch and Bound based on the Alternating Direction Method of Multipliers, and A* algorithm. The performance of the three algorithms has been compared against the commercially available solver Mosek. The Model Predictive Controller with integral action using a Differential Evolution algorithm has been implemented and tested on a laboratory test bench. The fault tolerance of multi-chamber cylinder drives with respect to valves failing in an open or closed position has been tested. A fault tolerant controller based on the Model Predictive Controller with integral action has been implemented. Finally a sensitivity study has been performed to investigate which parameters have the most adverse effects on the performance of a multi-chamber cylinder controlled with a model predictive controller.

6.1 Answering the research questions

Conducting these tasks has focused on answering the research questions posed in chapter 2.3.

> *What performance may be expected if multi-chamber cylinders are used for the control of systems with large inertias like cranes?*

It has been found that under controlled conditions, such as known load, known trajectory and optimized pressure levels, multi-chamber cylinders have the possibility to greatly improve the energy efficiency of low-speed, high-force applications such as cranes compared to a Load Sensing system.

However, when the conditions mentioned before change either position tracking, energy efficiency or both suffer. In some cases the position tracking of the multi-chamber cylinder can be ensured by using Model Predictive Control with integral action, but this reduces the energy efficiency of the system.

The oscillatory motion of the multi-chamber cylinder can be quantified better with a Total Harmonic Distortion value than with a Root Mean Square of the position error signal. The first one describes the ratio between a trajectory signal and the oscillations due to switching, while the Root Mean Square of position error is comprised of all errors including phase lag in tracking. In order to reduce oscillations in motion and improve energy efficiency the force resolution can be manipulated by changing pressure levels instead of adding more pressure rails or using cylinders with more chambers. A simple analytical method is proposed for choosing the pressure levels if a force trajectory is available.

The commonly held opinion is that multi-chamber cylinders cannot work with small inertias because the inertia is unable to filter the oscillations due to switching. This has been found not to be completely correct. The oscillations can be reduced by manipulating the force resolution, but the stability of the system depends on the amount of time it takes for a force shift to happen. In order to use a smaller mass - faster valves and smaller chambers are needed together with appropriately selected pressure levels.

How robust are multi-chamber cylinder drives with respect to valve faults?

Multi-chamber cylinder drives are found to be robust to valve faults, because of the redundancy in valve system. Even without additional control structures certain faults do not significantly affect the performance of the drive, specifically valves failing in a closed position are less dangerous. Valves failing in an open position have a much larger effect on the available force resolution and were thus found to be more dangerous. In both cases, after the faulty valve is identified adding a single matrix to the cost function of the controller recovered position tracking performance in most cases. This happens at the cost of increased energy use.

Which system parameters (inertia, noise, etc.) are important to multi-chamber cylinder performance?

It was found that system delays such as valve delay, computation delay, pressure dynamics, and variations in the mass of the system have the greatest effect on multi-chamber cylinder performance. In the laboratory test a velocity feedback was obtained from the available position measurement and this was found to be feasible, but the system is sensitive to the frequency at which this estimation is done. Also, the system was found not to be sensitive to noise on the velocity measurement when that is available. The system was found not to be sensitive to changes in the levels of the pressure rails.

How do different optimization algorithms affect the performance of model predictive control applied to multi-chamber cylinders?

It was found that Model Predictive Control offers better performance than the simpler Direct Force Control. The complexity of the Model Predictive Controller can be mitigated by using a short prediction horizon of four steps which was used throughout the project. The A* algorithm can be used to find a local minimum much faster than the Differential Evolution algorithm without compromising the performance of the controller.

6.2 Future Work

The following tasks are proposed as future work:

- The system should be implemented, validated and evaluated on a real crane with particular interest on the trajectory generation for the Model Predictive Controller.
- Research should be devoted to finding ways to retrofit existing offshore systems. Many cranes have multiple differential cylinders working in parallel and are supplied by a constant pressure rail system. Utilizing some of these already available components can reduce the initial investment required from multi-chamber cylinder systems. The task is not straight forward, because for instance the crane structure has limitations on how the cylinders can be used. Space limitations, transmission line effects and other considerations will have to be taken into account on a system level.
- Pressure lines are an essential part of the secondary control of a multi-chamber cylinder, but not a lot of attention is devoted on how to create and balance these pressure lines on large applications.
- A more concentrated effort should be devoted to the use of neural networks in the approximation of a Model Predictive Controller. The machine learning field is showing good results in the control of autonomously driven vehicles and the automation of mining tasks. It can be expected that this will extend to other areas of industry.
- The Model Predictive Control in this thesis focused on switching between force levels. Model Predictive Control has also been used to control the pressures in the cylinder's chambers during this transition. The two controllers can be used at the same time. This makes the system exhibit both continuous and discrete behaviour. Systems of this type are called hybrid systems and there is a field of research devoted

to analyzing and controlling them. Tools and methods from this field could perhaps give improved results.

Part IV

Papers

Paper A

Digital Hydraulic Technology for Linear Actuation: A state of the art review

Viktor Donkov, Torben Ole Andersen, Matti Linjama, Morten Kjeld Ebbesen

This paper has been submitted for publication in
International Journal of Fluid Power, 2020.
It received a decision of Revisions Required on 15.09.2020.
The paper has been resubmitted on 16.09.2020.

Digital Hydraulic Technology for Linear Actuation: A state of the art review

Viktor Donkov[1], Torben Ole Andersen[1], Matti Linjama[2], Morten Kjeld Ebbesen[3]

1 Aalborg University, Aalborg, Denmark, vhd@et.aau.dk

2 Tampere University of Technology, Tampere, Finland

3 University of Agder, Grimstad, Norway

Abstract.

This paper analyses the current state of the art in linear actuation with digital hydraulics. Based on the differences in their aims the paper partitions the area into four actuation concepts - parallel valve solutions, single switching valve solutions, multi-chamber cylinders, and multi-pressure cylinders. The concepts will be evaluated on accuracy and smoothness of motion, switching load, reliability, efficiency and the number of components required.

Keywords. State of the art, Digital hydraulics, Switching valves

1. INTRODUCTION

Hydraulic systems are a popular actuation solution in a number of industries. The high force-to-size ratio is the main reason for their popularity. Applications intended to move large masses (e.g. lifting mechanisms, digging machines) or to work with hard materials (e.g. steel rolling, paper mills, some drilling applications) are areas where hydraulics is and has been an attractive solution.

Unfortunately, the overall efficiency of the hydraulic systems can be low depending on the work area; part loading situations can be especially problematic. The cost of energy has been increasing as the world tries to move towards greener solutions and this puts pressure on traditional hydraulics to evolve. Digital hydraulics is one of the fields concerned with improving the energy efficiency and reliability of traditional hydraulics [1], [2]. The field has been growing and the theoretical work dominating the field until now is starting to produce commercially viable results.

It is important to note that for the purposes of this paper the field of digital hydraulics does not refer to concepts in which digital sensors are used in standard systems i.e. electronic

load-sensing. It also does not refer to the digitization trend associated with Industry 4.0 or the Internet of things. In this paper digital hydraulics is the field of study in which hydraulic components (most often valves) are either turned on or off (opened or closed). This on/off nature is the digital part of digital hydraulics.

In fact, in recent years several digital hydraulic solutions have successfully been implemented in industrial applications [3]. In [3] Winkler et al. mention that a micro-positioning system for milling machines for Daimler has been working since 2014; a gap control solution for paper mills was successfully brought to market by Valmet [3]; and a digital hydraulic tilting system for the Finish Pendolino trains was introduced in 2015 [3]. The company Valmet has published a document in which they claim that digital hydraulics can reduce lost profit due to reliability by up to 35000 EUR per year [4]. The most widely cited state of the art paper in digital hydraulics was published in 2011 [5], but since then the field has changed considerably. This is the reason for making this new state of the art paper.

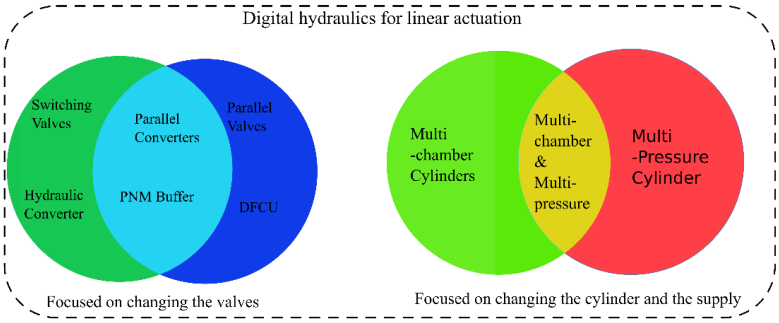

Figure 1 Digital Hydraulic fields and their overlap

The papers have been divided into four actuation concepts, but the different concepts overlap as seen in Figure 1. The proposed division is based on the changes on the system level. The first two areas focus primarily on changing the valve system between a traditional cylinder and its pressure supply. Section 2 discusses solutions in which a proportional valve can be exchanged with a number of parallel on/off valves. Section 3 contains papers in which a single on/off is used to modulate the flow. The other two sections focus on changing the actuator and/or the pressure supply. In section 4 cylinders with multiple pressure lines will be discussed and section 5 contains papers which tackle multi-chamber cylinders. In each section, subsections are devoted to the concept itself, to the key results of the papers, and to a discussion evaluating the concept. The Concept and Discussion subsections offer a bird's eye view for a reader unfamiliar with the field of digital hydraulics. The papers listed in the Papers section can be used as an index by a reader experienced in the concepts or interested in more details. Each discussion subsection will focus on evaluating the digital hydraulic concept according to accuracy, switching load, reliability, efficiency and the number of components required.

2. PARALLEL VALVE FLOW CONTROL

2.1. Concept

The idea behind the parallel valve flow control concept is to use several on/off valves - of either the same or different sizes - connected in parallel in order to simulate a variable orifice. Opening specific valves varies the cumulative opening area of the flow path. One of these variable orifices is usually called a Digital Flow Control Unit (DFCU).

One idea behind using flow control units is to arrange four of them as seen in Figure 2. Each flow control unit can allow or restrict the flow between one chamber and one flow source. If a specific flow requirement coincides with a valve opening combination, no continuous switching is required. On the other hand, if the required flow falls between two combinations, the valves need to be switched between the two flow steps in order to achieve the average flow. This leads to a trade-off between tracking accuracy and control effort that needs to be managed. The combination of four DFCUs to simulate a proportional valve has been called a Digital Independent Metering Valve (D-IMV). Controlling each DFCU separately can lead to improved efficiency due to the independent metering of the forward and return flows.

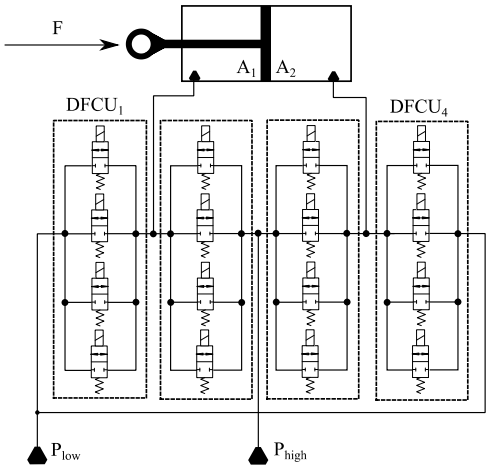

Figure 2 D-IMV concept built from 4 DFCUs

A comparison between the flow capacity of an example DFCU with 4 binary coded valves and 4 equally coded valves can be seen in Figure 3. In order for both DFCUs to have the same maximum flow capacity, the binary coded sizes are 1:2:4:8, while the equally coded valves all have size 3.75. The total area is 15 in both cases, when all the valves are open, but the equally coded DFCU's resolution is worse. Therefore, in order to get the same resolution, the equal sized valves should be 15 with a relative size of 1. The disadvantage is obviously using more valves, but the benefit is that all valves have the same properties and it does not matter which one is opened or closed. In comparison, the binary coded DFCU

achieves the same resolution with fewer valves, but the drawback is that more dangerous switching events can happen. Dangerous use in this sense is when for instance changing from combination 7 to combination 8 requires that the valves with areas 1, 2, and 4 are closed and the valve area 8 is opened. Due to unknown delays and valve dynamics, a small time period is present when all valves could be closed or all valves could be open. This results in rapid flow changes.

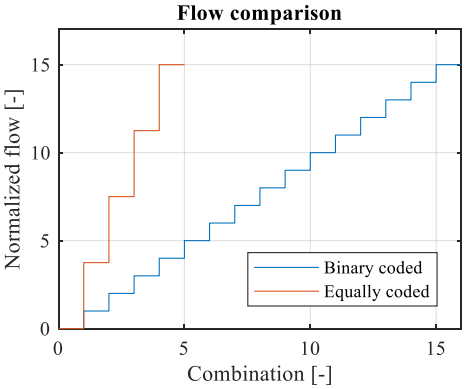

Figure 3 Binary coded vs Equally coded 4 bit valve flows

Model-based control has been a good way to decide which valves should be opened to follow a specific velocity reference. Papers in Subsection 2.2.1 deal with this subject. As mentioned in the introduction, there is some overlap with other fields and attempts to improve the resolution through Pulse Width Modulation (PWM) have been made. These papers are collected in Subsection 2.2.2. Some interesting papers dealing with reliability and fault detection among other things are described in Subsection 2.2.3.

2.2. Papers

2.2.1. Model-based control

Papers [6], [7], [8] and [9] are some of the first developments by Linjama et al. in controlling a cylinder with DFCU's. In the four mentioned papers 4 DFCU units are used to define 4 flow directions. Each cylinder chamber can be connected to the pressure supply or to the tank similar to the architecture in Figure 2. The block diagram of the controller can be seen in Figure 4. In these papers only one DFCU can be opened per chamber. The flow through a DFCU can be calculated analytically using the orifice equation. This is the model part of the model based controller. The major issue is controllability at low velocities. This was researched in [10] and [11].

In [10] and [11], the authors allowed three of the DFCU's to be active at a time. This allows a chamber to be connected to the supply and the tank at the same time. The inclusion improves controllability at low velocities at the cost of energy efficiency. Furthermore when the chamber is connected to two pressures through two different orifices the final pressure in the chamber cannot be calculated analytically any more. Instead, a numerical solution has

to be found for each combination. The method uses Newton-Raphson iterations to find the steady state solutions to the systems equations. The system has 20 valves with two states each, which results in 10^6 possible state combinations. To implement the controller in real time, the search area is reduced by analysing the flow balance of each chamber separately by first only considering two active DFCU's. In this way, the state equations still have an analytical solution and a control combination can be selected. The combinations involving three active DFCU's, which are in the vicinity of this combination, are then solved numerically using the Newton-Rhapson method. Further research has iterated upon this basic structure. The papers presented in this subsection are mainly concerned with the robustness of the controller, the computational complexity and accuracy of the valve model used in the model based controller, or obtaining laboratory results.

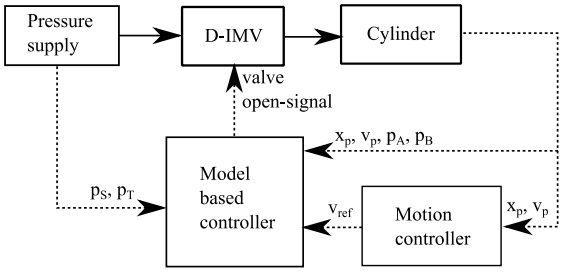

Figure 4 Model based DFCU controller

In [12], Siivonen et al. implemented the DFCU control method from [11] in a mobile hydraulic mining application. Instead of the normal square root of the pressure difference used in the orifice equation, a general power exponent is used. This power exponent is a tuning parameter for each valve and was found experimentally in laboratory conditions. The control structure was then tuned based on these results. The authors of [12] then tested the system outside of laboratory conditions and found that due to the change in operating conditions the control performance was reduced.

In [13], [14], [15], and [16] Linjama et al. try to design a more robust motion controller through robust design and mixed sensitivity. According to the authors in [13], the system was stable with 407 % increase in the load mass and a 50 % reduction in bulk modulus.

Several papers address the valve model used in the model based controller. The general exponent method describes DFCU flows better, but it is computationally intensive. In [17] Linjama et al. transform the system equations into scalar form and use Ridders' method to solve the equations faster. In [18], Linjama et al. present a new valve model based on third or fourth order polynomials. This also reduces the computation time.

In [19] and then in [20], Stauch et al. propose a new valve model, which can be inverted. The new model allows valves to be open one by one until the desired flow is reached. With this method no search algorithm iterations are needed. The method imposes that the valves are coded with a binary coding. The controller allows the position and force tracking to be

decoupled. If the position controller is prioritised, good position tracking is possible even with low inertia systems or poor DFCU resolutions.

Several papers focus on reducing the computation complexity of the controller without changing the valve model. In [21], Huova et al. investigate the possibility of decreasing the computational complexity of the controller established in [11]. The authors introduce a table-based switching cost, instead of the on-line search algorithm. The simplified controller runs 194 times faster. In [22], Ersfolk et al. implement the model based controller on a GPU. The computation time is reduced from 1350 ms on a sequential ARM processor to 7.19 ms on the GPU.

Several papers focus on implementing the control on a wheeled excavator. First, in [23] the system is designed using commercial components. The aim was to achieve a flow rate of up to 400 l/min. The DFCU had 4 control edges with 7 bits each. Four of the valves in each edge had orifices resulting in a binary coding for the first 5 bits as 1:2:4:8. Valves 6 and 7 are opened at the same time to give the 16 in the series 1:2:4:8:16. In [24] Ketonen et al. use this valve system to realise independent metering valve control with digital hydraulic valves on a 21-ton Volvo EW210C excavator through a simulation study. A grading cycle was followed and the results showed that the digital independent metering control could reduce energy consumption by 28-42 %. Finally, in [25] Ketonen et al. present the conversion of a Volvo EW210C wheeled excavator from a standard load sensing system into a digital hydraulic system with parallel connected on/off valves. The tests showed a 36 % reduction in input energy for a grading work cycle. The authors plan further modifications in order to improve the efficiency.

2.2.2. Introducing PWM in DFCU control

A major problem of DFCUs is that a low number of valves, results in poor flow resolution. Several authors have tackled the possibility of improving DFCU resolutions through introducing Pulse Width Modulation (PWM) into the control structure. In essence, if a valve is repeatedly closed and opened in such a way that during one control period it is only open for half of the time, then that valve has delivered approximately half the flow. The ratio dictating how much of the time should the valve be open is known as a duty cycle.

In [26] Huova et al. discuss this possibility. Inside the code, two of the valves are treated as 5 artificial ones with a binary coding. In essence, these two valves act like 10 binary coded valves. The DFCU has 4 valves, but acts like a DFCU with 12 valves. The largest artificial valve corresponds to a 50 % duty cycle of the real valve. The improved resolution resulted in a minimum achieved velocity of 1 mm/s from a maximum of 350 mm/s. This is a max/min velocity ratio of 350. The 4 bit DFCU proposed by [10] discussed in the previous section achieved a ratio of 50.

In [27] Paloniity et al. propose a similar scheme where pulse frequency modulation is used on one of the bits of the DFCU in order to achieve even smaller opening areas. Paloniity et al. report that the method is effective at improving controllability as the average error for a slow trajectory has been reduced by a factor of approximately 4 compared with just the Pulse Number Modulation (PNM) technique.

In [28] Paloniity et al. present a method for improving the resolution and the linearity of a digital hydraulic valve system using equal sized on/off valves. The improvement comes

from combining pulse width modulation and pulse frequency modulation into the control structure. All the valves in the DFCU are modulated, but it is done according to a circular buffer. In this buffer a valve is moved to the back of the buffer when it switches state. This ensures that the same valve is not actuated several times in a row, unless no other valves are available. In this way, according to the authors, PFM and PWM are combined and the result is a more equal distribution of the switching duty for the valves, and a wider range within which average flow is linearly proportional to the duty cycle. The method is tested in a laboratory experiment using a vertical differential cylinder with a mass load of 50 kg. Eight prototype valves are used in each of the two DFCUs. The maximum position error during the trajectory is reportedly below 0.2 mm. In comparison, the PNM method achieved 0.8 mm.

In [29] Siivonen et al. designed, simulated and tested a digital valve system for a water hydraulic system. The valve package consisted of 16 prototype on/off valves. The control method used is from [28]. After 60 days of testing Siivonen et al. state that despite some problems with the valves, performance was still good as the digital solution exceeded the application's accuracy requirements of 133 μm on the cylinder position. Furthermore it fit within the physical size limitations and had lower water cleanliness requirements.

2.2.3. Other papers

In [30] Siivonen et al. present a method for detecting and diagnosing faults. Only pressure and position measurements are needed to distinguish the faults. The procedure is simple, so it does not require a lot of computations, but it is based on a number of tests which are conducted while the cylinder is not following a trajectory. The procedure cannot be used on-line, which is a disadvantage.

In [31], Laamanen et al. discuss the possibility of reducing pressure peaks in the system due to actuation time uncertainty of the digital valves. The authors examine the possibility of including a weight on the more dangerous switching events. They also examine if the Fibonacci coding has better properties than the popular binary coding. The authors find that even though the dangerous switching events are avoided, the selected event can still exhibit the same property. For instance, when the flow should switch from valves 1, 2 and 3 open to just 4 open, the controller chooses 1 and 4 to be opened. They also find that Fibonacci sequence is theoretically better suited to avoid pressure peaks, due to the smaller steps between flow levels and the possibility of choosing different combinations with the same flow output.

Another benefit of DFCUs is that the components connected in parallel are naturally fault tolerant. As Siivonen et al. write in [32] the systems fault tolerance depends on the software and if faults can be detected online and the control structure is changed to reflect this, all digital hydraulics based on parallel valve combinations can have a degree of fault tolerance. A drawback to including fault tolerance is that the computation requirements are increased.

In [33] Lähteenmäki et al. and then later on Ketonnen et al. [34] make a pressure relief valve out of an DFCU through changing the control structure. The DFCU was made of 16 parallel connected equal sized on/off valves. The DFCU was compared to a standard pressure relief valve. The two valves showed similar performance on the test stand with the DFCU

achieving a smaller pressure peak. The authors point out that a different pressure relief valve could have performed better.

In [35] Huova et al propose a positioning method for a cylinder based on the on/off valves in a digital valve system realized with DFCUs. The method modulates the flow to one chamber at a time. Due to this the piston position changes by very small step sizes and achieves a position accuracy of ±1 µm. In order to achieve this small motion, the model of the valve and the model of the cylinder are used to calculate how much fluid a small opening pulse in one chamber would achieve. The experimental setup used is a symmetric cylinder connected to four DFCUs. The valve has an opening and closing time of 2 ms due to booster electronics. The initial error is 70 µm. The smallest bit executes a 6.3 ms pulse to reduce the error to 4 µm. A second pulse then brings the error down to 0.3 µm. The authors note that some practical limitations are present if the position overshoots and the controller has to move the cylinder in the other direction. This is due to the static friction force, which was not considered in the controller design.

2.3. Discussion

The conclusion based on this collection of papers is that DFCUs improve hydraulic efficiency only through independent metering control. The flow to each chamber is still throttled which is a major source of losses in hydraulics.

The position accuracy and smoothness of motion offered by the concept is on par or better than standard proportional valves because they are both based on throttling control. The major advantage of the concepts is the improved reliability. Since multiple components are actuated in parallel, malfunctions are not critical. The seat type valves used also reduce the sensitivity to oil cleanliness and leakages. Switching between flow levels does not need to happen continuously. Furthermore, some concepts are designed in such a way as to spread the switching load across all the valves. Overall, this is the digital hydraulic architecture that has the smallest switching load. Component-wise the change to multiple smaller, equally sized valves, that have simpler design can even be beneficial in some cases. In the reviewed papers, multiple experimental results show that it is possible to achieve good results with current valve technology, and it is ready to be implemented more widely, but it can be argued that the benefits are smaller due to the reliance on throttling control. It can also be noticed that a lot of the papers focus on computational complexity.

3. SINGLE VALVE SWITCHING CONTROL

3.1. Concept

Single valve switching control - an alternative digital hydraulics concept - is based on power electronics theory. Instead of using a proportional orifice open to a certain level, a single on/off valve is used. This valve is opened and closed rapidly in order to give an average flow over time using either PWM or Pulse Frequency Modulation (PFM). In this case, one valve is needed per flow path as seen in Figure 5. At this point, this can still be considered throttling control.

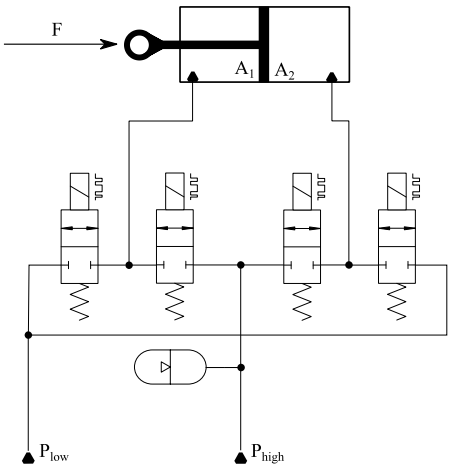

Figure 5 Concept for controlling a cylinder with switching valves

The idea of using modulation techniques in hydraulics comes down to a simple idea. If a valve can deliver a certain amount of flow in a certain amount of time, then keeping the valve open for a fraction of the time will mean it delivers a fraction of the flow. The inertia and compressibility of the hydraulic fluid, as well as the delay and travel time of the spool complicate this concept. A representation of a duty cycle can be seen in Figure 6. What models and methods to use in order to achieve the concept is a major question in the field.

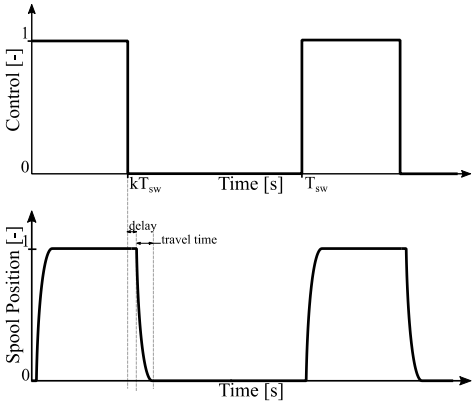

Figure 6 Representation of the concept of duty cycle

The concept can be further augmented by continuing the analogy between electrical systems and hydraulic system. The inertance of the fluid can act as inductance in the system and this can be increase by using long fluid lines. The compressibility of the fluid can act as capacitance. In such a way it can be possible to realise Buck or Boost converters in a hydraulic system. An illustration of the method can be seen in Figure 7. The concept allows the inertia of the fluid in the long hose to produce a localized pressure drop in front of the check valve. In this way the check valve opens and fluid can be drawn from the low pressure side. In the case of retraction, the same concept comes into play and return fluid can be forced back to the supply line. This improves efficiency and allows energy regeneration.

A benefit of these concepts is the possibility of achieving an average flow chosen by a duty cycle according to the well-known PWM technique. The flow resolution of a DFCU is limited by the number of available valves, while the flow resolution of a switching valve is limited by its switching frequency. With a high enough switching frequency the duty cycle can be considered a continuous input to the system. Switching valves have been introduced into DFCUs in order to improve flow resolution without increasing the number of valves.

A disadvantage of the concept is that the valve has to switch constantly in order to achieve any flow level different from the maximum. Furthermore, to achieve good control, the frequency of the valve should preferably exceed the natural frequency of the system by a factor of up to 20 as stated by Gradl et al. [36]. To offset this Gradl et al. proposed that several valves can be operated in parallel with a phase shift allowing higher frequencies to be achieved.

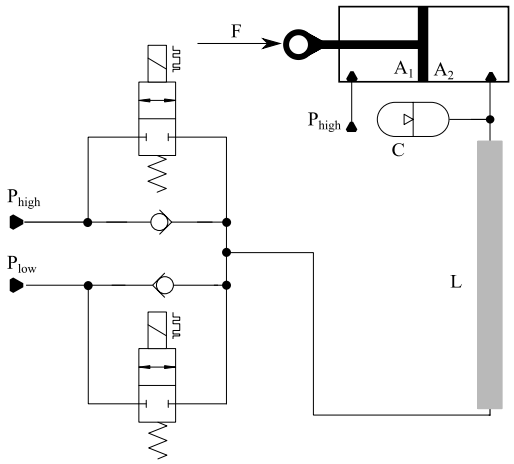

Figure 7 Concept for a Hydraulic Buck Converter (HBC)

The repeated opening and closing of the valves can lead to flow and pressure pulsations. The authors of [36] also propose that instead of modulating the width of the pulse, a specific pulse can be repeated leading to Pulse Count Modulation (PCM). In this way a pulse can be

designed such that for a specific system the second pulse removes the oscillations introduced by the first one. Another way to dampen the pulsations is to include an accumulator just before the cylinder as seen in Figure 7. This reduces pulsations, but it also increases the softness of the system. A softer system in this case means a reduce position tracking performance.

The HBC concept greatly benefits from valves, which can open and close very fast. This allows for higher control frequencies. The flow pulsations introduced in the system have less effect if the modulation frequency is high enough. Due to current valve technology limitations, valves have a minimum duty cycle, a maximum modulation frequency and other issues, which researchers are trying to address.

Papers discussing the concept in Figure 4 are described in Subsection 3.2.1. Papers discussing digital hydraulic converters are described in Subsection 3.2.2. The newest development of these concepts have moved into quite complicated control structures to take into account the non-linearity and softness of the system. Another research path has focused on designing converters using a linear model of the system and these papers are described in Subsection 3.2.3. Pressure pulsations have been identified as a major issue with switching control. Most papers in the other three subsections deal with the issue by introducing capacitive elements. In Subsection 3.2.4 active solutions to the pressure pulsations issue are discussed.

3.2. Papers

3.2.1. Replacing proportional valves with switching valves

In [37], Tsuchiya et al. investigate the possibility of PWM digital hydraulic control of a table actuated by hydraulic cylinders. The authors show that it is possible to increase the smoothness of the table's motion by changing the phase between the valve, which supplies flow to one chamber, and the valve which drains fluid from the other chamber.

In [38] Plöckinger et al. use the same test bench as in [26], but instead of using a mix of DFCU and PWM, they use PWM only. One valve was used for each of the four flow paths. The valves have a response time of 1.8 ms. In order to avoid ballistic operation of the valve, the minimum duty cycle of the valve was selected based on the PWM frequency. Thus higher frequencies resulted in larger minimum duty cycles. This corresponded to worse controllability at small velocities with high PWM frequencies (100 Hz) and better controllability with the lower PWM frequency (25 Hz). On the other hand, the pressure pulsations in the fluid decreased in size with increased PWM frequency i.e. 40 bar at 25 Hz to approximately 10 bar at 75 Hz.

In [39], Šimic et al. present the control of a differential cylinder with new digital piezo DPVL-2 valves. Each of the four flow paths has a valve controlled by PWM. The switching response of the time is below 0.3 ms for 100 % control signal. In order to achieve the fast response time of the valve it is actuated by four piezo elements. The fast valves resulted in improved overshoot and 15 % less energy consumed. Unfortunately, the valves are not commercially available.

3.2.2. Converters

In [40] Kogler et al. designed and tested a hydraulic buck converter. Two valves have been used as can be seen in Figure 7. A minimum duty cycle of 20 % and a maximum of 60 % has been selected at the 100 Hz PWM frequency. The converter charges and discharges an accumulator. The results are compared with those obtained from the same system controlled by a proportional valve. The hydraulic buck converter achieved a 34 % reduction in average energy consumption and no significant pressure ripple can be noticed in the measurements.

In [41] Kogler et al. present some further developments on the concept. They identify that the accumulator used to attenuate the pressure before the load introduces softness and non-linearity in the system, which prevents a simpler proportional (P) controller from achieving satisfactory performance. The authors then develop a Flatness Based Controller (FBC) in the second part of the publication [42]. The system can be transformed to a special class of flat system according to the authors. Kogler et al. develop a non-linear observer with a time varying observer gain in order to get full state feedback. The output of the flatness based controller is converted to a duty cycle from the static characteristics of the hydraulic buck converter. The sophisticated control technique allows the hydraulic converter to give the same positional accuracy as the system with the proportional valve and a P controller, but with significantly better efficiency.

In [43] the authors construct a test stand and test the concept. The results agree with the previous articles - the FBC is more accurate than the P controller and the HBC is more energy efficient than a conventional setup. Pressure oscillations are still a problem for the concept as can be seen in the measurements. This is despite the accumulator at the HBC output, which is meant to attenuate the pressure. Kogler et al. propose that much faster valves would solve the pressure pulsation problems and possibly make the accumulators obsolete, but for the time being, they will research the possibility of using several HBC in parallel.

In [44] Scheidl et al. present four cases in which digital fluid system are better solutions compared with the standard one. Two examples stand out: the control of a gap for rolling mills and the control of mould oscillations. Both of these systems already have low bandwidths making it easier to implement the solution.

In [45] Gradl et al. design and manufacture a stepper converter prototype. The converter is made out of two slave cylinders, which are controlled by fast switching valves. One slave cylinder steps up, meaning that the master cylinder is extended, and one steps down - doing the opposite. The paper also describes the design of a fast switching plate-type check valve and a combined hydrostatic hydrodynamic bearing. These were needed to improve the converter performance. Specifically an improvement in energy efficiency of approximately 15 % was seen due to these components. The energy efficiency compared with resistance control of the cylinder was reported as 30 % higher.

In [46] Lukachev et al. present the building of a prototype of an elementary hydraulic switching control drive concept for heavy load actuation. An analytical model of the transmission line and the cylinder itself is developed according to previous research, and it is further augmented to include the influence of the rod side chamber and the dead volume in the valve block. A laboratory experiment is prepared where a cylinder pushes a 1.5 ton mass. The valves used in the experiment are four Bosch Rexroth WES spool type on/off valves. There are four valves because each line has two valves in parallel. The extra valves

are used to increase the apparent switching frequency of the converter as it is seen by the cylinder. The PWM frequency is set to 200 Hz. The authors conclude that the tested switching control drive provided dynamics sufficient for rolling mill actuators and aim to implement the design in a real industrial application.

In [47] a gas-loaded accumulator is used in order to tune the dynamics of the system for a smooth behaviour of the drive. Two PWM valves drive a single acting ram with an attached weight of 500 kg. The accumulator reduces the natural frequency of the drive, so it can still achieve smooth motion even with the valve-imposed limitations on switching frequency. The authors compensate for the added softness with a passivity-based controller. A simulation is conducted in which the PWM frequency was set to 50 Hz. The movement of the cylinder appears to be smooth and the pressure ripple due to switching appears to be below 20 bar. Kogler at et al. mention that in the future experimental work will be done and the influence of line dynamics will be included.

3.2.3. Converter control based on linear models

The performance of hydraulic converters depends on the frequency of the system on which they are applied. Kogler et al. states in [48] that the hydraulic system contains non-linear components, which can make the analysis difficult in the frequency domain alone. The authors propose a mixed time-frequency domain model that needs to be solved iteratively in order to simulate the system with a high degree of accuracy.

De Negri et al. show in [49] and later in [50], that it is possible to use a linear model to predict the average value of the controlled pressure as well as the flow rate in several parts of the system. In [50] Nostrani et al. show the design process of a hydraulic step-down switching converter with considerations for the losses in the inertance tube and the switched valve. This is done through a steady state analysis. The results of the analysis are then compared with a non-linear simulation of the system. A hydraulic test rig is used to validate the non-linear simulation. The authors report that when the system was operated in open-loop configuration, the load pressure, the flow rate, and the efficiency predicted by the steady-state model matched the results of the dynamic simulation. According to this, the steady state equation can be used to design hydraulic step-down switching converters.

In [51] De Negri et al. present a steady state analysis of a step-down hydraulic converter. The model is used to calculate the average load pressure and average flow to the system as a function of duty cycle. The theoretical values are compared with experimental results. The minimum and maximum recorded flow rates deviate from the theoretical ones but the average flow rate agrees better.

In [52], Nostrani et al. attempt to control a system consisting of two cylinders. One cylinder is controlled by a conventional proportional valve, while the other is controlled by PWM. The chosen PWM frequency is 32 Hz. The authors find that the valve is not fast enough for position control of the system. During movement the control signal of the valve reached saturation and kept the valve fully opened or closed, which made the losses in the system equivalent to the conventional system. The digital solution resulted in 17 % better efficiency, when performing velocity control.

3.2.4. Active damping of pressure pulsations due to switching

In [53] Scheidl et al. point out that one of the major issues with digital hydraulics is still pressure and flow pulsations. Some of the work done in investigating the pressure oscillations due to switching is presented here.

In [54], Pan et al. investigate the possibility of attenuating the pressure spikes in a system by active damping. The system consists of a length of pipe with three transducers along the length, a pressure supply on one side and a proportional valve, which can divert flow just before the load, which is in this case a throttling orifice. The method consists of estimating the pressure wave through the pipe by using the transducer measurements and annihilating it by introducing an opposing pressure wave with the valve. This is done at the expense of energy loss. The pressure pulsation frequency is 85 Hz while the proportional valves bandwidth is 350 Hz.

In [55], Pan et al. use a piezo-electric switching valve instead of the proportional valve from the previous test. The control structure is adaptive and it reduces the pressure pulsations significantly. The piezo-electric valve has a bandwidth of 425 Hz, while the pressure pulsations in the system have a maximum frequency of 40 Hz.

In a similar way in [56] Kogler et al. investigate the pressure wave propagation due to digital valve switching. Again, three transducers are used to measure the wave. Instead of using a valve at the end of the pipe, to attenuate the fluid borne noise, the authors investigate the opening trajectory of the switching valve. They find that by using a slower opening or a smoother trajectory the pressure oscillations can be reduced. Kogler et al. further point out that it is possible to design the pipe system in such a way as to force the pressure wave to bounce back from the end of the pipe and annihilate itself.

In [57], Peng et al. presents the concept of a zero-flowrate-switching controller. The author uses an extra flow line between the pressure supply and the cylinder chamber, which is specifically designed to resonate at the frequency of the PWM signal. The pressure in the system is supplied by a piston pump, which means that the supply pressure is pulsating with a certain frequency as well. The valve can be switched exactly when there is no flow across it by using the flow waves within the system. At the same time the pressure pulsations do not reach the cylinder chamber because at that point the flow is supplied by the second flow line. The resulting switching losses in the system are reduced from 158 W to 1.5 W, but this requires a valve with an opening/closing time of 2 ms.

3.3. Discussion

With regard to accuracy and smoothness of motion it can be said that state of the art control in this field has achieved smooth motion on par with throttling control. The switching load due to this is increased compared with parallel valve solutions, because a constant switching frequency is selected. It can be noticed that papers in the field have focused on systems with a natural frequency of 100 Hz or less. The reliability of this architecture suffers, due to the increased switching load, which does put a lot of strain on the valve. It can be said that having parallel connected converters can improve reliability, because of the added redundancy. This is not clear though, because the apparent switching frequency which the system sees drops with each faulty converter. The load on the valves grows when the natural frequency of the system is increased. The efficiency of systems with hydraulic converters is

much improved and this can be said to be the main benefit of the technology. The number of components required to make the concept work is difficult to pin down. Parallel converters or switching valves seem to be needed in order to actuate systems with a steady motion. Each converter requires a state of the art switching valve, a long hose and possibly an accumulator. At the same time fewer valves are needed. The computational complexity of the controllers in this field are not high compared with those used in the other fields. This is due to the fact that no optimization problem needs to be solved at each instant. The active damping of pressure pulsations presented in subsection 3.2.4 seems to be impossible as of yet, because the valves used to attenuate the vibrations are in the 400 Hz bandwidth range and this is not possible with commercially available valves.

4. MULTI-PRESSURE ACTUATORS

4.1. Concept

Multi-pressure actuators work on a similar principle as multi-chamber chamber cylinders in the sense that they are controlled by switching between different force levels. A differential cylinder is connected to different pressure lines in order to achieve different force outputs. Multi-pressure systems with only three pressures were proposed first. The low number of pressure lines required that throttling was still used in order to achieve any controllability. In order to achieve good controllability without throttling, seven or more pressures might be needed. Since switching losses scale with the difference between the initial and final pressure, having many pressure lines can greatly reduce losses. In order to create these many pressure lines a pressure transformer was proposed by [58]. One high pressure rail is connected to the rod side chamber of a row of small cylinders as can be seen in Figure 8.

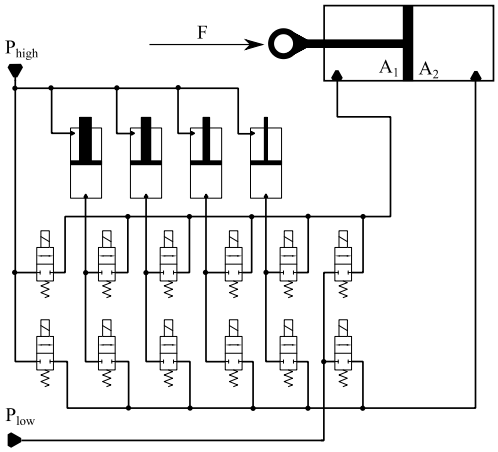

Figure 8 Concept for a multi-pressure cylinder with 6 pressures

The ratio between piston and rod side produces different pressures in the piston side chamber. These chambers are used as the constant pressure rails. The prototype in [58] was built with rather small cylinders for the pressure line. The pistons of these cylinders move when fluid is extracted from the pressure rail. Care needs to be taken not to drain too much fluid from a single pressure rail, because this reduces the resolution of the controller.

There are few papers available for the digital concept of switching between multiple pressure lines. The following subsection has not been further divided for this reason. The main advantages of the concept is its energy efficiency and so most papers are concerned with that. The main problems to be solved are how to balance energy flows from pressure lines to cylinder chamber, how to achieve smooth motion despite the switching nature of the control and the computational complexity of the controller.

4.2. Papers

In [59], Dengler et al. propose to use multiple pressure lines in the control of a linear actuator in a wheel loader. The middle pressure line is supplied by an accumulator. The control structure is based on a model prediction algorithm, which attempts to optimise the energy consumption of the pump. In the cost function, extracting energy from the high pressure line without charging the medium pressure line has a prohibitive cost. The state equations for all control combinations are solved and the two energies in the two pressure rails are calculated for the next time step. The authors then use a proportional valve and throttle the flow to get the correct chamber pressures. The article shows that the resulting controller is 13 % more efficient than a load sensing solution.

In [60], Stauch et al. propose the use of a digital hydraulic inspired accumulator to store and recover energy. The accumulator has a multi-area piston type design. The top part is filled with gas, which is the spring as in a conventional accumulator, but the bottom part consists of several concentric annular areas with different sizes. Each area can be switched between a load port and a low pressure port. This makes the accumulator function in a manner similar to a multi-chamber cylinder. The authors simulate a case in which a cylinder moving a weight is used. The weight is first lifted. This discharges the accumulator. Then the weight is lowered which charges the accumulator. The weight is then lifted again but it does not reach the same height due to the throttling losses and the friction in the system.

In [61] a three-pressure multi-pressure actuator is investigated. A state-space representation of the system is obtained and used to find a Linear Quadratic Regulator (LQR) which controls force and back pressure by outputting flow references for the two cylinder chambers. A set of switching rules are defined based on the available pressures and the possible flow directions (i.e. flow from low to high pressure is not possible). Then the inverse valve model is used to realize the flow reference set by the LQR. In order to avoid any flow spikes during switching between pressure lines, the switch happens over a period of 100 ms. Both pressure lines are connected to the cylinder at 50 ms and are each providing half of the flow. The resulting energy use was reduced by 49.3 % on average for the six test cases, despite the fact that cross-port leakage occurs. The reduction in question is in comparison with the same system using two pressure rails.

In [62] Linjama et al. discuss the possibility of combining the energy storage concept from [59] together with the multi-chamber accumulator [60] or a secondary controlled multi-chamber cylinder. In both cases, the idea is to have an energy storage unit providing the peak power for each actuator as opposed to a unified energy storage solution. This reduces the need to transfer large power quantities from the main power storage to each actuator. The energy peaks are handled locally at the actuators instead. A further benefit is that the energy storage for each actuator can be designed separately. The size and pre-charge of the accumulator influence the efficiency of the system as discussed in [63]. This information is used to conclude that designing multiple actuators with different loading conditions and a single storage system can be difficult. The main issue with both the proposed solutions in [62] is the size of the accumulator. Larger accumulators will be able to supply the system better, but they are bulkier. Smaller accumulators can furthermore have problems with heat dissipation due to the smaller amount of fluid in the system.

In [58] a two chamber cylinder is controlled by switching between multiple pressure lines. Huova et al. propose 100 pressure lines instead of the more common three. A more realistic prototype with 7 pressure lines is tested. The authors compare the energy losses with those of a four-chamber cylinder. The losses are 3.5 kJ for the multi-chamber cylinder and 2.49 kJ in for the multi-pressure cylinder.

In [64] Huova et al. study a multi-pressure actuator to drive a mobile hydraulic boom mock-up. The authors consider the possibility of opening one or two valves between a chamber and a pressure line. This changes the maximum flow capacity of the valve and so changes the force resolution at velocities different than zero. They also consider the possibility of allowing crossflow between pressure lines. The authors find that at low velocities only changing the number of valves opened does not improve the resolution. In order to get good resolution both PNM and crossflow have to be allowed. The inclusion of crossflow does produce losses, but the authors have removed the most costly combinations. The experimental results show an average energy loss over movement distance between 10 and 14 J/mm depending on the controller and the loading conditions. Huova et al. study the source of the power losses in the system and find that 65 % are due to the on/off valve.

In [65] Linjama et al. develop a force controller for a multi-pressure cylinder. The system has six possible pressures to choose from, but each line has two valves connected in parallel. Two chambers, six pressures lines and two valves per line result in 24 valves and 2^{24} combinations. The two valves connected to each chamber do not have different sizes, so opening either one is equivalent to opening the other. The total number of unique combinations is 28^2, because there are two chambers. A cost function is used to evaluate the control combinations by enumerating all of them. The system is experimentally tested on a seesaw bench reported in other papers. The energy efficiency measure was comparable with the results of a multi-chamber cylinder actuating the same test stand.

In [66] Linjama et al. collect results and reflect on a 2-year research project for the improvement of fuel efficiency in hydraulic working machines. The main finding of the project is that hybridization can reduce fuel consumption by 15 %. The most effective solution is the combination of independent metering and hybridization where a 28 % reduction is seen. It is noted that multi-pressure systems have the potential to reduce fuel consumption by 36 %. The inertia of the luffing and extension joints was too low for the system to be implemented, so they used a standard load sensing system with 4/3 proportional

valves for those two actuators. The multi-pressure system was only implemented on the swing and lift actuators.

4.3. Discussion

The results for multi-pressure cylinder and multi-chamber cylinders are very similar. Accuracy and smoothness of motion depends on the mass of the system and the force resolution. Energy efficiency is the main advantage of the architecture and results show that multi-pressure cylinders can be more efficient than multi-chamber cylinders. The switching losses can be reduced by both having smaller differences between pressure levels and by having smaller chambers in which the change happens. Switching frequency is not constant and is in general smaller than with a hydraulic buck converter. The number of components needed to make the concept work is rather high as in multi-chamber cylinders. A three-chamber three-pressure cylinder requires 12 valves, while a two-chamber, seven-pressure cylinder requires 14. Since the pressure lines are created locally at the cylinder itself, each actuator would require a transformer and having multiple multi-pressure cylinders does not reduce the number of needed components.

5. MULTI-CHAMBER CYLINDERS

5.1. Concept

Multi-chamber cylinders are hydraulic cylinders with more than two chambers. The authors in [67] explain that using the same constant pressure in different chambers produces different force levels. This can allow the four quadrant secondary control of a multi-chamber cylinder.

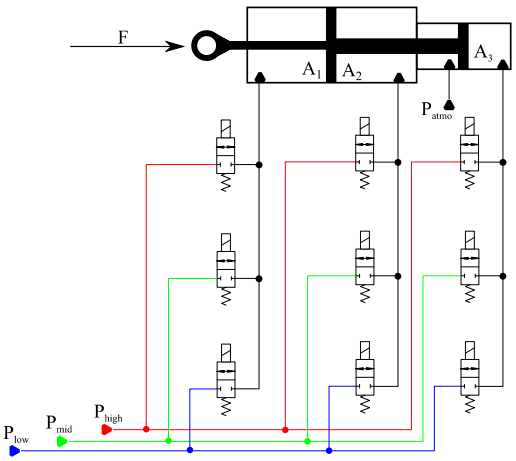

Figure 9 Cylinder used in Wavestar prototype

In Figure 9, a multi-chamber cylinder with four chambers can be seen. The cylinder is used in the Wavestar prototype [94]. In the figure, only three chambers are used. The fourth chamber is vented to tank. The cylinder can be connected to three pressure levels by a bank of on/off valves. The resulting force level the cylinder is able to produce can be seen in Figure 10. The resolution of the force depends on the number of chambers and number of pressure lines, which are available. A four-chamber cylinder with two pressure lines can produce $2^4 = 16$ forces, a three-chamber cylinder with three pressure lines can produce $3^3 = 27$ forces, and a four-chamber cylinder with three pressure lines can produce $3^4 = 81$ forces. More combinations can result in better performance, but it also necessitates more components and it makes choosing a force level more difficult.

A force trajectory can be followed by switching between these force levels. Since the valves are always on or off, there is no throttling. In a sense, the multi-chamber cylinder is a different way of creating a hydraulic converter, but instead of modulating the flow, the pressures are being modulated. The major source of losses in the system is switching, as the fluid in the chamber has to be compressed and decompressed depending on the case. Some authors propose throttling control as an inner loop of the force controller. That is - a force level above the reference is chosen and then the minimum amount of throttling is used to reach the force reference.

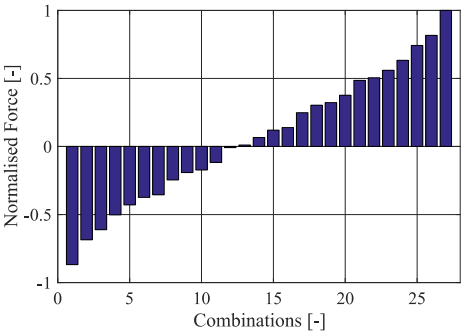

Figure 10 Normalised force levels, which the Wavestar prototype can produce

5.2. Papers

5.2.1. Multi-chamber cylinders with two pressure lines

In [67], the cylinder under consideration has four chambers with binary coding ratios. The chambers are either connected to a high pressure or low pressure line. Since there are four chambers and two pressure levels the actuator can provide 16 discrete force levels. The control structure optimises a cost function for the minimum force error while penalising excessive switching. The experiments show that a secondary controlled multi-chamber cylinder can have 60 % less losses than a standard proportional valve and cylinder solution. The authors identified the compressibility losses as the largest source of losses in the multi-chamber cylinder solution. Linjama et al. [67] also point out that the controllability at low velocities or with small system inertias is poor.

In [68], Huova et al. used a three-chamber cylinder with two pressure levels, but instead of on/off valves the system has DFCUs, which are used to control the velocity of the cylinder. It can be seen from the results that the velocity tracking is improved. The losses are still on average 60 % lower than for a standard load sensing system. The authors point out that if the cylinder is supposed to drive overrunning loads a higher load pressure is needed and then the losses are only 33 % smaller compared with a load sensing system. The reduction in losses is 50 %, if the hoses are excluded from the simulation and the chamber area ratio is changed.

In [69] Hansen et al. also optimise the chamber sizes of a four-chamber cylinder and determine that efficiency can be increased if the loading conditions are known.

In a similar fashion Belan et al. [70] investigate the possibility of using secondary controlled multi-chamber cylinder in aviation. The authors have developed a procedure for selecting cylinder areas.

In [71], [72], and [73] Linköping University and Volvo Construction Equipment discuss the possibility of using digital hydraulics to improve the efficiency of a mobile hydraulic machine. The concept utilises two constant pressure rails. The wheel loaders work functions are realised with multi-chamber cylinders. DFCU's are proposed for connecting the pressure rails to the chambers in order to efficiently control the transition from one force level to another. The authors propose a model based controller (MPC) for the cylinders. In [73] Heybroek et al. focus on the MPC of a multi-chamber actuator. The simulation results show a 5 % force error over 99 % of the cycle time. The overall energy efficiency is 71 %. The authors state that the controller requires a bandwidth of 1 kHz, but 100 Hz is the common capability of the electrical control units used in the excavator industry.

5.2.2. Multi-chamber cylinders with multiple pressure lines

In [74] and [75], Hansen et al. investigate the compressibility losses. The authors point out that when shifting from one pressure level to another, the pressure will overshoot the desired level due to the pressure dynamics. Hansen et al. propose that it is possible to introduce an intermediate pressure level. Thus the initial shift will result in a smaller energy loss, since the pressure drop across the valve will be smaller. When the overshoot reaches its maximum, the desired pressure level is introduced. Since at the time of the shift the new pressure level is equal to the system pressure, the energy loss would be zero. In order for such shifts to be possible a minimum performance requirement for the valves has been established in [76].

The work in [74], [75], [76], [77], [78] and [94] used a multi-chamber cylinder with three pressure lines to extract energy from waves. They achieved a 90 % efficiency over multiple operating conditions.

In [79], Hansen et al. present a test bench representing a part of the wave energy extractor presented in [78]. The authors faced a control problem as the fast switching time of the on/off valves resulted in under-damped chamber pressure responses. In order to avoid the pressure overshoot or cavitation, Hansen et al. stagger the opening of the valve over the opening period. An optimal opening trajectory is proposed. In order to follow the trajectory a parallel valves solution is used.

In [80], Hansen et al. further show that small shifting times lead to a better efficiency of the system, but they can also lead to larger pressure oscillations in the cylinder chambers. The optimal shifting time depends on the size of the chamber, which in turn depends on the current stroke of the cylinder. The authors proposed selecting opening times for every chamber as a trade-off. The authors then further expanded on their work in [81], where they investigate the influence of a box flow and a cosine flow shape. The conclusion is that the cosine input flow produces less oscillation, because it has a smoother shape and has a longer shifting time.

In [82], Dell'Amico et al. use a four-chamber cylinder and three pressure lines. The resulting structure can produce 81 different forces. The control structure consisted of a PI controller in the outer loop, which outputs the desired force reference. The force reference was compared with the possible steady state forces and the closest match was selected. The smoothness of the motion was improved by using a smaller load and placing a weight on unnecessary switching. When a larger weight was used the pressure to the larger chambers was switched, which resulted in larger fluctuations in velocity.

In [83], Niemi et al. attempt to use a multi-chamber cylinder together with a multi-pump approach. The cylinder has four chambers which can be connected to supply or load pressure. Instead of using a constant pressure rail, the authors have connected three pumps with different displacements to the same motor shaft. The pumps can pump either to the supply line, or directly to tank. This changes the flow output of the pumps. There are three pumps with binary coded displacements and four cylinder chambers, which results in 106 force-velocity combinations. The results showed several problems with the system. Since the supply pressure is dictated by the load force, when the cylinder is stopped against the load force, the supply pressure would rise to the demands of the load. If the cylinder then has to move in the opposite direction (with the load force) the high pressure would result in a velocity surge. The energy efficiency of the system is compared with other control structures on a similar setup. The system is more efficient than a proportional solution with a load sensing system, but not as efficient as [67].

In [84], Hansen at al. investigate the performance of a Force Selection Algorithm (FSA) and a Model Predictive Controller (MPC) algorithm for solving the tracking problem of a multi-chamber cylinder, while minimizing energy use. Two MPC algorithms are investigated and are compared to the FSA. The cylinder used has three chambers and three pressure lines. The middle pressure line's level is chosen as the average of the high and low pressures. The cylinder is pushing against a spring damper system. The time horizon of the MPC was varied from 0.2 to 0.8 s and the time step from 0.1 to 0.5 s respectively. The parameters chosen are 0.5 s and 0.1 s. In order to compare the algorithms, they were tuned so they have less than 3 mm mean squared error over the trajectory. The computation time for the MPC controllers where 38 s and 327 s, values much larger than the 0.5 s horizon. The results indicate that the energy efficiency of a position tracking multi-chamber cylinder can be improved significantly by using the MPC algorithm.

In [85], Donkov et al. investigate the energy saving potential of using a multi-chamber cylinder to actuate the inner jib of a knuckle-boom crane. In the simulation, a three-chamber cylinder is used along with three pressure lines. The controller is based on a simple FSA, where all switching is punished with the same weight without regard for actual losses involved. A parameter sweep is performed to find the optimal weight and the optimal

pressure for the mid pressure line, showing that the controller can perform better if the force levels are tailored to the load and the trajectory. A second controller is presented which has a large weight on the two valves, which connect chamber A and chamber B to high pressure. The two controllers showed close performance with regard to accuracy and energy efficiency, but at the same time, they exhibited different switching patterns. One controller would follow the force trajectory closer and switch less often, while the other switched more often to forces above and below the actual trajectory. The original controller which followed the force trajectory more closely had large force spikes during switching. The force controllers were compared to a traditional hydraulic system - a mobile hydraulic proportional valve and a constant pressure supply. The proportional valve achieved a root mean square (RMS) error of 2 mm while the force controller achieved 74 mm at best. At the same time the energy used was 0.89 MJ versus 0.22 MJ for the force controller.

In [86], Hansen et al investigate how a new MPC algorithm can lead to a significant increase in the harvested power of a wave energy converter with discrete fluid power take-off system. The discrete power take-off system is a three-chamber cylinder with three pressure lines. The losses considered in the MPC are losses due to switching and throttling losses associated with the displacement flow. The influence of the time horizon and the time step size on the controller are investigated. The authors report that average absorbed power increases when the prediction horizon is increased, but the gains flatten out in horizons longer than 4 s. The authors also report that average absorbed energy decreases as time step grows. In practice, a value of 200 ms was chosen, because it takes 50 ms for the pressure shift to occur in the chamber. These dynamics are omitted in the MPC, because they are assumed to happen much faster than the time step. Three cost functions are tested - one without losses, one with switching losses, and one with switching and throttling losses. Harvested power was largest in all tests with the third cost function.

In [87], Donkov et al. discuss the possibility of using MPC to control the multi-chamber cylinders actuating a realistically sized crane. This is a simulation study only. In the simulation, a large weight is added to the load, after both inner and outer jibs are extended, to simulate the crane picking up something heavy. The FSA and the MPC are compared against a system with a load sensing pump, proportional valves, and normal cylinders. It is shown that the MPC performs better than the normal cylinders and the FSA in terms of energy efficiency. It is also shown that the large change in weight causes a constant error in the MPC and furthermore reduces its energy efficiency. This is found to be due to the change in the model, which is not reflected in the algorithm.

In [88], Hansen et al. investigate the long term effect of valve shifting time on a mechanical structure driven by a multi-chamber cylinder. A three-chamber, three-pressure cylinder is controlled with a FSA. The simulation is run for 100 wave periods and the force shifts are recorded. These force shifts are converted to an equivalent fatigue load using Miners rule. The results show that harvested energy decreases with increasing valve shifting time, but the fatigue load generally decreases.

In [89], Hansen et al. conduct a hardware-in-the-loop validation of a MPC controlled multi-chamber cylinder. The test bench is two cylinders pushing against each-other. One simulating a wave load, while the other simulates the power take-off system of a wave energy converter. Five different cost functions are compared in terms of energy efficiency, but also in term of computation time. The more complicated cost functions took longer to

compute, but also extracted more energy. The least complicated cost function took 16 ms, while the most complicated took 85 ms. In both cases this was below the MPCs prediction horizon, meaning that it is possible to run these controllers in real time.

In [90], Donkov et al. investigate a fault-tolerant MPC. A seesaw test bench was driven by a three-chamber, three-pressure cylinder. The faults investigated where valves stuck closed and valves stuck open. A simulation study was performed in which the system was investigated with and without a fault tolerant controller. It was shown that in general valves stuck closed produce a smaller effect on the system. Furthermore, the system can operate normally if the fault is detected. In the case where valves are stuck open, the effects were much larger - often resulting in an inability to move the cylinder. Two cases were tested on the test bench to validate the simulations, but modelling errors and undiscovered faults gave inconclusive results.

5.2.3. Multi-chamber cylinders for exoskeletons

In [91], a digital cylinder drive is studied for a knee joint of an exoskeleton. A four-chamber cylinder is used and the aim is to examine the jerkiness of the motion due to force transitions, when the system is used for getting up from a crouching position. The multi-chamber cylinder is made up of three differential cylinders connected in parallel. Only two pressure lines are used. The valves used are 3/3 two-way switching valves. This reduces the number of valves from eight to four. The control structure is described as a simple model predictive controller. The initial and desired angle of the leg are used to compute a position, velocity and acceleration trajectory for the cylinder. It is noted that valve size is a problem as the ones used in the simulation would have to be attached to the upper body. A different trajectory - fast walking, and experimental results are suggested as future work.

In [92], Scheidl et al. continue the investigation of a multi-chamber cylinder for the knee joint of an exoskeleton. In this case the focus is on the valves system. In order to reduce the size and weight of the four valves, they are changed from electrically actuated to pilot pressure actuated. In the new design the pilot pressure for the four valves is controlled by one proportional valve. Moving the spool of the one valve causes the pilot pressure to change and the four valves to switch states making this a hydraulic binary counter. These valves switch from one state to another in 50 ms, but the authors claim that this can be reduced by changing the switching trajectory.

5.2.4. Discussion

Multi-chamber cylinders rate lower than throttling based approaches such as parallel valves, in terms of accuracy and smoothness of motion. The actual performance depends on the size of the system, the trajectory and the available force levels. In terms of switching load, the switching frequency and the switching events can be reduced compared with the switching valve or the hydraulic buck converter concepts. The reduced switching load can also lead to improved reliability. Furthermore, the components operate in parallel, so it is possible to avoid using faulty components without affecting the system. The efficiency of multi-chamber cylinders can be considered their main advantage with proven efficiency of the cylinder of 98 % in multiple loading conditions. This efficiency can be destroyed though by the inefficiency of the pressure rails if they are not constructed in a smart way (e.g. throttling a high pressure rail in order to create a medium pressure rail). The concept does not require

many components - each chamber requires a number of valves equal to the number of pressure rails. On the other hand, pressure rails may require multiple pumps, accumulators and possibly significant length of hose. This can be offset if the pressure lines supply multiple actuators. The multi-chamber cylinder itself can be costly as it is a more complicated component than a differential cylinder. In terms of control the current trend is towards MPC over FSA. The computational complexity associated with MPC is an issue.

6. GENERAL CONCLUSION

The general conclusion for these concepts is presented in table form in Table 1. Pluses and minuses have been assigned to each category. A ± denotes either average result or that the result depends on how you implement the technology. Simple pluses and minuses do not represent the full reality of the differences between technologies and furthermore subjectivity cannot be avoided, but the table can be used to give an estimate of the subject area. The mobile-hydraulic industry in particular has so far shown the largest interest in digital hydraulics, specifically Bosch-Rexroth and Volvo, which have collaborated on some of the papers cited e.g. [93], [72].

Table 1 Result of state of the art review

	Parallel Valves	Switching Valves	Multi-chamber cylinders	Multi-pressure cylinders
Accuracy	++	++	±	±
Energy efficiency	±	+	++	++
Switching	+	--	-	-
Extra Components	+	±	-	--
Computational Complexity	+	+	-	-
Robustness	++	-	+	+

In terms of accuracy parallel valves and switching valves have been give very good results. This is a reflection of the fact that parallel valves can use throttling and micro-positioning with single pulses. Papers concerning switching valves also report accurate smooth motion with the complex flatness based controllers. The other two concepts get average results, because most papers in these fields focus energy efficiency more.

Multi-pressure cylinders and by extension multi-chamber cylinders with multiple pressure lines are very efficient and as such are given the highest mark in this category. Switching valves are given a good result, because the field contains both HBC and throttling based concepts. Parallel valves are given an average result, because they still rely on throttling

control. They are more efficient that a standard proportional valve solution, because they can throttle the flows to the cylinders chambers separately.

Concerning switching, parallel valves require the least amount of it. The concept controls velocity directly and with possible cross-port leakage good resolution can be achieved with relatively few valves. Multi-chamber and multi-pressure cylinders require switching between forces in order to follow a trajectory, but the control structures try to punish this. That is to say switching will only occur when it is needed. In the case of switching valves, a constant switching frequency is used to the PWM controllers. For this reason switching valves are given the worst score.

In the "Extra components" category multi-pressure cylinders are given the worst score, because they require a transformer for each cylinder. Multiple multi-chamber cylinders can be actuated from the same pressure rail. Switching valves are given an average result, because HBC require extra check valves and hoses, but at the same time, two valves might be enough to actuate a cylinder.

Multi-pressure and multi-chamber cylinders receive low scores in computational complexity, because the field seems to be moving towards the use of MPC. Depending on the prediction horizon, this can be quite complex. No computational problems have been reported in the field of switching valves and multiple papers address the computational complexity of parallel valve controllers.

In terms of robustness, parallel valves receive the highest grade since all the valves are essentially equal. In multi-pressure and multi-chamber cylinders some valves can be more important i.e. those connecting to the low-pressure line. Switching valves incur the highest switching load and based on that have been given the lowest grade.

In the field of parallel valves a trend can be seen towards reducing the number of valves. In order to do this more switching is introduced. In the field of switching valves, the trend seems to be to incorporate multiple HBCs in parallel. In both fields, increasingly complicated control structures are receiving more attention compared with physical changes to concept or architecture.

The field of multi-chamber cylinders is moving towards MPC and trying to solve the computation problem associated with it. The field of multi-pressure cylinders is still new and not enough papers are present in order for a trend to be detected, though it can be expected that the field will follow the others and control strategies will receive more attention.

7. ACKNOWLEDGMENTS

This research was funded by the Research Council of Norway, SFI Offshore Mechatronics, project number 237896/O30.

8. REFERENCES

[1] M Sc Arto Laamanen and Matti Vilenius. Is it time for digital hydraulics. In The eighth Scandinavian international conference on fluid power, 2003.

[2] Rudolf Scheidl, Matti Linjama, and Stefan Schmidt. Is the future of fluid power digital? Proceedings of the Institution of Mechanical Engineers, Part I: Journal of Systems and Control Engineering, 226(6):721–723, 2012.

[3] Bernd Winkler. Recent advances in digital hydraulic components and applications. In Proc. of The Ninth Workshop on Digital Fluid Power, Aalborg, Denmark, 2017.

[4] Valmet. Digital hydraulics, 2016. [Online]. Available: https://www.valmet.com/globalassets/media/downloads/whitepapers/process-improvements-and-parts/wpp digihydraulics.pdf

[5] Matti Linjama. Digital fluid power: State of the art. In 12th Scandinavian International Conference on Fluid Power, Tampere, Finland, May, pages 18–20, 2011.

[6] Matti LINJAMA, Kari T KOSKINEN, and Matti VILENIUS. Pseudo-proportional position control of water hydraulic cylinder using on/off valves. In Proceedings of the JFPS International Symposium on Fluid Power, volume 2002, pages 155–160. The Japan Fluid Power System Society, 2002.

[7] Matti Linjama, Kari T Koskinen, and Matti Vilenius. Accurate trajectory tracking control of water hydraulic cylinder with non-ideal on/off valves. International Journal of Fluid Power, 4(1):7–16, 2003.

[8] Matti Linjama, Mikko Huova, Pontus Boström, Arto Laamanen, Lauri Siivonen, Lionel Morel, Marina Waldèn, and Mati Vilenius. Design and implementation of energy saving digital hydraulic control system. In Proceedings of the 10th Scandinavian International Conference on Fluid Power, Tampere , Finland, 2007.

[9] M Linjama and M Vilenius. Digital hydraulic control of a mobile machine joint actuator mockup. In Bath Workshop on Power Transmission and Motion Control, volume 2004, page 145. PROFESSIONAL ENGINEERING PUBLISHING, 2004.

[10] Matti Linjama and M Vilenius. Improved digital hydraulic tracking control of water hydraulic cylinder drive. International Journal of Fluid Power, 6(1):29–39, 2005.

[11] Matti LINJAMA and Matti VILENIUS. Energy-efficient motion control of a digital hydraulic joint actuator. In Proceedings of the JFPS International Symposium on Fluid Power, volume 2005, pages 640–645. The Japan Fluid Power System Society, 2005.

[12] L Siivonen, M Linjama, M Vilenius, and P Anttonen. Accurate flow control with digital valve system. In Proceedings of the 51st National Conference on Fluid Power March 12-14, 2008, IFPE 2008, Las Vegas, USA, 2008.

[13] Matti Linjama. Robust control of digital hydraulic servo actuator.

[14] Matti Linjama, Mikko Huova, and Kalevi Huhtala. Model-based force and position tracking control of an asymmetric cylinder with a digital hydraulic valve. International Journal of Fluid Power, 17(3):163–172, 2016.

[15] Matti Linjama, Mikko Huova, Otso Karhu, and Kalevi Huhtaka. Energy efficient tracking control of a mobile machine boom mockup. In The Eight Workshop on Digital Fluid Power, Tampere, Finland, May, pages 268–278, 2016.

[16] Matti Linjama, Mikko Huova, Otso Karhu, and Kalevi Huhtala. High-performance digital hydraulic tracking control of a mobile boom mockup. In The 10th International Conference on Fluid Power, Dresden, Germany, March, pages 37–48, 2016.

[17] Matti Linjama. On the numerical solution of steady-state equations of digital hydraulic valve-actuator system. In The Eight Workshop on Digital Fluid Power, Tampere, Finland, May, pages 144–155, 2016.

[18] Matti Linjama and Mikko Huova. Numerically efficient flow model for on/off valves. In The Seventh Workshop on Digital Fluid Power, Linz, Austria, February, pages 164–172, 2015.

[19] C Stauch, J Rudolph, and F Schulz. Some aspects of modelling, dimensioning, and control of digital flow control units. In Proc. 7th Workshop on Digital Fluid Power, DFP15, Linz, Austria, pages 101–113, 2015.

[20] Christian Stauch and Joachim Rudolph. Control-oriented modelling and development of a model-based switching algorithm for a digital hydraulic independent metering cylinder drive. Proceedings of the Institution of Mechanical Engineers, Part I: Journal of Systems and Control Engineering, page 0959651816629315, 2016.

[21] Mikko Huova, Miika Ahopelto, Ville Ahola, Matti Linjama, and Kalevi Huhtala. Characteristics of digital hydraulics with commercial controllers. In The Seventh Workshop on Digital Fluid Power, Linz, Austria, February, pages 114–128, 2015.

[22] Johan Ersfolk, Pontus Bostrlöm, Ville Timonen, Jam Westerholm, Jonatan Wiik, Otso Karhu, Matti Linjama, and MarinaWaldèn. Optimal digital valve control using embedded gpu. In The Eight Workshop on Digital Fluid Power, Tampere, Finland, May, pages 239–250, 2016.

[23] Miikka Ketonen and Matti Linjama. High flowrate digital hydraulic valve system. In Proc. of The Ninth Workshop on Digital Fluid Power, Aalborg, Denmark, 2017.

[24] Miikka Ketonen and Matti Linjama. Simulation study of a digital hydraulic independent metering valve system on an excavator. In Proceedings of 15th Scandinavian International Conference on Fluid Power, June 7-9, 2017, Linköping, Sweden, number 144, pages 136–146. Linköping University Electronic Press, 2017.

[25] Miikka Ketonen and Matti Linjama. Digital hydraulic imv system in an excavator–first results.

[26] M Huova and A Plöckinger. Improving resolution of digital hydraulic valve system by utilizing fast switching valves. In: Laamanen, A. & Linjama, M.(eds.). Proceedings of the Third Workshop on Digital Fluid Power, October 13-14 2010, Tampere, Finland, 2010.

[27] M Paloniitty, M Linjama, and K Huhtala. Equal coded digital hydraulic valve system-improving tracking control with pulse frequency modulation. Procedia Engineering, 106:83–91, 2015.

[28] Miika Paloniitty and Matti Linjama. High-linear digital hydraulic valve control by an equal coded valve system and novel switching schemes. Proceedings of the Institution of Mechanical Engineers, Part I: Journal of Systems and Control Engineering, 232(3):258–269, 2018.

[29] Lauri Siivonen, Miika Paloniitty, Matti Linjama, Harri Sairiala, and Salvador Esqué. Digital valve system for iter remote handling–design and prototype testing. Fusion Engineering and Design, 2019.

[30] Lauri Siivonen, Matti Linjama, Mikko Huova, and Matti Vilenius. Pressure based fault detection and diagnosis of a digital valve system. Power Transmission and Motion Control (PTMC 07), pages 67–79, 2007.

[31] A. Laamanen, M. Linjama, and M. Vilenius. On the pressure peak minimization in digital hydraulics, pages 107–121. Tampere University of Technology, 2007. Contribution: organisation=iha,FACT1=1.

[32] Lauri Siivonen, Matti Linjama, Mikko Huova, and Matti Vilenius. Jammed on/off valve fault compensation with distributed digital valve system. International Journal of Fluid Power, 10(2):73–82, 2009.

[33] T Laehteenmaeki, M Ijas, and E Mäkinen. Characteristics of digital hydraulic pressure reducing valve. In: Johnston, DN & Plummer, A.(eds.). Fluid Power and Motion Control (FPMC 2010), 15-17 September 2010, University of Bath, UK, 2010.

[34] M. Ketonen, M. Huova, M. Heikkilä, M. Linjama, P. Boström, and M. Wald´en. Digital hydraulic pressure relief function. In ASME/BATH 2012 Symposium on Fluid Power and Motion Control, pages 138–151. American Society of Mechanical Engineers, 2012.

[35] Mikko Huova, Matti Linjama, Lauri Siivonen, Till Deubel, Heino Försterling, and Edgar Stamm. Novel fine positioning method for hydraulic drives utilizing on/off-valves. In BATH/ASME 2018 Symposium on Fluid Power and Motion Control. American Society of Mechanical Engineers Digital Collection, 2018.

[36] Christoph Gradl and Rudolf Scheidl. A basic study on the response dynamics of pulsefrequency controlled digital hydraulic drives. In ASME/BATH 2013 Symposium on Fluid Power and Motion Control, pages V001T01A022–V001T01A022. American Society of Mechanical Engineers, 2013.

[37] Sojiro Tsuchiya, Hironao Yamada, and Takayoshi Muto. A precision driving system composed of a hydraulic cylinder and high-speed on/off valves. International Journal of Fluid Power, 2(1):7–16, 2001.

[38] Andreas Plöckinger, Mikke Huova, and Rudolf Scheidl. Simulation and experimental results of pwm control for digital hydraulics. In Proceedings of The Fifth Workshop on Digital Fluid Power, Tampere. The Digital Fluid Power Workshop series, 2012.

[39] Marko Šimic and Herakovič. High-response hydraulic linear drive with integrated motion Sensor and digital valve control. In The 10th International Conference on Fluid Power, Dresden, Germany, March, pages 49–58, 2016.

[40] Helmut Kogler, Rudolf Scheidl, Michael Ehrentraut, Emanuele Guglielmino, Claudio Semini, and Darwin G Caldwell. A compact hydraulic switching converter for robotic applications. Proc. Fluid Power and Motion Control, September, Bath, pages 55–66, 2010.

[41] Helmut Kogler and Rudolf Scheidl. Linear motion control with a low-power hydraulic switching converter-part i: Concept, test rig, simulations. Proceedings of the Institution of Mechanical Engineers, Part I: Journal of Systems and Control Engineering, 229(8):677–684, 2015.

[42] Helmut Kogler and Rudolf Scheidl. Linear motion control with a low-power hydraulic switching converter-part ii: Flatness-based control. Proceedings of the Institution of Mechanical Engineers, Part I: Journal of Systems and Control Engineering, 229(9):818– 828, 2015.

[43] Helmut Kogler and Rudolf Scheidl. Energy efficient linear drive axis using a hydraulic switching converter. Journal of Dynamic Systems, Measurement, and Control, 138(9):091010, 2016.

[44] Rudolf Scheidl, Bernd Winkler, Helmut Kogler, Peter Ladner, Rainer Haas, and Evgeny Lukachev. Digital fluid technologies for the steel industry. BHM Berg-und Hüttenmännische Monatshefte, 161(11):504–509, 2016.

[45] Christoph Gradl and Rudolf Scheidl. Performance of an energy efficient low power stepper converter. Energies, 10(4):445, 2017.

[46] Evgeny Lukachev and Rudolf Scheidl. Hydraulic switching type position control of a large cylinder drive. In 2018 Global Fluid Power Society PhD Symposium (GFPS), pages 1–6. IEEE, 2018.

[47] Helmut Kogler, Markus Schöberl, and Rudolf Scheidl. Passivity-based control of a pulse-width mode operated digital hydraulic drive. Proceedings of the Institution of Mechanical Engineers, Part I: Journal of Systems and Control Engineering, 233(6):656–665, 2019.

[48] Helmut Kogler, Rudolf Scheidl, and Michael Ehrentraut. A simulation model of a hydraulic buck converter based on a mixed time frequency domain iteration. In ASME/BATH 2013 Symposium on Fluid Power and Motion Control, pages V001T01A006–V001T01A006. American Society of Mechanical Engineers, 2013.

[49] Victor J De Negri, Pengfei Wang, Andrew Plummer, and D Nigel Johnston. Behavioural prediction of hydraulic step-up switching converters. International journal of fluid power, 15(1):1–9, 2014.

[50] Marcos P Nostrani, Alessio Galloni, Henrique Raduenz, and Victor J De Negri. Design and optimization of a fast switching hydraulic step-down converter for position and speed control. In Proceedings of 15: th Scandinavian International Conference on Fluid Power, June 7-9, 2017, Linköping, Sweden, number 144, pages 361–369. Linköping University Electronic Press, 2017.

[51] Victor J De Negri, Marcos P Nostrani, Pengfei Wang, D Nigel Johnston, and Andrew Plummer. Modelling and analysis of hydraulic step-down switching converters. International Journal of Fluid Power, 16(2):111–121, 2015.

[52] Marcos Nostrani, Alessio Galloni, Henrique Raduenz, and Victor De Negri. Theoretical and experimental analysis of a hydraulic step-down switching converter for position and speed control. In The Eight Workshop on Digital Fluid Power, Tampere, Finland, May, pages 157–175, 2016.

[53] Rudolf Scheidl, Bernd Winkler, and Andreas Plöckinger. Digital fluid power in the 7th year of dfp workshops. In The Seventh Workshop on Digital Fluid Power, pages 4–8. The Digital Fluid Power Workshop series, 2015.

[54] Min Pan, D Nigel Johnston, Andrew Plummer, Sylwester Kudzma, and Andrew Hillis. Active control of pressure pulsation in a piping system using measured dynamic flow rate. In ASME/BATH 2013 Symposium on Fluid Power and Motion Control, pages V001T01A013–V001T01A013. American Society of Mechanical Engineers, 2013.

[55] Min Pan, Nigel Johnston, and Andrew Hillis. Active control of pressure pulsation in a switched inertance hydraulic system. Proceedings of the Institution of Mechanical Engineers, Part I: Journal of Systems and Control Engineering, 227(7):610–620, 2013.

[56] Helmut Kogler, Rudolf Scheidl, and Bernd Hans Schmidt. Analysis of wave propagation effects in transmission lines due to digital valve switching. In ASME/BATH 2015 Symposium on Fluid Power and Motion Control, pages V001T01A057–V001T01A057. American Society of Mechanical Engineers, 2015.

[57] Shuang Peng. The concept of a zero-flowrate-switching controller. In The Eight Workshop on Digital Fluid Power, Tampere, Finland, May, pages 187–199, 2016.

[58] Mikko Huova, Arttu Aalto, Matti Linjama, Kalevi Huhtala, Tapio Lantela, and Matti Pietola. Digital hydraulic multi-pressure actuator–the concept, simulation study and first experimental results. International Journal of Fluid Power, pages 1–12, 2017.

[59] Peter Dengler, Marcus Geimer, and René von Dombrowski. Deterministic control strategy for a hybrid hydraulic system with intermediate pressure line. In ASME/BATH 2012 Symposium on Fluid Power and Motion Control, pages 334–347. American Society of Mechanical Engineers, 2012.

[60] C Stauch, F Schulz, P Bruck, J Rudolph, and Gewerbepark Eschberger Weg. Energy recovery using a digital piston-type accumulator. In Proceedings of the Fifth Workshop on Digital Fluid Power. Tampere: Tampere University of Technology, pages 57–73, 2012.

[61] Niels Henrik Pedersen, Sören Christian Jensen, Rico Hjerm Hansen, Anders Hedegaard Hansen, and Torben Ole Andersen. Control of an energy efficient hydraulic cylinder drive with multiple pressure lines. 2018.

[62] Matti Linjama, Mikko Huova, Matti Pietola, Jyri Juhala, and Kalevi Huhtala. Hydraulic hybrid actuator: Theoretical aspects and solution alternatives. In Proceedings of the 14th Scandinavian International Conference on Fluid Power SICFP, volume 15, pages 20–22, 2015.

[63] H. Hänninen, J. Kajaste, and M. Pietola. Optimizing hydraulic energy recovery system of reach truck. In ASME/BATH 2012 Symposium on Fluid Power and Motion Control, pages 110–122. American Society of Mechanical Engineers, 2012.

[64] Mikko Huova, Arttu Aalto, Matti Linjama, and Kalevi Huhtala. Study of energy losses in digital hydraulic multi-pressure actuator. In Proceedings of 15th Scandinavian International Conference on Fluid Power, June 7-9, 2017, Linköping, Sweden, number 144, pages 214–223. Linköping University Electronic Press, 2017.

[65] Matti Linjama and Mikko Huova. Model-based force and position tracking control of a multi-pressure hydraulic cylinder. Proceedings of the Institution of Mechanical Engineers, Part I: Journal of Systems and Control Engineering, 232(3):324–335, 2018.

[66] Adj Prof Matti Linjama, Tech Mikko Huova, M Sc Jyrki Tammisto, Tech Mikko Heikkilä, Seppo Tikkanen, Tech Jyrki Kajaste, Tech Miika Paloniitty, and Matti Pietola. Hydraulic hybrid working machines project–lessons learned.

[67] Matti Linjama, HP Vihtanen, Ari Sipola, and Matti Vilenius. Secondary controlled multichamber hydraulic cylinder. In The 11th Scandinavian International Conference on Fluid Power, SICFP, volume 9, pages 2–4, 2009.

[68] Mikko Huova, Arto Laamanen, and Matti Linjama. Energy efficiency of three-chamber cylinder with digital valve system. International Journal of Fluid Power, 11(3):15–22, 2010.

[69] Anders Hedegaard Hansen, Rico Hjerm Hansen, and Henrik C Pedersen. Optimisation of working areas in discrete hydraulic power take off-system for wave energy converters. In Proceedings of the 5th Workshop on Digital Fluid Power. Tampere University of Technology, 2012.

[70] Henri C Belan, Cristiano C Locateli, Birgitta Lantto, Petter Krus, and Viktor J De Negri. Digital secondary control architecture for aircraft application. In Proc. 7th Workshop on Digital Fluid Power, DFP15, Linz, Austria, pages 22–40, 2015.

[71] Karl Pettersson, Kim Heybroek, Per Mattsson, and Petter Krus. A novel hydromechanical hybrid motion system for construction machines. International Journal of Fluid Power, 18(1):17–28, 2017.

[72] Kim Heybroek, Erik Norlin, and A Sipola. Hydraulic multi-chamber cylinders in construction machinery. In Hydraulikdagarna, March 16-17, 2015, 2015.

[73] Kim Heybroek and Johan Sjöberg. Model predictive control of a hydraulic multichamber actuator: A feasibility study. IEEE/ASME Transactions on Mechatronics, 23(3):1393–1403, 2018.

[74] Rico H Hansen, Torben O Andersen, and Henrik C Perdersen. Analysis of discrete

pressure level systems for wave energy converters. In Fluid Power and Mechatronics (FPM), 2011 International Conference on, pages 552–558. IEEE, 2011.

[75] Rico H Hansen, Anders Hansen, and Torben O Andersen. Influence and utilisation of pressure propagation in pipelines for secondary controlled discrete displacement cylinders. In Applied Mechanics and Materials, volume 233, pages 72–75. Trans Tech Publ, 2012.

[76] Rico Hjerm Hansen, Torben Ole Andersen, and Henrik C Pedersen. Determining required valve performance for discrete control of pto cylinders for wave energy. 2012.

[77] Rico H Hansen, Anders Hansen, and Torben O Andersen. Simulation of utilisation of pressure propagation for increased efficiency of secondary controlled discrete displacement cylinders. In Applied Mechanics and Materials, volume 233, pages 3–6. Trans Tech Publ, 2012.

[78] Rico H Hansen, Morten M Kramer, and Enrique Vidal. Discrete displacement hydraulic power take-off system for the wavestar wave energy converter. Energies, 6(8):4001–4044, 2013.

[79] Rico H Hansen, Torben O Andersen, Henrik C Pedersen, and Anders H Hansen. Control of a 420 kn discrete displacement cylinder drive for the wavestar wave energy converter. In ASME/BATH 2014 Symposium on Fluid Power and Motion Control, pages V001T01A021–V001T01A021. American Society of Mechanical Engineers, 2014.

[80] Anders Hedegaard Hansen and Henrik C Pedersen. Energy cost of avoiding pressure oscillations in a discrete fluid power force system. In ASME/BATH 2015 Symposium on Fluid Power and Motion Control, pages V001T01A044–V001T01A044. American Society of Mechanical Engineers, 2015.

[81] Anders Hansen and Henrik Pedersen. Reducing fatigue loading due to pressure shift in discrete fluid power force systems. In 9th FPNI Ph. D. Symposium on Fluid Power, pages V001T01A002–V001T01A002. American Society of Mechanical Engineers, 2016.

[82] Alessandro DellAmico, Marcus Carlsson, Erik Norlin, and Magnus Sethson. Investigation of a digital hydraulic actuation system on an excavator arm. In 13th Scandinavian International Conference on Fluid Power; June 3-5; 2013; Linköping; Sweden, number 092, pages 505–511. Linköping University Electronic Press, 2013.

[83] Olli Niemi-Pynttäri, Matti Linjama, Arto Laamanen, and Kalevi Huhtala. Parallel pump-controlled multi-chamber cylinder. In ASME/BATH 2014 Symposium on Fluid Power and Motion Control, pages V001T01A014–V001T01A014. American Society of Mechanical Engineers, 2014.

[84] Anders H Hansen, Magnus F Asmussen, and Michael M Bech. Energy optimal tracking control with discrete fluid power systems using model predictive control. In Proceedings of the Ninth Workshop on Digital Fluid Power, Aalborg, Denmark, pages 7–8, 2017.

[85] Viktor Donkov, Torben Ole Andersen, Morten Kjeld Ebbesen, and Henrik Clemmensen Pedersen. Applying digital hydraulic technology on a knuckle boom crane. In The Ninth Workshop on Digital Fluid Power, 2017.

[86] Anders Hedegaard Hansen, Magnus F Asmussen, and Michael M Bech. Model predictive control of a wave energy converter with discrete fluid power power take-off system. Energies, 11(3):635, 2018.

[87] Viktor Hristov Donkov, Torben Ole Andersen, Henrik Clemmensen Pedersen, and

Morten Kjeld Ebbesen. Application of model predictive control in discrete displacement cylinders to drive a knuckle boom crane. In 2018 Global Fluid Power Society PhD Symposium (GFPS), pages 408–413. IEEE, 2018.

[88] Anders H Hansen, Magnus F Asmussen, and Torben O Andersen. Valve shifting time in a digital fluid power system-energy efficiency versus fatigue loading. In Proceedings of the 6th International Conference on Control, Mechatronics and Automation, pages 128–132. ACM, 2018.

[89] Anders H Hansen, Magnus F Asmussen, and Michael M Bech. Hardware-in-the-loop validation of model predictive control of a discrete fluid power power take-off system for wave energy converters. Energies, 12(19):3668, 2019.

[90] Viktor Donkov, Torben Andersen, Morten Kjeld Ebbesen, Matti Linjama, and Miika Paloniitty. Investigation of the fault tolerance of digital hydraulic cylinders. In the Sixteenth Scandinavian Conference on fluid power, Tampere, Finland, 2019

[91] Eva Holl, Rudolf Scheidl, and Sulaymon Eshkabilov. Simulation study of a digital hydraulic drive for a knee joint exoskeleton. In ASME/BATH 2017 Symposium on Fluid Power and Motion Control. American Society of Mechanical Engineers Digital Collection, 2017.

[92] Rudolf Scheidl and Simon Mittlböck. A hydraulic piloting concept of a digital cylinder drive for exoskeletons. In BATH/ASME 2018 Symposium on Fluid Power and Motion Control. American Society of Mechanical Engineers Digital Collection, 2018.

[93] Hermann Mehling and Daniel Weiler. Digital hydraulics valve stage, October 13 2015. US Patent 9,157,461.

[94] Rico Hjerm Hansen. Design and control of the powertake-off system for a wave energy converter with multiple absorbers. Videnbasen for Aalborg Universitet VBN, Aalborg Universitet Aalborg University, Det Teknisk-Naturvidenskabelige Fakultet, The Faculty of Engineering and Science, 2013.

Paper B

Applying Digital Hydraulic Technology on a Knuckle Boom Crane

Viktor Donkov, Torben Ole Andersen, Morten Kjeld Ebbesen, Henrik Clemmensen Pedersen

This paper has been published in the proceedings of
The Ninth Workshop on Digital Fluid Power, September 7-8, 2017, Aalborg, Denmark.

Applying Digital Hydraulic Technology on a Knuckle Boom Crane

Viktor Donkov[1], Torben Ole Andersen[1], Morten Kjeld Ebbesen[2], Henrik Clemmensen Pedersen[1]

[1]Aalborg University
Pontoppidanstraede 111
9220 Aalborg East, Denmark
E-mail: vhd@et.aau.dk
Phone: +45 7159 7943

[2]Adger University
Jon Lilletuns vei 9
4879 Grimstad, Norway

ABSTRACT

This paper aims to evaluate the benefits and disadvantages of applying a digital hydraulic concept to actuate a knuckle boom crane. The standard cylinders of the knuckle boom crane will be substituted with multi-chamber cylinders of comparable size. The performance of one of the multi-chamber cylinders will be compared with the standard differential cylinder. The standard cylinder will be actuated with a constant pressure supply, a proportional directional valve and a proportional controller. Control performance and energy consumption for the two configurations have been considered. It is concluded that more research is needed into the control strategies in order to improve robustness and performance.

KEYWORDS: Digital hydraulics, Multi-chamber cylinder, Knuckle Boom cranes

1 Introduction

Hydraulic systems are a popular actuation solution in a number of industries. The high torque-to-size ratio is often stated as the reason for their popularity. Solution based on electric motors have to rely on often large gear ratios in order to achieve high torque/force low speed outputs. For this reasons applications intended to move large masses (lifting mechanisms, digging machines) or to work hard materials (steel rolling, some drilling applications) are attractive areas for hydraulics. Unfortunately the overall efficiency of the hydraulics transmission can be low depending on the work area. Specifically, part loading situations can be problematic due to the dissipative nature of throttling, which occurs over the proportional valve. This paper will examine the performance of digital hydraulic technology, specifically secondary controlled multi-chamber cylinders, on a large scale lifting mechanism-a knuckle boom crane.

Multi-chamber cylinder can experience problems with achieving smooth motion at low velocities, due to a smaller resolution of force outputs at low velocities [1]. This problem does depend on the mass of the system, what one decides to consider as low velocity and how often the pressures in the cylinder can be switched. The current state of the art in the control of multi-chamber cylinders involves the selection of an appropriate

pressure for each chamber and then throttling the flow with digital flow control units as in [1] or [2]. These controllers have achieved much smoother motion than the simpler controller, but they are generally more complex as well. The aim of this paper is to evaluate the performance of a simpler controller in order to establish the magnitude of possible problems for a system of this scale. This will be used to consider the need for more complex controllers and furthermore used as a baseline for the possibility of applying other digital hydraulic concepts. An often cited paper about secondary control of multi-chamber cylinders is [3]. In this paper the four chambers of a cylinder are pressurised to one of two pressure levels to produce different forces. The algorithm is shown to be very efficient, but some problems in the smoothness of the motion of the cylinder are evident. A different approach was applied by [4], were a 3 chamber cylinder is connected to 3 pressure lines. The middle pressure was used when switching from low to high pressure and vice-versa. This was shown to reduce the switching losses indtroduced by the compressibility of the hydraulic fluid. The focus of [4] was on energy efficiency, while the cylinder was part of a power take-off system in the Wavestar wave energy extraction concept. Due to this, trajectory tracking was not the main aim. In [5], Dengler et al propose to use multiple pressure lines in the control of a linear actuator in a wheel loader. The pump only maintains the pressure in the high pressure line. The control structure is based on a model prediction algorithm, which attempts to optimise the energy consumption of the pump over a horizon. In the cost function extracting energy from the high pressure line without charging the medium pressure line accumulator has a prohibitive cost. The algorithm in this paper will take inspiration from the one in [3], but an additional pressure line will be added as in [4]. Then the choice of middle pressure and controller parameters will be investigated. Furthermore the algorithm will be augmented with weights on the high pressure lines for the two larger chambers, in order to investigate the energy efficiency and position tracking of the controller if the middle pressure line is preferred in order to evaluate the possibility of applying an algorithm similar to [5]. In section 2, the dimensions of the knuckle boom crane are presented. In section 3 the model of the system is described. The control is discussed in section 4. The performance of the controllers will be presented and discussed in section 5. The paper ends with conclusions and future work in section 6.

2 Test Case

A two link knuckle boom crane has been selected as an investigation case. Knuckle boom cranes are popular in shipping and off-shore drilling industries. Knuckle boom cranes are characterised by high force, low speed operation modes. The large mass of the machine can result in a good match for digital hydraulics as it will naturally dampen some of the motion introduced by pressure pulsation. A picture of an example knuckle boom crane can be seen in Fig.1. The two cylinders connecting the column to the first link (inner jib) will be the focus of this paper. In the paper the two cylinder will considered as one cylinder of equivalent size and power, furthermore there are crane models of this size, which have a single cylinder actuating the inner jib e.g. the knuckle boom crane in [6]. The standard differential cylinder will be substituted with the three chamber multi-chamber cylinder seen in Fig.2. Each of the on-off valves in the circuit are assumed to have the same discharge coefficient and eigen frequency as the original proportional valve. The dimensions of the test case crane have been selected to reflect the scale of real knuckle boom crane. The dimensions used can be seen in table 1.

Figure 1: Knuckle Boom Crane example provided by National Oilwell Varco.©

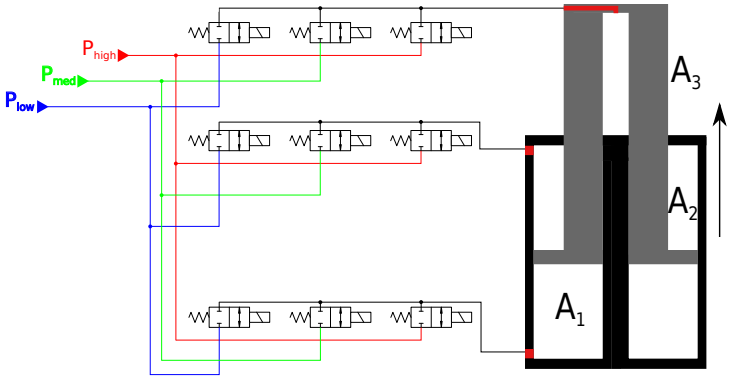

Figure 2: Representation of the multi-chamber cylinder used in the paper

Body	Length [m]	Mass [kg]
Inner Jib	10.8000	5600
Outer Jib	9.6000	2710
Cylinder 1	1.755	1500
Cylinder 2	1.33	750

Table 1: Crane dimensions

In this case a simple trajectory will be used where only the first cylinder will lift and lower the entire structure. Test trajectory for this situation can be seen in figure 3.

3 Model

The modelling section has been divided into a mechanical part and a hydraulic part. The mechanical part remains unchanged with both cylinder types.

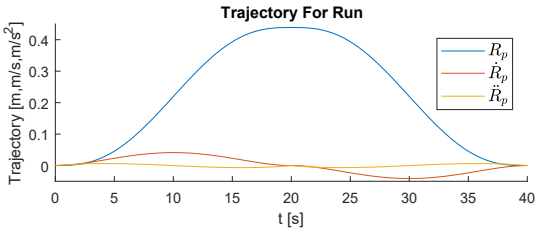

Figure 3: Reference Trajectory

3.1 Mechanical part

The non-linear equations describing the mechanical part of the model will be presented here in a very short form. According to [7] Newton's second law of motion for a multi body system can be expressed as:

$$\begin{bmatrix} M & D^T \\ D & 0 \end{bmatrix} \begin{bmatrix} \dot{v} \\ \lambda \end{bmatrix} = \begin{bmatrix} g_{ext} - b \\ \gamma \end{bmatrix} \tag{1}$$

where

M	is the matrix of masses and inertias around the center of mass of each link
D	the constraint Jacobian found from the kinematic constraints of the system
λ	is the vector of Lagrange multipliers
$\dot{v}$	is a vector of the linear and rotational acceleration of the bodies
g_{ext}	the vector of external forces, including gravity, Coriolis and cylinder forces
b	contains the velocity cross product terms
γ	is calculated from the derivation of the kinematic constraints of the system

There are 7 bodies with 6 coordinates which means that $\dot{v} \in \mathbb{R}^{42}$ as seen in Eq. (2). In this case the bodies include the column(1), inner jib(2), the first cylinder (broken into two bodies 3 and 4), the outer jib (5), and the second cylinder (6, 7). This also makes the mass matrix $M \in \mathbb{R}^{42\times 42}$.

$$\dot{v} = \begin{bmatrix} \ddot{r}_1 \\ \dot{\omega}_1 \\ \vdots \\ \ddot{r}_7 \\ \dot{\omega}_7 \end{bmatrix} \quad q = \begin{bmatrix} r_1 \\ \Theta_1 \\ \vdots \\ r_7 \\ \Theta_7 \end{bmatrix} \tag{2}$$

The mechanical system is modelled as 7 revolute joints and two parallel constraints (forcing the cylinder and piston bodies to be parallel) similar to how a knuckle boom crane was modeled in [6]. This makes D a 39×42 matrix. According to the Nikravesh method [7] the kinematic constraints of the system can be expressed as a non-linear function of the general coordinates of the multi body system. The theory states that when the constraints are not violated the kinematic constraints function $\Phi(q)$ returns zero. The specific equations for each joints are standard and can be found in [7]. The function can be differ-

entiated according to time to produce:

$$\Phi(q) = 0 \tag{3}$$
$$\dot{\Phi}(q,v) = Dv = 0 \tag{4}$$
$$\ddot{\Phi}(q,v,\dot{v}) = D\dot{v} + \dot{D}v = 0 \tag{5}$$
$$\gamma = D\dot{v} \tag{6}$$
$$\gamma = -\dot{D}v \tag{7}$$

This makes γ a 39×1 vector. With these extra equation the number of unknowns and equations in Eq. (1) become equal and can be solved simultaneously. Finally b is the cross product of velocities as seen in Eq. (8) and $b \in \mathbb{R}^{42}$.

$$b = \begin{bmatrix} 0^{3\times 1} \\ \tilde{\omega}_1 J_1 \omega_1 \\ \vdots \\ 0^{3\times 1} \\ \tilde{\omega}_7 J_7 \omega_7 \end{bmatrix} \tag{8}$$

where $\tilde{\omega}_1$ is the skew symmetric matrix constructed from the elements of ω_1 in order to represent cross product. This concludes the modelling of the mechanical part.

3.2 Hydraulic part

The non-linear equations describing the change in pressure are

$$\dot{p} = C(Q_{move} + Q_{valve}) \tag{9}$$

where $\dot{p}$ is a vector of pressure gradients for each chamber. C is the matrix of hydraulic capacitances. Q_{move} is the change in chamber volumes due to the velocity of that piston as seen in Eq. (10). Q_{valve} is the flow delivered by the valves. For the two cylinders with two chambers each, there are 4 pressure equations so $\dot{p} \in \mathbb{R}^4$. The bulk modulus of each chamber varies with the current pressure in the chamber. In Eq. (9), the vectors Q_{move} and Q_{valve} are defined as:

$$Q_{move} = \begin{bmatrix} -A_{1,1}\dot{x}_{p1} \\ A_{1,2}\dot{x}_{p1} \\ -A_{2,1}\dot{x}_{p2} \\ A_{2,2}\dot{x}_{p2} \end{bmatrix} \tag{10}$$

$$Q_{valve} = \begin{bmatrix} Q_{v,1}(u) \\ Q_{v,2}(u) \end{bmatrix} \tag{11}$$

$$Q_{v,1}(u) = \begin{cases} k_q u S(p_s - p_{1,1})\sqrt{(|p_s - p_{1,1}|} \\ k_q u S(p_{1,2} - p_t)\sqrt{(|p_{1,2} - p_t|} \end{cases} \quad u \geq 0$$
$$\begin{cases} k_q u S(p_s - p_{1,2})\sqrt{(|p_s - p_{1,2}|} \\ k_q u S(p_{1,1} - p_t)\sqrt{(|p_{1,1} - p_t|} \end{cases} \quad u < 0 \tag{12}$$

Here $A_{i,j}$ again stands for the area of the i-th cylinders j-th chamber. $\dot{x}_{p1}$ is the velocity of the 1st cylinder piston in the direction of the cylinder. $Q_{v,1}(u)$ is short for $Q_{v,1}(u,p,p_s,p_t)$,

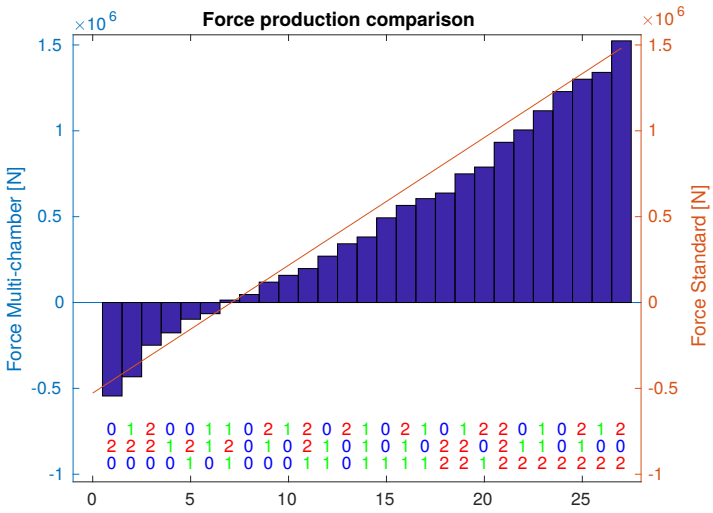

Figure 4: Forces the standard and multi-chamber cylinders can produce with the chosen pressures

which is the non-linear orifice equation describing the flow the valve delivers at the current spool position and pressure drops. In the case, where multi-chamber cylinders substitute the normal cylinders, some changes in the equations arise. The multi-chamber cylinder is chosen to have 3 chambers. Two chambers are delivering positive force (chosen as pushing) and one chamber delivers negative force (pulling). Three on-off valves are connected to each chamber of the cylinder. They connect the chamber to 3 constant pressure rails. A representation of the cylinder can be seen in Fig.2. The 3 chamber areas have been chosen in a ratio of $A_1 : A_2 : A_3 = 4 : 2 : 1$. The actual areas chosen so the cylinder produces a maximum positive force corresponding to the original cylinder. The three pressures are selected as $p_{high} = 22\ MPa$, $p_{mid} = 9\ MPa$ and $p_{low} = 1\ MPa$. The middle pressure is selected through a parameter sweep discussed in section 4.2. The high and low pressure are close to the ones used in the normal cylinder case, so the two cylinder can be compared in force production easily. The comparison can be seen in Fig.4. Since there are three chambers the pressure gradient vector (9) becomes $\dot{p} \in \mathbb{R}^6$. The matrix of hydraulic capacitance also grows to a 6×6. The spools of the on-off valves can only take values as $u \in [0, 1]$. The discharge coefficient and eigen frequency of the on-off valves are considered to be the same as the proportional ones.

4 Control

4.1 Classic control

A standard Proportional controller is used on the standard cylinders. The non-linear model has been linearised around cylinder middle position, which should be close to the lowest eigen-frequency of the cylinder. A velocity feedforward term is added to improve the trajectory tracking capabilities of the controller. A gain scheduling is introduced with a

gain and a velocity feedforward term for each direction of movement.

4.2 Secondary Controlled Multi-chamber cylinder

For the secondary controlled multi-chamber cylinder situation a simple force controller is chosen. The controller was originally suggested in [3] and since then has been augmented and improved with digital flow control units as in [1]. In [3], the controller switches between two constant pressure rails and the cylinder has four chambers. In [8] it was shown that having a third pressure rail with a value between the maximum and minimum pressure can result in a more efficient performance. The reason is that switching between pressures was identified as the largest source of losses for multi-chamber cylinders. The switching losses for a chamber which switches from one pressure $p(t)$ to another pressure p_s have been defined by [8] as:

$$E_{loss,\beta} = E_{supply} - E_{vol} = \int_0^\infty p_s Q(t)dt - \int_0^\infty p(t)Q(t)dt \tag{13}$$

These losses occur, because the flow exiting a constant pressure rail is the same as the one entering the cylinder chamber. Since fluid power is defined as the flow times the pressure at which it is delivered, the power exciting the pressure rail is larger than the one entering the cylinder. The excess energy is converted to heat over the valve. With further mathematical manipulation Hansen et al [8], prove that the losses for the chamber depend on the initial pressure p_0 and the end pressure p_1, the chamber volume V and the bulk modulus β:

$$E_{loss,\beta} = \frac{1}{2}(p_1 - p_0)^2 \frac{V}{\beta} \tag{14}$$

If the difference between p_1 and p_0 is small the switching loss is also small. Furthermore, because the pressure difference appears in the power of two in Eq. (14), switching to an intermediate pressure before switching to a high pressure can reduce losses considerably. The control algorithm can be expressed as choosing a control combination u_i where i is one of the 27 possible combinations, which minimises a cost function seen Eq. (15) . Each u_i is a vector of 9 binary values for the 9 valves - $u_i = [u_{i,1}, u_{i,2}, \cdots, u_{i,9}]$.

$$u_i = \underset{u_i}{argmin} \left\{ |F_{ref} - F_i| + W u_{change} \right\} \quad i = 1, \cdots, 27 \tag{15}$$

where

F_{ref}	is a force reference
F_i	is the force produce by valve combination i
W	is a weight to be chosen
u_{change}	is a binary values, which is equal to 1 if combination i is different from the current valve combination

The control algorithm selects one of the $3^3 = 27$ valve combinations (3 chambers and 3 possible pressures), which would produce a different force F_i. The aim is for this force to be as close as possible to a force reference. The force reference is obtained by using the non-linear model and the reference trajectory to determine a feedforward signal as seen in Eq. (17). In order to account for the fact that the discontinuous controller will not be

able to follow the continuous force trajectory perfectly, a position and a velocity error are added to the reference as seen in Eq. (18)

$$e = x_{ref} - x_p \quad \dot{e} = \dot{x}_{ref} - \dot{x}_p \tag{16}$$

$$F_{ff} = D(x_{ref})\ddot{x}_{ref} + C\dot{x}_{ref} + G(x_{ref}) \tag{17}$$

$$F_{ref} = F_{ff} + G_1 e + G_2 \dot{e} \tag{18}$$

where e and $\dot{e}$ are position and velocity errors, respectively. F_{ff} is a feedforward term calculated from the non-linear 1 degree model of the system in actuator space. $D(x)$ and $G(x)$ are functions for mass and gravitational force as seen by the cylinder. C is the viscous friction coefficient of the cylinder. G_1 and G_2 are gains. As mentioned before pressurising and de-pressurising chambers is associated with losses. That is the purpose of the "W" term. To select the middle pressure level and the weight on switching a parameter sweep is performed. The energy used to follow the trajectory as a function of weight and middle pressure can be seen in Fig.5. The root-mean-square of the position error can be seen in Fig.6. Here the energy used to track the trajectory is defined as

$$E_{sum} = \int_0^{t_{end}} p_{high} Q_{high}(t)dt + \int_0^{t_{end}} p_{med} Q_{med}(t)dt + \int_0^{t_{end}} p_{low} Q_{low}(t)dt \tag{19}$$

where Q_s, Q_{med} and Q_{low} are the flows exiting the pressure lines. It can be seen that

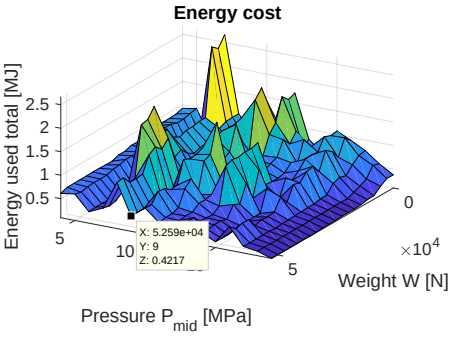

Figure 5: Energy used total as a function of weight and mid pressure

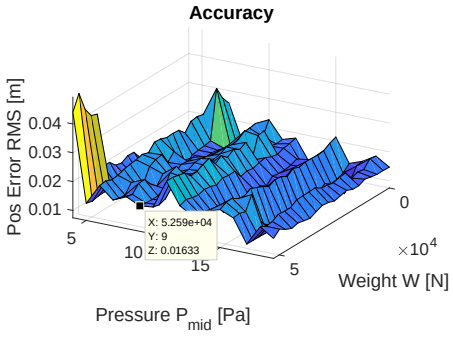

Figure 6: Tracking accuracy as a function of weight and mid pressure

there are multiple points with similar costs. Furthermore it can be seen that certain combinations of middle pressure and switching weight result in very poor performance. For most cases the middle pressure has a much larger effect on the efficiency of the system, compared with the effect of a different weight on the switching. The highlighted point is selected with a middle pressure $p_{mid} = 9\ MPa$ and a weight $W = 52590\ N$.
Since the valve are not infinitely fast first a "close valves" command is given and after 25 *ms* the "open valves" command is given. After another 25 *ms* a new combination is chosen. According to this the controller chooses a new combination every 50 *ms* and so it can be considered to be running at 20 Hz.

4.3 Augmented controller

A lot of attention within digital hydraulics has been devoted to minimising losses. Considering Eq. (13), changing the pressure level of a chamber is not desired. But in [5],

there is a preference for using the middle chamber pressure, because that pressure line is connected to an accumulator which stores regenerated energy. In order to examine how the algorithm performs if the middle pressure line is preferred an additional weight has been added to the controller. The augmented algorithm is:

$$u_i = \underset{u_i}{argmin} \{|F_{ref} - F_i| + W u_{change} + W_{large} u_{i,3} + W_{large} u_{i,6}\} \quad i = 1, \cdots, 27 \tag{20}$$

where $u_{i,3}$ and $u_{i,6}$ are the valves used to connect the high pressure rail to chambers A and B. W_{large} is an arbitrary weight chosen large enough to prevent the controller from using combination with higher pressures. Once again a parameter sweep has been conducted to determine how the middle pressure and the weight on switching will affect the performance. The effect on the energy used to follow the trajectory can be seen in Fig.7. The root-mean-square of the position error can be seen in Fig.8. It can be seen that the

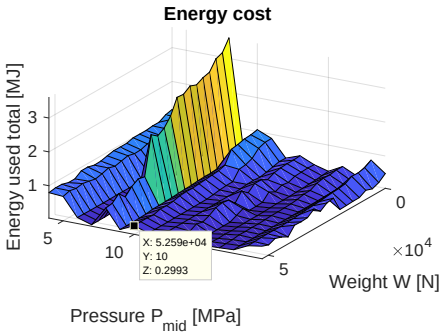

Figure 7: Energy used total as a function of weight and mid pressure

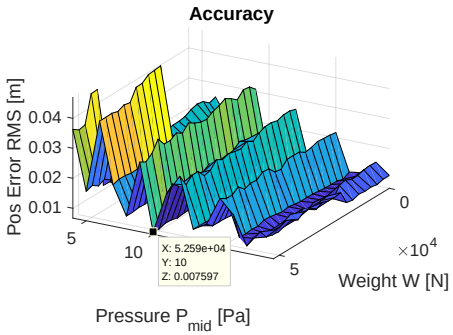

Figure 8: Tracking accuracy as a function of weight and mid pressure

pressure level has an even larger effect on the costs. Furthermore better performance can generally be obtained by using a larger medium pressure. A point close to the one used for the original controller is chosen. The medium pressure is raised from 9 *MPa* to 10 *MPa*, because of the large tracking error at 9 *MPa*. The large tracking error for some pressures is introduced, because the controller prefers not to use the high pressure line in chambers A and B. This reduces the force resolution. In the cases where the error is not increased, the available forces match the trajectory better.

5 Results

The trajectory tracking of the 3 controllers can be seen in Fig.9. Better tracking performance can be achieved by either selected a different pressure or increasing the gains G_1 and G_2. A different pressure was not selected, because the point chosen was apparently optimal according to Fig.5 and Fig.6. It is obvious that the proportional controller follows the trajectory better.

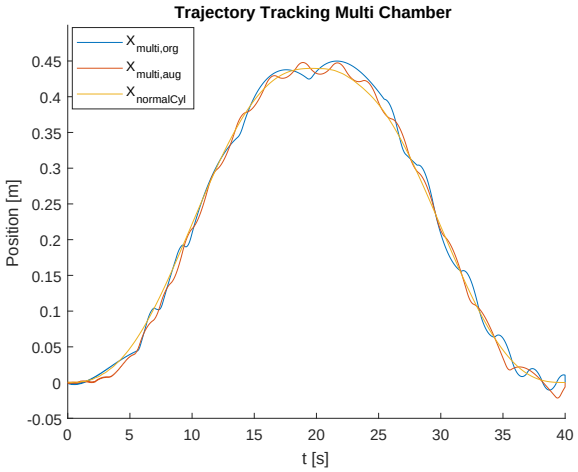

Figure 9: Trajectory tracking with the different controllers

The energy used to follow the trajectory by the 3 controllers can be seen in Fig.10. Both multi-chamber cylinders use less energy than the standard cylinder. But they use nearly the same amount of energy as each other.

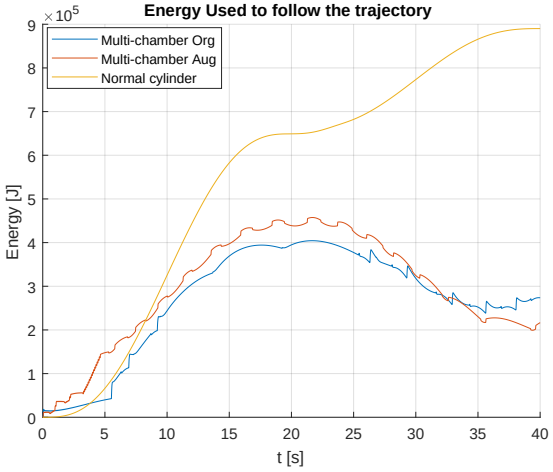

Figure 10: Energy used to follow the trajectory

To investigate the difference between the controllers the energy used by each chamber can be seen in Fig.11 for the original controller and in Fig.12 for the augmented one. It can be seen that the original controller uses more energy through chamber A but also returns more energy through chamber B. This is because both A and B chamber are connected to the same high pressure. In comparison chamber A in the augmented controller uses nearly half the energy, but very little energy is returned through chamber B. During the lowering motion, chamber A in original controller is switched between high and medium pressure. This reduces the efficiency of energy regeneration.

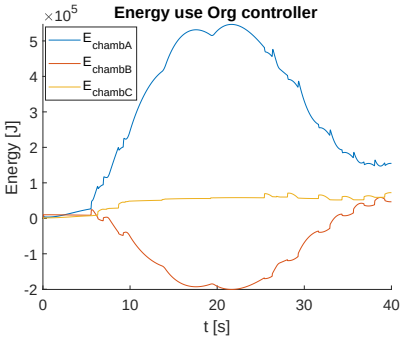

Figure 11: Energy used to follow the trajectory by chamber

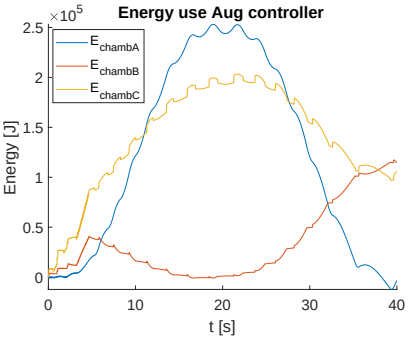

Figure 12: Energy used to follow the trajectory by chamber

The chamber pressures can be seen seen in Fig.13 and Fig.14. Fig.13 shows that for a large part of the trajectory the pressures do not change for the original controller. Furthermore both of the large chambers are connected to the high pressure. The lack of switching of the large chamber with few switches of the smallest chamber to middle pressure explain why this the middle pressure and weigth were determined as near optimal. In comparison the augmented controller switches more often, but it is the second and third chambers that are switching. This enables chamber A to regenerate all of the energy it had used in the first half of the trajectory. Very little energy is regenerated through Chamber B for the first half of the trajectory and it uses a lot of energy in the second half. Most of the energy is lost due to the switching in chambers B and C. The large amount of switching just before the 5 second mark is due to the velocity feedback. Reducing or removing it completely avoided this problem, but the overall tracking of the controller was much poorer.

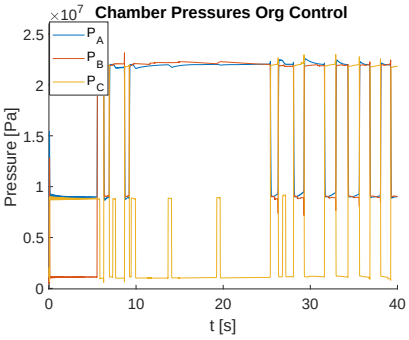

Figure 13: Pressures used to follow the trajectory

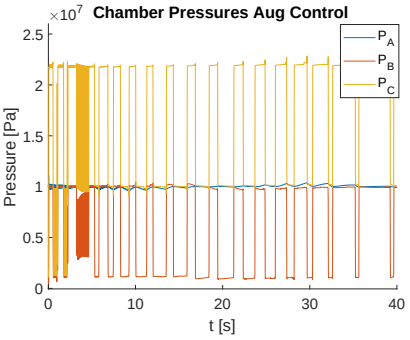

Figure 14: Pressures used to follow the trajectory

The forces used by the multi-chamber cylinder force controllers can be seen in Fig.15. It can be seen that the force produced by the multi-chamber cylinder with the original controller is very close to the predetermined feedforward signal. It can be seen that when lowering the jib, the original controller produces huge force spikes. This is due to dangerous switching combinations that involve switching the pressure of all the chambers simultaneously. In this paper, it has been assumed that the valves have no uncertainty in

closing time. In reality this is not the case and it has been shown that the problem can be much larger and it is difficult to avoid [9]. To test the robustness of the controllers they

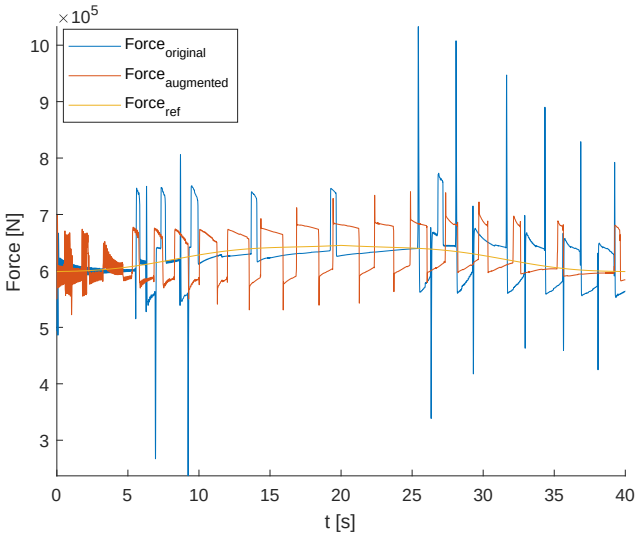

Figure 15: Forces applied by the different controllers

have been tested under different conditions. The conditions involve a trajectory which is two times faster, and a trajectory that is two times slower. Then the weight and inertia of the outer jib have been doubled and the three trajectories are run again with both controllers. The results can be seen in table 2 and table 3.

Results with original load

	Energy used [MJ]			Error RMS [m]		
Velocity	Normal	Increased	Decreased	Normal	Increased	Decreased
Normal Cyl	0.89007	0.89308	0.88867	0.002	0.0026	0.0013
Contr Org	0.27357	0.28364	0.71907	0.0097	0.0113	0.0098
Contr Aug	0.21672	0.14764	0.22810	0.0074	0.0124	0.0074

Table 2: Result of simulations with different trajectories

6 Conclusion and future work

Some conclusions can be made based on the results in this paper.

- Energy wise the knuckle-boom crane is a good fit for digital hydraulic technology.
- The tracking performance of the multi-chamber cylinder force controllers is not satisfactory, because for instance due to the lengths of the links an error of 0.0188 m as seen in Fig.9, result in a deviation of ≈ 0.45 m of the tool center point of the crane.

Results with increased load

	Energy used [MJ]			Error RMS [m]		
Velocity	Normal	Increased	Decreased	Normal	Increased	Decreased
Normal Cyl	0.89455	0.91036	0.89207	0.0054	0.0087	0.0028
Controller Org	0.47680	0.39424	0.79168	0.0078	0.0090	0.0088
Controller Aug	0.37959	0.28645	0.65295	0.0118	0.0180	0.0133

Table 3: Result of simulations with different trajectories and increased load

- Tracking wise the two multi-chamber controllers are robust in the sense that changing the load and velocity of the trajectory does not degrade the tracking performance considerably.
- The energy use of the multi-chamber force controllers cannot be said to be robust as seen in table 2, specifically the result with a decreased velocity trajectory and the original controller.
- The choice of middle pressure level and switching weight is not trivial, because their effect on the energy and error cost are non-linear as seen in the parameter sweep plots Fig.5, Fig.6,Fig.7 and Fig.8.
- If the middle pressure line changes significantly during the operation of the system the performance of the controller may also change, as seen in the results of the parameter sweeps in Fig.6 and Fig.8.
- The weight on switching is meant to prevent chattering situations such as the one in Fig.14, but this cannot be guaranteed with a preselected constant weight.
- Slower trajectories with a larger load may result in more switching which can bring the overall efficiency of the controller down considerably as seen in table 3.
- The size of the chambers needs to be taken into account when switching as shown in [8] and [10].

Based on these consideration a model predictive controller, which can optimise over a certain horizon, might be a good solution. In [11] a model predictive controller is used to drive a multi-chamber cylinder and the results are compared with a controller similar to [4] and the ones used in this paper. The model predictive controller showed better tracking performance while still using less energy.
Also in [6] a knuckle-boom crane with flexible bodies is considered. It should be investigated if any resonance modes might be excited in the structure.
Further it should be investigated if it is beneficial to have more pressure rails. The increased force resolution should result in less switching. It appears that a tendency has emerges towards towards multiple pressures, but normal cylinder. Instead of 3 pressure lines Huova et al. propose 100 in [10], but probalby due to practical reasons a prototype with 7 pressure line is tested instead and 6 are used in [12]. Since the pressure difference between the steps is smaller the compressibility losses are reduced. This is due to some extent because the smaller force steps result in smaller losses, when switching between them, but also as seen Fig.15 if a force combination is very close to the force reference the controller doesn't need to switch as often. Adding an additional pressure line has a much

smaller effect on the force resolution, than an additional chamber. On the other hand having more than two chambers in a cylinder introduces force steps, which can result in a large force uncertainty while switching.

7 ACKNOWLEDGMENT

The research in this paper has received funding from The Research Council of Norway, SFI Offshore mechatronics, project number 237896/O30.

References

[1] M. Huova, A. Laamanen, and M. Linjama, "Energy efficiency of three-chamber cylinder with digital valve system," *International Journal of Fluid Power*, vol. 11, no. 3, pp. 15–22, 2010.

[2] K. Pettersson, K. Heybroek, P. Mattsson, and P. Krus, "A novel hydromechanical hybrid motion system for construction machines," *International Journal of Fluid Power*, vol. 18, no. 1, pp. 17–28, 2017.

[3] M. Linjama, H. Vihtanen, A. Sipola, and M. Vilenius, "Secondary controlled multi-chamber hydraulic cylinder," in *The 11th Scandinavian International Conference on Fluid Power, SICFP*, vol. 9, 2009, pp. 2–4.

[4] R. H. Hansen, M. M. Kramer, and E. Vidal, "Discrete displacement hydraulic power take-off system for the wavestar wave energy converter," *Energies*, vol. 6, no. 8, pp. 4001–4044, 2013.

[5] P. Dengler, M. Geimer, and R. v. Dombrowski, "Deterministic control strategy for a hybrid hydraulic system with intermediate pressure line," in *ASME/BATH 2012 Symposium on Fluid Power and Motion Control*. American Society of Mechanical Engineers, 2012, pp. 334–347.

[6] M. K. Bak and M. R. Hansen, "Analysis of offshore knuckle boom crane-part one: modeling and parameter identification," *Modeling, Identification and Control*, vol. 34, no. 4, p. 157, 2013.

[7] P. E. Nikravesh, *Computer-aided analysis of mechanical systems*. Prentice-Hall, Inc., 1988.

[8] R. H. Hansen, T. O. Andersen, and H. C. Perdersen, "Analysis of discrete pressure level systems for wave energy converters," in *Fluid Power and Mechatronics (FPM), 2011 International Conference on*. IEEE, 2011, pp. 552–558.

[9] A. Laamanen, M. Linjama, and M. Vilenius, *On the pressure peak minimization in digital hydraulics*. Tampere University of Technology, 2007, pp. 107–121, contribution: organisation=iha,FACT1=1.

[10] M. Huova, A. Aalto, M. Linjama, K. Huhtala, T. Lantela, and M. Pietola, "Digital hydraulic multi-pressure actuator–the concept, simulation study and first experimental results," *International Journal of Fluid Power*, pp. 1–12, 2017.

[11] A. Hansen, M. Asmussen, and M. Bech, "Energy optimal tracking control with discrete fluid power systems using model predictive control," *submitted to The Ninth Workshop on Digital Fluid Power*, 2017.

[12] M. Huova, A. Aalto, M. Linjama, and K. Huhtala, "Study of energy losses in digital hydraulic multi-pressure actuator," in *The 15th Scandinavian International Conference on Fluid Power*, 2017.

Paper C

Application of Model Predictive Control in Discrete Displacement Cylinders to Drive a Knuckle Boom Crane

Viktor Donkov, Torben Ole Andersen, Morten Kjeld Ebbesen, Henrik Clemmensen Pedersen

This paper has been published in the proceedings of
The Global Fluid Power Society PhD Symposium, July 18-20, 2018, Samara, Russia.

Application of Model Predictive Control in Discrete Displacement Cylinders to Drive a Knuckle Boom Crane

Viktor Hristov Donkov
Dept. of Energy Technology
Aalborg University
Aalborg, Denmark
vhd@et.aau.dk

Torben Ole Andersen
Dept. of Energy Technology
Aalborg University
Aalborg, Denmark
toa@et.aau.dk

Henrik Clemmensen Pedersen
Dept. of Energy Technology
Aalborg University
Aalborg, Denmark
hcp@et.aau.dk

Morten Kjeld Ebbesen
Dept. of Engineering Sciences
University of Agder
Grimstad, Norway
morten.k.ebbesen@uia.no

***Abstract*—In this paper, two Discrete Displacement Cylinders (DDCs) are used to drive the boom of a knuckle boom crane. DDCs operate by connecting one of several available pressure levels to each chamber in order to produce different forces. A trade-off exists with such systems, between the accuracy of tracking and energy dissipation due to switching. A popular way to approach this problem is a Force Shifting Algorithm (FSA). However, in this paper, the trade-off is managed by use of a Model Predictive Control (MPC) algorithm. The tracking accuracy and energy efficiency of the MPC and FSA strategies for DDCs are compared to a PID strategy for standard cylinders. The comparison is obtained by use of a computer simulation of a knuckle boom crane performing a realistic load cycle. The load cycle consists of the crane extending to pick up a load and then retracting to place it at an appropriate location. The main results show that MPC can deliver smoother and more accurate motion than FSA, while using less energy. Compared with standard cylinders and PID control, MPC uses less energy, but due to the switching of chamber pressures, the motion is smoother with the standard strategy. Both FSA and MPC can have degraded performance when a large change in load is introduced.**

***Index Terms*—Discrete Displacement Cylinders, Knuckle Boom Crane, Model predictive control**

I. Introduction

Digital hydraulics is a field receiving a lot of attention in recent years. The field attempts to improve the efficiency of hydraulic systems by making sure that each component operates at peak efficiency despite the changing conditions. A sub field of digital hydraulics is the study of multi-chamber cylinders or Discrete Displacement Cylinders (DDC). DDCs can offer up to 60% reduction in power loss [1] compared with a standard cylinder. This is achieved by connecting the various cylinder chambers to constant pressure rails by on/off valves. The number of chambers and pressure levels defines the number of force combinations which are available. Unfortunately, the resulting motion of the cylinder can be jerky if a small number of combinations are available. Surges in motion can also occur if the system has a small inertia. This can be a problem as in some applications (i.e. cranes) the inertia in the system can vary greatly. Most control strategies applied to DDCs involve a trade-off between the smoothness of motion and the energy efficiency of the cylinder. The trade-off is usually tied to a heuristic method involving a user selected weight [1], and a timer which prevents further switching of a chamber [7]. In another digital hydraulics field (hydraulic buck converters) choosing the switching pattern for the entire trajectory shows very promising result. Using the optimised control series as a pure feedforward signal has lead to reduced pressure pulsations [2]. It stands to reason that optimising with more information can lead to a better trade-off, but in practical application uncertainties and disturbances will interfere with the optimality of the signal. For this reason Model Predictive Control (MPC) stands out as a good candidate for control. In [3] a MPC control structure was tested on a DDC pushing against a linear spring damper. The MPC's performance was compared with a Force Selection Algorithm (FSA) and it was concluded that the MPC achieved better accuracy in a more energy efficient manner. In this article MPC will be applied to two DDCs in a simulation study. In this simulation the DDCs will be actuating the jibs of a knuckle boom crane in order to follow a realistic loading scenario.

In section II, the dimensions of the knuckle boom crane are presented and the model of the system is described. The control is discussed in section III. The performance of the controllers will be presented and discussed in section IV. The paper ends with conclusions and future work in section V.

978-1-5386-4785-1/18/$31.00 ©2018 European Union

II. Application and model

Knuckle boom cranes are high force low speed systems which often move large masses. The cranes are widely used in offshore drilling platforms. A picture of a knuckle boom crane can be seen in Fig.1. The hydraulic circuit for the system can be seen in Fig.3. For the case where DDCs are used instead, the hydraulic circuit for one cylinder can be seen in Fig. 4. The three pressure lines are assumed to have constant pressure. Their creation has not been considered.

The test trajectory for this situation starts the crane at a so called origin point, extends it to point 2 to pick up a load of

Fig. 1. Knuckle Boom Crane example provided by National Oilwell Varco.©

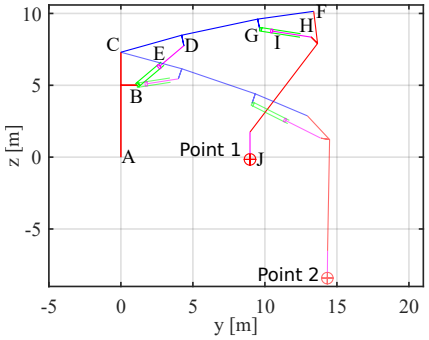

Fig. 2. Simplified representation

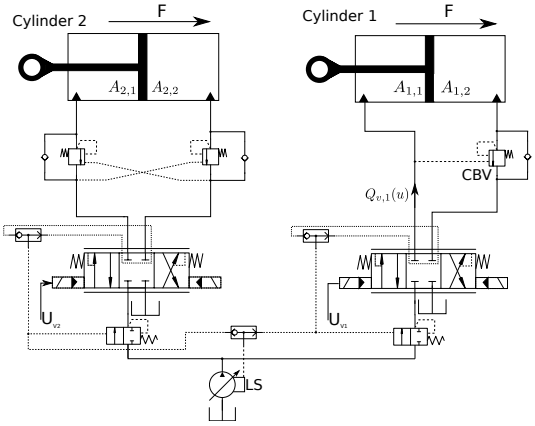

Fig. 3. Knuckle Boom Crane hydraulic circuit

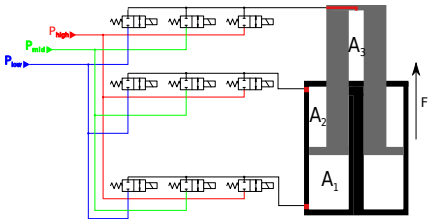

Fig. 4. Representation of the multi-chamber cylinder used in the paper

20000 kg and finally retracts the crane back to point 1. The location of these points can be seen in Fig. 2

The crane structure has been modeled according to the Nikravesh method [5]. The mechanical equations can be seen in Eq. (1). In the equation M is matrix of masses and inertias for each body, D is the constraint Jacobian, λ is the vector of Lagrange multipliers, $\dot{v}$ is a vector of the linear and rotational acceleration of the bodies, g_{ext} is the vector of external forces (including gravity and cylinder forces), b is the gyroscopic term, and γ is calculated from the derivation of the kinematic constraints of the system.

$$\begin{bmatrix} M & D^T \\ D & 0 \end{bmatrix} \begin{bmatrix} \dot{v} \\ \lambda \end{bmatrix} = \begin{bmatrix} g_{ext} - b \\ \gamma \end{bmatrix} \tag{1}$$

The crane has 8 bodies (each cylinder is divided in 2 bodies). The bodies are column, inner jib, cylinder and piston 1, outer jib, cylinder and piston 2, and the load. They can be seen in Fig.2. There are 3 linear and 3 rotational coordinates used to describe the location of each body creating a generalised coordinate vector $q \in \mathbb{R}^{48\times 1}$ and the accelerations of the system are collected in $\dot{v}$ as seen in Eq. (2).

$$\dot{v} = \begin{bmatrix} \ddot{r}_1 \\ \dot{\omega}_1 \\ \vdots \\ \ddot{r}_8 \\ \dot{\omega}_8 \end{bmatrix} \quad q = \begin{bmatrix} r_1 \\ \Theta_1 \\ \vdots \\ r_8 \\ \Theta_8 \end{bmatrix} \tag{2}$$

The mechanical system is modelled as 7 revolute joints (A,B,C,D,F,G,H in Fig.2) and two parallel constraints (E,I in Fig.2) similar to how a knuckle boom crane was modeled in [4]. The load is constrained with a distance constraint (between point J and the tip of the jib in Fig.2). Finally b is the gyroscopic term seen in Eq. (3), J_i is the matrix of mass moment inertia of body i and so on.

$$b = \begin{bmatrix} 0^{3\times 1} \\ \tilde{\omega}_1 J_1 \omega_1 \\ \vdots \\ 0^{3\times 1} \\ \tilde{\omega}_8 J_8 \omega_8 \end{bmatrix} \tag{3}$$

where $\tilde{\omega}_1$ is the skew symmetric matrix constructed from the elements of ω_1 in order to represent cross product.

As previously mentioned the cylinder forces are included in g_{ext}. The cylinder forces are calculated from the pressure and area of each cylinder chamber. The one dimensional force calculated in this way is converted into a three dimensional force vector by using the unit vector of the cylinder orientation.

The hydraulic schematic for the knuckle boom crane can be seen in Fig. 3. The system comprises of two cylinders, controlled through pressure compensated directional proportional valves. The system is supplied by a variable displace-

ment pump with load sensing (LS) capabilities. This makes the system more efficient than the constant pressure supply considered in [6], because throttling losses are reduced. The change in pressure in the chambers has been modelled as Eq. (4). C is the hydraulic capacitance of the chamber, and Q_{move} and Q_{valve} are the change in volume and the flow through the valve, respectively.

$$\dot{p}_p = \underbrace{\frac{\beta_1}{V_1}}_{C}\left(\underbrace{-A_1\dot{x}_p}_{Q_{move}} + \underbrace{Q_{v,1}(u)}_{Q_{valve}}\right) \tag{4}$$

The flow through the valve to the chamber is simplified, because the mobile hydraulic valve is pressure compensated. In the forward path it is given as a percentage of the maximum flow. When returning flow the standard orifice equation is used as seen in Eq. (5). Here k_q is the discharge coefficient, p_p is chamber pressure, $S(*)$ is the sign function, and u is the spool position.

$$Q_{v,1}(u) = \begin{cases} Q_{max}u & u \geq 0 \\ k_q u S(p_p - p_t)\sqrt{(|p_p - p_t|} & u < 0 \end{cases} \tag{5}$$

For the second chamber, the opening of the Counterbalance valve (CBV) is calculated as Eq. (6). In this equation $x_{cbv1,1}$ is the normalised CBV opening, R is the ratio of the CBV, p_{CP} is the crack pressure, and K_s is the spring stiffness converted to bar.

$$x_{cbv1} = \begin{cases} \frac{p_p R + p_r - p_{CP}}{K_s} & p_p R + p_r > p_{CP} \\ 0 & p_p R + p_r < p_{CP} \\ 1 & p_p R + p_r - p_{CP} > K_s \end{cases} \tag{6}$$

The flow from the piston side chamber to tank, which passes through the counterbalance valve is calculated by the orifice equation. In order to simplify the model the fluid volume between the CBV and the directional valve has been omitted. Instead the two orifices (CBV and direction valve) are considered as a single equivalent orifice as in Eq. (7).

$$A_{eq} = \begin{cases} \sqrt{\frac{1}{\frac{1}{(|u|A_{dv})^2} + \frac{1}{(x_{cbv1}A_{check})^2}}} & |u|, x_{cbv1} > 0 \\ 0 & |u|, x_{cbv1,1} = 0 \end{cases} \tag{7}$$

For the DDC cylinder the same equation as Eq. (4) has been used for each chamber. The DDCs used in this article have 3 chambers as can be seen in Fig. 4. The 3 chamber areas have been chosen in a ratio of $A_1 : A_2 : A_3 = 4 : 2 : 1$. The actual areas have been chosen so the cylinder produces a maximum positive force corresponding to the original cylinders. The comparison can be seen in Fig. 5, where 0, 1, 2 correspond to low, mid and high pressure respectively, and the rows correspond to chambers A_1, A_2, and A_3 from top to bottom.

III. Control

In this article three control structures will be used on the system - standard PID with pressure feedback and a velocity feedforward, a FSA as in [1], and an MPC. FSA control of a knuckleboom crane with DDC has been attempted in [6] and

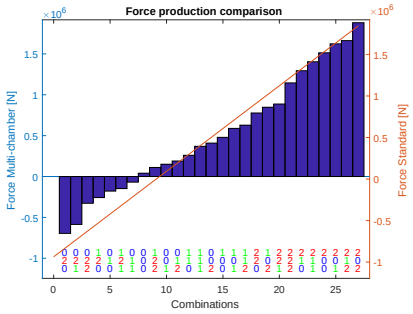

Fig. 5. Forces the standard and multi-chamber cylinders can produce with the chosen pressures

will not be elaborated in detail. In essence the algorithm tries to follow a force reference. The pressures for each chamber are selected according to

$$u = \underset{u}{argmin}\ \{|F_{ref} - F_i| + Wu_{change}\} \quad i = 1, \cdots, 27 \tag{8}$$

In this equation $u \in \mathrm{R}^{9\times 1}$ is a vector of valve opening, F_i are the 27 possible force combinations, Wu_{change} is the weight and combination change indicator. For more information on FSAs the reader is directed to the following references [1] and [7]. In [6] it was found to be beneficial not to select the middle pressure level manually. Instead, the pressure level and the weight on switching were selected through an optimisation algorithm.

The third control structure used in this article is a MPC. The controller uses a model of the system to predict several future time steps. The future output of the model is a function of the current and future control inputs. The predicted states are included in a cost function turning the control problem into an optimisation problem. The optimisation problem is solved by an optimisation algorithm. MPC applied to a DDC for the purpose of position tracking has been attempted in [3]. The DDC was working against a linear spring damper and the load was inertial in nature. Furthermore, a non-linear equation for calculating losses was used in the cost function. Due to the integer constraint on the inputs and the non-linear cost function, a genetic algorithm was used to solve the optimisation problem. In this case the MPC was shown to produce a more energy efficient, smoother, and more accurate motion than the FSA control. In our investigation the mass moment of inertia of the system is changing due to the moving parts of the crane and the varying load. The position reference is continuous while the inputs are still constrained to integers. The resulting problem is a Mixed Integer Program. The input to the system is a vector of the states of the 9 valves. Each valve can either be closed or opened. The trend of the losses is captured through a linear equation. In this way the cost function, becomes linear and convex (if integrality constraint

is relaxed). The control algorithm can be stated as

$$u(k) = \underset{\hat{u}}{argmin}\ \{J\} \tag{9}$$

where $u(k)$ is the vector of valve openings which will be applied to the system, $\hat{u} \in \mathrm{R}^{9M\times 1}$ is the vector of predicted inputs up to the horizon M i.e. $\hat{u} = [u(k); u(k+1); \cdots ; u(M);]$. The cost function to be optimised is:

$$J = \hat{e}^T \hat{Q} \hat{e} + |F\hat{u}|_1 \tag{10}$$

Here $\hat{e}$, $\hat{Q}$ are an error vector and a weight matrix in order to obtain a quadratic form. With a cost function of this form the optimisation problem becomes a generalised lasso. Furthemore, since the F matrix is the difference matrix seen in Eq. (11), the problem becomes total variation denoising [10].

$$\begin{aligned} &if \quad && i == j \\ &\quad && F(i,j) = -V_{chamb_n} \tfrac{p_z}{p_{high}} \\ &elseif \quad && j == i + 9 \\ &\quad && F(i,j) = V_{chamb_n} \tfrac{p_z}{p_{high}} \\ &else \\ &\quad && F(i,j) = 0 \\ &end \end{aligned} \tag{11}$$

The multiplication of F and $\hat{u}$ produces a vector

$$F\hat{u} = \begin{bmatrix} V_{chamb_1} \frac{p_t}{p_{high}}(-u_1(k) + u_1(k+1)) \\ V_{chamb_1} \frac{p_{mid}}{p_{high}}(-u_2(k) + u_2(k+1)) \\ \cdots \\ V_{chamb_3} \frac{p_{high}}{p_{high}}(-u_9(M-1) + u_9(M)) \end{bmatrix} \tag{12}$$

Taking the norm of this vector gives a measure of the number of switchings for all the valves. This term punishes excessive switching and thus reduces the losses associated with switching. V_{chamb_n} is the volume of the chamber n, where $n = \{1, 2, 3\}$. This weight punishes switching of chambers with larger volumes. The ratio $\frac{p_z}{p_{high}}$, where $p_z = \{p_t, p_{mid}, p_{high}\}$, punishes switching of larger pressures. In [3] the input to the system is considered to be one of the 27 possible forces similar to Eq. (8). The optimal input is then constrained to be a member of one of these 27 forces. In order to calculate the losses associated with switching between two forces a lookup table matches forces to chamber pressures. The losses are then calculated according to

$$E_{switching} = \sum_{k=1}^{M} \sum_{n=1}^{3} \frac{V_{chamb_n}}{2\beta} |p(k) - p(k-1)|^2 \tag{13}$$

The Eq. (12) models the same behaviour by using a linear transformation and avoiding the need for a look-up table. Clearly Eq. (13) has a quadratic term so the results are not the same, but the trend is kept, because larger differences between the old and new pressure result in larger losses. The constraints in the system also have to be included. The first constraint limits the values in $\hat{u}$ between 0 and 1

$$\hat{0} \leq \hat{u} \leq \hat{1} \tag{14}$$

where $\hat{0}$ and $\hat{1}$ denote vectors of appropriate size. Another constraint is that only one pressure line can be connected to a chamber at a time. This avoids short circuiting the supply lines which can lead to losses and unforeseen movement of the cylinders. To enforce this constraint the following equation is used

$$L\hat{u} = \begin{bmatrix} u_1(k) + u_2(k) + u_3(k) \\ \vdots \\ u_7(M) + u_8(M) + u_9(M) \end{bmatrix} \quad L\hat{u} == \hat{1} \tag{15}$$

Since the elements of $u(k)$ are constrained to be integers the result is that only one valve can be open to a chamber at a time. The error over several time steps is

$$\hat{e} = \begin{bmatrix} e(0) \\ e(1) \\ \vdots \\ e(M) \end{bmatrix} \tag{16}$$

Since the controller is meant to follow a position reference, the error term for each time step is selected as Eq. (17). Only the position reference will be followed because of the way $\hat{Q}$ is selected.

$$e(k) = \begin{bmatrix} 0 \\ 0 \\ 0 \\ x_{ref}(k) \\ v_{ref}(k) \end{bmatrix} - \begin{bmatrix} p_1(k) \\ p_2(k) \\ p_3(k) \\ x_p(k) \\ v_p(k) \end{bmatrix} \tag{17}$$

The cost function for optimisation involves this error vector included as a quadratic form with a weight matrix $\hat{Q}$ i.e. $\hat{e}\hat{Q}\hat{e}$. The weight matrix itself will be composed as $\hat{Q} = diag\{Q, Q, \cdots, P\}$ where Q and P are diagonal matrices with elements:

$$Q = diag\{0, 0, 0, W_1, 0\} \quad P = diag\{0, 0, 0, W_2, 0\} \tag{18}$$

The two weights punish position error only. W_1 will punish position error for all time except the last time step, while W_2 will punish only the position error at the last time step. If it is desired to follow the velocity reference as well another weight can be introduced e.g. $Q = diag\{0, 0, 0, W1, W_v\}$. This doubles the optimisation variables and increases the solution time. Since a relatively long prediction horizon M=5 was selected in this article the velocity reference was not included. For the prediction model a difference equation was used in which $x(k)$ is the state vector for time instance k, A is the state matrix, B is the input matrix, $u(k)$ is the vector of 9 valve states. The vector A_{grav} is a constant gravitational term. The gravitational term was added to the model, because a large steady state error was observed otherwise. It can be expected that counteracting the gravitational term accounts for a large part of the force production in crane systems. The procedure was to calculate the torque due to gravity at joints C and F in Fig. 2 for a specific configuration and load. This torque was then converted into an equivalent force on each cylinder and its final effect on acceleration is $A_{grav} = [0, 0, 0, 0, F_{grav}T_s/M_{eq}]^T$. In reality

as the cranes moves away from the linearisation point, both the equivalent mass and the equivalent force change. In the linear model they are kept constant.

$$x(k+1) = Ax(k) + Bu(k) - A_{grav} \tag{19}$$

The state vector and input vector were selected as

$$x = \begin{bmatrix} p_1 \\ p_2 \\ p_3 \\ x_p \\ v_p \end{bmatrix} \qquad u = \begin{bmatrix} u_1 \\ \vdots \\ u_9 \end{bmatrix} \tag{20}$$

This makes the matrix $A \in \mathrm{R}^{5\times5}$ with the following entries

$$A = \begin{bmatrix} 0 & 0 & 0 & 0 & 0 \\ 0 & 0 & 0 & 0 & 0 \\ 0 & 0 & 0 & 0 & 0 \\ 0 & 0 & 0 & 1 & Ts \\ \frac{A_1 T_s}{M_{eq}} & -\frac{A_2 T_s}{M_{eq}} & \frac{A_3 T_s}{M_{eq}} & 0 & 1 \end{bmatrix} \tag{21}$$

The input matrix $B \in \mathrm{R}^{5\times9}$ is

$$B = \begin{bmatrix} p_t & p_{mid} & p_{high} & 0\,0\,0 & 0\,0\,0 \\ 0\,0\,0 & p_t & p_{mid} & p_{high} & 0\,0\,0 \\ 0\,0\,0 & 0\,0\,0 & p_t & p_{mid} & p_{high} \\ 0 & & \cdots & & 0 \\ 0 & & \cdots & & 0 \end{bmatrix} \tag{22}$$

In essence the pressure dynamics are ignored in order to simplify the problem. The valves require 15 ms to open or close. Furthermore when switching from one pressure to another one valve needs to be closed before the other is opened. This avoids short circuiting the flow lines and uncertain changes in the pressure chamber. The sample time is selected as $T_s = 45$ ms. It was observed that the pressure in the chamber is able to reach that of the constant pressure rail in most cases with this controller sampling.

Using this model the future evolution of the system can be described by:

$$\begin{bmatrix} x(1) \\ x(2) \\ \vdots \\ x(M) \end{bmatrix} = \begin{bmatrix} B & 0 & \cdots & 0 \\ AB & B & \cdots & 0 \\ \vdots & \vdots & \ddots & \vdots \\ A^{M-1}B & A^{M-2}B & \cdots & B \end{bmatrix} \begin{bmatrix} u(1) \\ u(2) \\ \vdots \\ u(M-1) \end{bmatrix} + \begin{bmatrix} A \\ A^2 \\ \vdots \\ A^M \end{bmatrix} x(0) - \begin{bmatrix} I & 0 & \cdots & 0 \\ A & I & \cdots & 0 \\ \vdots & \vdots & \ddots & \vdots \\ A^{M-1} & A^{M-2} & \cdots & I \end{bmatrix} A_{grav} \tag{23}$$

This can also be written as

$$\hat{x} = G\hat{u} + \hat{x_o} - \hat{A}_{grav} \tag{24}$$

In order to tune the controller two scalar weights are put in the cost function:

$$J = \hat{e}^T w_{pos} \hat{Q} \hat{e} + |w_{enrg} F \hat{u}|_1 \tag{25}$$

The scalars w_{pos} and w_{enrg} can be found through an exhaustive search. These will be the two parameters for tuning the controller. In this case they were tuned by hand for each cylinder. The weights W_1 and W_2 are selected with a ratio 1:2 i.e $W_2 = 2W_1$. This is introduced with the desire to reduce the greediness of the optimisation with regard to the initial position error. With this ratio future errors are associated with a larger weight. However, the weight on switching is the same for all time instants. The result is that switching in the future is slightly more preferable to the algorithm.

IV. Simulation Results

The knuckle boom crane in the simulation study has the following size: the inner jib has a length of 13.750 m and the outer jib has a length of 9.241 m.

For the case with the standard cylinders the load sensing pump has a maximum pressure of 300 bar. The pump pressure is always selected as 35 bar higher than the largest load pressure. The crack ratio of the CBVs has been selected as 5:1 and the crack pressure has been selected as 235 bar and 260 bar for cylinder 1 and 2 respectively. The inflow compensated mobile valve can deliver a maximum of 160 l/min to each cylinder.

For the DDCs the three pressure levels are $p_t = 10$ bar, $p_{mid} = 100$ bar and $p_{high} = 300$ bar. The lines are assumed to be created and maintained separately. They are also assumed to have no limitation on the amount of fluid they can supply. The area ratio is 4:2:1 as mentioned before. The on/off valves are assumed to have a response time of 15 ms and a discharge coefficient of 114 $\frac{l}{min\sqrt{bar}}$.

The weight W, which reduces switching in the FSA has been selected as 5000. The rather small number for shifting penalty is due to the slow rate at which the force reference changes. In [6] the force reference was generated with a PD filter. The derivative of the position error improved stability, but it also increased the rate of switching. In this paper the force reference is being generated with a PI filter. This resulted in the low switching weight. The optimisation problem has been set up in Yalmip [8] with the MOSEK solver [9]. As mentioned before, the prediction horizon was selected as M=5. This gives the following sizes for the optimisation variables $\hat{e} \in \mathrm{R}^{25\times1}$ and $\hat{u} \in \mathrm{R}^{45\times1}$. The sampling time for the controller was selected as 45 ms. The MOSEK solver automatically selected a MIP algorithm. The simulation was conducted on a Windows 10 laptop with an Intel(R) Core(TM) i7-5600U running at 2.6 GHz. The average time the solver took to solve the optimisation is 0.23 s. This time is of course not implementable in a real time controller. Using a 3 time step horizon leads to solver times of 0.15 s, which is still too large. The efficiency of the algorithm will be investigated in the future.

The tracking results of the three control structures can be seen in Fig. 6 and Fig. 7. It can be seen that the large increase in load leads to a large error for the MPC and FSA. Furthermore it can be seen that in the first part of the trajectory, the MPC has smoother motion than the FSA algorithm. The tracking in case of a constant load of 200 kg was also tested. The

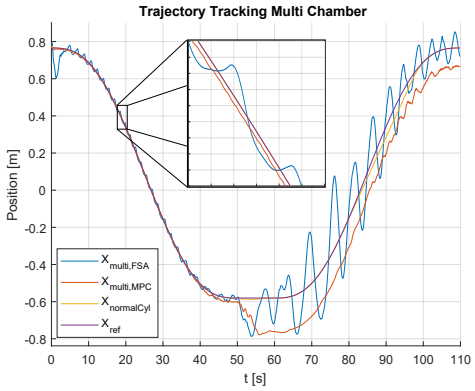

Fig. 6. Tracking results of the first cylinder with a changing load.

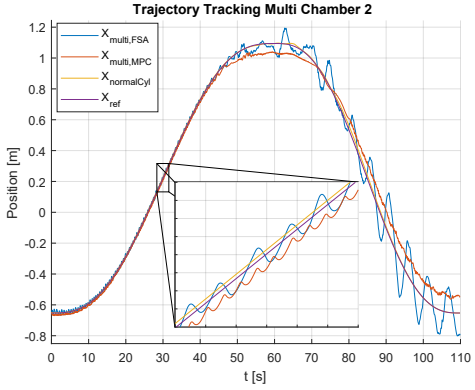

Fig. 7. Tracking results of the second cylinder with a changing load.

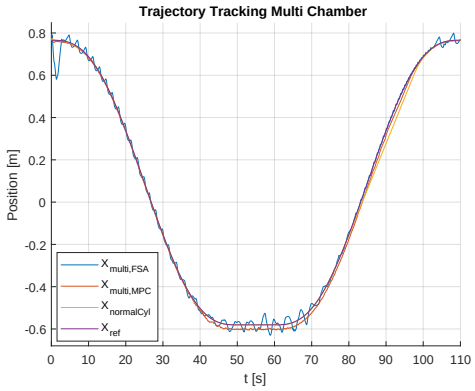

Fig. 8. Tracking results of the first cylinder with a constant load.

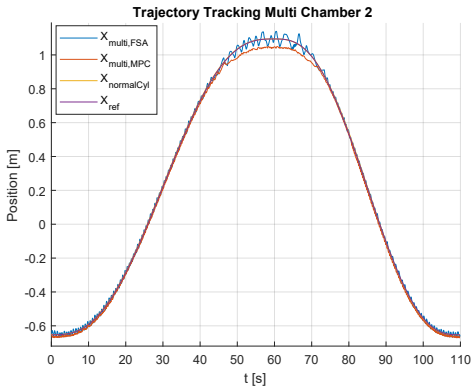

Fig. 9. Tracking results of the second cylinder with a constant load.

results can be seen in Fig. 8 and Fig. 9. It can be seen that the MPC has problems with accuracy in the area where the second cylinder is fully extended. At this point the equivalent mass is furthest from the value included in the linear model.

The energy used to follow these trajectories for each cylinder is defined as the integration of the flow leaving the constant pressure rails

$$E_{sum} = \sum_{i=1}^{3} \int_{0}^{t_{end}} p_i Q_i(t) dt \tag{26}$$

For the normal cylinder with a load sensing pump a similar equation is used but the pressure used is the higher load pressure. Summing the energy use for the two cylinders for the three situations results in the following Fig. 10. It can be seen that for the first part of the trajectory the MPC and the FSA follow the trajectory by using less energy than the standard cylinder. In the first part of the trajectory the MPC uses close to the same amount of energy as the FSA algorithm. In the second part where the load changes the FSA uses more energy than the MPC and the normal cylinder case. If the load is kept constant then the the MPC achieves the best energy efficiency as can be seen in Fig. 11.

V. Conclusion and Future Work

In this article 3 control structures have been implemented on a simulated knuckle boom crane. Two of the strategies use DDCs in order to increase the efficiency of the hydraulic system. A different formulation for MPC of DDC has been proposed here compared with [3]. The proposed structure uses a linear transformation to represent energy losses in the DDC. The MPC uses the least amount of energy of the three control structures. Furthermore the motion of the cylinders with the MPC is smoother than the motion with the FSA. When the load is increased, the MPC stops being accurate. The integral part of the force reference generation of the FSA can compensate for the change in load better than the MPC. It

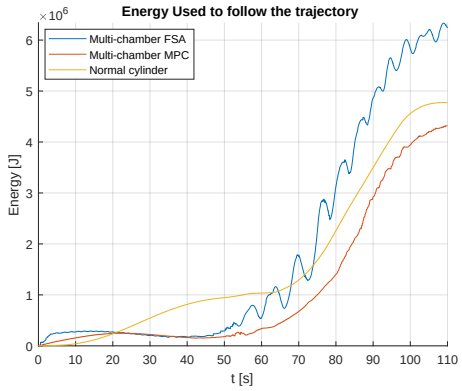

Fig. 10. Energy used by the system if changing load.

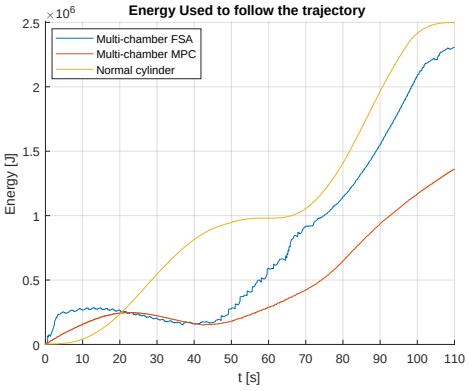

Fig. 11. Energy used by the system if constant load.

was observed that increasing the proportional gain of the force reference generation filter lead to much better accuracy for the FSA. The oscillations around the position reference after the change in load were completely removed. Unfortunately this also lead to a serious increase in energy consumption, which defeats the purpose of using DDCs. It can be observed that the MPC has a steady state error in the middle of the trajectory even with the constant load condition. This is where the equivalent mass in the linear model is furthest from the actual one. It is concluded that for both MPC and FSA large increases in the load on the system can lead to very poor performance.

For future work possible load or model estimation is proposed, as it is obvious that the MPC is not able to cope with the large non-linearity of the 100 times increase in load mass.

The structure of the optimisation problem is standard and this may allow a wider selection of tools to be applied to the problem in the future. The current solving time cannot be used for a real time implementation. Future work will have to address this.

The fact that a clear link is present between each valve and its effect on the system, can allow the straightforward introduction of fault tolerant additions in the form of constraints in the optimisation problem. This is also proposed as future work.

Finally it has been proposed in [11] that having 7 or more pressure lines can lead to very efficient control of a boom. Furthermore, in [12] an optimisation of the configuration of a DDC for wave energy extraction was conducted in order to find the number of chambers and pressure lines, which would lead to highest energy extraction. The optimisation was conducted with a brute force approach. The MPC structure outlined in the current study could easily be expanded to incorporate 20 or more different pressure levels and 4 or more cylinder chambers. Then a single simulation run can be conducted in order to obtain statistical information, about which chambers and which pressure lines are used most often for a common load case. In this situation the rather long optimisation time would be of lesser concern, since brute force optimisation with a simulation for each possible combination would also involve a lot of time. Investigating the possibility of such a design procedure is proposed for future work.

ACKNOWLEDGMENT

The research in this paper has received funding from The Research Council of Norway, SFI Offshore mechatronics, project number 237896/O30.

REFERENCES

[1] M. Linjama, H. Vihtanen, A. Sipola, and M. Vilenius, “Secondary controlled multi-chamber hydraulic cylinder” , The 11th Scandinavian International Conference on Fluid Power vol. 9, pp. 2–4, 2009.

[2] R. Haas, and E. Lukachev, “Optimal Feedforward Control of a Digital Hydraulic Drive” The Seventh Workshop on Digital Fluid Power, Linz, pp. 2–4, 2009.

[3] A. Hansen, M. Asmussen, and M. Bech, “Energy optimal tracking control with discrete fluid power systems using model predictive control”, The Ninth Workshop on Digital Fluid Power, Aalborg, 2017.

[4] M. Bak, and M. Hansen, “Analysis of offshore knuckle boom crane-part one: modeling and parameter identification” Modeling, Identification and Control, vol. 35, num. 4, pages 157–165, 2013.

[5] Parviz E. Nikravesh, “Computer-aided analysis of mechanical systems”, Prentice-Hall, Inc. 1988.

[6] V. Donkov, T. Andersen, M. Ebbesen, H. Pedersen, “Applying Digital Hydraulic Technology on a Knuckle Boom Crane”, The Ninth Workshop on Digital Fluid Power, Aalborg, 2017.

[7] R. Hansen, M. Kramer, and E. Vidal, “Discrete displacement hydraulic power take-off system for the wavestar wave energy converter”.

[8] J. Löfberg, “YALMIP : A Toolbox for Modeling and Optimization in MATLAB”, In Proceedings of the CACSD Conference, 2004.

[9] ”MOSEK ApS”, “The MOSEK optimization toolbox for MATLAB manual. Version 7.1 (Revision 28)”, ”http://docs.mosek.com/7.1/toolbox/index.html” , 2015.

[10] S. Boyd, N. Parikh, E. Chu, B. Peleato, J. Eckstein, “Distributed optimization and statistical learning via the alternating direction method of multipliers, Foundations and Trends in Machine Learning 3.1 , pp. 1-122, 2011.

[11] M. Huova, A. Aalto, M. Linjama, K. Huhtala, T. Lantela, M. Pietola, “Digital hydraulic multi-pressure actuator the concept, simulation study and first experimental results”, International Journal of Fluid Power, Vol. 18, Iss. 3, 2017.

[12] A. Hansen, H. Pedersen, “Optimal configuration of a discrete fluid power force system utilised in the PTO for WECs”, Ocean Engineering, Vol. 117, pages 88–98, 2016.

Paper D

Investigation of the Fault Tolerance of Digital Hydraulic Cylinders

Viktor Donkov, Torben Ole Andersen, Morten Kjeld Ebbesen, Matti Linjama, Miika Paloniity

This paper has been published in the proceedings of
The Sixteenth Scandinavian Conference on Fluid Power, May 22-24, 2019, Tampere, Finland.

Investigation of the fault tolerance of digital hydraulic cylinders

Viktor Donkov[1], Torben Andersen[1], Morten Kjeld Ebbesen[2], Matti Linjama[3] , Miika Paloniitty[3]

[1]Aalborg University
Pontoppidanstraede 111
9220 Aalborg East, Denmark
E-mail: vhd@et.aau.dk

[2]University of Agder
Jon Lilletuns vei 9
4879 Grimstad, Norway

[3]Tampere University of Technology
Korkeakoulunkatu 10
FI-33720 Tampere, Finland

ABSTRACT

This paper investigates the fault tolerance of Discrete Displacement Cylinders (DDCs) controlled with a Model Predictive Controller(MPC). Due to the nature of DDCs there are multiple components such as several pressure chambers, constant pressure rails, and on/off valves, which operate in parallel. Some of these components do similar jobs, i.e. more than one cylinder chamber provides a positive force when pressurized. This modularity in design is an often stated benefit of digital hydraulics because failed components have less influence on the behaviour of the whole system. The exact influence of faults in the components, when the fault is detected and when it is not, is shown through a sensitivity study. Certain faults are tested in a laboratory setting to verify the simulation results. The results show that different component failures lead to different types of loss of capability of the system because the components are not equivalent in size. Furthermore the results show that the performance of the system is better when the fault is detected and the controller is able to take appropriate action.

KEYWORDS: Discrete Displacement Cylinders, Digital Hydraulics, Fault Tolerance

1. INTRODUCTION

Digital hydraulics started as an attempt to increase the energy efficiency of classic hydraulic systems by exchanging more complex components with simple components, which are either fully on or off. In certain ways, it tries to emulate the benefits electrical power systems have acquired from the use of transistors. This trend tries to make parts simpler and shift the functionality of the system from hardware to software. The main benefit and goal of the trend is energy efficiency, but there can be other benefits as well. Some digital hydraulic systems require multiple components operating in parallel. In this paper the focus will be on Discrete Displacement Cylinders (DDCs). DDCs are cylinders with more than two chambers. In order to produce different force levels the pressure in the different chambers is changed by connecting them to one of several pressure lines. The number of chambers together with the number of possible pressure levels define the resolution of the force output. Furthermore, a larger number of possible pressure levels also increases the energy efficiency of the system as the losses introduced by switching from one pressure to another are reduced when the two pressures are closer together [8]. The number of valves which are needed to connect the cylinder and the pressure lines grows proportionally. From one perspective the increased number of components is a minus due to the more complicated maintenance, but from a different perspective the large number of components such as valves and accumulators providing pressure means that only a certain subset of them are needed for a particular loading. In this article the extent of this inherent fault tolerance will be investigated. The faults investigated are valves stuck open and valves stuck closed. This is done because valves in digital hydraulic

systems are under considerable load, and these are common failure modes for them [3]. Fault tolerance for digital flow control units has been investigated for instance in [2]. For this reason failures in one valve, when more valves are connected in parallel, will not be investigated. Instead, if several valves are used in a pressure line, all will experience a failure. In section 2 the test setup will be presented. In section 3 the mathematical model describing it will be presented. This model will be used to test the majority of the faults, with only some of them implemented on the real test stand. In section 4.4 the model will be verified showing a good agreement with reality. In section 5 the faults will be described and the results will be shown. Finally in section 6, conclusions will be drawn and possible future work will be suggested.

2. TEST STAND

The test stand (Fig.1) is a commonly used test stand for digital hydraulics at Tampere University. The stand consists of a metal bar connected at the center with two places for extra mass to be attached on each end. The metal bar acts as a seesaw and in this case is actuated by a four-chamber cylinder. A constant velocity on/off pump supplies the system. In order to create the constant pressure rails three accumulators are used. The controller is implemented on a Dspace RealTime(RT) target using Matlab's compiler feature. The cylinder chambers are connected to the pressure rails through 21 type KSDE Rexroth valves, another four valves are used for charging the pressure rails. The hydraulic circuit can be seen in Fig.6. The large amount of valves is required because chamber A1 is four times larger than chamber A2. For the pressure in these chambers to rise equally fast, the same ratio of flow should be delivered to both of them. Since the valves are the same size, chamber A1 uses four valves per pressure line, chamber B1 uses two valves, and chamber A2 uses one valve. With three pressures to connect to, the total number of valves are twelve, six, and three. With different sized valves and a new manifold specifically designed for this circuit, fewer components could have been used. The amount of hoses and fittings would have been reduced as well. This would have increased the energy efficiency of the system. Due to monetary and time reasons this was not done. Instead the manifolds and valves already available were arranged in a way that provides the desired capabilities. The specific components used in the test stand can be seen in Tab.1.

Figure 1. Test stand

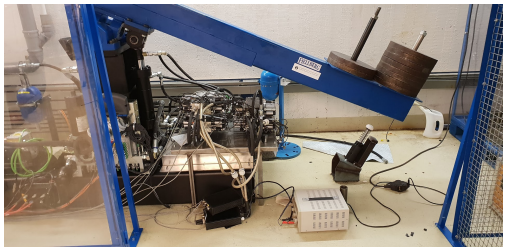

Figure 2. Hydraulics

Table 1. Components of the test stand

Component	Specification	Component	Specification
Cylinder	Norrhydro 85/63/40/28-250	Valves	Rexroth KSDE 10 L/min@5bar
Accumulators x 3	4 L	Pump	Rexroth UPE2 7 L/min
RT target	Dspace ds1006 1 core 2GHz		

3. MODEL

This section presents the mathematical model describing the test stand. The section is divided into two parts - the mechanical model of the seesaw and the hydraulics system which will drive the cylinder.

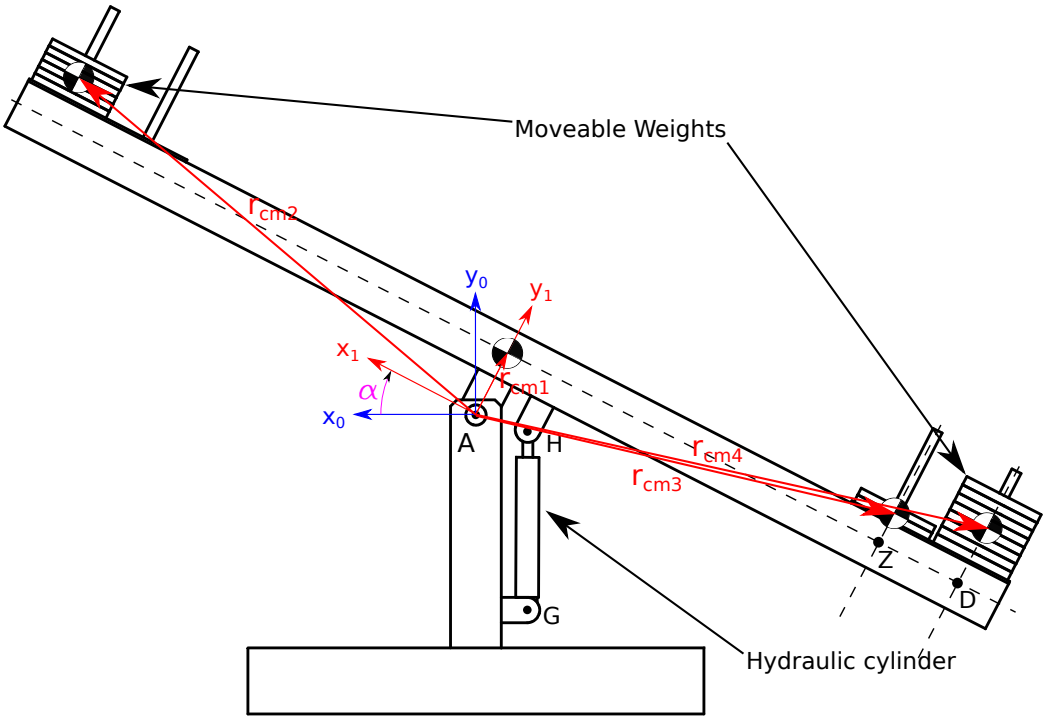

Figure 3. Kinematics

3.1. Seesaw model

Fig.3 shows the naming convention used in the model. The angle α is defined as the rotation between the stationary reference system denoted as $[x_0, y_0]$ and the rotating reference system denoted $[x_1, y_1]$, as seen in Fig.3. The cylinder is attached on the right side of the column. With that in mind, the cylinder stroke is smallest at $\alpha = 0.5$. The axis x is positive to the left, because the coordinate systems have been defined for the cylinder attached to the left of the column as in [4], this convention has been kept here for consistency. The lengths of the vectors in the appropriate coordinate systems can be seen in Tab.2. In order to calculate the load force the gravitational forces due to the 4 point masses are converted to a torque around point A using the kinematics of the system. This torque is them converted to a one dimensional force acting along the length of the cylinder. The torque due to gravity depends on angle α. The ratio between cylinder force and torque around point A also varies with α. The kinematics are also used to convert the total system inertia to a equivalent mass attached to the top of the cylinder. This mass varies with the same parameter as the load force. In Fig.4 and Fig.5 the calculated values for the load force and the equivalent mass on the cylinder according to the rotation angle α can be seen. The connection between cylinder stroke and α is used to make a one dimensional model with the nine valve as inputs and the cylinder stroke as output.

Table 2. Table of vector lengths in the appropriate coordinate system

Vector	x [m]	y [m]
AZ_1	-1.65	0.26
AD_1	-2	0.26
AH_1	-0.2025	0.05
AG_0	- 0.205	-0.760

3.2. Hydraulics

The hydraulics circuit used can be seen in Fig.6

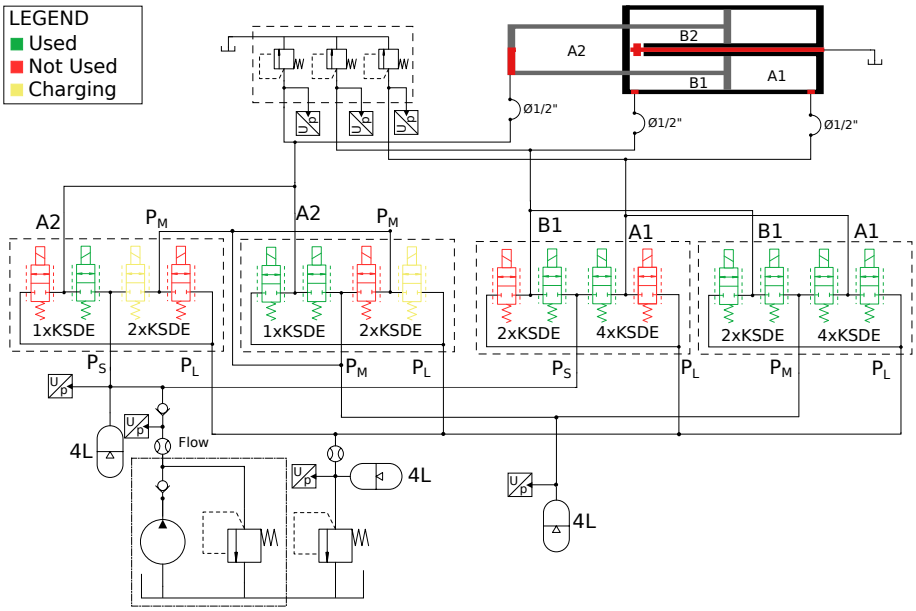

Figure 6. Hydraulic Circuit

3.2.1. Cylinder

The cylinder has four chambers, but only three will be used. According to this, the cylinder provides force as

$$F_{cyl} = A_{A1}p_{A1} - A_{B1}p_{B1} + A_{A2}p_{A2} \tag{1}$$

where the A_{A1} stands for area of chamber $A1$, and p_{A1} is the pressure in that chamber. The three pressure lines p_S, p_M, and p_L are selected as 12 MPa, 3 MPa, and 1 MPa respectively. The three chamber areas have

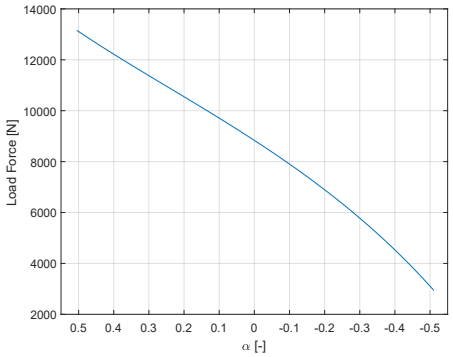

Figure 4. Load force as a function of α.

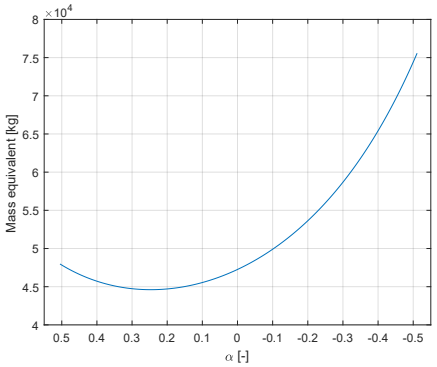

Figure 5. Equivalent mass seen by the cylinder as a function of α.

sizes according to the diameters in Tab.1. The available force levels can be seen in Fig.7. The blue dot at 9 kN corresponds to the average of the load force. This is taken from the trajectory and the load force calculated in Fig.4.

3.2.2. Hoses

The hoses in the system are modelled according to the method used in [5]. The time derivatives of the flow and the pressure for each hose segment are modelled as

$$\dot{Q}(k) = \frac{A\,(p(k) - p(k+1))}{L\rho} \tag{2}$$

$$\dot{p}(k) = \frac{\beta(p(k))}{AL}\,(Q(k-1) - Q(k)) \tag{3}$$

where A and L are the area and length of the hose segment, ρ is the density of oil, and (k) denotes segment number, $\beta(p(k))$ is the bulk modulus of the oil as a function of the pressure in that segment. Fig.8 also illustrates this convention. Losses in the hoses and fittings are ignored.

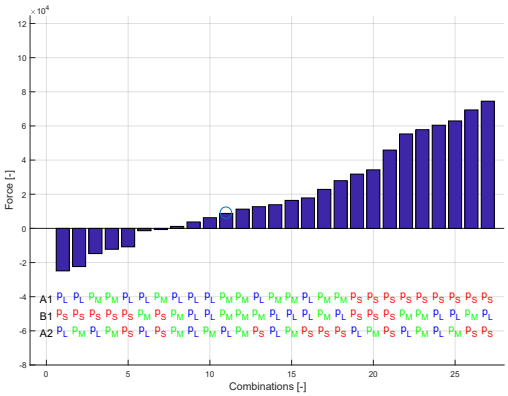

Figure 7. Available force levels

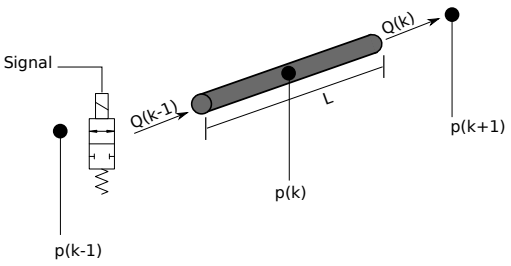

Figure 8. Model of the hoses between the cylinder chamber and the valve.

3.2.3. Accumulator

The accumulators are modelled according to the method used in [5]. The model is based on the temperature and volume of the gas as

$$\dot{T} = \frac{T_{wall} - T}{\tau} - \frac{RT\dot{V}_g}{c_v V_g} \tag{4}$$

$$\dot{V}_g = \dot{p}_{acc}\frac{V_{oil}}{\beta_v} - Q_{in} \tag{5}$$

where T_{wall} is the temperature of the accumulator wall, τ is the heat exchange time constant, R is the thermal resistance of the accumulator, c_v is the heat capacitance, $\dot{p}_{acc}$ is the gradient of the pressure in the accumulator, V_{oil} is the volume of the oil, β_v is the bulk modulus of the oil, and Q_{in} is the flow of oil into the accumulator. The volume of the oil is found from the current volume of the gas and the size of the accumulator

$$V_{oil} = V_{acc} + V_0 - V_g \tag{6}$$

From these equations the change in pressure of the hydraulic fluid can be described by

$$\dot{p}_{acc} = \frac{Q_{in} + \frac{1}{1+\frac{R}{c_v}}\frac{V_g}{T}\frac{1}{\tau}\,(T_{wall} - T)}{\frac{V_{oil}}{\beta_v} + \frac{1}{1+\frac{R}{c_v}}\frac{V_g}{p_{acc}}} \tag{7}$$

From Eq.4, Eq.5 and Eq.7 the dynamics of an accumulator can be described. A simple combinatorial logic based controller is used to charge the p_S and p_M accumulators. A threshold is selected as 0.5 MPa below the desired pressure. For the high pressure line, if p_S falls below this value (11.5 MPa), the pump is turned on. For the middle pressure line, if p_M reaches 2.5 MPa charging doesn't start unless the high pressure line is above the desired value. That is AND(p_M <2.5 MPa, NOT(p_S < 11.5 MPa)). If the charging condition is fulfilled two valves are opened between the high and middle pressure lines. The charging occurs with a large pressure drop across the charging valves and is very inefficient. The two valves between middle and low pressure lines can be used to drain the accumulators. This is done by opening all of the charging valves which connects p_S to p_M to p_L.

4. CONTROL

The cylinder is controlled with a Model Predictive Controller (MPC). The problem is be optimized with the differential evolution algorithm as in [1]. The MPC is based on [6]. Since it was shown in [6] that the controller has problems with changing mass and load force, the algorithm will be augmented by incorporating integral action according to the method used in [7].

4.1. Prediction

A linear model will be used to predict the system states:

$$x_c(k+1) = A_c x_c(k) + B_c u(k) \tag{8}$$

$$y(k) = C_c x_c(k) \tag{9}$$

In this equation x_c is a state vector containing the three pressures in the chambers p_{A1}, p_{B1} and p_{A2}, the position and velocity of the cylinder. $u(k)$ is a vector of nine Boolean values - indicating whether a valve is open or closed, $y(k)$ is the position of the cylinder. The specifics and a longer discussion of the system can be seen in the previously mentioned reference [6]. In order to introduce the integral action into the controller a new control vector has to be introduced: $\Delta u(k) = u(k) - u(k-1)$. Furthermore, a "change in system state" vector is introduced: $\Delta x_c(k) = x_c(k) - x_c(k-1)$ which allows the system equations to be rewritten as:

$$\Delta x_c(k+1) = A_c \Delta x_c(k) + B_c \Delta u(k) \tag{10}$$

$$y(k+1) - y(k) = C_c A_c \Delta x_c(k) + C_c B_c \Delta u(k) \tag{11}$$

A few more steps are needed. A new state vector is introduced as:

$$\bar{x}(k) = \begin{bmatrix} \Delta x_c(k) \\ y(k) \end{bmatrix} \tag{12}$$

This allows the rewriting of Eq.10 and Eq.11 into:

$$\bar{x}(k+1) = \bar{A}\bar{x}(k) + \bar{B}\Delta u(k) \tag{13}$$

$$y(k) = \bar{C}\bar{x}(k) \tag{14}$$

Here the matrices are defined as:

$$\bar{A} = \begin{bmatrix} A_c & 0 \\ C_c A_c & I \end{bmatrix} \quad \bar{B} = \begin{bmatrix} B_c \\ C_c B_c \end{bmatrix} \quad \bar{C} = \begin{bmatrix} 0 & I \end{bmatrix} \tag{15}$$

were I and 0 are an identity matrix and a matrix of zeros with the appropriate sizes.

For multi-step prediction a new output vector is defined as:

$$\hat{y} = G\Delta\hat{u} + \hat{x}_o \tag{16}$$

where $\hat{y}$ and $\Delta\hat{u}$ are:

$$\hat{y} = \begin{bmatrix} y(k+1) \\ y(k+2) \\ \vdots \\ y(k+M) \end{bmatrix} \qquad \Delta\hat{u} = \begin{bmatrix} \Delta u(k) \\ \Delta u(k+1) \\ \vdots \\ \Delta u(k+M) \end{bmatrix} \tag{17}$$

The matrices are built as:

$$G = \begin{bmatrix} B & 0 & \cdots & 0 \\ AB & B & \cdots & 0 \\ \vdots & \vdots & \ddots & \vdots \\ A^{M-1}B & A^{M-2}B & \cdots & B \end{bmatrix} \tag{18}$$

$$\hat{x}_o = \begin{bmatrix} \bar{C}\bar{A} \\ \vdots \\ \bar{C}\bar{A}^M \end{bmatrix} \tag{19}$$

where M is the prediction horizon.

4.2. Cost function

Now that the system's states are predicted the optimal control vector has to be chosen according to some condition. Since the aim is to follow a position trajectory, the position state can be selected as an output by choosing the correct C_c matrix. Then an error vector can be defined as

$$\bar{e} = \begin{bmatrix} e(k) \\ e(k+1) \\ \vdots \\ e(M) \end{bmatrix} = \begin{bmatrix} r(k) \\ r(k+1) \\ \vdots \\ r(M) \end{bmatrix} - \begin{bmatrix} y(k) \\ y(k+1) \\ \vdots \\ y(M) \end{bmatrix} \tag{20}$$

where $r(k)$ is the position reference for time instant k. This vector can be included in the cost function that is to be minimized. In [6] the cost function J was chosen as:

$$J = \omega_1 \hat{e}^T \hat{Q} \hat{e} + \omega_2 |F\hat{u}|_1 \tag{21}$$

where $\hat{Q}$ is a diagonal matrix with weight and F is a difference matrix built according to [6]. This cost function has some good properties - it is always positive and lower bounded, so it exhibits convex properties. The first term punishes error, while the second punishes pressure switching, which has been shown to be the major source of losses in a DDC [8]. Cost functions of this shape are fairly often used [9], but unfortunately the squaring of matrices proved too heavy to be completed online by the RT target. For this reason the cost function was simplified to

$$J = \omega_1 |\hat{e}|_1 + \omega_2 |F\hat{u}|_1 \tag{22}$$

The cost function is still positive definite and lower bounded, but the calculations are completed much faster. For the RT implementation a population of 50 combinations with a maximum setting of 100 generations always completed in less than the 60 ms. This was the setting on the watchdog timer. This timer was selected because the comparatively low inertia and the fast trajectory required from the controller to run at this frequency. The population size and maximum generations were selected to ensure that the computations are completed in the required time. With larger population size and more generations a better optimum can be found at each time step. This of course requires better hardware.

4.3. Delay compensation

In order to cope with the delays of the valves and the computation delay, delay compensation has been implemented similar to [10]. With a lower frequency controller these delays can be ignored, but due to the low inertia

of the test stand a rather fast switching frequency of 16.6667Hz (60 ms) is required. The delay compensation is implemented by further delaying the selected command, so that the the force is delivered at the correct instant. The prediction is moved one step forward to match this. In the laboratory case, the calculation delay and transfer delay is large enough on its own, so no artificial delay is added.

The difference can be seen in Fig.9 and Fig.10. The red line is the force calculated by the controller. The blue line is the actual delivered force. It can be seen in Fig.9 that due to the valve delay and the pressure dynamics the actual force reaches the desired value with a substantial delay. With delay compensation, the delivered force matches the desired force more accurately. This improves both accuracy and energy efficiency; otherwise force commands could be achieved one time step later leading to excessive switching.

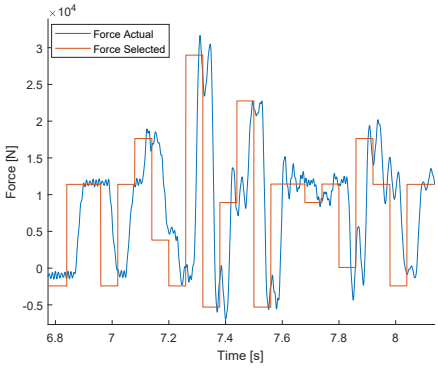

Figure 9. Without delay compensation

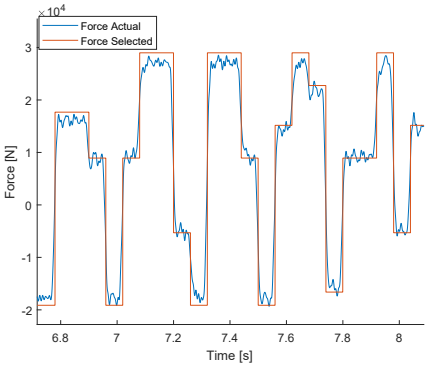

Figure 10. With delay compensation

4.4. Velocity estimation

With the delay compensation using the predicted pressures, the only real feedbacks to the controller are position and velocity. A velocity sensor was not available, so the velocity was estimated from the position signal. The position signal itself has noise which interferes with the proper estimation, so the position signal was filtered with

$$x_{p,filt}(k) = \frac{\Sigma x_p(k \cdots k-4) - max(x_p(k \cdots k-4)) - min(x_p(k \cdots k-4))}{3} \tag{23}$$

where $x_{p,filt}(k)$ is the filtered cylinder position at time instant k, and it depends on the previous four sampled values. The sampling was done at 1000 Hz. From this filtered signal the velocity could be obtained by

$$\dot{x}_{p,est} = \frac{5x_{p,filt}(k) + 3x_{p,filt}(k-1) + x_{p,filt}(k-2) - x_{p,filt}(k-3) - 3x_{p,filt}(k-4) - 5x_{p,filt}(k-5)}{35t_{s,vel}} \tag{24}$$

where $t_{s,vel}$ is the sample time for the estimation, which was chosen to be 5 ms. Both filter and velocity estimation are done according to [11].

4.5. Model Verification

Fig.11 shows the comparison between a real trajectory run and a simulation. In this test no faults are introduced. Fig.12 shows the comparison, but when a fault between chamber A2 and the supply pressure is introduced for the whole trajectory. In both test runs the simulation behaves similarly to the real plant. These verification tests were done with the controller in the closed loop.

For the first test run (Fig.11), the efficiency measure of the simulation is 19.93 J/mm. This is calculated by taking the energy used to follow the trajectory and dividing it by the total length of movement. The accuracy of the simulation run is 449.61 m. This was calculated by taking the difference of the reference and the

actual position of the cylinder, then finding the absolute value of this error for sampled time instances and then summing the values.

For the real system, the position error sum is 1510 m and the efficiency measure is 46.77 J/mm. The position error number differs significantly from the simulated case, but the actual tracking performance appears quite similar in the figure. A possible reason is that a small difference gets integrated fast to a large value. More importantly the efficiency measure differs significantly. The reason for this was found to be the fact that the pressures in the accumulators were dropping faster than in the model. When the supply pressure in the middle line reached a low enough value it was charged from the high pressure accumulator by opening two valves connected in parallel. This rather costly charging wastes a lot of energy. Since the middle pressure drops slower in the simulation the costly charging is not used and energy efficiency is improved. The reason for this difference could not be found in the limited time in which the test stand was available, but possible reasons are valve opening overlap and errors in the simulation model. For the fault case, the simulation's position error is 920.29 m and the efficiency measure is 21.84 J/mm, whereas for the real test stand the position error is 1498 m and the efficiency measure is 44.30 J/mm. The model does not describe the real situation perfectly, but since the goal of the paper is to find if the system is able to function under specific faults this level of agreement was considered satisfactory for the purpose of the fault tolerance study.

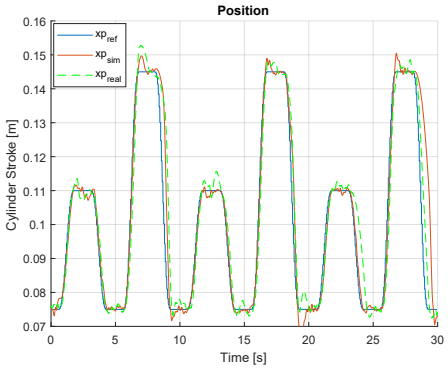

Figure 11. Comparison of model and real measurements without fault

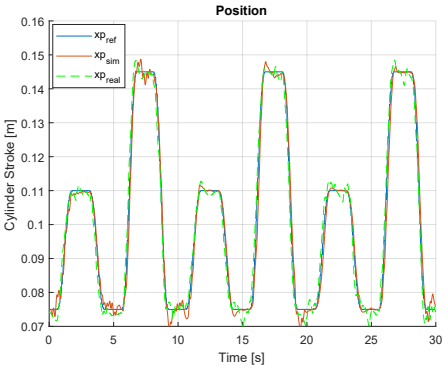

Figure 12. Comparison of model and real measurements with fault

5. FAULT TOLERANCE STUDY

For the fault study a fault in the valve between a chamber and a pressure line is introduced for the entire trajectory run. The same trajectory is used for all tests. Two types of faults are studied - a valve stuck closed and a valve stuck open. For chamber A1 where four valves are used per pressure line the fault is introduced in all four valves. In this sense the four valves are considered as one big valve. The same is done for chamber B1. Later in this section a weight is introduced in the control structure in order to improve the fault tolerance of the system. For the study it is assumed that the fault is detected and isolated. The actual fault detection and isolation have not been investigated in this paper and are instead left for future work. Multi-chamber cylinders are inherently fault tolerant to some faults. This can be seen in Tab3. In this table faults are denoted as "$*$ to $\bullet$", which can be understood as a fault in the valve connecting pressure line $*$ to chamber $\bullet$. The results, which can be considered critical, i.e. total inability to complete the work, have red coloured cells. Most often in these cases, the cylinder would reach one or the other end stop and stay there. For instance when chamber A1 is always connected to the high pressure line, the cylinder force is too large for the cylinder to move in the negative direction.

The basis for the fault tolerance in this part of the study is the fact that some of these valves do not need to be used to follow the predefined trajectory. It can be seen that the faults in the low pressure line are the most

critical, because they result in failures. In almost all cases the fault resulted in degraded performance in either the accuracy or the energy efficiency of the controller.

Table 3. Results with valve stuck closed without detection

Fault	Pos Error	Energy	Fault	Pos Error	Energy	Fault	Pos Error	Energy
p_s to A1	615.57	20.32	p_m to A1	1694.33	33.62	p_l to A1	12220.05	18.03
p_s to B1	1417.39	18.52	p_m to B1	659.43	26.85	p_l to B1	9062.45	14.41
p_s to A2	810.23	20.16	p_m to A2	735.09	25.70	p_l to A2	9231.42	19.53

The results for the same faults, but with a fault tolerance addition to the controller can be seen in Tab.4. The same convention has been followed, and the critical faults are coloured in red. If the fault is detected, the fault tolerance is improved as can be seen by the fact that some of the faults which were critical have been recovered from. The only thing necessary to introduce the fault tolerance in the controller is to augment the cost function as

$$J = \omega_1 \left|\hat{e}\right|_1 + \omega_2 \left|W_f F \hat{u}\right|_1 \tag{25}$$

where W_f is a diagonal matrix with a large weight at the position of the faulty valve and ones at all other positions of the diagonal. The cost of using that particular valve becomes very large and other force combinations are preferred. The weight selected here was chosen arbitrarily large, until those valves are never picked by the controller. In the case where a valve is stuck open, the weights can be put on the other two pressure lines. This makes combinations, where the valve (which is stuck open) is chosen to be open, is preferred. Using these weights is an easy way to represent constraints in a differential evolution algorithm. For all faults the weight on position error ω_1 had to be increased. This was necessary due the fact that the controller now needs to pick less energy efficient combinations.

Table 4. Results with valve stuck closed with detection

Fault	Pos Error	Energy	Fault	Pos Error	Energy	Fault	Pos Error	Energy
p_s to A1	490.19	36.45	p_m to A1	486.97	20.67	p_l to A1	1034.89	22.83
p_s to B1	509.69	18.22	p_m to B1	414.85	21.49	p_l to B1	590.81	46.28
p_s to A2	422.55	29.98 6	p_m to A2	487.97	24.86	p_l to A2	376.04	30.12

The same investigation has been done for faults where the valve is stuck open instead. The results are presented in Tab.5 and Tab.6. It can be seen that valves stuck open lead to critical failures in almost all cases when the the fault is not detected. Part of the severity of the failures is the fact that when a valve is stuck closed, it influences the performance only if the controller chooses to use it. If a valve is stuck open, it influences the performance at all times. It also leads the controller to short-circuit the pressure lines. This drains the accumulators, and the available pressures change significantly. The results in Tab.6 show that with proper detection and changes to the controller the fault can be recovered from. Again the weight on position error had to be increased in order to force the controller to use the more costly switching combinations more often.

Table 5. Results with valve stuck open without detection

Fault	Pos Error	Energy	Fault	Pos Error	Energy	Fault	Pos Error	Energy
p_s to A1	38422.09	13.38	p_m to A1	4208.14	29.85	p_l to A1	15956.17	1.43
p_s to B1	31687.24	15.63	p_m to B1	596.53	21.75	p_l to B1	2735.25	46.93
p_s to A2	31879.61	9.23	p_m to A2	16711.33	49.24	p_l to A2	13078.48	21.69

Table 6. Results with valve stuck open with detection

Fault	Pos Error	Energy	Fault	Pos Error	Energy	Fault	Pos Error	Energy
p_s to A1	23455.80	13.65	p_m to A1	473.98	25.87	p_l to A1	853.26	17.15
p_s to B1	17781.12	20.80	p_m to B1	522.98	20.05	p_l to B1	876.16	12.58
p_s to A2	778.69	38.51	p_m to A2	618.81	22.57	p_l to A2	721.17	32.92

6. CONCLUSION AND FUTURE WORK

In this paper an investigation of the fault tolerance of multi-chamber cylinders was conducted. To facilitate this study a mathematical model of the test stand was created. Tests were conducted to verify that the model exhibits similar behaviour to the real test stand. Model predictive control with fault tolerance capabilities was implemented in the model and on the real system. A study of the fault tolerance of the controller was performed both when the fault is detected and isolated and when it is not. During this study it was found that faults where the valve is stuck open are the most critical. Furthermore, it was found that when the fault is detected and isolated, the controller can function normally by utilizing different switching patterns. Some faults are severe enough that even with this fault tolerant controller they cannot be recovered from. For future work online fault detection and isolation should be investigated in order for this fault tolerant control strategy to be useful.

ACKNOWLEDGMENT

The research in this paper has received funding from The Research Council of Norway, SFI Offshore mechatronics, project number 237896/O30.

7. REFERENCES

References

[1] A. Hedegaard Hansen, M. F Asmussen, and M. M. Bech, "Model predictive control of a wave energy converter with discrete fluid power power take-off system," *Energies*, vol. 11, no. 3, p. 635, 2018.

[2] L. Siivonen, M. Linjama, M. Huova, and M. Vilenius, "Jammed on/off valve fault compensation with distributed digital valve system," *International Journal of Fluid Power*, vol. 10, no. 2, pp. 73–82, 2009.

[3] N. C. Bender, H. C. Pedersen, A. Plöckinger, and B. Winkler, "Reliability analysis of a hydraulic on/off fast switching valve," in *Proc. of The Ninth Workshop on Digital Fluid Power, Aalborg, Denmark*, 2017.

[4] M. Linjama and M. Huova, "Model-based force and position tracking control of a multi-pressure hydraulic cylinder," *Proceedings of the Institution of Mechanical Engineers, Part I: Journal of Systems and Control Engineering*, vol. 232, no. 3, pp. 324–335, 2018.

[5] A. H. Hansen, H. C. Pedersen, and R. H. Hansen, "Validation of simulation model for full scale wave simulator and discrete fuild power pto system," in *9th JFPS International Symposium on Fluid Power*. Japan Fluid Power System Society, 2014.

[6] V. H. Donkov, T. O. Andersen, H. C. Pedersen, and M. K. Ebbesen, "Application of model predictive control in discrete displacement cylinders to drive a knuckle boom crane," in *2018 Global Fluid Power Society PhD Symposium (GFPS)*. IEEE, 2018, pp. 408–413.

[7] M. A. Stephens, C. Manzie, and M. C. Good, "Model predictive control for reference tracking on an industrial machine tool servo drive," *IEEE Transactions on Industrial Informatics*, vol. 9, no. 2, pp. 808–816, 2013.

[8] R. H. Hansen, T. O. Andersen, and H. C. Perdersen, “Analysis of discrete pressure level systems for wave energy converters,” in *Fluid Power and Mechatronics (FPM), 2011 International Conference on*. IEEE, 2011, pp. 552–558.

[9] S. Boyd, N. Parikh, E. Chu, B. Peleato, J. Eckstein *et al.*, “Distributed optimization and statistical learning via the alternating direction method of multipliers,” *Foundations and Trends® in Machine learning*, vol. 3, no. 1, pp. 1–122, 2011.

[10] P. Cortes, J. Rodriguez, C. Silva, and A. Flores, “Delay compensation in model predictive current control of a three-phase inverter,” *IEEE Transactions on Industrial Electronics*, vol. 59, no. 2, pp. 1323–1325, 2012.

[11] A. Harrison and D. Stoten, “Generalized finite difference methods for optimal estimation of derivatives in real-time control problems,” *Proceedings of the institution of mechanical engineers, part I: journal of systems and control engineering*, vol. 209, no. 2, pp. 67–78, 1995.

Paper E

An analysis of Model Predictive Control with Integral Action Applied to Digital Displacement Cylinders

Viktor Donkov, Torben Ole Andersen, Morten Kjeld Ebbesen

This paper has been submitted for publication in
Modeling, Identification and Control 2020.

Modeling, Identification and Control, Vol. 31, No. 1, 2020, pp. 1–15, ISSN 1890–1328

An analysis of Model Predictive Control with Integral Action applied to Digital Displacement Cylinders

Viktor Donkov [1] Torben Ole Andersen [1] Morten Kjeld Ebbesen [2]

[1] *Department of Energy Technology, Aalborg University, Pontoppidanstraede 111, 9220 Aalborg East, Denmark. E-mail:* vhd@et.aau.dk

[2] *Department of Engineering Sciences, University of Agder, Jon Lilletuns vei 9, 4879 Grimstad, Norway.*

Abstract

This article aims to analyze Model Predictive Control (MPC) for the control of multi-chamber cylinders. MPC with and without integral action has been introduced. Three different optimization algorithms have been used to solve the optimization problem in the MPC. The different algorithms have been compared with an industrial solver. The influence of changing mass, choosing a different middle line pressure, system delays, signal noise, velocity estimation, and changing pressure levels has been investigated. It is concluded that for the small prediction horizon used in the paper a simple algorithm such as A* can produce results as good as the previously used Differential Evolution algorithm in less than half the time. It is further concluded that unknown software delays and unknown changes in mass have the largest effect on system performance.

Keywords: Model Predictive Control, Digital Displacement Cylinders, Optimization

1 Introduction

Digital displacement cylinders are cylinders with multiple chambers, which is why they are also known as multi-chamber cylinders. The differently sized areas allow the cylinder to change its force output, by connecting them to low or high pressure lines Linjama et al. (2009). Switching between these forces can allow the cylinder to follow a desired trajectory in an energy efficient way. The switching also causes undesirable vibrations in the cylinder's movement. According to Linjama et al. (2009) multi-chamber cylinders are only good for moving large masses, which help to filter out the vibrations. While this is true the minimum mass requirements have not clearly been investigated. The cylinders force resolution is defined by the number of chambers, their relative size, and the number of pressures, which it can be connected to. The authors have been using a middle pressure line to reduce the losses due to switching Hansen et al. (2011), Hansen et al. (2017). Usually this pressure is selected as the midpoint between the minimum and maximum pressures in the system. In the case of Hansen et al. (2011) a system with four pressures is discussed but the pressures in the pressure rails are still equally distributed. In Donkov et al. (2017) the value of the middle pressure rail is selected through a parameter sweep and it is shown that the value of the middle pressure value can vastly improve energy efficiency. A simulation of the entire trajectory run is used for each evaluation, which makes the method slow. Two algorithms are used in the control of multi-chamber cylinders - Force Selection Algorithm (FSA) used in Huova et al. (2010) and Hansen et al. (2011), and Model Predictive Control (MPC) used in Donkov et al. (2018), Hansen et al. (2018). In Heybroek and Sjöberg (2018) both algorithms are used in

doi:10.4173/mic.2020.1.1

a sense as a FSA is used to generate a pressure reference and then a MPC is used to control the valves during the switching event. In Hansen et al. (2017) and Donkov et al. (2018) it was shown that MPC can perform better than FSA for position tracking problems, but in these papers and others the computational burden of the algorithm is mentioned as a significant issue. In Donkov et al. (2018) the MPC could not deal with the changing load. In Donkov et al. (2019) MPC with integral action was applied to deal with this, but since the focus in Donkov et al. (2019) was on fault tolerance the effects were not really properly investigated. Furthermore delay compensation was introduced to deal with the considerable computation delay and the long time between a given command to switch pressures and the actual event occurring. This was also not discussed. This paper will attempt to address some of these problems. First a system will be described in Sec. 2. This system will be used for all of the tests. Then the MPC used in Donkov et al. (2018) and the addition of integral action as in Donkov et al. (2019) will be presented in Sec. 3. Furthermore, the properties of the cost functions used in Donkov et al. (2018) and Donkov et al. (2019) will be analysed. Then three different optimization algorithms will be presented in Sec. 4. One of the algorithms will be chosen for further study of the system in Sec. 5, where the influence of changing mass, changes in middle pressure line, reference changes and system delay will be discussed.

2 Model

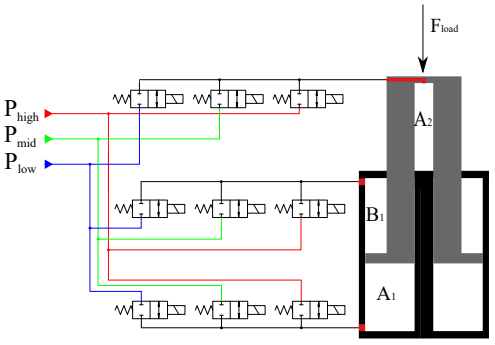

Figure 1: Representation of the multi-chamber cylinder used in the paper

The model used to investigate the system is a three chamber multi-chamber cylinder with a constant mass. The equations are as follows.

$$\dot{p}_i = \frac{\beta_i}{V_i}\left(A_i \dot{x}_p + Q_{v,i,n}(u)\right) \tag{1}$$

$$Q_{v,i,n}(u) = k_q u S(p_i - p_n)\sqrt{(|p_i - p_n|} \tag{2}$$

$$\ddot{x}_p = \frac{1}{m}\left(F_{cyl} - F_g - F_{fric}\right) \tag{3}$$

where $\dot{p}_i$, β_i, V_i, and A_i are the pressure gradient, bulk modulus, volume, and area of chamber i. x_p, $\dot{x}_p$, and $\ddot{x}_p$ are the position, velocity and the acceleration of the piston. $Q_{v,i,n}(u)$ is the flow to chamber i, through valve n. The flow is defined by the orifice equation with k_q being the valve specific coefficient, p_n being the n^{th} pressure line and u being the normalized valve opening. $S(*)$ stands for the sign function. m is the mass of the system, F_{cyl} is the force provided by the cylinder, F_g is the gravitational load, and F_{fric} is the frictional force modelled by the LuGre model. The system parameters are taken from Donkov et al. (2018) and Ho Cho et al. (2016), with a major difference that the cylinder is considered to push a constant mass instead of a changing inertia. This is done in order to simplify the analysis. The LuGre friction model is described by

$$F_{fric} = \sigma_0 z + \sigma_1 \dot{z} + \sigma_2 \dot{x} \tag{4}$$

$$\dot{z} = \dot{x} - \frac{|\dot{x}|}{g(\dot{x})} z \tag{5}$$

$$g(\dot{x}) = \frac{1}{\sigma_0}\left[F_c + (F_s - F_c)e^{-(\dot{x}/v_{str})}\right] \tag{6}$$

where z is the average deflection of the bristles, σ_0, σ_1, and σ_2 are friction parameters. $g(\dot{x})$ is a non-linear function describing the effects of the different friction forces, where F_c is the Coulomb friction, F_s is the static friction, and v_{str} is the Stribeck velocity. The parameters for this friction model have been obtained experimentaly for this specific cylinder by Ho et al. in Ho Cho et al. (2016). All parameters are collected in Tab. 1.

2.1 Force level number and density

The operation of the controller is heavily influenced by the possible force levels. The equation for the number of possible force levels is:

$$F_{num} = {n_c}^{n_p} \tag{7}$$

where F_{num} is the number of force levels that are available, n_c is the number of chambers and n_p is the number of pressure lines. Some researchers have chosen to use a four-chamber cylinder with two pressure lines - this gives 16 force levels. Others have chosen to use a three-chamber cylinder with three pressure lines - this gives 27 force levels. Others have chosen to use a normal differential cylinder with 7 pressure lines - this

Table 1: System parameters

A_1	0.0051 m^2	F_s	1214/-1646 N
A_2	0.0026 m^2	F_c	500/-600 N
A_3	0.0013 m^2	v_{str}	0.026/-0.035 m/s
k_q	2.3570e^{-7} m^3/Pa	σ_0	$8e^6/-6e^6$ N/m
m	50000 kg	σ_1	$7e^2/-7e^2$ N/ms^{-1}
F_g	9000 N	σ_2	$1e^4/-9e^3$ N/ms^{-1}

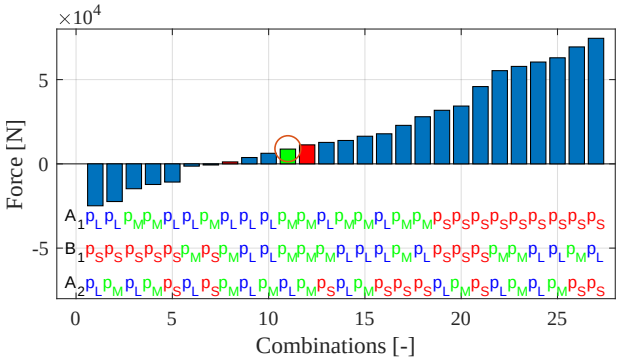

Figure 2: Force resolution of a three-chamber, three-pressure cylinder.

gives 128 force levels. The cost of switching between two pressures depends on the pressure and the volume as:

$$E = \frac{1}{2}\frac{V}{\beta}\left(p_1 - p_0\right)^2 \tag{8}$$

It stands to reason that having smaller differences between pressure levels improves efficiency more than having smaller chambers in which the switch can occur, because the pressure difference is squared. This would suggest that having more pressure lines is always better than having more chambers. An argument for increasing the number of chambers can be made, since all chambers are in use. On the contrary there might be 20 possible pressure lines, but a trajectory might require the use of only two of them. The number of force levels alone is not the only important thing. As mentioned above, it can be expected that trajectories will not utilise the entire force range of the cylinder. An example of this can be seen in Fig. 2. Here a constant force of 9000 N is needed (denoted with a red circle). Since it is very difficult to have a force which exactly matches the load the controller will have to switch constantly. In Fig. 2 the two forces with the smallest cost between them have been coloured in red. Changing pressure of the middle line value does not change the maximum and minimum forces of the cylinder, but it does change the distribution of possible forces. Here a mid pressure line of 30 bar has been chosen through a parameter sweep with a full model simulation for each point in the space (20 pressure values between 20 and 100 bar). A less time consuming method can be utilized to choose the value of the mid pressure line for a certain load by using Eq. (8). For each possible mid pressure value all combinations between a force above and a force below a target can be arranged. The cost of each combination can be found through Eq. (8) and the minimum can be selected. Fig. 3 shows the results for such an analysis when the target is the afore mentioned 9000 N. The analysis suggests that the mid pressure line should be even smaller than the previously selected 30 bar. This can be attributed to the fact that in the analysis only the average required force is considered. By doing the same sweep, but this time summing the cost for each force in the known force trajectory gives the result shown in Fig. 4. In the figure it can be seen that for this trajectory a mid pressure value of 30 bar gives the smallest amount of switching loses. This agrees with the results of the exhaustive search. The benefit is that the analysis can be conducted in a matter of seconds where as the parameter sweep can take up to several hours. The improved costs and force density around the load comes at a price of course - there is only one force level between 34000 N and 55000 N.

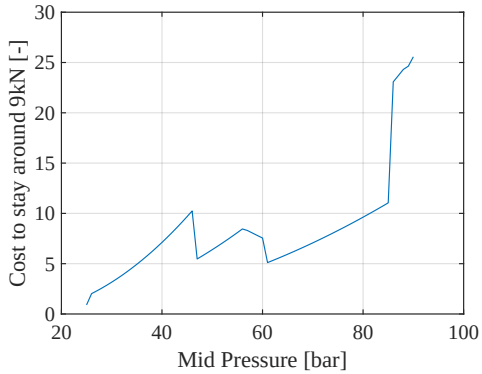

Figure 3: Cost to stay in one place with a load of 9 kN with different mid pressure levels

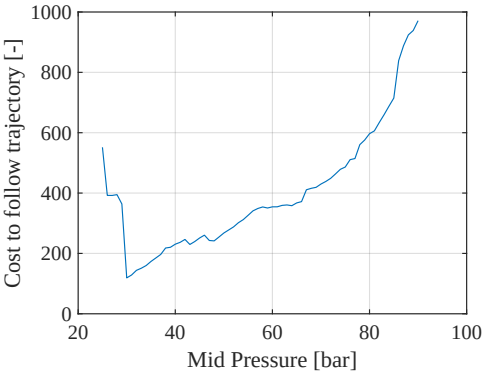

Figure 4: Cost to follow trajectory with different mid pressure levels

3 Control

The control structure will be a Model Predictive Controller (MPC). The controller has already been tested on a similar system in Donkov et al. (2018). Here it is repeated in brief terms for consistency in notation. The controller chooses a control signal based on an optimisation of a cost function J. The elements of the cost function are usually connected with the outputs of a physical representation of the system e.g a model. So in order to use MPC a model of the multi-chamber cylinder should be established. The one used in Donkov et al. (2018) was:

$$x(k+1) = Ax(k) + Bu(k) - A_{grav} \tag{9}$$
$$y(k+1) = Cx(k) \tag{10}$$

where $x(k)$ are the five internal states of the system at time step k which are p_A, p_B, p_C, v_p, x_p. These in turn are the three chamber pressures, the velocity of the piston, and the position of the piston respectively. $u(k)$ is the vector of valve openings. Once again from Donkov et al. (2018) A, B, and C can be defined as:

$$A = \begin{bmatrix} 0 & 0 & 0 & 0 & 0 \\ 0 & 0 & 0 & 0 & 0 \\ 0 & 0 & 0 & 0 & 0 \\ 0 & 0 & 0 & 1 & Ts \\ \frac{A_1 T_s}{M_{eq}} & -\frac{B_1 T_s}{M_{eq}} & \frac{A_2 T_s}{M_{eq}} & 0 & 1 \end{bmatrix} \tag{11}$$

$$B = \begin{bmatrix} p_t & p_{mid} & p_{high} & 0\,0\,0 & 0\,0\,0 \\ 0\,0\,0 & p_t & p_{mid} & p_{high} & 0\,0\,0 \\ 0\,0\,0 & 0\,0\,0 & p_t & p_{mid} & p_{high} \\ 0 & & \cdots & & 0 \\ 0 & & \cdots & & 0 \end{bmatrix} \tag{12}$$

It can be noticed that no pressure dynamics are present in the model. The pressures in the system are directly defined by the valve vector and the matrix B. An equivalent mass M_{eq}, areas A_1, B_1, and A_2, and the sampling time T_s define the dynamics of the model. The magnitudes of these can be seen in Tab. 1, with the exception of T_s, which is 60 ms. Furthermore it was shown in Donkov et al. (2018), that the controller can work much better if the disturbance force is constant and known. In the referenced article the disturbance force was a load due to gravity, which is why it is denoted with A_{grav} in Eq. (9). The use of MPC with integral action can be a solution to problems with disturbances and modelling errors Stephens et al. (2013). According to Stephens et al. (2013) in order to introduce integral action the two things need to be introduced - the change in control $\Delta u(k) = u(k) - u(k-1)$ and change in system state $\Delta x(k) = x(k) - x(k-1)$. With these definitions Eq. (9) can be rewritten as

$$\Delta x(k+1) = A\Delta x_c(k) + B\Delta u(k) \tag{13}$$
$$y(k+1) - y(k) = CA\Delta x_c(k) + CB\Delta u(k) \tag{14}$$

Then a new state vector has to be introduced

$$\bar{x}(k) = \begin{bmatrix} \Delta x_c(k) \\ y(k) \end{bmatrix} \tag{15}$$

The system equations become

$$\bar{x}(k+1) = \bar{A}\bar{x}(k) + \bar{B}\Delta u(k) \tag{16}$$
$$y(k) = \bar{C}\bar{x}(k) \tag{17}$$

where

$$\bar{A} = \begin{bmatrix} A & 0^{n\times m} \\ CA & I^{m\times m} \end{bmatrix} \tag{18}$$

$$\bar{B} = \begin{bmatrix} B \\ CB \end{bmatrix} \tag{19}$$

$$\bar{C} = \begin{bmatrix} 0^{m\times n} & I^{m\times m} \end{bmatrix} \tag{20}$$

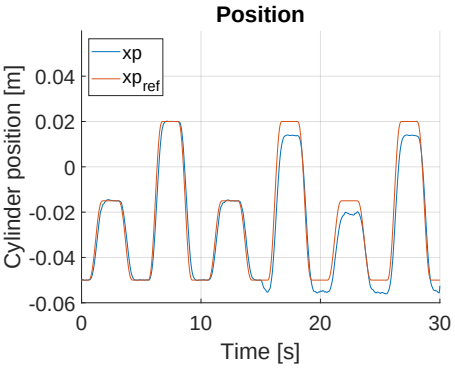

Figure 5: Position of cylinder without integral action MPC.

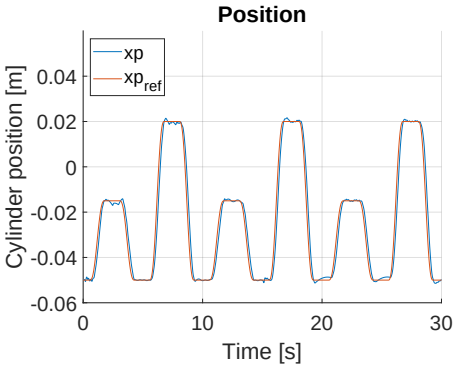

Figure 6: Position of cylinder with integral action MPC.

This can also be written as

$$\hat{y} = G\Delta\hat{u} + \hat{x}_o \tag{21}$$

where

$$G = \begin{bmatrix} \bar{B} & 0 & \cdots & 0 \\ \bar{A}\bar{B} & \bar{B} & \cdots & 0 \\ \vdots & \vdots & \ddots & \vdots \\ \bar{A}^{M-1}\bar{B} & \bar{A}^{M-2}\bar{B} & \cdots & \bar{B} \end{bmatrix} \tag{22}$$

$$\hat{x}_o = \begin{bmatrix} \bar{C}\bar{A} \\ \vdots \\ \bar{C}\bar{A}^{H_p} \end{bmatrix} \tag{23}$$

This is the model which will be used to predict the piston position of the multi-chamber cylinder for M steps ahead. The effect of a changing load on the original controller can be seen in Fig. 5. In this figure the load force on the cylinder is 0 N for the first 15 seconds and increases to 9000 N for the rest of the simulation. When the load increases an offset appears just as in Donkov et al. (2018). The effect of the integral action controller can be seen in Fig. 6.

3.1 Cost Function Analysis

The cost function used for the optimisation problem is

$$J = ||\hat{r} - (GQ\hat{u}_{full} + \hat{x}_o)||_2^2 + |F\hat{u}_{full}|_1 \tag{24}$$

where $\hat{r}$ is the reference vector. The symbol $\hat{u}_{full}$ denotes the vector of valves which starts with the current valve combination followed by the vector to be found by optimisation. These variables can only take on values of 0 or 1. This denotes the valve being open or closed. The matrix Q is used to connect the vector $\hat{u}_{full} \in \{0, 1\}$ with the difference vector $\Delta\hat{u} \in \{-1, 0, 1\}$. One shows the actual valve opening, while the other shows the change in control action. By this definition of Q, $\Delta\hat{u}$ can be defined as $Q\hat{u}_{full} = \Delta\hat{u}$. In this case $(GQ\hat{u}_{full} + \hat{x}_o) = G\Delta\hat{u} + \hat{x}_o = \hat{y}$. The first part of the cost function is then $||\hat{r} - \hat{y}||_2^2$, which is the second norm squared of the position error of the cylinder. The cost function can also be rewritten as:

$$J = || - GQ\hat{u}_{full} + (\hat{r} - \hat{x}_o)||_2^2 + |F\hat{u}_{full}|_1 \tag{25}$$

$$J = \left|\left|T\hat{u}_{full} + \hat{j}\right|\right|_2^2 + |F\hat{u}_{full}|_1 \tag{26}$$

Putting the cost function on the form (26) makes it a well known optimization problem called classic lasso. F is a difference matrix which calculates the cost of switching from one pressure to another.

$$F(i,j) = \begin{cases} -V_{chamb_n}p_z, & if\ i = j \\ V_{chamb_n}p_z, & else if\ j = i + 9 \\ 0, & otherwise \end{cases} \tag{27}$$

where V_{chamb_n} is the volume of the chamber connected to this valve, p_z is the normalized pressure in the pressure line connected to this valve.
In order for the optimization to agree with the model $\hat{u}$ has to be constrained to:

$$\hat{0} \leq \hat{u} \leq \hat{1} \tag{28}$$

Furthermore, since only one pressure line should be connected to each chamber an additional constraint is added:

$$L\hat{u} = \begin{bmatrix} u_1(k) + u_2(k) + u_3(k) \\ \vdots \\ u_7(M) + u_8(M) + u_9(M) \end{bmatrix} \quad L\hat{u} == \hat{1} \tag{29}$$

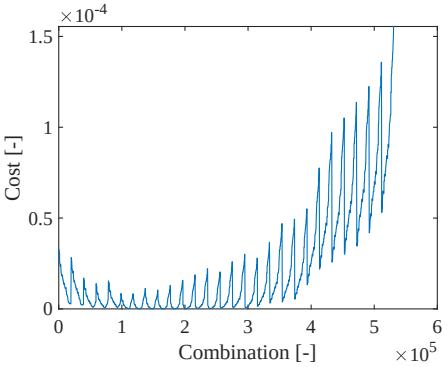

Figure 7: Cost of position accuracy.

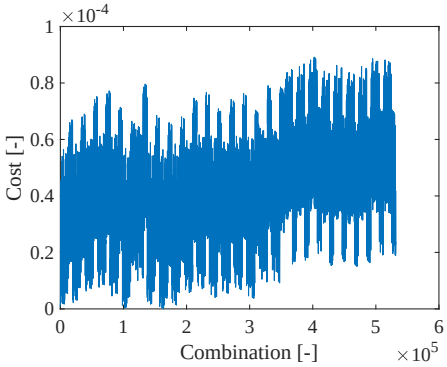

Figure 8: Cost of switching scaled with w.

Finally, because no throttling should occur with this controller, the input vector is constrained to only having the integer values $\hat{u} \in \{0, 1\}$.

The cost function is made of two parts - the cost of not following the reference, and the cost incurred due to switching between two pressure lines. The two costs for a prediction horizon of 4 steps can be seen in Fig. 7 and Fig. 8.

The switching cost function can be considered convex (IFF the integrality constraint is dropped from $\hat{u}_{full}$), because the first one is constructed by taking an affine system $\hat{y}$ to the second power, and the second function is a norm, which makes it always affine.

In Fig. 9 the two parts of the cost function have been plotted against each-other with yellow points being specific combinations of valve openings. A Pareto optimal front can be identified by the points which are not dominated by any other points in atleast one dimension. In this case the front has been denoted with red points.

The two cost functions can be added with the weighted sum method in order to find a preferred trade-off. This is illustrated in Fig. 10.

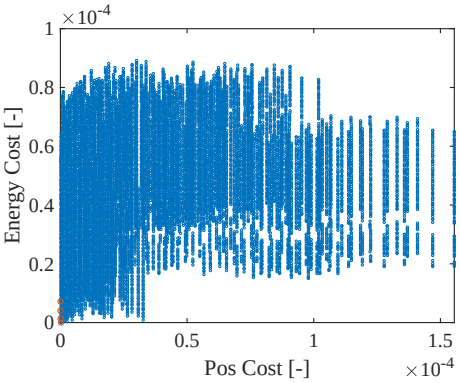

Figure 9: Pareto front.

4 Algorithms

Many different algorithms can be used to solve the problem defined in Eq. (26). Due to the integrality constraint on the inputs the problem is known as mixed-integer programming and is not convex. Some of the algorithms include stochastic optimization algorithms, branch and bound algorithms and enumeration. It is often difficult to determine which algorithm to use on a specific problem without testing it out. So far most DDC control has focused on stochastic algorithms (differential evolution in particular) and enumeration methods. In this section both differential evolution and branch and bound methods will be implemented and their performance will be investigated.

Differential Evolution

The differential evolution algorithm is a stochastic algorithm inspired by natural processes Storn (1995). It can solve a large variety of problems including the mixed-integer non-linear problems of the kind discussed in this paper. The algorithm has been proven to work for this specific controller in Hansen et al. (2017) and Donkov et al. (2019). The algorithm can be applied to the problem of controlling a DDC as described in Fig. 11. In it x stands for the current population, *ind* is a matrix of TRUE/FALSE values, *rand* is a random number generator outputting values between 0 and 1, and CR is a number describing the crossover

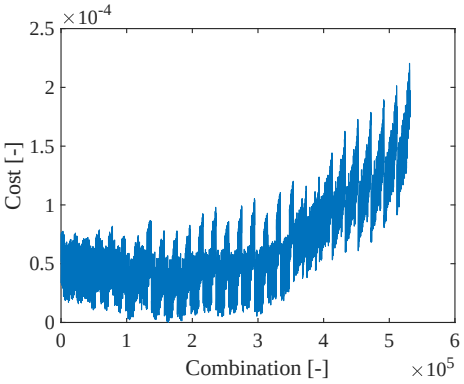

Figure 10: Combined cost for energy and position.

ratio. $mod(*,*)$ is the modulus function returning the remainder of the division of two numbers. Notation $x(min(f) == f)$ is taken from Matlab and stands for those members of x which produce the minimum value of f. In the algorithm a population of size $[NP, D]$ is initiated, where NP is the size of the population and D is the control horizon for the MPC. For each member in the population, a D-number of forces are selected based on a randomization of a initial seed. The seed can be a previous optimum or something else. In this implementation the seed was the force number 12 because that was a force level close to the constant load applied to the cylinder. It was found to be a good starting value. The randomization changed this force level within ±4 forces i.e. the initial population had forces between force levels 8 and 16. The algorithm then uses the cost function J to find the fitness of each member. Each new generation is created based on the best members from the previous generations and a random mutation. The crossover ratio CR determines how many members can be kept from the previous generation.

The mutation was done according to:

$$x_{new} = x_{r_1} + F(x_{best} - x_{r_1}) + F(x_{r_2} - x_{r_3}) \quad (30)$$

where r_1, r_2, and r_3 are randomly chosen vectors from the previous population, which are different from each other. The first part: $x_{r_1} + F(x_{best} - x_{r_1})$, moves the new population towards the best solution from the previous iteration, since if $F = 1$, the equation simplifies to x_{best}. The second part: $F(x_{r_2} - x_{r_3})$, prevents the algorithm from converging prematurely as it moves the answer in a random direction. As the algorithm converges, the population becomes more and more homogeneous and so the effect of the second part is reduced.

In theory the algorithm will converge to a global minimum provided the size of the population is large enough, the number of generations is large enough and the population is mutated in such a way as to explore the entire solution space. Generally speaking settings which allow the algorithm to converge faster are also more likely to result in local instead of global minima. The algorithm was implemented on a single-core 2 GHz dSpace microcontroller in Donkov et al. (2019). In that setup populations larger than 50 and with more than a 4 step prediction could not run in real time (<60 ms for the specific system). Even these numbers were not possible without first changing the cost function. Profiling the algorithm code showed the bottleneck in the evaluation of the cost function. Initially the cost function was selected for its convexity, but the DE method does not depend on convexity or the gradient of the cost function. The cost function J has a 2-norm squared. The squaring of matrices was identified as computational intensive, so instead the $sum(*)$ and $abs(*)$ functions from Matlab were used:

Figure 11: Differential Evolution

```
x = Initiate(seed) ;
stop = 0 ;
f = J(x) ;
while stop ==0 do
    x_new = Mutate(x, min(f));
    ind = rand > CR ;
    x_new(ind) = x(ind) ;
    f = J(x_new) ;
    h_indx = mod(G,Tf)+1 ;
    h(h_indx) = sum(f) ;
    G = G + 1 ;
    best = x(min(f) == f);
    x = x_new ;
    if std(h) > Tol OR G ≥ G_max then
        stop = 1 ;
    end
end
```

$$cost_x = sum(abs(\hat{e}_{np})) \quad (31)$$

The vector $cost_x$ has size $\Re^{NP,1}$ and represents the costs of following the reference of each individual member in the population of size NP. Similarly the cost of switching can be collected as:

$$cost_E = sum(abs(Fx)) \quad (32)$$

where F is the difference matrix and x is the current population. The final cost vector is then:

$$cost_{full} = cost_x + cost_E \quad (33)$$

It can be seen that for each individual member of the

population the cost function was changed from (26) to

$$J = \left| |T\hat{u}_{full} + \hat{j}| \right|_1 + |F\hat{u}_{full}|_1 \tag{34}$$

The effects of this can be seen in Fig. 12. The algorithm was considerably sped up due to the reduction of mathematical operations. In fact the lines of code, which took the most time are the ones used to create the matrix x. Furthermore, the cost function can be sped up in Matlab by vectorizing the calculations. Instead of evaluating each member of the population in a FOR loop, the entire population can be evaluated at once by collecting all the control input vectors in a population of size NP to a matrix of size $pop \in \Re^{D\times 9,NP}$.

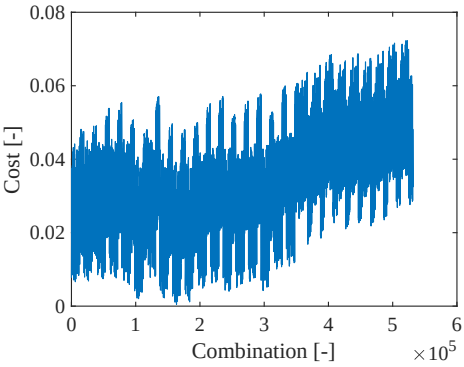

Figure 12: Position error and switching cost combined into one cost function.

$$pop = [\hat{u}_{full,1}, \hat{u}_{full,2}, \cdots, \hat{u}_{full,np}] \tag{35}$$

$$\hat{j}_{np} = \left[\hat{j}, \hat{j}, \cdots, \hat{j}\right] \tag{36}$$

Then the entire population can be evaluated as

$$\hat{e}_{np} = Tpop + \hat{j}_{np} \tag{37}$$

After these changes the runtime of the code was reduce from $\approx$ 2 s to $\approx$ 30 ms. The small number of members in each population, the low number of populations and the changes to the cost function were expected to produce poor results, but in fact valve problems and measurement noise had a larger effect. For this article the function was written with both the flat cost function from Eq. 34 and the Lasso from Eq. 26 using Matlab 2019. The two functions were then compiled to MEX files with the Matlab coder application. Both were then tested on the same laptop. In the newer version of Matlab the two cost functions take the same time to complete. This can attribute to either improvements in Matlab's compiler or the difference in how the hardware handles the compiled code. The performance of the algorithm will be presented and compared after the other algorithms are also discussed.

Branch and bound

A branch and bound algorithm was also developed. The algorithm consists of several steps as can be seen in Fig. 13.

Figure 13: Branch and bound based on ADMM

```
while stop == 0 do
    x_opt, f_opt = ADMM(J, A) ;
    if Binary(x_opt) OR I > I_max then
        stop = 1 ;
    end
    x_b = BranchVar(x_opt) ;
    A_1 = AddConstaintOne(x_b) ;
    x_1, f_1 = ADMM(J,A_1) ;
    A_0 = AddConstaintZero(x_b) ;
    x_0, f_0 = ADMM(J,A_0) ;
    if f_0 > f_1 then
        A = A_1 ;
    else
        A = A_0
    end
    I = I + 1 ;
end
```

The algorithm removes the integerality constraint and solves the resulting convex problem using a normal convex solver. Then a variable is chosen on which to branch. In this case the two branches are - "the variable is constrained to be 0" and "the variable is constrained to be 1". The two minimums are then compared and the smaller one is selected, provided all the constraints are satisfied. If at this point all the variables are integers the algorithm is stopped. If not, then another variable to branch on is selected. The variable being selected is chosen chamber by chamber. That is to say that the vector is scanned from beginning to end. When a value is found which is not within the tolerance of being an integer, it is selected for branching. The other two valves connected to the same chamber are also examined and the one with the largest value is chosen for branching. This is done because the constraint in Eq. (29) forces only one valve to be open per chamber. If the minimum is smaller with the chosen valve being equal to 1, then the other two are already branched and the next chamber can be examined. If instead the variable is selected to be 0, it is still not clear which of the other two variables should be 1.

The other part of the algorithm is the convex solver. In this case an Alternating Directions Method of Multipliers (ADMM) algorithm was selected. This algorithm was chosen because it shows good properties for solving the lasso problem. The method consists of separating the cost function into two separate functions

$$f(x) = 0.5 \left|\left|Tx + \hat{j}\right|\right|_2^2 + |Fx|_1 \tag{38}$$

$$g(z) = I(z) \tag{39}$$

where $f(x)$ is the original cost function and $g(z)$ is an indication function connected with the constrains as

$$I(z) = \begin{cases} 0 & x \in C \\ \text{inf} & \text{otherwise} \end{cases} \tag{40}$$

In this case C is the set $Ax = b$ satisfying the constraints Eq. (29) and $x \geq 0$. Then the problem can be described as:

$$\min(f(x) + g(z)) \tag{41}$$

$$subject\ to\ \ x - z = 0 \tag{42}$$

The ADMM iterations to solve this problem are:

$$x^{k+1} = \min(f(x) + 0.5\rho \left|\left|x^{k+1} - z^k + u^k\right|\right|_2^2) \tag{43}$$

$$z^{k+1} = \min(g(z) + 0.5\rho \left|\left|x^{k+1} - z^{k+1} + u^k\right|\right|_2^2) \tag{44}$$

$$u^{k+1} = u^k + x^{k+1} + z^{k+1} \tag{45}$$

For this type of problem the proximity functions of the x and z iteration are known Gaines et al. (2018).

A* search

Another algorithm which will be tested is the A* search algorithm. At each step the algorithm chooses the node with the smallest cost and explores its branches. Each branch deeper represents one more simulation step. For this reason the algorithm is searching for a node number above 20440 which represents nodes in the 5th simulation step. For the specific case here each node branches into 27 possible new combinations. A pseudo code textbox describing the algorithm can be seen in Fig. 14. Without any heuristic the algorithm tends to search through the tree width first, since both position and switching costs grow with each simulation step. This can result in a large number of explored branches or relatively few if the position error has grown enough. An example of the latter can be seen in Fig. 15. In order to help the algorithm to converge faster an heuristic is implemented as well. The heuristic is based on the distance of a certain combination to an oracle. In order to obtain an oracle the integrality constraint is dropped and the much simpler problem is solved using ADMM. Unfortunately the heuristic only works if

Figure 14: A* search

```
N = [1, 0, 0] ;
stop = 0 ;
while stop ==0 do
    n_branch, n_cost = min(N(:,2));
    n_new = Branch(n_branch) ;
    n_new,costs = J(n_new) ;
    f = J(x_new) ;
    N = AddNodes([ n_new, n_new,costs,
     n_branch]) ;
    N = RemoveNode(n_branch) ;
    if n_new > Goal AND n_new,costs < N(:,2)
     then
        stop = 1 ;
    end
end
```

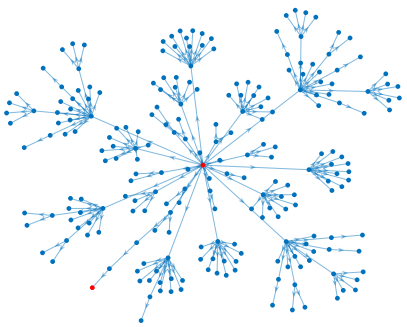

Figure 15: Tree exploration without heuristic. Explored nodes 229.

the ADMM produces results above 0.5 for a specific valve which can then be rounded to 1. An example where the heuristic is rounded and where it is not can be seen in Fig. 17 and Fig. 16 respectively. In the second case only one third of nodes were explored. It can be observed that at each each following time step the number of summed elements is increased. This can lead to a situation in which every node on a level is explored before the next level is explored. The heuristic and the tuning need to take this into account. It can also be observed that during the first steps the chosen pressure levels do not affect the position error directly. This leads to a situation where the cost of changing force has a larger effect on the cost function.

The algorithm was still slow to complete in this form so a modification was introduced. Instead of predicting

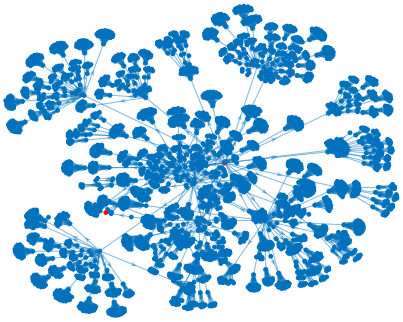

Figure 16: Tree exploration with heuristic but no rounding. Explored nodes = 3423.

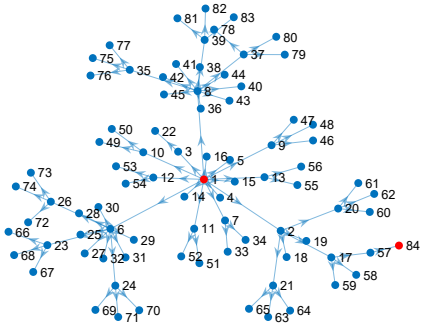

Figure 17: Tree exploration with heuristic with rounding. Explored nodes = 84.

only until the current step in each node, the prediction for the entire horizon with the current node's force level is conducted. For example for node 10, which corresponds to the choice of force 9 at the first time step, the prediction is for the full 5 time steps with force 9 being kept constant. This prevents the optimization algorithm to find combinations in which a more costly step is taken first in order to use a much cheaper step later in the prediction horizon. This greatly increased performance time-wise, while not considerably degrading the accuracy of the controller, due to the nature of the system.

Algorithm results

The performance of the various algorithms has been tested and presented in Fig. 19 and Fig. 18. The initial conditions for the tests consist of 32 different initial conditions. These are created from all the combinations of two parameters. One parameter is the current force level. The second parameter is the position reference. This corresponds to a change in the position reference for the final step from -5 mm to +5 mm. In the table the notation (1,1) then corresponds to a situation where all the valves are closed and the desired movement is in the negative direction.

The different algorithms find similar optimum values in most cases. The only exception is the branch and bound algorithm which in most cases gives a poorer result. In order to show how these small variations affect the accuracy of the controller full simulation runs are conducted with each algorithm. Each test is repeated ten times and the values in Tab. 2 are the average and the standard deviation. Instead of RMS sum of position error, only the absolute sum of errors is used for the Accuracy measure. This is done, because when these numbers are divided by the large number of sample the variations become very small numbers which are difficult to compare.

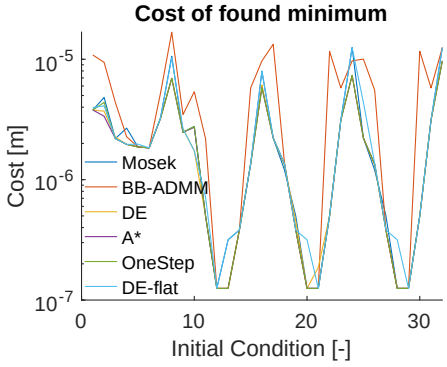

Figure 18: The value of the minimums found by the algorithms

It can be seen that the branch and bound algorithm has the worst results in term of accuracy, energy use and simulation time. It is also important to notice that the A* and OneStep algorithm have the same accuracy and energy use. This shows that in its current implementation the A* cannot find the global optimum. On the other hand it can also be noticed that the accuracy of the controller compared with the DE controller is not much different. Furthermore the OneStep algorithm completes the computation in $\approx 1/3$ of the time.

Table 2: Result for full simulation

	BB-ADMM	DE	DE-Flat	A*	OneStep
Accuracy [m]	1260.99±0.00	843.90±8.29	916.30±119.49	859.62±0.00	859.62±0.00
Energy use [J/mm]	21.15±0.00	5.03±0.69	4.48±1.04	7.44±0.00	7.44±0.00
Sim Time [s]	197.50±12.85	131.01±17.49	121.75±7.43	64.87±34.84	41.50±8.19

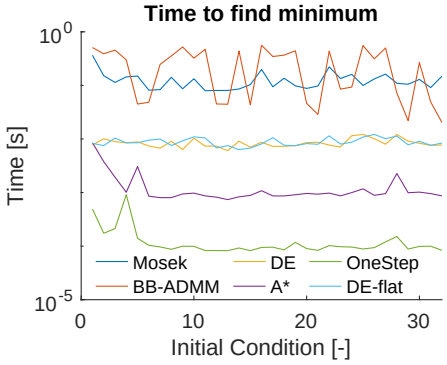

Figure 19: Time needed to find the minimum with different algorithms

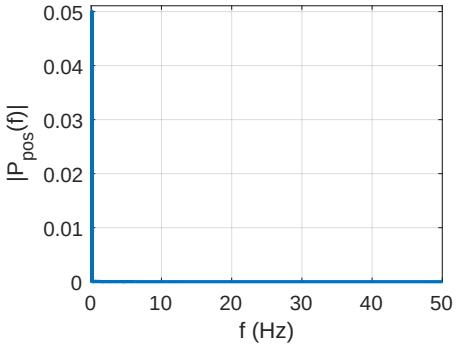

Figure 20: The single-sided amplitude spectrum of the position signal.

It can also be noticed that while DE and DE-Flat have variations in their results. The other algorithms do not. This is, because these two algorithms are stochastic based. The variation of the DE-Flat algorithm is quite large. In one of the ten tests the algorithm fails to find an optimum and gives an incorrect force command. The cost to switching back to a better force level is quite high and by the time the cylinder is following the trajectory again the results of that run are poor. This illustrates the issue with using stochastic algorithms to solve time sensitive problems.

5 Parameter variation

The effect of different algorithms has been explored in the previous section. In this section one of the algorithms is chosen and the effects of the variation of different system parameters will be examined. The performance of the algorithm under varying conditions will be examined according to the root-mean-square sum of error over time, the energy used over time and the total harmonic distortion. All test results are normalized with a so called base run where mass is 50 ton, software delays are 30 ms, no position or velocity noise is present, the pressure lines are constant and all signal are available.

5.1 THD analysis and reference variation

In order to analyse the effect of parameter variation it was decided that the sum of error and the energy use of the simulation might not be enough. The total harmonic distortion analysis is based on Fast Fourier Transforms (FFT) and can show the ratio between the main amplitude present in a signal and other frequencies such as harmonics or noise. Compared with the RMS sum of error the analysis shows whether position error comes from switching activity or if it comes from a phase shift between the reference and the actual position. In order to calculate the THD, the FFT of the position, velocity, and force output signals of the cylinder were collected. FFT produces a single-sided amplitude spectrum of the analysed signal. For instance the position signal was analysed and the results can be seen in Fig. 20. The FFT has broken down the original position signal into a large number of smaller composite sine-wave signals. In the figure the y-axis shows the amplitude of these components and the x-axis shows their frequency. The following formula was used in order to calculate THD based on the signal P1:

$$THD = \frac{\sqrt{(\sum_{f=1}^{L} P_{pos}(f)^2) - max(P_{pos}(f))^2}}{A_{ref,rms}} \quad (46)$$

Table 3: Sine wave testing

Sine freq [Hz]	Error sum [m]	Energy measure[J/mm]	THD [%]
0.1	0.0024	6.36	1.25
0.2	0.0047	2.66	1.79
0.4	0.0102	4.40	1.43
0.6	0.0171	8.02	4.99
0.8	0.0356	8.36	48.04

In the equation L is the length of the amplitude spectrum signal. This is determined by the sampling frequency. Since the signal was obtained from a simulation a very high sampling frequency of 10000 Hz could be chosen. $P_{pos}(f)$ is the value of the signal at frequency f i.e. the amplitude of the sine-wave with this frequency. In the figure it can be seen that the reference trajectory with a frequency of 0.2 Hz and an amplitude of 0.05 m is clearly seen. $max(P_{pos}(f))$ is the maximum value of the signal. In this case it will correspond to the previously mentioned spike due to the reference. It is important to notice that the spice does not necessarily equal the reference, as the controller might over or undershoot. $A_{ref,rms}$ is the RMS value of the reference signal. In Tab. 3 the results of five test are shown. The position reference is a sine wave with the indicated frequency. The length of the trajectory is always the same - 3 periods of the sine wave. THD results closer to 0 are better. It can be seen that position error, energy use and THD do not vary the same way. The trajectory with a frequency of 0.2 Hz has two times larger error, but uses three times less energy. At the same time the smoothness of motion has not degraded considerably as is indicated by the THD. It can be concluded that the error is largely due to phase shift between position and trajectory. It can be seen that at faster frequencies the controller is no longer able to follow the trajectory with the same accuracy until at 0.8 Hz the error and THD become extremely large.

A standard cylinder with a proportional control valve, which can employ throttling control would produce THD values very close to zero. Outside of simulation studies it can be expected that the multi-chamber cylinder would produce results with higher THD. The same THD analysis can be applied to the force output of the cylinder the results can be seen in Fig. 21. The constant load can be seen as a spike at 0 Hz. The result of the force switching can be seen as two mountains on either side of the 8 Hz mark, which repeat periodically. This plot can give an indication of the force spikes in the cylinder.

The THD value is well established in electrical and audio engineering and multiple standards define acceptable limits. The field of digital hydraulics does not have such standards, but perhaps as the field expands it can establish them in conjunction with industry.

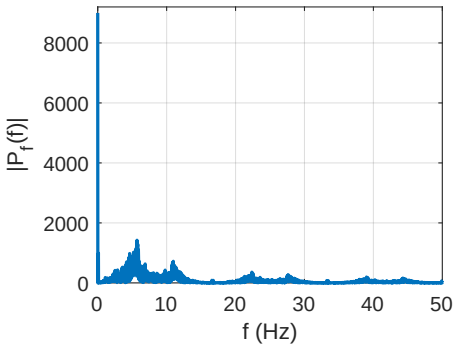

Figure 21: The single-sided amplitude spectrum of the force output signal.

5.2 Changing mass

In order to test how the controller reacts to a change in load mass, this parameter has been varied from 25 ton to 100 ton. In Fig. 22 the mass is varied but the controller uses only 50 ton in the model of the system. It can be seen that reducing the mass below 40 ton increases error significantly. It can be seen that THD increases much faster. At 25 ton the RMS sum of position error is 5 times larger compared with the base run. In Fig. 23 when the mass is changed the new value is given to the controller and the prediction matrices are recalculated. This reduces both error and THD.

When inertia is reduced the system's frequency increases. In order to investigate if a multi-chamber cylinder can operate with low mass - the mass and switching frequency of the controller have been swept individually. The accurate values are supplied to the controller, so the model agrees with the parameters. The sweep has been extended in one direction until the controller is no longer accurate due to the large mass.

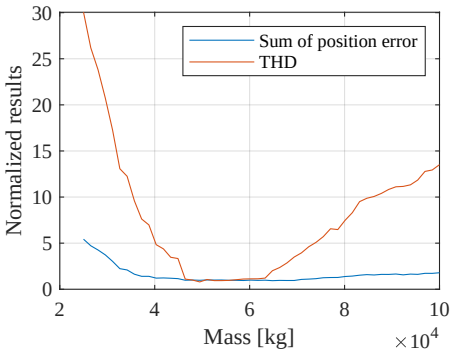

Figure 22: Result from varying mass without providing the controller the correct value.

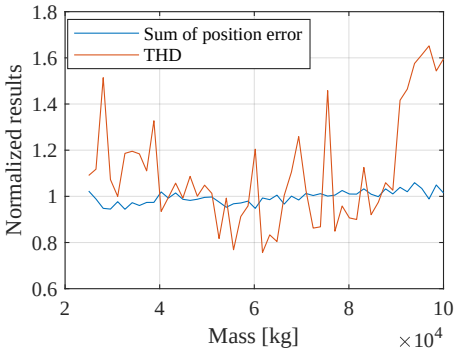

Figure 23: Result from varying mass and providing the controller the correct value.

With different tuning(increased penalty on position error) this error can be reduced. Increasing the switching frequency helps with this problem, but very quickly a lower bound is found. Since one valve requires 15 ms to close and then the other requires 15 ms to open, the controller cannot run faster than 40 ms. Changing tuning parameters does not help with the instability due to very low system inertia. It was found that with this size of cylinder and valves with these properties the system needs at least 15 ton of equivalent mass for the controller to be stable.

5.3 System delays

The system delays have a large effect on the performance of the controller. The delays are of a significant size compared with the sampling time of the model. In order to deal with this, the output of the controller is further delayed as discussed previously. If the added delay together with the system delays perfectly matches one sample of the model, it can be said that the delay can be cancelled out. This is of course never the case, since the delay compensation is static and user chosen and the real delays are variable and potentially unknown. In this study the representation of the system delay is varied, while the user chosen delay is kept constant at 30 ms. The results in Fig. 24 illustrate how much does the performance degrade depending on difference in delay.

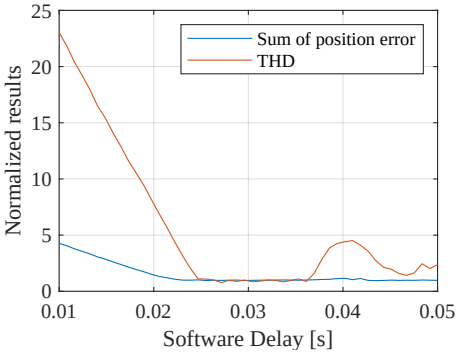

Figure 24: Result from varying system delays.

For close to 5 ms in either direction there is no noticeable increase in error. Beyond this error and THD increase. Once again THD increases faster than the position error.

5.4 Noise and velocity estimation

In this study the difference in performance when noise is present on the position measurement and velocity measurement are presented. The size of the white noise is varied with a gain. A low pass filter with a cut-off frequency of 160 Hz is used to filter out the noise, because it can be expected that both noise and filtering would be present on any implementation of the system. Because of the gain the maximum noise level varies from 0 mm in the first test to 1.25 mm in the last. As a reference the real system has a noise size of 0.3 mm. The effect of noise on the position measurement can be seen in Fig. 25. The effect of noise on the velocity measurement can be seen in Fig. 26. Finally, it cannot be certain that a velocity measurement is available on all systems. A test was conducted were the velocity is estimated from the position measurement using the same method as in Donkov et al. (2019). The frequency of this estimation process was varied by changing the

sampling time t_s and the results can be seen in Fig. 27.

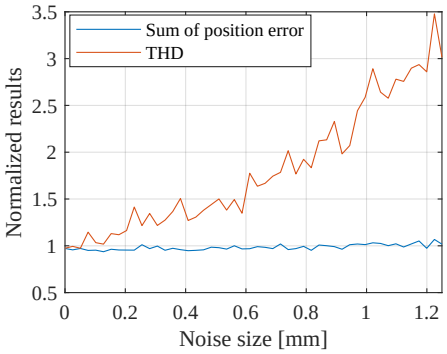

Figure 25: Result from varying position noise level.

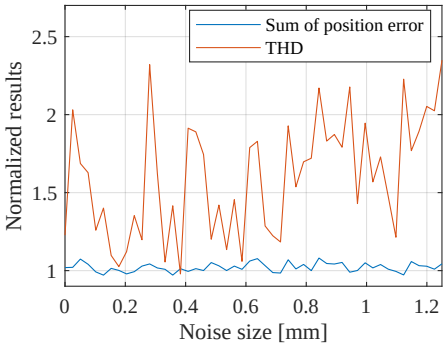

Figure 26: Result from varying velocity noise level.

These tests show that noise has little effect on the position error, but it increases THD. It can also be seen that at 0 mm velocity noise THD has increased by 20 % compared with the base run. The only difference between the two is that in this test the velocity signal is filtered even though the noise gain is zero. The same is true for the position noise test, but the THD there has not increased. It can be concluded that the phase shift introduced by the filter has increased THD, but the controller is only sensitive to phase shifts in velocity and not position. The results also show that if velocity is estimated with a high enough frequency it does not effect performance. In Donkov et al. (2019) the sampling rate of the velocity estimation was 5 ms. It can be concluded that this contributed to the poor laboratory results in that study.

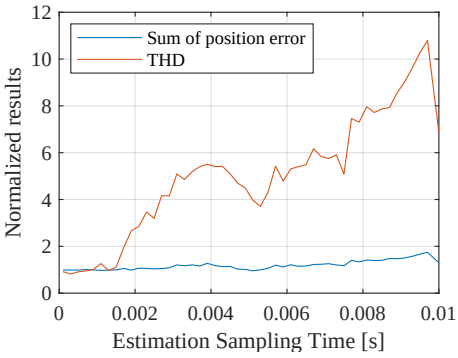

Figure 27: Result from varying the frequency of velocity estimation.

5.5 Supply pressure change

It can be expected that the pressure of the supply lines will not be perfectly constant. In this test the value of the middle pressure line is changed, but the controller is not updated. The results can be seen in Fig. 28.

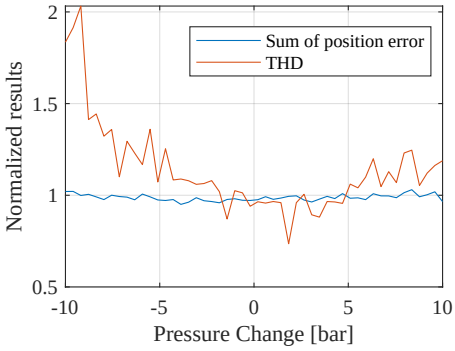

Figure 28: Result from varying the

In this test also the position error is not significantly changed by the variation of the parameter, but the THD raises to twice its original value when the pressure line magnitude is reduced by nine bar.

6 Conclusion

In this paper, a multi-chamber cylinder with MPC with integral action has been investigated through a sensitivity study. Several different optimization algorithms have been tested for the specific problem. The DE algorithm produces the best results regarding time and

accuracy at larger time horizons, but at smaller time horizons of 4 steps a simpler iterative algorithm or the A* search can find similar results faster. Another benefit of the A* algorithm is that it is not based on stochastic methods, so it delivers the same performance every time. The systems performance depends on several factors. It can be seen that the integral action of the MPC can overcome some parameter variations, but this usually comes at the cost of increased control effort. The factors, which have the largest impact on the system performance are changes in mass, changes in system delays and the frequency of velocity estimation. If the exact mass is known and provided to the controller, multi-chamber cylinders can work with masses as low as 15 ton. In order to drive systems with lower inertia - smaller cylinders, faster valves and faster controllers need to be used. The THD number can give a good indication of the vibrations the controller will introduce due to switching, but the number is meaningless without some well established standards.

Acknowledgments

This research was funded by the Research Council of Norway, SFI Offshore Mechatronics, project number 237896/O30.

References

Donkov, V., Andersen, T., Ebbesen, M. K., Linjama, M., and Paloniitty, M. Investigation of the fault tolerance of digital hydraulic cylinders. In *The 16th Scandinavian International Conference on Fluid Power, SICFP*. 2019.

Donkov, V., Andersen, T. O., Ebbesen, M. K., and Pedersen, H. C. Applying digital hydraulic technology on a knuckle boom crane. In *The Ninth Workshop on Digital Fluid Power*. 2017.

Donkov, V. H., Andersen, T. O., Pedersen, H. C., and Ebbesen, M. K. Application of model predictive control in discrete displacement cylinders to drive a knuckle boom crane. In *2018 Global Fluid Power Society PhD Symposium (GFPS)*. IEEE, pages 408–413, 2018.

Gaines, B. R., Kim, J., and Zhou, H. Algorithms for fitting the constrained lasso. *Journal of Computational and Graphical Statistics*, 2018. 27(4):861–871.

Hansen, A. H., Asmussen, M. F., and Bech, M. M. Energy optimal tracking control with discrete fluid power systems using model predictive control. In *Proceedings of the Ninth Workshop on Digital Fluid Power, Aalborg, Denmark*. pages 7–8, 2017.

Hansen, A. H., Asmussen, M. F., and Bech, M. M. Model predictive control of a wave energy converter with discrete fluid power power take-off system. *Energies*, 2018. 11(3):635.

Hansen, R. H., Andersen, T. O., and Perdersen, H. C. Analysis of discrete pressure level systems for wave energy converters. In *Fluid Power and Mechatronics (FPM), 2011 International Conference on*. IEEE, pages 552–558, 2011.

Heybroek, K. and Sjöberg, J. Model predictive control of a hydraulic multichamber actuator: A feasibility study. *IEEE/ASME Transactions on Mechatronics*, 2018. 23(3):1393–1403.

Ho Cho, S., Niemi-Pynttäri, O., and Linjama, M. Friction characteristics of a multi-chamber cylinder for digital hydraulics. *Proceedings of the Institution of Mechanical Engineers, Part C: Journal of Mechanical Engineering Science*, 2016. 230(5):685–698.

Huova, M., Laamanen, A., and Linjama, M. Energy efficiency of three-chamber cylinder with digital valve system. *International Journal of Fluid Power*, 2010. 11(3):15–22.

Linjama, M., Vihtanen, H., Sipola, A., and Vilenius, M. Secondary controlled multi-chamber hydraulic cylinder. In *The 11th Scandinavian International Conference on Fluid Power, SICFP*, volume 9. pages 2–4, 2009.

Stephens, M. A., Manzie, C., and Good, M. C. Model predictive control for reference tracking on an industrial machine tool servo drive. *IEEE Transactions on Industrial Informatics*, 2013. 9(2):808–816.

Storn, R. Differential evolution-a simple and efficient adaptive scheme for global optimization over continuous spaces. *Technical report, International Computer Science Institute*, 1995. 11.

ISSN (online): 2446-1636
ISBN (online): 978-87-7210-810-0 AALBORG UNIVERSITY PRESS